NASA CR-165123
August 1980

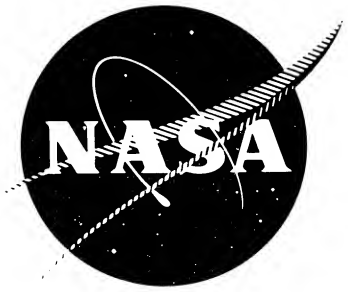

EVALUATION OF THE CYCLIC BEHAVIOR OF AIRCRAFT TURBINE DISK ALLOYS

PART II
FINAL REPORT

By B. A. Cowles, J. R. Warren, and F.K. Haake

Pratt & Whitney Aircraft Group
Government Products Division

Prepared for
National Aeronautics and Space Administration

NASA Lewis Research Center
Contract NAS3-21379

FOREWORD

An evaluation of the cyclic behavior of several nickel-base superalloy turbine disk materials for aircraft gas turbine engine applications was performed from July 1978 through March 1980. The authors wish to express their gratitude to several Pratt & Whitney Aircraft employees who made significant contributions to the program effort. These include Messrs. D. P. Shoemaker, J. M. Lieske II, D. L. Sims, E. J. Drumheller, and E. H. Hindle III, who performed the majority of the materials testing. Special thanks are extended to Mr. E. I. Veil, who conducted the metallographic and fractographic analyses.

This program was conducted under the cognizance of Mr. M. C. VanWanderham, General Supervisor of the Mechanics of Materials and Structures section of the Materials Engineering and Technology Department at Pratt & Whitney Aircraft Group, Government Products Division.

TABLE OF CONTENTS

ILLUSTRATIONS

ILLUSTRATIONS (Continued)

ILLUSTRATIONS (Continued)

ILLUSTRATIONS (Continued)

ILLUSTRATIONS (Continued)

ILLUSTRATIONS (Continued)

LIST OF TABLES

SUMMARY

Several nickel-base aircraft turbine disk superalloys representing various strengths and processing histories were evaluated at 650°C for resistance to fatigue crack initiation and propagation under cyclic and cyclic/dwell conditions. Controlled strain low-cycle fatigue (LCF) and controlled load crack propagation tests were performed and results utilized to provide a direct comparison among the alloys. In addition, limited fractographic and metallographic analyses were conducted, and tests were performed on selected alloys to evaluate the effects of hold times, mean stresses, stress-dwell cycle types, inert environment, and contractor test methods.

At the lower total strain ranges of interest for aircraft turbine disk applications, the alloys exhibited generally increasing initiation life with increasing tensile strength for both cyclic (0.33 Hz) and cyclic/dwell (900-sec hold per cycle) conditions. Rank order of the alloys by LCF initiation life changed substantially at higher strain ranges, approaching the rank order expected from monotonic tensile ductilities (for total strain ranges above approximately 1.8%). The effect of the 900-sec (15-min) hold time fatigue life varied significantly from alloy to alloy. Generally, the higher-strength, finer-grained alloys exhibited more significant reductions in fatigue life due to the dwell. In general, the effects of mean strain were found to be negligible for the conditions evaluated and the effects of mean stress were pronounced. For the type cycles evaluated, at high strain ranges the mean stress was near zero and did not contribute to reduction in life. At low strain ranges, however, mean stresses were large and significant reductions in LCF lives occurred.

Crack growth rates generally increased with increasing tensile strength. Crack growth testing conducted with a 900-sec dwell at maximum tensile load in air showed the same trends as the 0.33 Hz testing with larger absolute differences in crack growth rates, and, as in the initiation tests, the higher strength, finer grained alloys were more severely affected by the hold time. Waspaloy and IN 100 tested in an argon environment at 0.33 Hz demonstrated crack growth rates at low ΔK levels approximately a factor of 2 slower than the same alloys tested in air. Air and argon crack growth rates converged at higher ΔK levels.

Low-cycle fatigue data generated by P&WA and GE generally agreed with some differences in the cyclic (0.33 Hz) test data. Differences in LCF life are probably attributable to specimen machining and surface preparation. Comparison of Contractor crack growth testing and data analysis procedures showed crack growth data obtained at 0.33 Hz for the GE K_b bar specimen to be approximately two times faster than that obtained from the compact type specimen. At 900-sec dwell times, K_b bar data was much faster than the CT specimens, with diminishing differences at low ΔK levels.

Additional creep-fatigue cyclic evaluations were performed on the IN 100 samples at 650°C. Changing dwell time from zero to 30, 120, and 900 sec resulted in corresponding reductions in life with very minimal changes in cyclic creep strain range. Reductions in life are attributed primarily to exposure time at 650°C rather than cyclic creep deformation damage. Comparison of basic tensile stress-hold with tensile strain-hold cycles showed no significant differences provided test variables, such as mean stress, strain range, and hold time were comparable. Mean stress and accumulated creep strain (in stress-hold cycles) both significantly affected LCF life. Life differences between stress-hold and strain-hold cycles were attributed to mean stress and cumulative creep strains.

Overall, the relationship of strength and grain size to LCF and crack growth capability were found to be valid, in general. The effects of mean stress, hold times, and environment were significant, and more pronounced for the higher strength alloys. Finally, the relative cyclic performance of the alloys would not be expected to relate simply to strength or any other single material property, but would depend on specific usage conditions.

INTRODUCTION

Recent strength advances in wrought powder metallurgy superalloys offer the potential for increasing the performance and reducing the weight of gas turbine aircraft engines. Coupled with lower cost processing methods, such as hot-isostatic pressing (HIP), the net result could be substantially reduced system life-cycle costs. After an alloy has been developed, critical evaluations must be conducted to define its capability to enable utilization of that capability in the design, manufacture, and service of components. The cyclic behavior and capability of the new powder metallurgy alloys become extremely important when they are considered for turbine disk applications. In many engine designs, these disks are often low-cycle fatigue (LCF) limited.

Before these powder-metallurgy alloys can be incorporated into engine turbine disk designs a comparison of their cyclic fatigue behavior must be made with reference to an alloy in current use. Then an objective assessment of total-crack initiation plus crack propagation-fatigue life can be made to determine if the strength advances in wrought powder-metallurgy superalloys have resulted in corresponding increases in LCF capability, and if HIP processed alloys have cyclic lives substantially the same as their wrought powder counterparts. In addition, the effects of mean stress or strain on LCF life, the effect of environment on crack growth rate, and the effect of varying hold time on LCF life must be understood both to successfully use current alloys and to facilitate development of improved alloys for turbine disk applications.

This program follows two earlier NASA contracts which evaluated the cyclic behavior of several aircraft turbine disk alloys. In the earlier programs, Pratt & Whitney Aircraft Group (P&WA) evaluated the cyclic behavior of conventionally wrought Waspaloy produced from ingot, fully HIP low carbon powder Astroloy, HIP plus forged low carbon powder Astroloy, HIP plus cross-rolled powder metallurgy NASA IIB-7, and GATORIZED® powder IN 100.[1] General Electric Company (GE) evaluated INCO 718 produced from ingot, HIP powder René 95, and HIP plus forged powder metallurgy René 95.[2]

The objectives of this program included evaluation of an additional alloy, providing a comparison of contractor test methods, determination of crack initiation and early propagation mechanisms for various alloys, and determination of the effects of mean stress or strain, various creep-fatigue cycle forms, and environmental effects on crack initiation and crack growth behavior for two of the alloys. As in earlier programs, the cyclic behavior of the alloys was evaluated from two aspects: crack initiation and crack propagation. The test methods utilized to establish this behavior were axially-loaded strain control LCF tests for initiation and load-controlled cyclic crack growth rate fracture mechanics tests for propagation. Tests were conducted under both cyclic and cyclic/dwell conditions at 650°C (1200°F).

The alloys selected for this program included HIP MERL 76 which is an advanced alloy currently undergoing trial disk production development at P&WA under NASA MATE program sponsorship, HIP plus forged René 95 currently used by GE, GATORIZED IN 100 which is an advanced alloy currently used by P&WA, and conventionally forged Waspaloy which is a current, widely used disk alloy produced from ingot.

HIP MERL 76 represented the new alloy not previously evaluated. René 95 which was previously tested by General Electric was included to provide a comparison of Contractor test methods and results. IN 100 and Waspaloy were selected for evaluation under cyclic and cyclic/dwell conditions and in an inert environment because these alloys are representative of relative extremes in processing methods and cyclic behavior for currently used turbine disk alloys.

MATERIAL PROCUREMENT AND QUALIFICATION

Four nickel-base superalloys for aircraft gas turbine engine disks were evaluated for resistance to fatigue crack initiation and propagation under both cyclic and cyclic/dwell conditions at elevated temperature. Results provide comparisons of a conventionally forged superalloy produced from ingot with three advanced alloys produced from pre-alloyed powder in the wrought, hot isostatically pressed (HIP) , and the HIP plus forged forms. These results are also directly comparable with alloys previously evaluated and reported (Reference 4).

The listing below details the four alloys evaluated under this program. Table 1 describes the chemical compositions and heat treatments.

TABLE 1
NOMINAL CHEMICAL COMPOSITIONS[1] AND HEAT TREATMENTS

Element	*Alloy 1 HIP MERL 76*	*Alloy 2 René 95*	*Alloy 3 Waspaloy*	*Alloy 4 GATORIZED™ IN 100*
Carbon	0.022	0.065	0.06	0.07
Manganese	0.02 max	0.15 max	0.75 max	0.020 max
Sulfur	0.01 max	0.015 max	0.02 max	0.010 max
Phosphorous	0.01 max	0.015 max	—	0.010 max
Silicon	0.10 max	0.50 max	0.75 max	0.10 max
Chromium	12.40	13.0	19.5	12.40
Cobalt	18.50	8.0	13.5	18.50
Molybdenum	3.20	3.50	4.0	3.20
Titanium	4.32	2.50	3.0	4.32
Aluminum	5.00	3.50	1.4	4.97
Boron	0.02	0.01	0.065	0.02
Zirconium	0.06	0.05	0.07	0.06
Tungsten	—	3.50	—	0.05 max
Iron	0.30 max	0.50 max	2.0 max	0.30 max
Copper	0.07 max	—	0.10 max	0.07 max
Lead	0.0002 max	—	10 ppm max	0.0002 max
Tantalum[2]	—	0.2 max	—	0.04 max
Vanadium	—	—	—	0.78
Hafnium	0.40	—	—	—
Nickel	Balance	Balance	Balance	Balance
Heat Treatment[3]				
Solution, Stabilization, and Age	1163°C/2 hr/OQ 871°C/0.67 982°C/0.75 760°C/16	1092°C/1 Hr 538°C Molten Salt Bath Quench 760°C/16 hr	1024/4/OQ 843/4/AC	1121/2/OQ 871/40 min/AC 649/24/AC 760/4/AC

[1]Nominal Composition—Percent by Weight
[2]Tantalum and Columbium for Alloy 4
[3]Heat Treat Conditions — Nominal
Temperature — °C/Time-hr/Air Cool — AC, Oil Quench — QC

Alloy 1— HIP MERL 76: an advanced, high-strength powder metallurgy superalloy. Trial production of full-sized turbine disks is currently underway at P&WA/Commercial Products Division (CPD) in East Hartford, CT under NASA MATE program sponsorship. HIP MERL 76 was supplied by the Government through P&WA/CPD. Material was received in the form of four rough-cut sections from a fully-HIP'd JT10D 1st-stage turbine disk, as shown in figure 1. This figure also shows the specimen cutup layout. Composition and material tensile qualification test results for this forging are presented in tables 2 and 3, respectively.

Alloy 2 — HIP plus forged René 95: an advanced powder metallurgy turbine disk alloy currently in use by GE. HIP plus forged René 95 was supplied by NASA in the form of a fully heat treated turbine disk segment. Composition and material qualification test results (supplied by NASA) for this forging appear in tables 4 and 5, respectively. Figure 2 presents the specimen cutup schematic.

Alloy 3 — Wrought Waspaloy produced from cast ingot. Waspaloy is widely used as a turbine disk alloy in engines, such as P&WA JT8D, JT9D, and TF30. Waspaloy was produced in the form of a JT9D 3rd-stage turbine disk forging taken from a production run of this part. This disk was produced by the Ladish Company and is representative of the material in current use. Composition and material qualification test results for this forging are presented in table 6. Figure 3 shows the specimen cutup schematic.

Alloy 4 — GATORIZED IN 100: an advanced powder metallurgy turbine disk alloy currently used in the turbine and high-pressure compressor disks of the F100 engine. The IN 100 was obtained as a fully heat treated disk/pancake forging segment. Composition, heat treatment, and material qualification test results for this forging are presented in table 7. Test specimen machining was in accordance with the layout presented in figure 4. Test specimens machined from the forging consisted primarily of axial strain control LCF specimens and modified compact tension specimens for crack growth rate, as shown in figure 5.

The LCF specimens were oriented tangentially in the forgings and the compact specimens were oriented such that crack growth direction would be approximately radial to the disk forging. Tensile tests were conducted at 650°C (1200°F) to provide a comparison of monotonic strengths and ductilities among the alloys at a representative temperature. Table 8 presents the results of these tests.

Optical and electron micrographs representing the microstructure for each of the alloys appear in figures 6 through 9. The microstructure of HIP MERL 76 is shown in figure 6. This material has an ASTM grain size of 8.5 to 10.5. HIP plus forged René 95 is characterized in figure 7. This alloy has a grain structure consisting of 60% unrecrystallized grains with ASTM grain size of 5 to 6 with occasional 4, necklaced by recrystallized grains finer than 8. The Waspaloy microstructure, figure 8, varied but was generally ASTM grain size 3 to 5 with occasional 2, and with some duplexing with 7 and finer. The IN 100 microstructure is shown in figure 9. This alloy is fine-grained with an ASTM grain size of 12.5 to 14.5 with occasional 11.5.

Further details of microstructure are given in a later section entitled "Evaluation of Fatigue Crack Initiation Mechanisms."

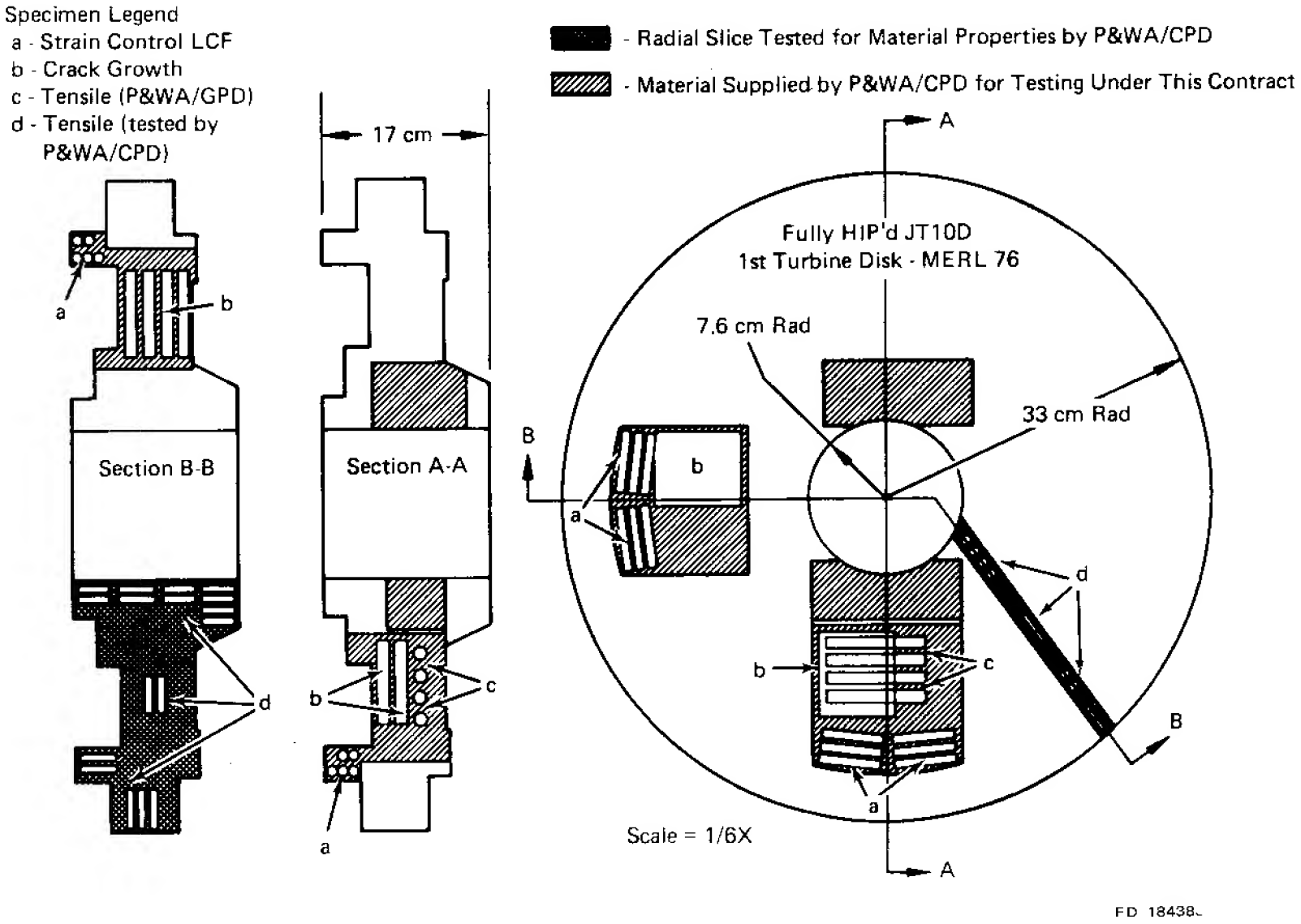

Figure 1. Material and Specimen Layout Plan for Fully HIP'd MERL 76 Disk

TABLE 2
CHEMICAL COMPOSITION AND HEAT TREATMENT—ALLOY 1, HIP MERL 76.
Identification: UDIMET Powder Blend No. 79003, JT10D 1st Turbine Disk S/N-102-2

Element	*Target Chemistry*	*Powder BN 7903*	*Disk 102-2*
Ni	R	R	R
Cr	11.9 - 12.9	12.51	12.0
Co	18.0 - 19.0	18.50	18.4
Mo	2.8 - 3.6	3.29	3.3
Al	4.85 - 5.15	4.93	5.1
Ti	4.15 - 4.50	4.20	4.2
Nb	1.20 - 1.60	1.46	1.41
Hf	0.30 - 0.50	0.39	0.48
B	0.016 - 0.024	0.02	0.02
Zr	0.04 - 0.08	0.05	0.045
C	0.015 - 0.03	0.026	0.023
Mn	0.02 max	0.008	ND
S	0.01 max	ND	ND
P	0.01 max	0.004	ND
Si	0.10 max	0.01	ND
Fe	0.30 max	0.05	ND
Cu	0.07 max	0.03	ND
Bi	0.05* max	0.02*	ND
Pb	2.0* max	1*	ND
O	100.0* max	92*	89*
N	50.0* max	18*	20*

R = Remainder
ND = Not Determined

Disk 102-2 was HIP consolidated at 1182°C/103 MPa/3hr
Heat Treatment:
1163°C/2 hr/Oil Quench +
871°C/0.67 hr +
982°C/0.75 hr +
649°C/24 hr +
760°C/16 hr

TABLE 3
TENSILE QUALIFICATION TEST RESULTS — ALLOY 1, HIP MERL 76
Identification: UDIMET Powder Blend No. 79003, JT10D 1st Turbine Disk S/N-102-2

Specimen S/N	*Location*	*Test Temp (°C)*	*0.2% YS*		*UTS*		*%El*	*%RA*	*Testing* Source*
			MPa	*ksi*	*MPa*	*ksi*			
102-2-5	Bore — ID	25	—	—	1612	233.9	19.7	19.7	CPD
102-2-9	Bore — ID	25	1153	167.4	1647	239.0	18.2	18.3	CPD
102-2-2	Adjacent to	25	1076	156.2	1581	229.5	16.5	16.9	CPD
102-2-8	Bore — ID	25	1059	153.7	1616	234.5	22.2	18.3	CPD
102-2-17	Rim	25	1067	154.9	1610	233.6	19.6	19.8	CPD
TARGET	—	25	1034	150.0	1482	215.0	15.0	15.0	—
102-2-1	Bore — ID	621	1084	157.4	1430	207.5	23.5	28.3	CPD
102-2-7	Bore — ID	621	1087	157.7	1437	208.6	21.7	23.9	CPD
102-2-6	Adjacent to	621	1042	151.2	1430	207.5	23.7	24.1	CPD
102-2-10	Bore — ID	621	1087	157.8	1470	213.3	18.0	16.9	CPD
102-2-3	Hub	621	1059	153.7	1450	210.4	26.6	24.1	CPD
102-2-4	Hub	621	1053	152.8	1416	205.4	23.2	26.7	CPD
102-2-13	Flange	621	1078	156.4	1421	206.2	22.7	26.7	CPD
102-2-14	Flange	621	1090	158.2	1453	210.9	23.3	22.7	CPD
102-2-11	Web	621	—	—	1364	198.0	27.1	24.6	CPD
102-2-12	Web	621	1039	150.8	1387	201.3	28.8	28.3	CPD
102-2-16	Rim	621	1079	156.6	1419	205.9	22.5	26.9	CPD
TARGET	—	621	1014	147.0	1365	198.0	22.0	12.0	—
F-4	Web	650	1031	149.5	1369	198.6	22.5	24.6	GPD
F-5	Web	650	1024	148.5	1361	197.4	24.0	25.5	GPD

*CPD: United Technologies Corp., Pratt & Whitney Aircraft Group, Commercial Products Division, East Hartford, Connecticut

GPD: United Technologies Corp., Pratt & Whitney Aircraft Group, Government Products Division, West Palm Beach, Florida

TABLE 4
CHEMCIAL COMPOSITION AND HEAT TREATMENT-ALLOY 2, HIP PLUS FORGED RENE 95 PRODUCED FROM PREALLOYED POWDER
Producer: Cartech VIM Heat No. V91085,
Preform C525,
Ladish Company Forging EX091

	Required	*Actual**
Chemical Composition:		
Carbon	0.04 to 0.09	0.08
Manganese	0.15 Max	0.01
Silicon	0.50 Max	0.06
Phosphorous	0.015 Max	0.005
Sulphur	0.015 Max	0.002
Chromium	12 to 14	12.8
Molybdenum	3.3 to 3.7	3.56
Cobalt	7 to 9	8.05
Titanium	2.3 to 2.7	2.56
Aluminum	3.3 to 3.7	3.57
Boron	0.006 to 0.015	0.01
Niobium	3.3 to 3.7	3.60
Tantalum	0.2 Max	0.01
Tungsten	3.3 to 3.7	3.59
Zirconium	0.03 to 0.07	0.053
Iron	0.5 Max	0.39
Hydrogen	0.001 Max	2 ppm
Oxygen	0.010 Max	66 ppm
Nitrogen	0.005 Max	0.003
Nickel	Balance	Balance

*Analysis of Master Powder Blend No. 55

Heat Treatment:
1092°C/1 Hr
538°C Molten Salt Bath Quench
760°C/16 hr

TABLE 5
QUALIFICATION TEST RESULTS — ALLOY 2, HIP PLUS FORGED
RENE 95
Identification: CarTech VIM Heat V91085/Preform No. C525
Ladish Company Forging EX 091 DFL Series -2
Specification: GE C50TF54

1. *Tensile*

Specimen Number	*Temperature* °C	(°F)	*0.2% YS* MPa	(ksi)	*UTS* MPa	(ksi)	*RA %*	*El%*
SR-1	Room Temperature		1172	(170)	1620	(235)	22.3	18.6
SR-2	Room Temperature		1179	(171)	1627	(236)	23.2	18.1
SR-3	Room Temperature		1186	(172)	1641	(238)	22.6	18.4
Average Values	Room Temperature		1179	(171)	1629	(236)	22.7	18.4
Spec Values								
C1-B	Room Temperature		1207	(175)	1544	(224)	12	10
C1-C	Room Temperature		1179	(171)	1524	(221)		
SR-4	650	(1200)	1110	(161)	1475	(214)	14.4	11.8
SR-5	650	(1200)	1124	(163)	1482	(215)	15.9	14.6
SR-6	650	(1200)	1131	(164)	1482	(215)	12.2	12.1
Average Values	650	(1200)	1122	(162.6)	1480	(214.6)	14.2	12.8
Spec Values								
C1-B	650	(1200)	1117	(162)	1427	(207)	10	8
C1-C	650	(1200)	1089	(158)	1407	(204)		

2. *Stress Rupture*

Specimen Number	*Temperature* °C	(°F)	*Stress* MPa	(ksi)	*Time to Failure, Hours*	*RA %*	*El %*
SR-7	650	(1200)	1034	(150)	280.8	6.3	2.2
SR-8	650	(1200)	1034	(150)	315.4	1.6	2.2
Spec Values							
C1-B	650	(1200)	1034	(150)	35		
C1-C	650	(1200)	1034	(150)	35		

TABLE 5
QUALIFICATION TEST RESULTS — ALLOY 2, HIP PLUS FORGED
RENE 95 (Continued)
Identification: CarTech VIM Heat V91085/Preform No. C525
Ladish Company Forging EX 091 DFL Series -2
Specification: GE C50TF54

3. Creep

Specimen Number	*Temperature* °C	(°F)	*Stress* MPa	(ksi)	*Time to 0.2% Plastic Deformation, Hours*
SR-9	593	(1100)	1034	(150)	205
SR-10	593	(1100)	1034	(150)	235
Spec Values					
C1-B	593	(1100)	1034	(150)	100
C1-C	593	(1100)	1034	(150)	100

4. Cyclic Rupture

Specimen Number	*Temperature* °C	(°F)	*Stress* MPa	(ksi)	*Cycles to Failure*	*Hours*
1	650	(1200)	1000	(145)	533	17.1
3	650	(1200)	1000	(145)	610	19.1
Spec Minimum Value	650	(1200)	1000	(145)	300	—

5. Residual Life

Specimen Number	*Temperature* °C	(°F)	*Stress* MPa	(ksi)	*Cycles to Failure*
1-B	538	(1000)	690	(100)	12.380
2-B	—	—	690	(100)	5.319

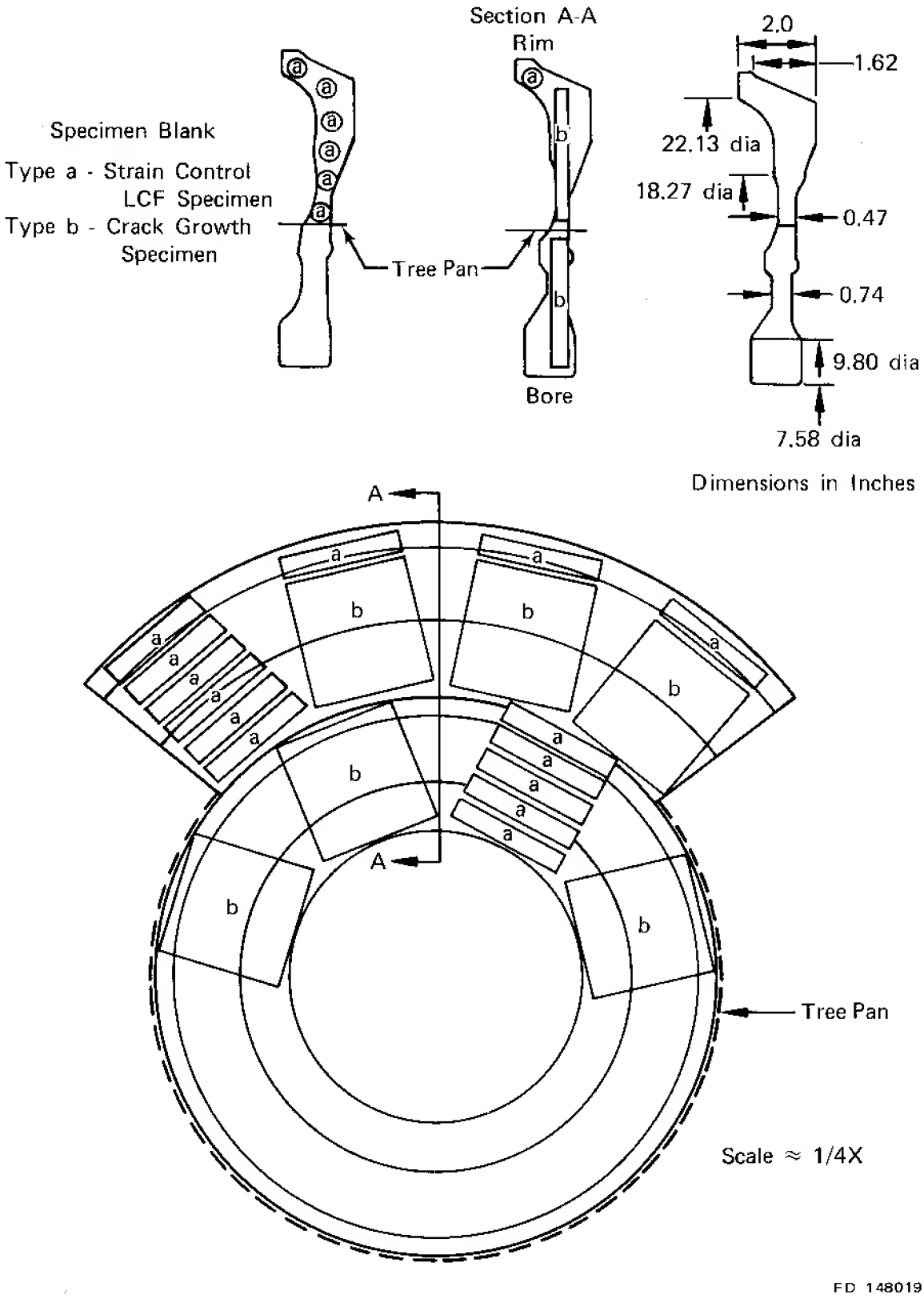

Figure 2. Material and Specimen Layout Plan for HIP and Forged René 95

TABLE 6
QUALIFICATION TEST RESULTS — ALLOY 3, WROUGHT WASPALOY PRODUCED FROM INGOT
Producer: Ladish Company
Heat Code: LRKB 2017

	Required	*Actual*
Chemical Composition:*		
Carbon	0.02 to 0.10	0.04
Manganese	0.75 max	0.01
Sulfur	0.020 max	0.005
Silicon	0.75 max	0.03
Chromium	18.0 to 21.0	19.25
Cobalt	12.0 to 15.0	13.58
Molybdenum	3.5 to 5.0	4.22
Titanium	2.75 to 3.25	3.09
Aluminum	1.20 to 1.60	1.29
Zirconium	0.02 to 0.12	0.048
Boron	0.003 to 0.010	0.0051
Iron	2.0 max	0.68
Copper	0.10 max	0.01
Bismuth	0.5 ppm max	0.5 ppm
Lead	10 ppm max	3.0 ppm
Nickel	Balance	57.48
Heat Treatment:	1010°C to 1038°C/4/OQ	1016°C/4/OQ
	843°C/4/AC	843°C/4/AC
	760°C/16/AC	760°C/16/AC

	Ultimate	*0.2% Yield*	*% EL*	*% RA*
Tensile Properties:				
Room Temperature				
Required Minimum	1241 MPa	862 MPa	15	18
Actual	1376.9 MPa	1060.4 MPa	21	31
538°C				
Required Minimum	1103 MPa	758 MPa	15	18
Actual	1240.4 MPa	934.9 MPa	22	28

	Required Min.		*Actual*	
	Time	*% EL*	*Time*	*% EL*
Stress Rupture Strength:				
732°C, 552 MPa	23 hr	12	56.8	18
816°C, 293 MPa	23 hr	12	42.5	26

**Percent by weight unless otherwise noted.*

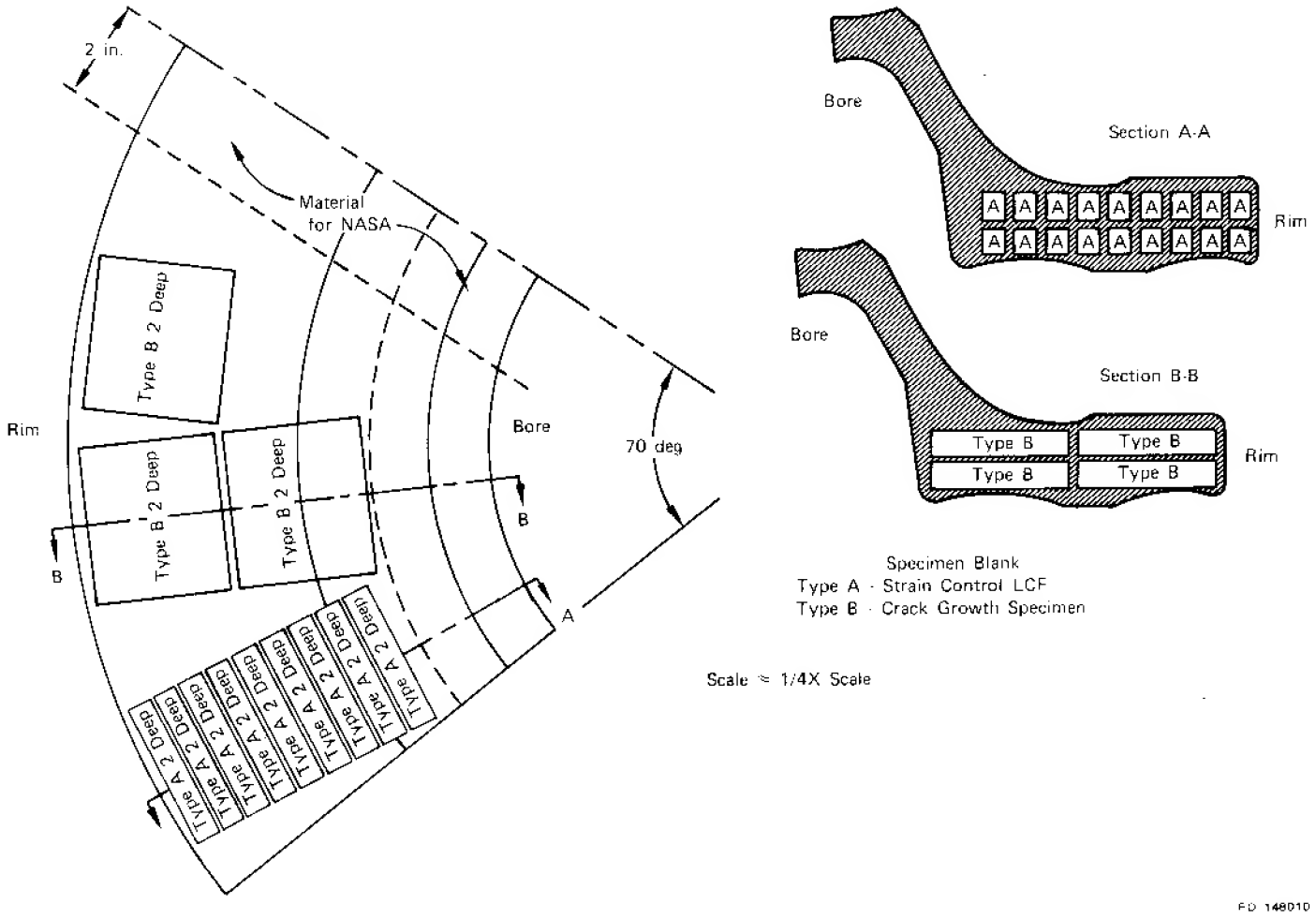

Figure 3. Material and Specimen Layout Plan for Wrought Waspaloy Disk Forging

TABLE 7
QUALIFICATION TEST RESULTS — ALLOY 4, GATORIZED®
IN 100 PRODUCED FROM PREALLOYED POWDER
Powder Source: Homogenous Metal
Forging Vendor: P&WA
Heat Code: BAQQ, H105-A10

	Required		
Chemical Composition	*Min*	*Max*	*Actual*
Carbon	0.05	0.09	<0.090
Manganese	—	0.020	0.02
Sulfur	—	0.010	<0.001
Phosphorus	—	0.010	0.006
Silicon	—	0.10	<0.10
Chromium	11.90	12.90	12.21
Cobalt	18.00	19.00	18.26
Molybdenum	2.80	3.60	3.20
Titanium	4.15	4.50	4.28
Aluminum	4.80	5.15	4.96
Vanadium	0.58	0.98	0.72
Boron	0.016	0.024	0.018
Zirconium	0.04	0.08	0.06
Tungsten	—	0.05	<0.05
Iron	—	0.30	<0.30
Copper	—	0.07	<0.07
Columbium and Tantalum	—	0.04	<0.04
Lead*	—	0.0002 (2 ppm)	<1 ppm
Bismuth*	—	0.00005 (0.5 ppm)	<0.3 ppm
Oxygen	—	0.010 (100 ppm)	76 ppm
Nickel	Remainder		Balance

Heat Treatment:	1121°C/2 hr/OQ 871°C/40 min/AC to below 371°C 649°C/24 hr/AC to below 371°C 760°C/4 hr/AC to below 371°C	1121°C/2 hr/OQ 871°C/40 min/AC to below 371°C 649°C/24 hr/AC to below 371°C 760°C/4 hr/AC to below 371°C

	Ultimate	*0.2% Yield*	*% El*	*% RA*
Tensile Properties 704°C				
Required Minimum	1172 MPa	1014 MPa	12	12
Actual	1269 MPa	1051 MPa	26.6	34.9

	Required Minimum		*Actual*	
	Time	*% El*	*Time*	*% El*
Stress Rupture Strength:				
732°C, 655 MPa	23 hr	5	26.8 hr	10.3

	Required Minimum Time to 0.2% Offset	*Actual*
Creep Strength:		
704°C, 552 MPa	100 hr	0.1% after 174.5 hr**

*If determined
**Creep on integral rings may be discontinued after 75 hr if 0.08% extension has not been exceeded.

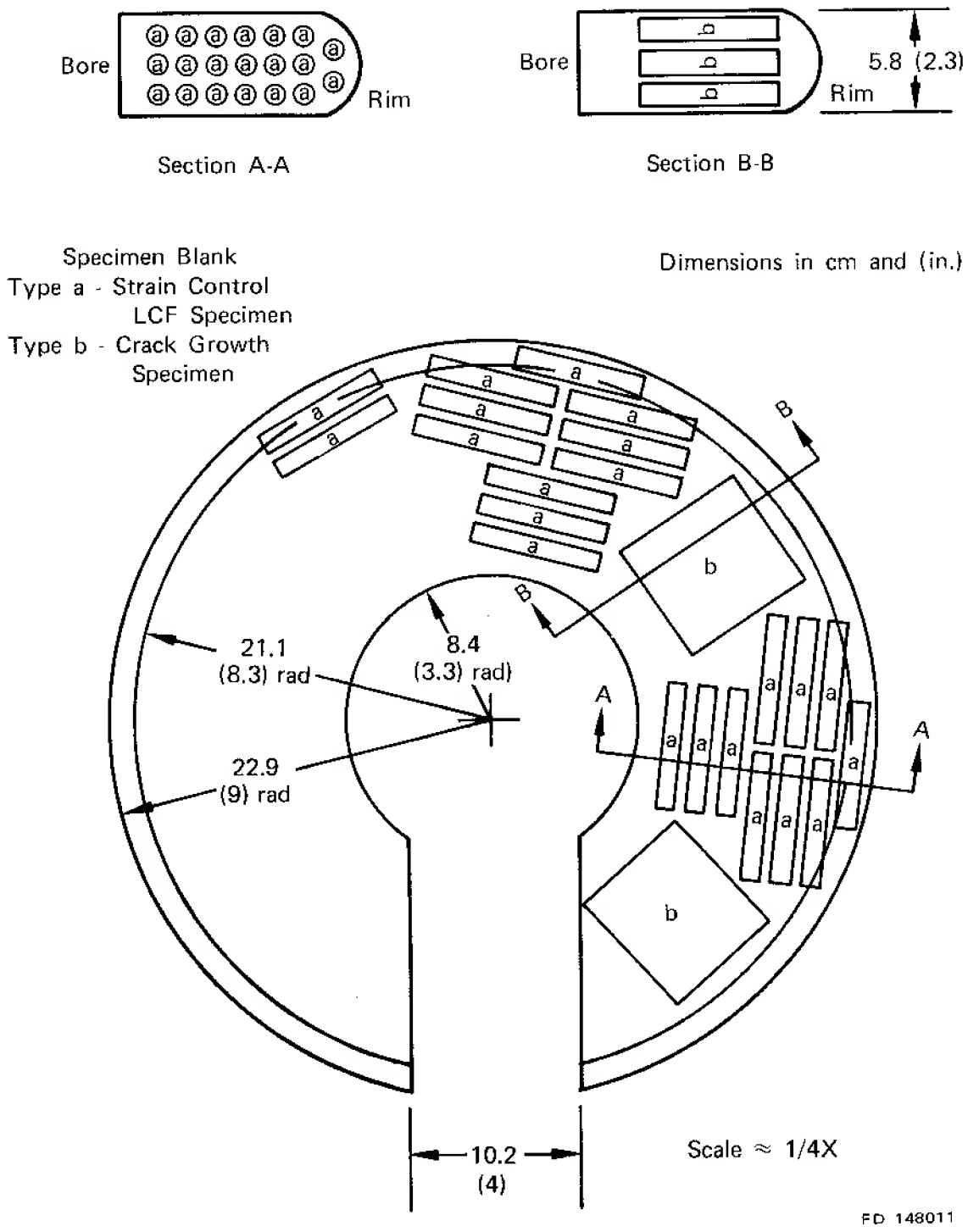

Figure 4. Material and Specimen Layout Plan for GATORIZED® IN 100 Pancake

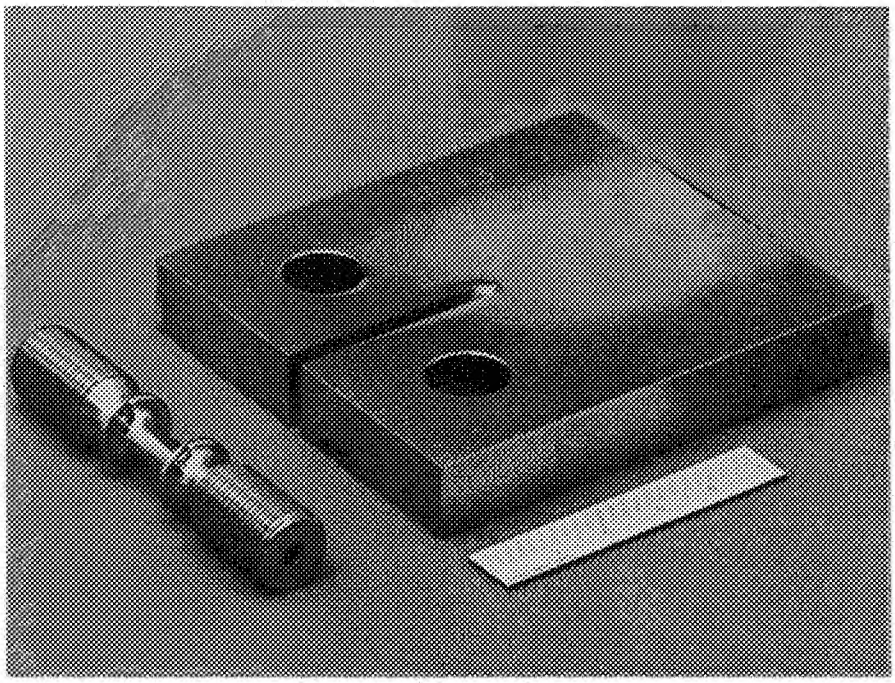

FE 169461

Figure 5. Strain Control LCF and Modified Compact Tension Specimens

TABLE 8
ELEVATED TEMPERATURE TENSILE PROPERTIES AT 650°C

Material	*Material Identification or Heat Code*	*Specimen Number*	*Ultimate Strength (MPa)*	*0.2% Yield (MPa)*	*EL (%)*	*RA (%)*
HIP MERL 76	UDIMET Blend 79003 Disk S/N 102-2	F-4	1369	1031	22.5	24.6
		F-5	1361	1024	24.0	25.5
René 95 (HIP + forged)	CarTech V91085 Preform C525	SR-4	1475	1110	11.8	14.4
		SR-5	1482	1124	14.6	15.9
		SR-6	1482	1131	12.1	12.2
Waspaloy	LRKB-2017	A4	1259	967	22.5	28.7
		A8	1266	947	20.5	25.2
IN 100	BAQQ,H105-A10	19	1359	1113	22.5	25.3
		20	1341	1107	21.0	24.6

*Results from disk/pancake forging BAKY-H45-A5, evaluated under NAS3-20367 (Reference 1), with identical shape and processing as BAQQ-H105-A10. The 704°C tensile results for these forgings were nearly identical.

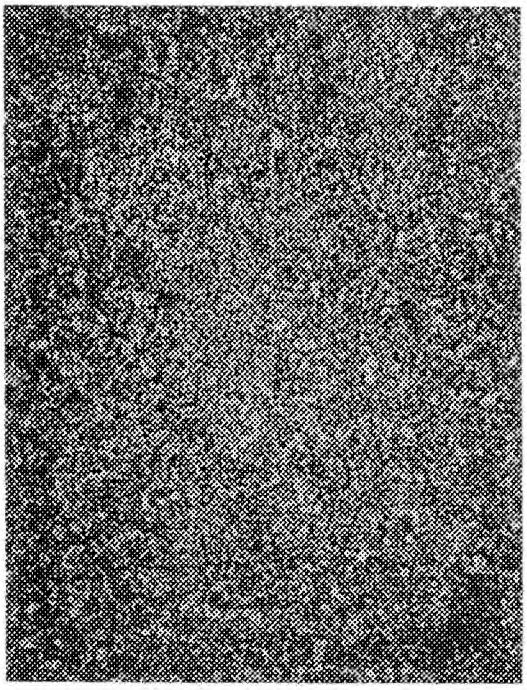

100X

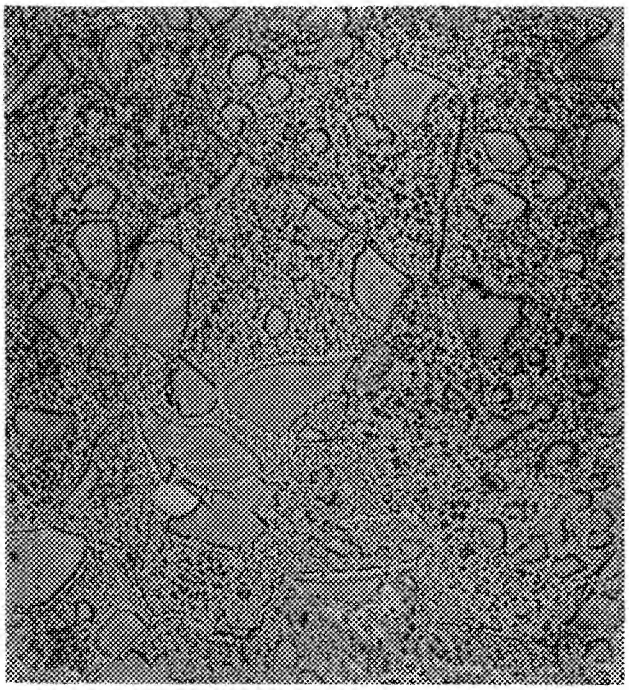

3,000X

1,000X

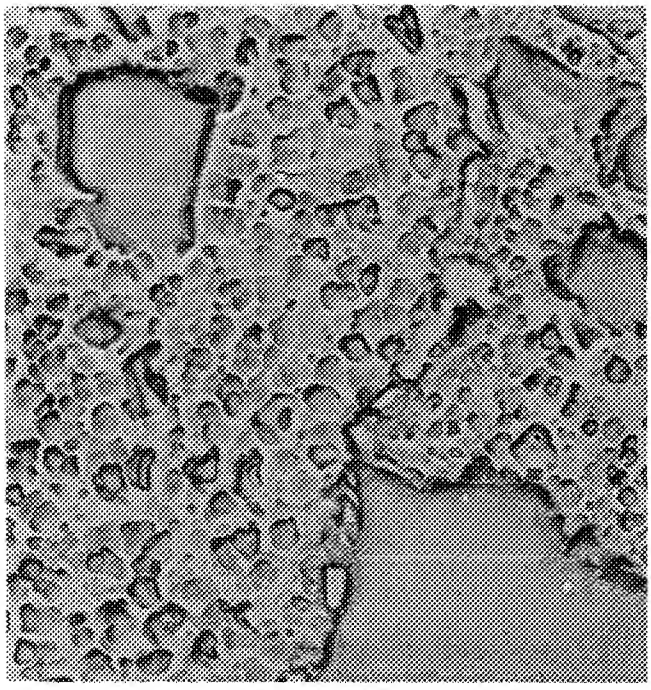

20,000X

FD 193467

Figure 6. Optical Microstructure and Transmission Electron Micrographs of Alloy 1, HIP MERL 76

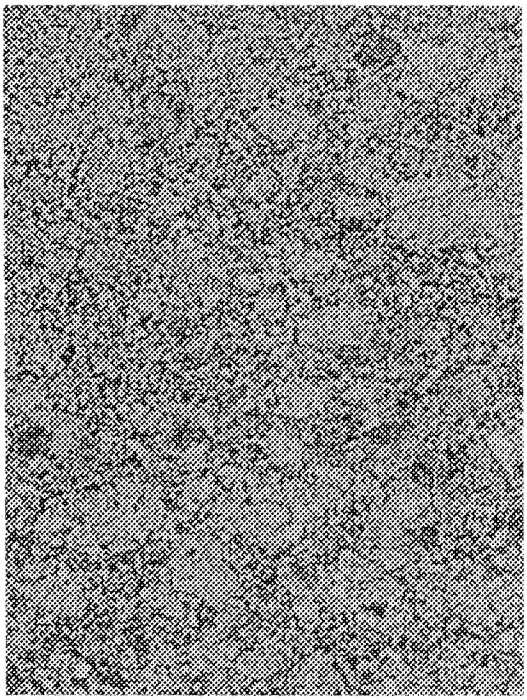

100X

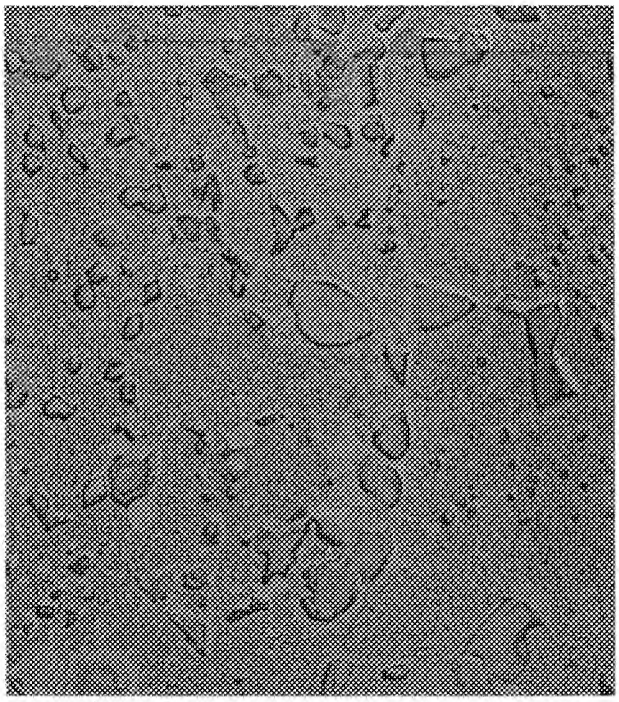

3,000X

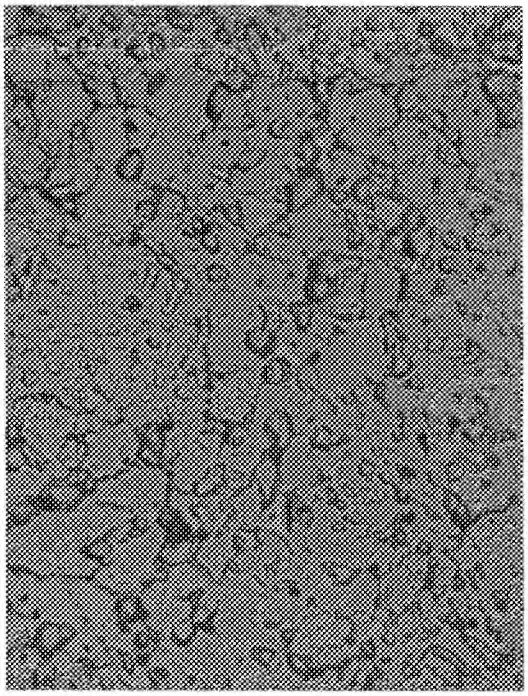

1,000X

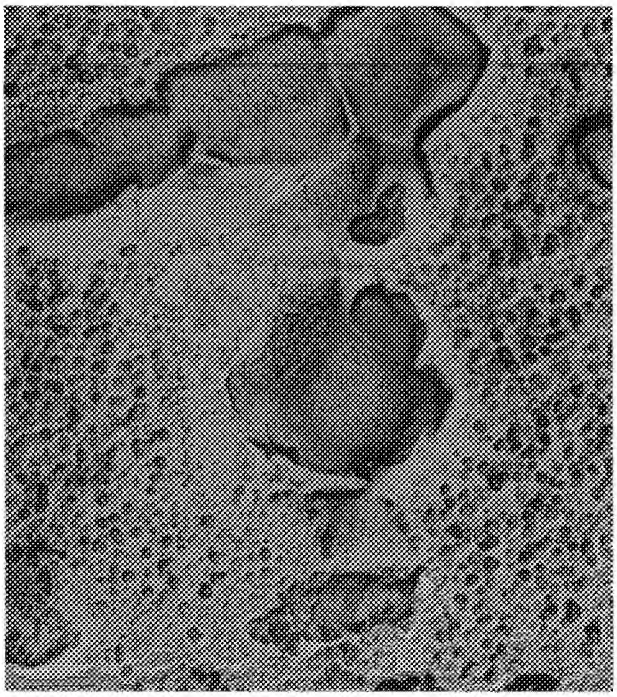

20,000X

FD 193468

Figure 7. Optical Microstructure and Transmission Electron Micrographs of Alloy 2, HIP plus Forged René 95

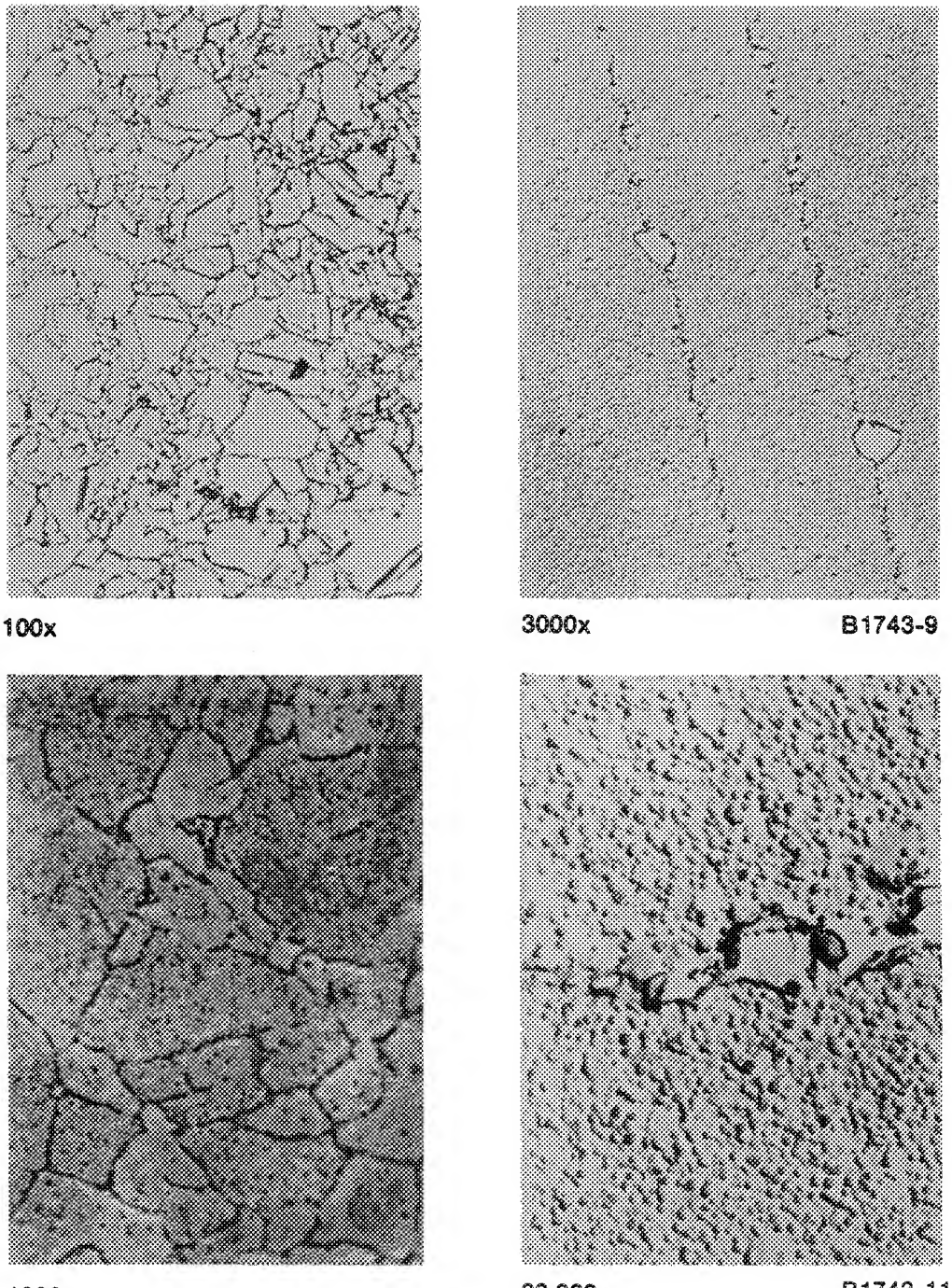

Figure 8. Optical Microstructure and Transmission Electron Micrographs of Alloy 3, Waspaloy

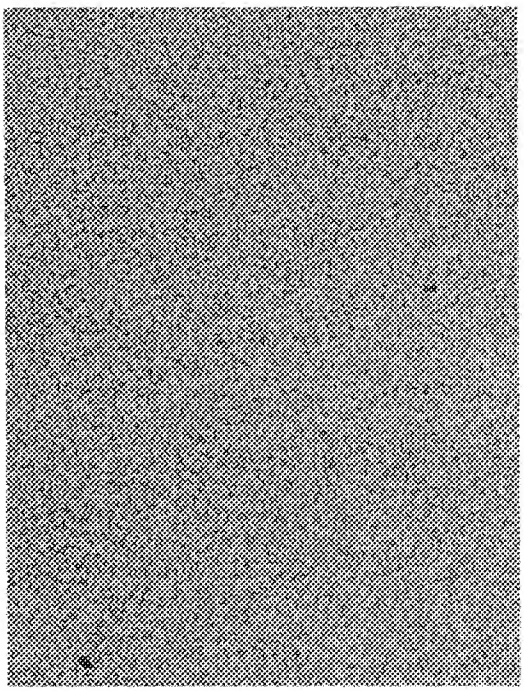

100X

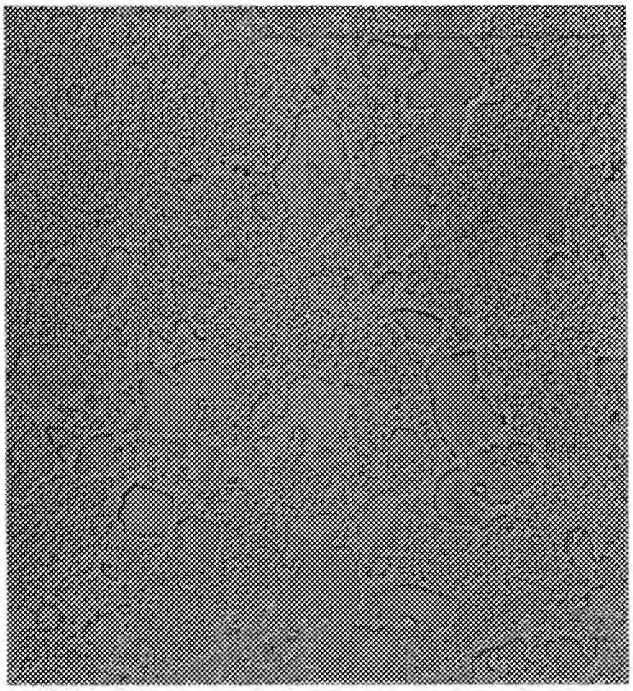

3,000X

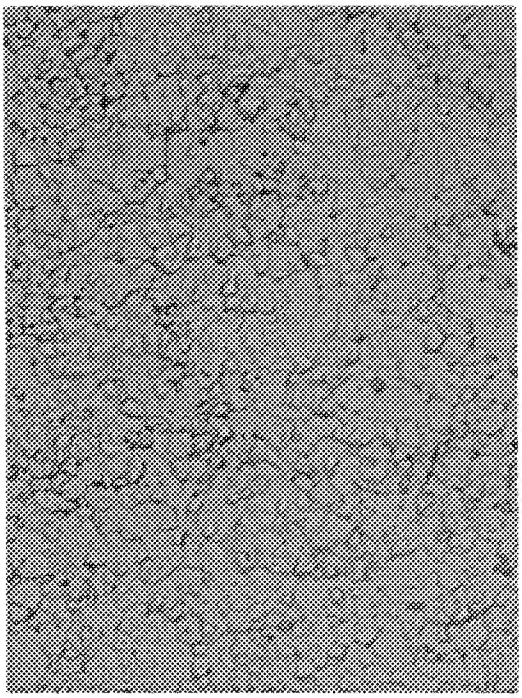

1,000X

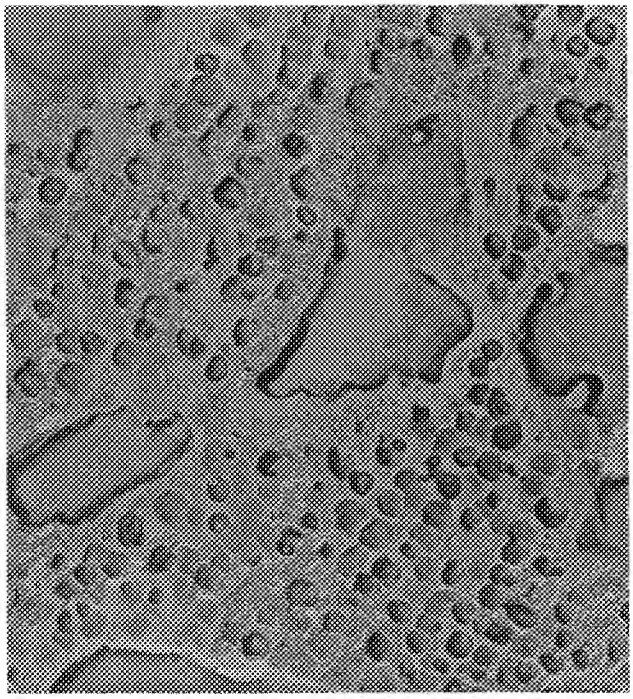

20,000X

FD 193469

Figure 9. Optical Microstructure and Transmission Electron Micrographs of Alloy 4, GATORIZED® IN 100

EVALUATION OF FATIGUE AND CYCLIC CRACK GROWTH

General

Strain control LCF and load-controlled crack growth tests characterized the cyclic behavior of the alloys under both cyclic and cyclic/dwell conditions. All testing was performed under isothermal conditions at 650°C (1200°F) which represents a typical operating temperature for the fracture critical areas of an advanced engine turbine disk. The cyclic tests were performed at a frequency of 0.33 Hz (20 cpm). Hold time per cycle for the cyclic/dwell tests was 900 sec (15 min) at maximum tensile strain for the LCF tests and at maximum tensile load for the crack growth tests. In addition, strain control LCF tests were conducted at other mean stresses, mean strains, variable cyclic hold times, and hold modes (stress hold vs strain hold) to determine the corresponding effects on LCF life. The latter two additional testing types are discussed later in this report under Creep-Fatigue Evaluations. Further crack growth tests were run in an inert atmosphere (argon) to measure the effects of oxidation on cyclic crack growth rates.

The experimental results provided data to directly compare the cyclic behavior of the four alloys tested herein and to make additional comparisons with the alloys tested under the previous NASA contracts NAS3-20367 and NAS3-20368 (reported in NASA CR-159409[1] and CR-159433,[2] respectively).

Strain Control LCF Testing

Currently, there are no industry-wide accepted ASTM procedures for strain control LCF testing at elevated temperatures. The techniques for data generation and analysis used in the program appear in the following paragraphs.

Testing Methods

Specimen

The specimen used in this program appears in figure 10 and the specimen print is shown in figure 11. Four basic requirements guided specimen design and development: (1) strain distribution be known over the gage section, (2) axial strain be accurately measurable, (3) minimum strain concentrations exist, and (4) failure location be in the gage section. Additional requirements included ease of installation and simplification of calculations necessary to establish machine operating parameters.

The specimen configuration, which includes integral machined extensometer collars, was determined experimentally using photoelastic and elastic/plastic strain analyses. A calibration procedure was established to relate the maximum strain to collar deflection during both the elastic and plastic portions of the strain cycle. Subsequently, finite-element and mathematical model analyses analytically verified the specimen design and calibration procedures.[3]

All test specimens were visually examined prior to testing in normal light and with fluorescent penetrant to screen for machining anomalies or surface discontinuities. Additionally, randomly selected samples underwent thorough dimensional inspection to ensure conformance to print requirements.

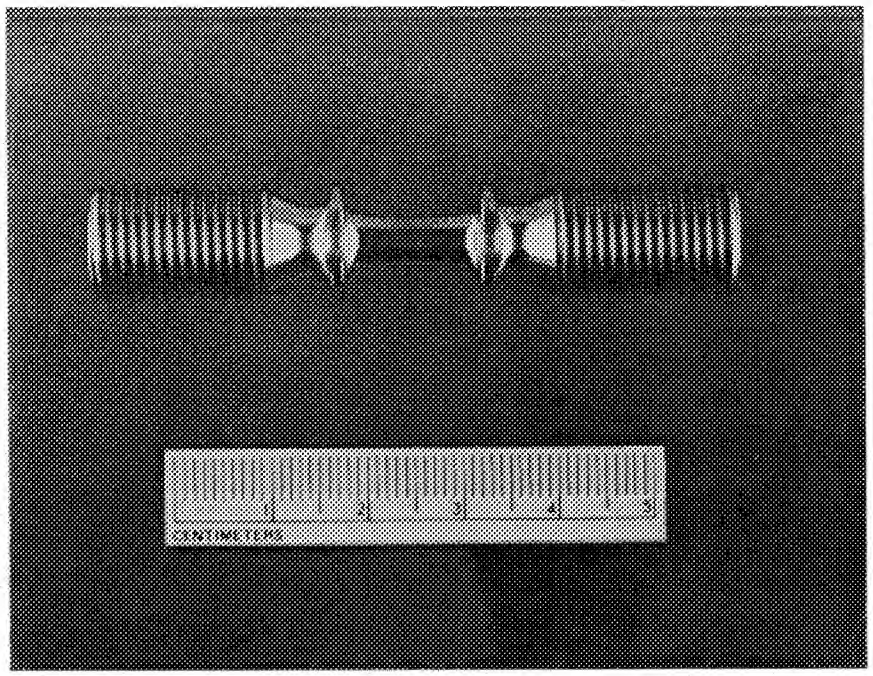

FE 169457

Figure 10. Strain Control LCF Specimen

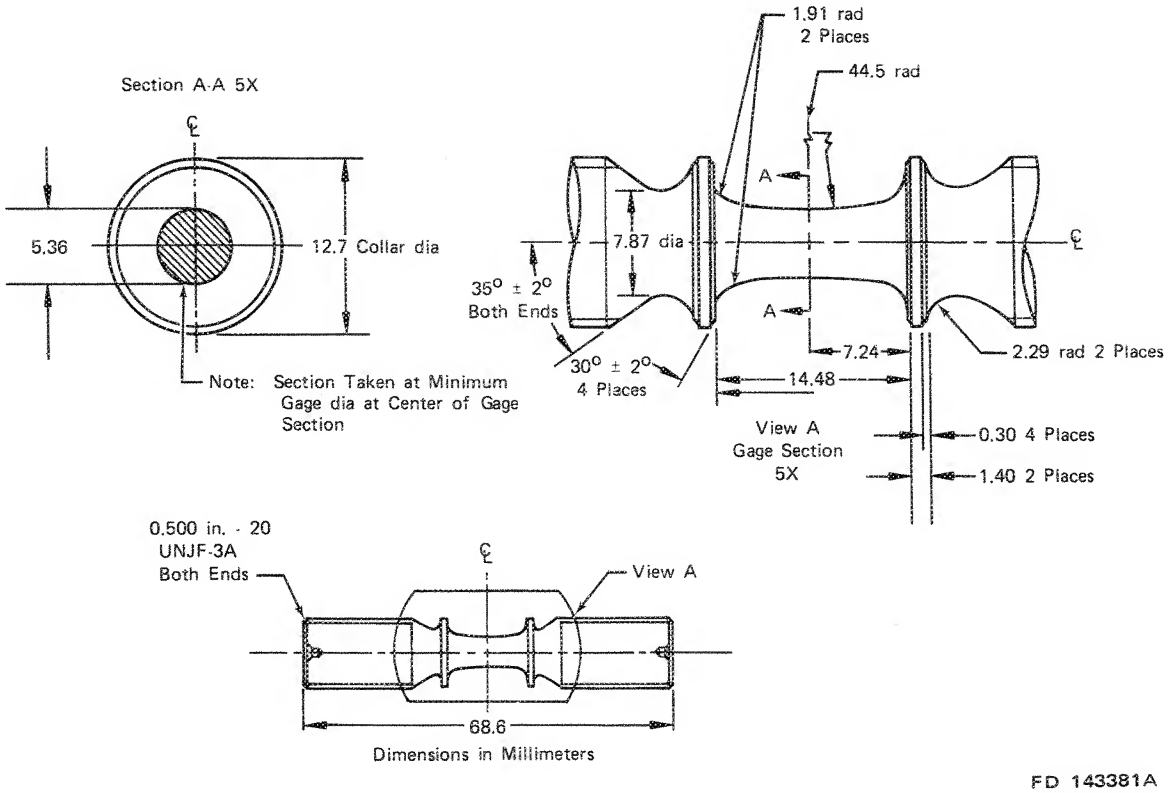

Figure 11. Strain Control LCF Specimen Details

Testing Procedures

All testing machines were controlled under a system of calibration and preventative maintenance schedules. System accuracies are within 2%. Approved calibration procedures, records, and National Bureau of Standards (NBS) traceability were retained for all test equipment from which data were obtained.

Isothermal strain control LCF characteristics were determined for this program using servohydraulic, closed-loop-on-axial strain LCF testing machines designed and built at P&WA/Florida. A typical test machine with controls and readout instrumentation is shown in figure 12.

Specimen axial strain was measured and controlled by means of a proximity probe extensometer. Split extensometer heads were attached to the specimen by mating the grooves in the heads with the integral collars on the specimen and bolting the assembly together. Collar deflection is measured and controlled via proximity probes. Load measurement is obtained by a commercial tension-compression load cell.

An x-y recorder was used for recording load vs strain plots at predetermined cyclic intervals during testing. The recorder was calibrated with the extensometer so that the ratio of specimen collar deflection to x-y recorder pen movement in the "x" direction was known. The "y" axis of the x-y recorder was calibrated with the load cell so the ratio of specimen load to x-y recorder "y" axis pen movement was known.

The strain control LCF tests were conducted at constant total strain ranges to establish cycles to failure generally in the 10^2 to 10^5 cycle life range.

The cyclic tests utilized a triangular strain-time waveform at a frequency of 0.33 Hz (20 cpm) with either a mean strain equal to zero (completely reversed strain cycle, $R_\epsilon = -1$), as shown in figure 13, or a mean strain equal to one-half the maximum strain (all-tensile strain cycle, $R_\epsilon = 0$), as shown in figure 14.

The cyclic/dwell test utilized the same ramp frequency and mean strains as the nondwell tests, but incorporated a hold time of 900 sec (15 min) at the maximum tensile strain. A typical dwell test waveform for the mean strain of zero case is shown in figure 15. Figure 16 details the all-tensile strain case.

All specimens were cycled to failure in the strain-controlled test mode with load-strain hysteresis plots obtained at intervals throughout the life of the specimen.

The number of cycles to complete specimen separation (N_f), and the number of cycles to produce a 5% drop in the cyclic load range (N_5) were determined for each test. The change in specimen compliance causing the drop in cyclic load range was used as an indicator for crack initiation.

The total strain and the elastic, inelastic, and creep strain components were determined at the specimen half-life ($N_{f/2}$) from the hysteresis plots taken during each test. The strain components are described and presented in figures 13 through 16.

All tests were conducted in air at 650°C (1200°F). Temperature was controlled uniformly over the specimen gage section using calibrated thermocouple and temperature readout and control instrumentation.

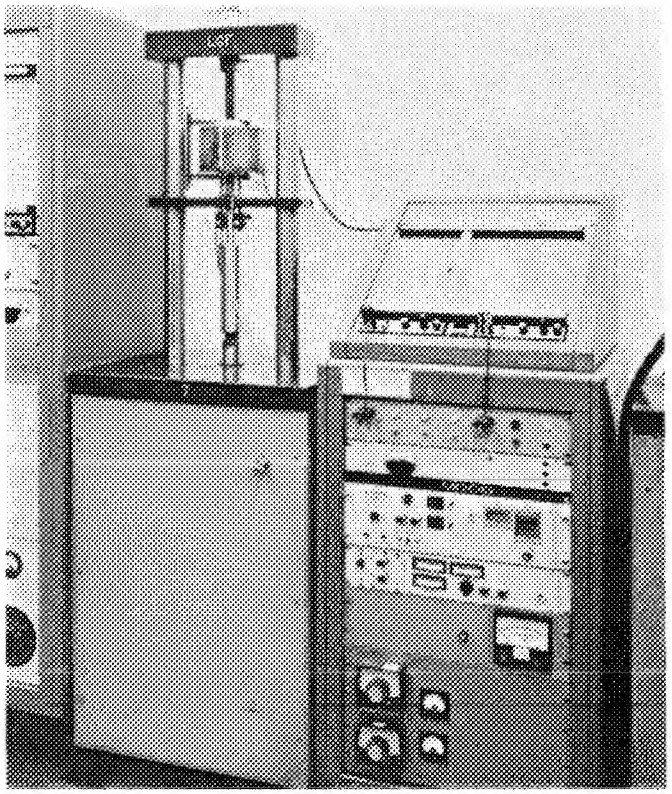

FC 39397

Figure 12. Servohydraulic Closed-Loop LCF Test Machine

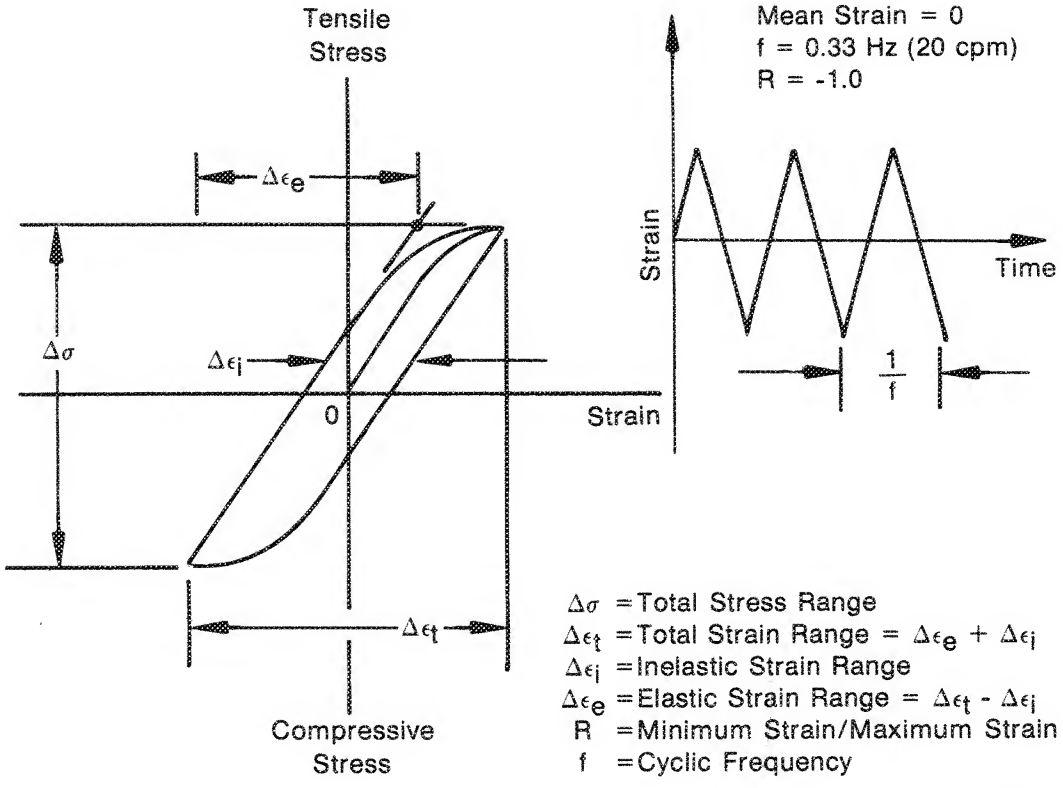

FD 135463B

Figure 13. Typical Cyclic (Nondwell) LCF Cycle, R_ϵ = -1

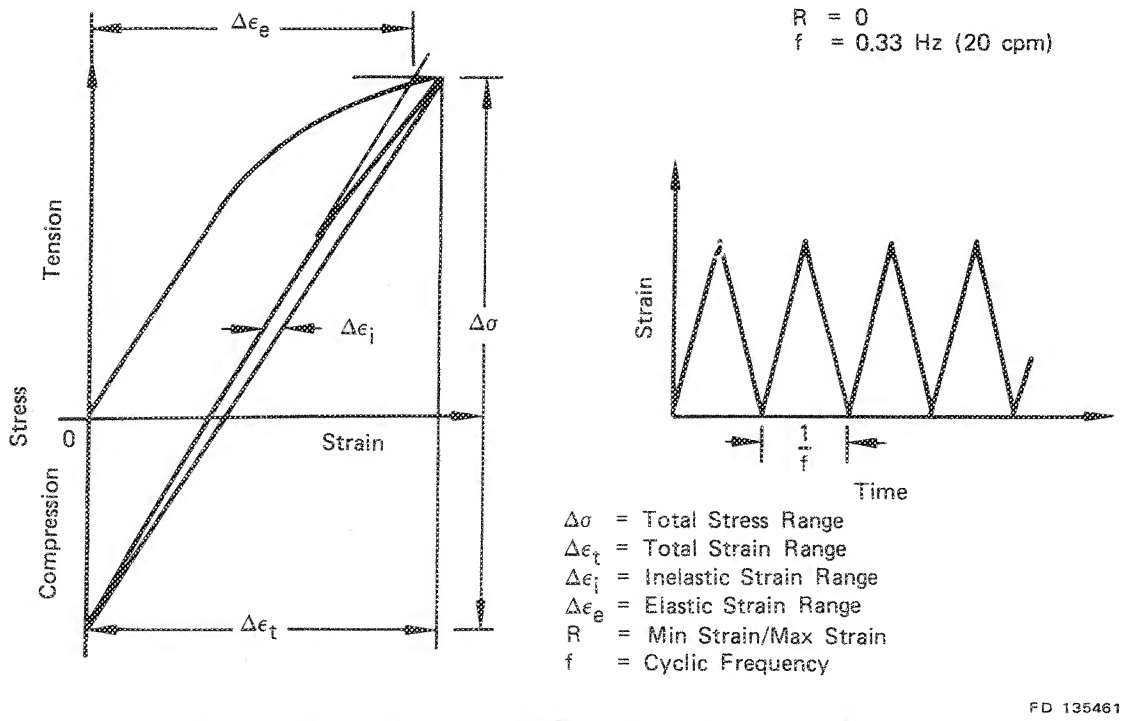

Figure 14. Typical Cyclic (Nondwell) LCF Cycle, R_ϵ = 0

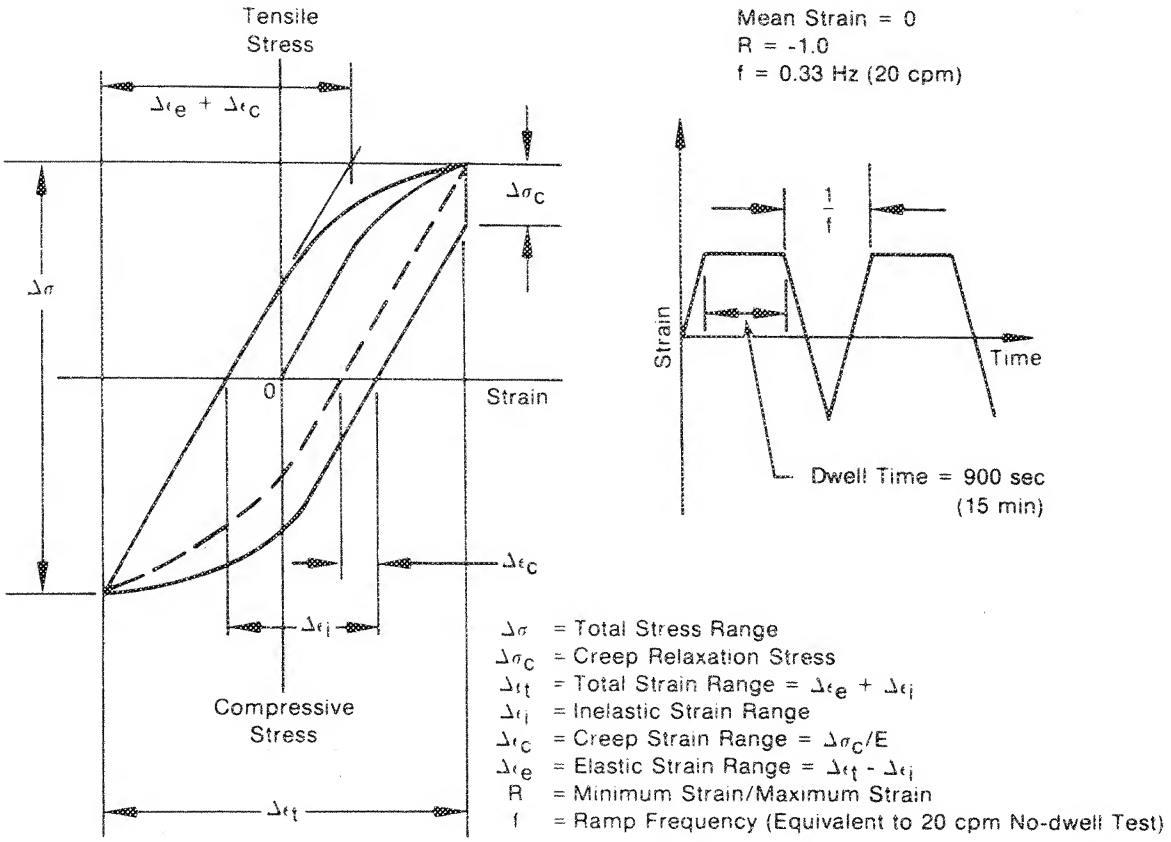

Figure 15. Typical Strain-Dwell LCF Test with R_ϵ = -1

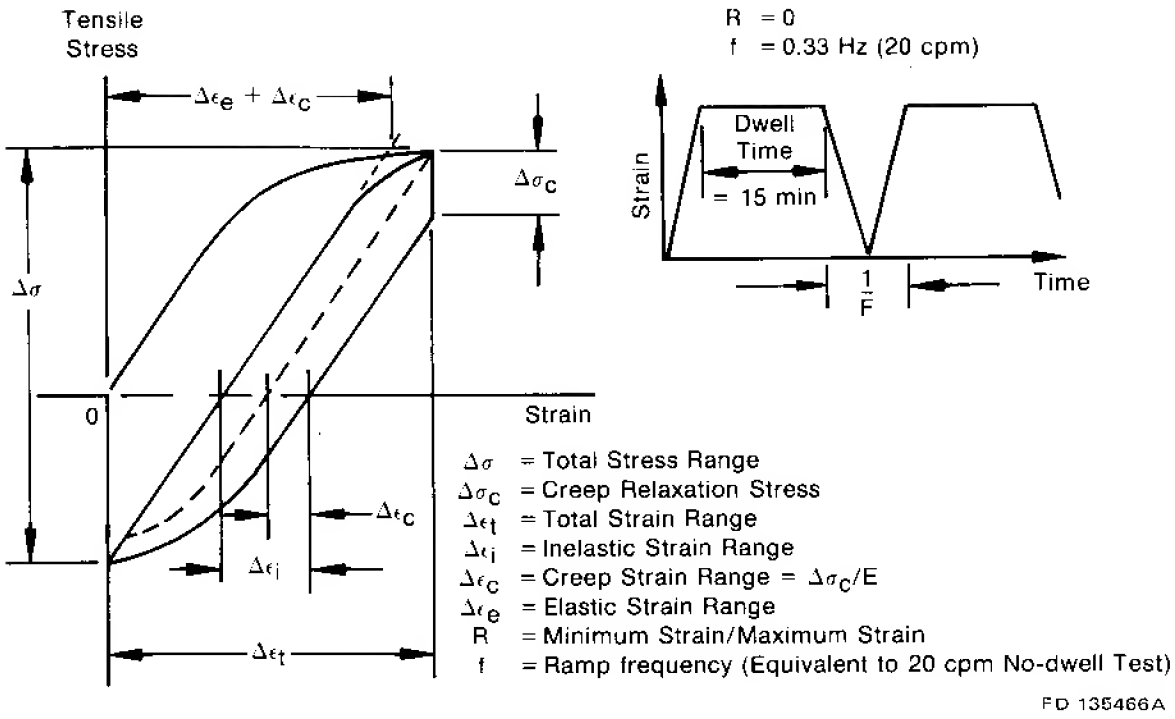

Figure 16. Typical Strain-Dwell LCF Test with $R_\epsilon = 0$

Low-Cycle Fatigue Test Results

A minimum of six cyclic tests and four cyclic/dwell tests were performed on each of the four turbine disk alloys involved in this contract. In addition, supplemental tests were conducted to investigate heat-to-heat or forging-to-forging LCF property variations in certain alloys, effects of high strain range on LCF life for several alloys tested in earlier contract work (NAS3-20367), and the effects of mean strain (strain R ratio) and mean stress of fatigue life.

Stress range and mean stress vs cycles for each test were determined from hysteresis plots generated periodically during the test. The data were analyzed by computer to estimate cycles to 5% stress range drop (N_5 life) and then the results were plotted. The 5% stress range drop occurred approximately within the last 10% of the total cyclic life for the majority of the tests. Typical stress-strain hysteresis loops at the specimen half-life ($N_f/2$) were recorded and are presented herein for all tests. Total strain range vs cycles to 5% stress range drop (N_5 life) and cycles to complete separation (N_f) are presented for each alloy. Each figure includes a strain range vs mean life regression curve.

The regression model used for the cyclic (0.33 Hz, 20 cpm) tests is a composite exponential function of the form $Y = AN^B + CN^D + E$, which relates total strain range (Y) to cyclic life (N). The inelastic strain component in this model is the AN^B term, and the elastic strain component consists of the $CN^D + E$ terms. The inelastic strain was statistically regressed as a log-linear (straight line on log-log paper) function ($Y_I = AN^B$). The elastic strain had the best statistically regressed curve fit as a nonlinear log (curved line on log-log paper) function ($Y_E = CN^D + E$).

The regression model used for the dwell (900-sec hold at max tensile strain) tests is a composite exponential function of the form $Y = AN^B + CN^D$, which relates total strain (Y) to cyclic life (N). The inelastic strain component in this model is the AB^N term, and the elastic strain component is the CN^D term. The inelastic strain was statistically regressed as a log-linear function ($Y_I = AB^N$). The elastic strain was also statistically regressed as a log-linear function ($Y_E = CN^D$) due to the limited quantity of dwell LCF test data.

Inelastic strain range data for all alloys has been adjusted to conform to the following reporting system:

If measured $\Delta\epsilon_i$ was:	*Then reported $\Delta\epsilon_i$ was:*
$\Delta\epsilon_i < 0.00005$	<0.0001
$0.00005 \leq \Delta\epsilon_i \leq 0.00008$	≤0.0001
$0.00008 < \Delta\epsilon_i < 0.00015$	0.0001

Required use of this system stemmed from the relative inaccuracies of the inelastic strain data on this order of magnitude and the significant effect that these data could exhibit on the linear regressions of inelastic strain. Inelastic strain range data less than 0.0001 was estimated based on plots of stress range vs inelastic strain constructed from test results with measurable inelastic strains, and was used for regression analyses.

The methodology of summing independent log-linear (or nonlinear) regressions of the elastic and inelastic strain components ($Y = Y_I + Y_E$ where Y = total strain, Y_I = inelastic strain, and Y_E = elastic strain) has been used with excellent agreement with the actual total strain data generated in this program. Figure 17 illustrates this method of component strain summation.

Fully Reversed LCF Tests (Mean Strain = 0, R_ϵ = -1)

Fully reversed strain cycle LCF tests were run for fully HIP'd MERL 76 and HIP plus forged René 95. These tests produced typical hysteresis loops and strain-time waveforms, as shown in figures 13 and 15. The following discussion details the test results achieved with each of the four alloys.

HIP MERL 76

Six cyclic tests (0.33 Hz) and five cyclic/dwell tests were completed with a fully reversed strain cycle. The dwell tests utilized a 900 sec hold time at maximum tensile strain. Three additional tests were conducted with an all-tensile strain cycle. (See Supplementary discussion.) Table 9 presents the test data.

Stress range and mean stress vs life plots are shown in figures 18 and 20 for the cyclic tests and figures 19 and 21 for the cyclic/dwell tests. Typical stress-strain hysteresis loops at the specimen half-lives for the cyclic and dwell tests are presented in figures 22 and 23.

Strain range vs life curves are presented in figures 24 and 25. These figures indicate that the 900 sec dwell reduces the fatigue life by a factor between 2 and 5, depending on total strain range. The stress range vs inelastic strain range relationship for the cyclic tests is presented in figure 26.

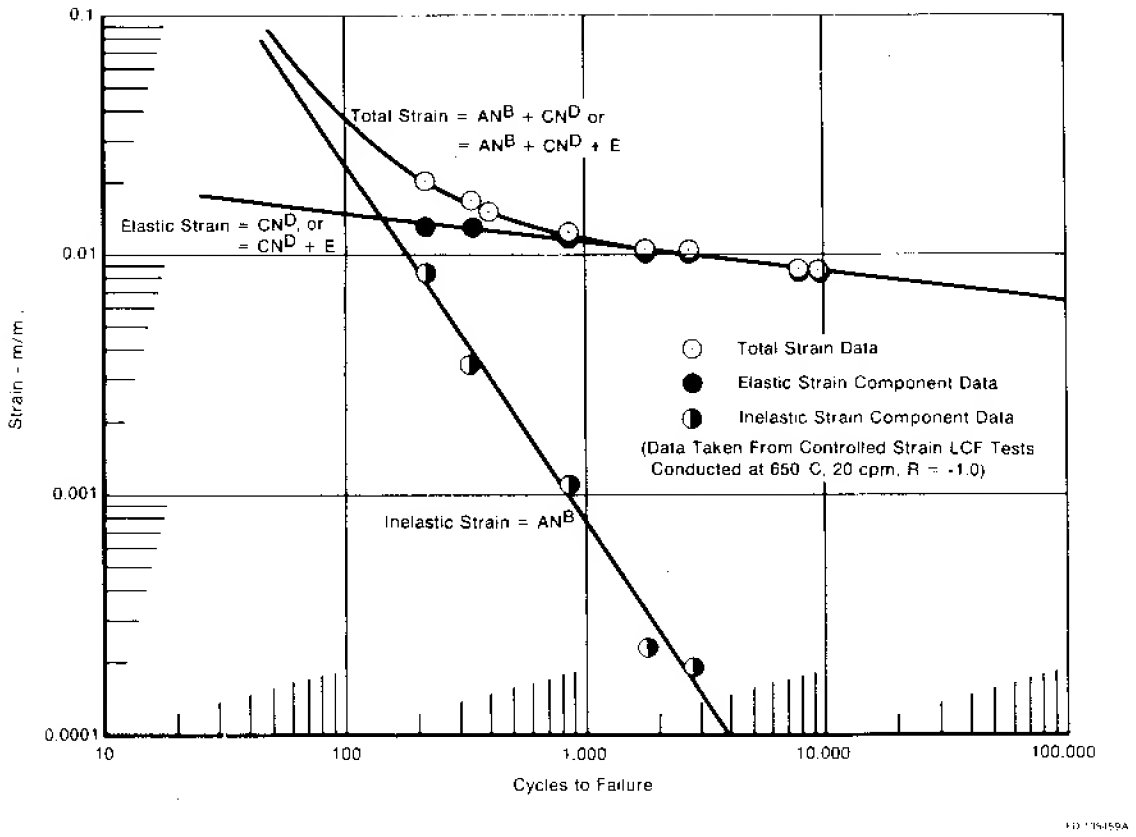

Figure 17. Composite Experimental Fatigue Life Model Using Summation of Elastic and Inelastic Strain Components

TABLE 9
CONTROLLED STRAIN LOW CYCLE FATIGUE RESULTS FOR HIP MERL 76
Testing Conducted at 650°C (1200°F) in Air

Spec S/N	Type* Test	Strain R Ratio (min/max)	Strain (m/m at $N_f/2$)				Mean Stress at $N_f/2$		Stress Range		Cyclic Stability	Cycles to Failure	
			Range	Elastic	Inelastic	Creep	MPa	ksi	Cycle 1	$N_f/2$		$N_5\%$	N_f
D-2	Cyclic	-1	0.0184	0.0158	0.0026	0	-45	-6.5	2431 MPa (352.6 ksi)	2634 MPa (382.2 ksi)	Hardens	240	271
D-7	Cyclic	-1	0.0151	0.0145	0.0006	0	-30	-4.4	2241 MPa (325.1 ksi)	2342 MPa (339.7 ksi)	Hardens	701	718
D-3	Cyclic	-1	0.0119	0.0118	0.0001	0	-60	-8.7	1985 MPa (287.9 ksi)	1995 MPa (289.4 ksi)	Stable	1,827	1,991
D-10	Cyclic	-1	0.0109	0.0108	≤0.0001	0	-15	-2.1	1817 MPa (263.6 ksi)	1798 MPa (260.7 ksi)	Stable	6,764	7,087
D-8	Cyclic	-1	0.0100	0.0099	<0.0001	0	15	2.1	1675 MPa (242.9 ksi)	1679 MPa (243.6 ksi)	Stable	26,521	28,117**
D-9	Cyclic	-1	0.0091	0.0091	<0.0001	0	25	3.6	1537 MPa (222.9 ksi)	1542 MPa (223.6 ksi)	Stable	120,817	124,323**
F-5	Cyclic	0	0.0117	0.0115	0.0002	0	194	28.2	1908 MPa (276.7 ksi)	1948 MPa (282.5 ksi)	Slight Hardening	1,567	1,714
F-1	Cyclic	0	0.0098	0.0098	<0.0001	0	212	30.7	1670 MPa (242.1 ksi)	1675 MPa (242.9 ksi)	Stable	3,925	4,152
F-6	Cyclic	0	0.0078	0.0078	<0.0001	0	354	51.3	1285 MPa (186.4 ksi)	1290 MPa (187.1 ksi)	Stable	20,465	24,645**
F-8	Cyclic/Dwell	-1	0.0152	0.0131	0.0021	0.0006	-113	-16.4	2270 MPa (329.3 ksi)	2339 MPa (339.3 ksi)	Hardens	237	264
F-9	Cyclic/Dwell	-1	0.0126	0.0118	0.0008	0.0003	-79	-11.4	2019 MPa (292.9 ksi)	2049 MPa (297.1 ksi)	Stable	799	815
F-4	Cyclic/Dwell	-1	0.0115	0.0109	0.0006	0.0002	-30	-4.3	1798 MPa (260.8 ksi)	1818 MPa (263.7 ksi)	Stable	1,370	1,394
F-7	Cyclic/Dwell	-1	0.0106	0.0102	0.0004	0.0002	5	0.7	1694 MPa (245.7 ksi)	1689 MPa (244.9 ksi)	Stable	1,833	2,065
F-11	Cyclic/Dwell	-1	0.0102	0.0099	0.0003	0.0001	-70	-10.1	1654 MPa (239.9 ksi)	1659 MPa (240.6 ksi)	Stable	—	2,861***

*— Cyclic tests conducted at 0.33 Hz (20 cpm)

Cyclic/Dwell tests have a 900 sec (15 min) hold time at the maximum tensile strain. Ramp frequency is the same as the cyclic tests.

**— Failure initiated at an internal inclusion

***— Premature failure due to electrical power outage.

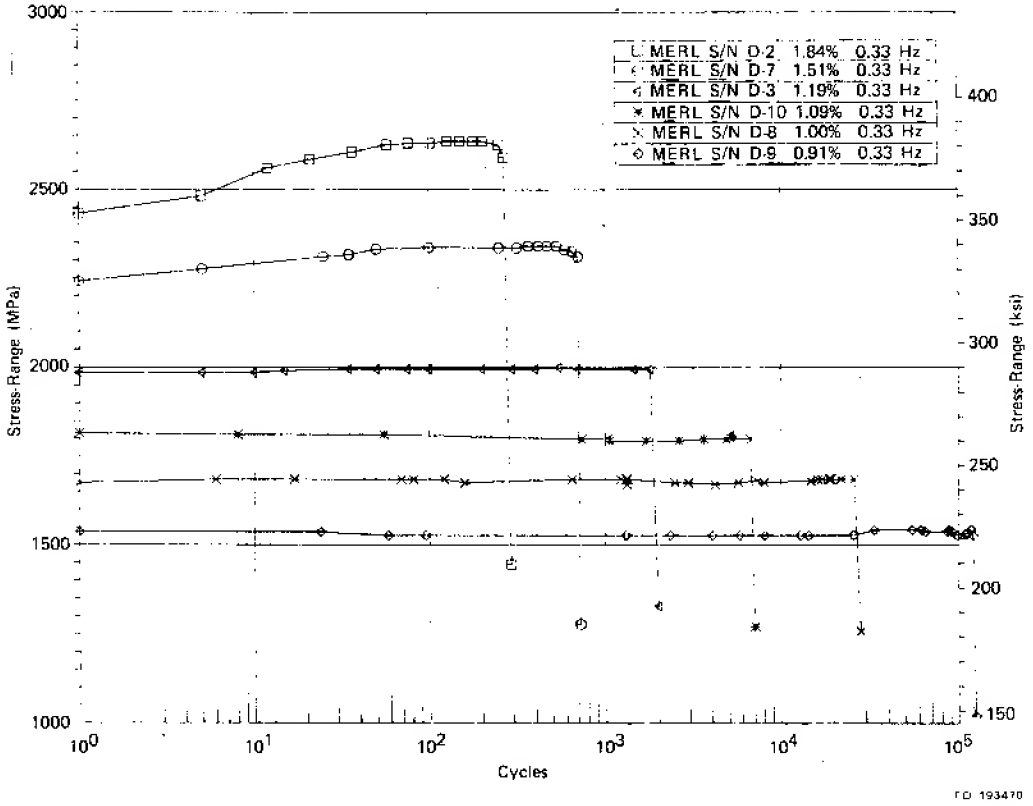

Figure 18 Stress Range vs Cycles for HIP MERL 76 (0.33 Hz, R_ϵ = -1)

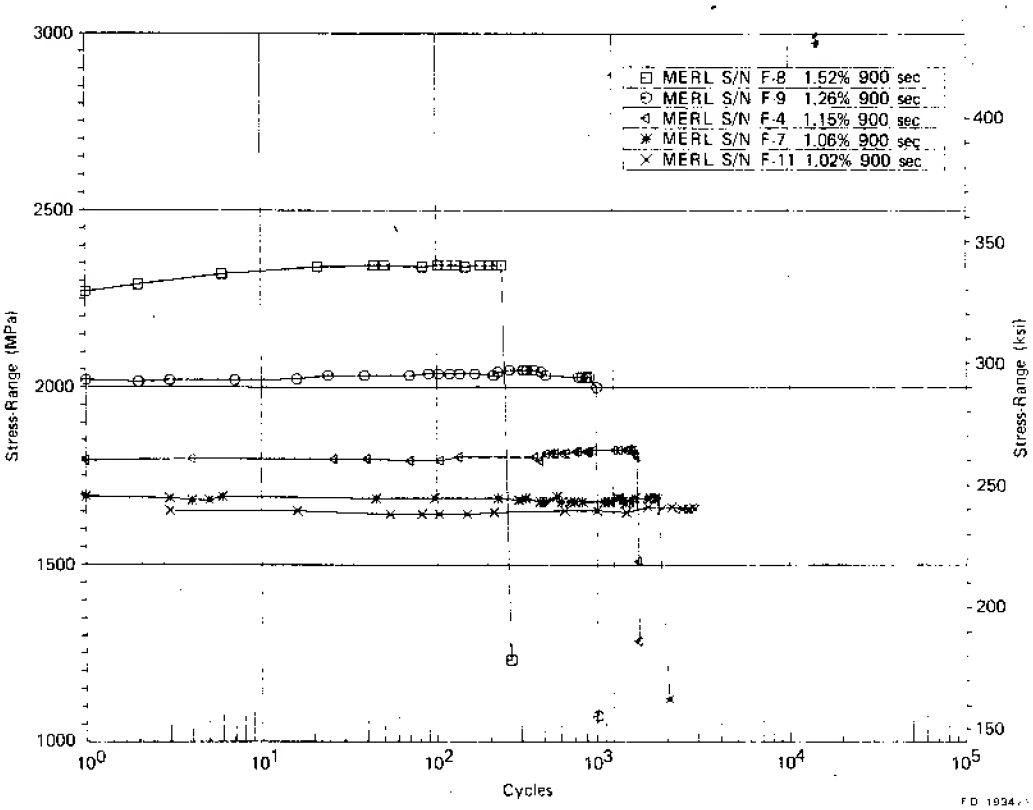

Figure 19. Stress Range vs Cycles for HIP MERL 76 (900-sec Dwell, R_ϵ = -1)

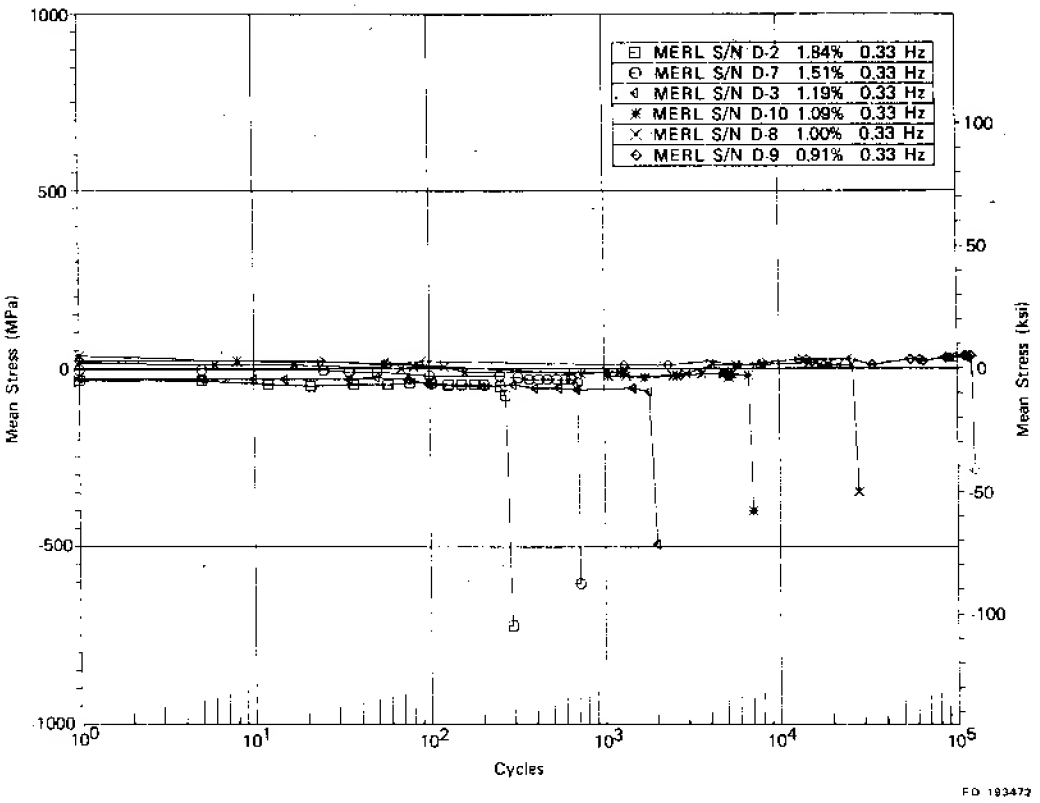

Figure 20. Mean Stress vs Cycles for HIP MERL 76 (0.33 Hz, R_ϵ = -1)

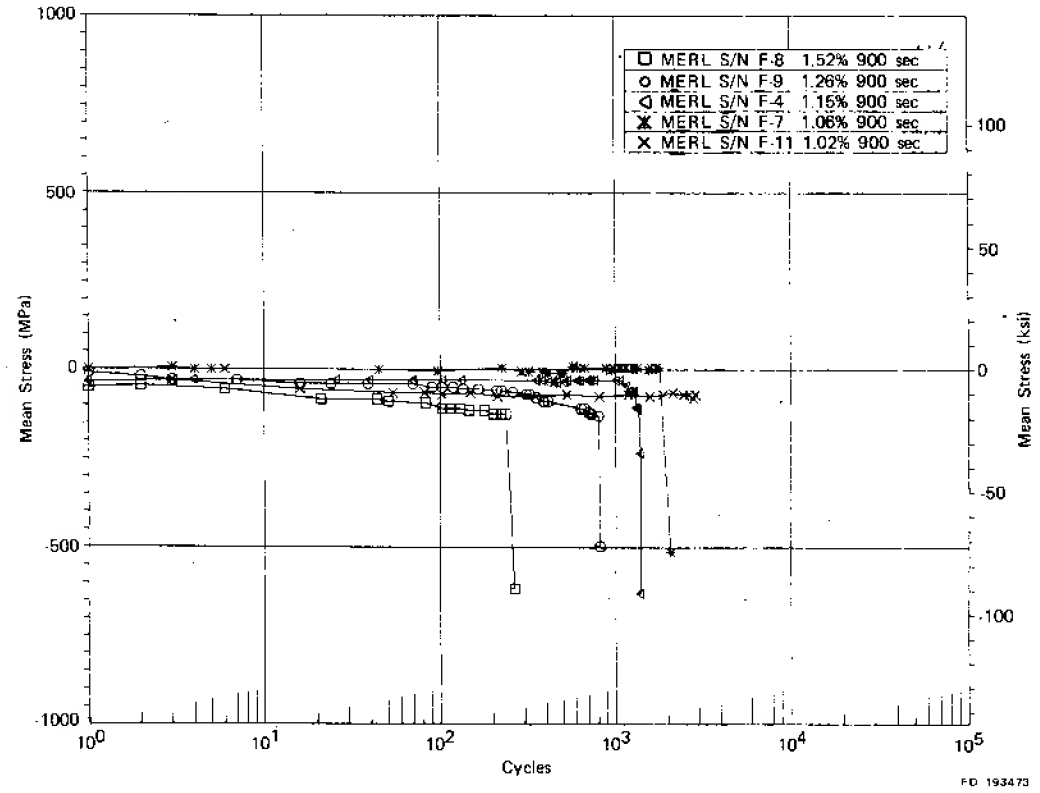

Figure 21. Mean Stress vs Cycles for HIP MERL 76 (900-sec Dwell, R_ϵ = -1)

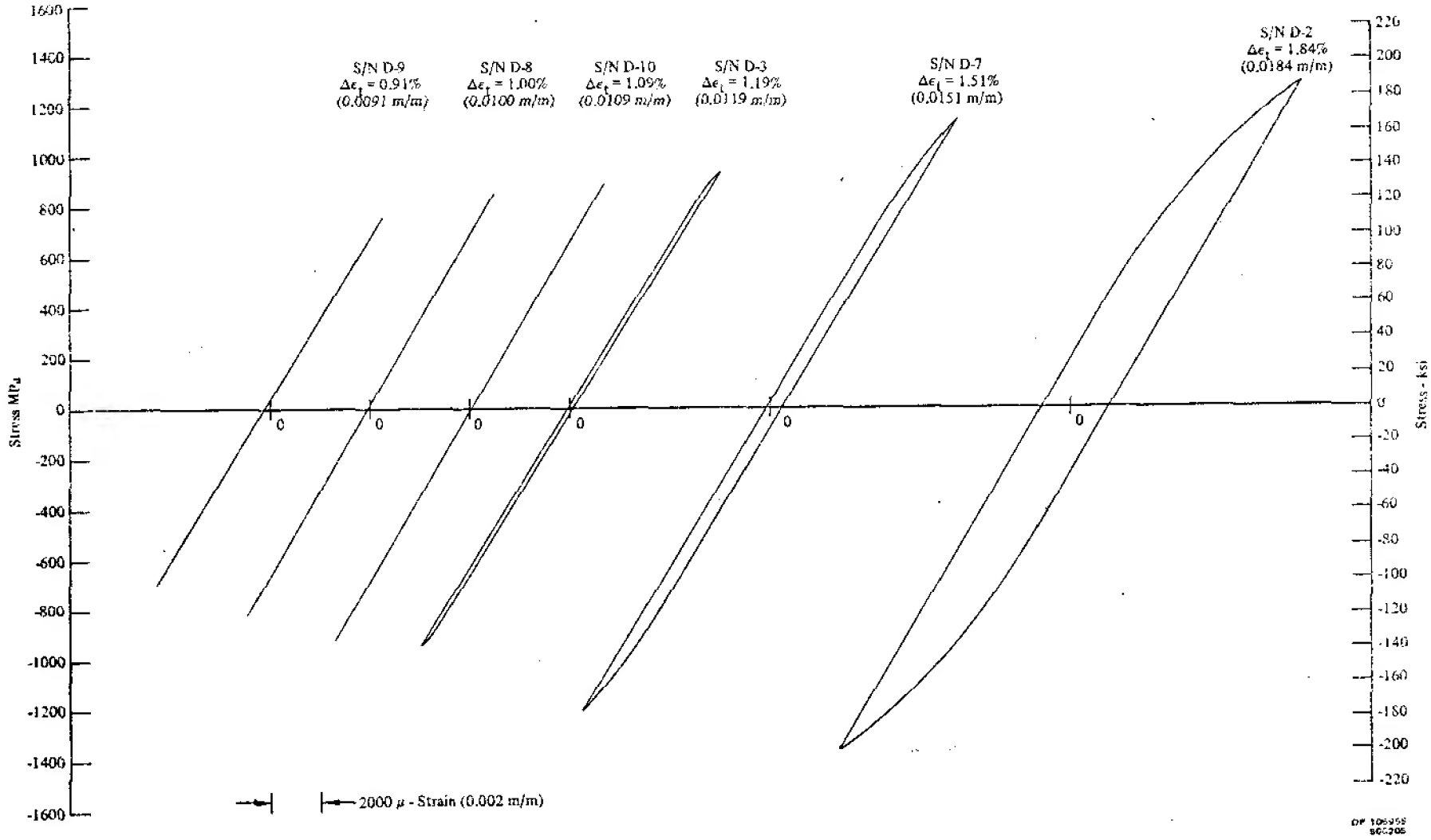

Figure 22. Typical Hysteresis Loops, HIP MERL 76 Cyclic Tests

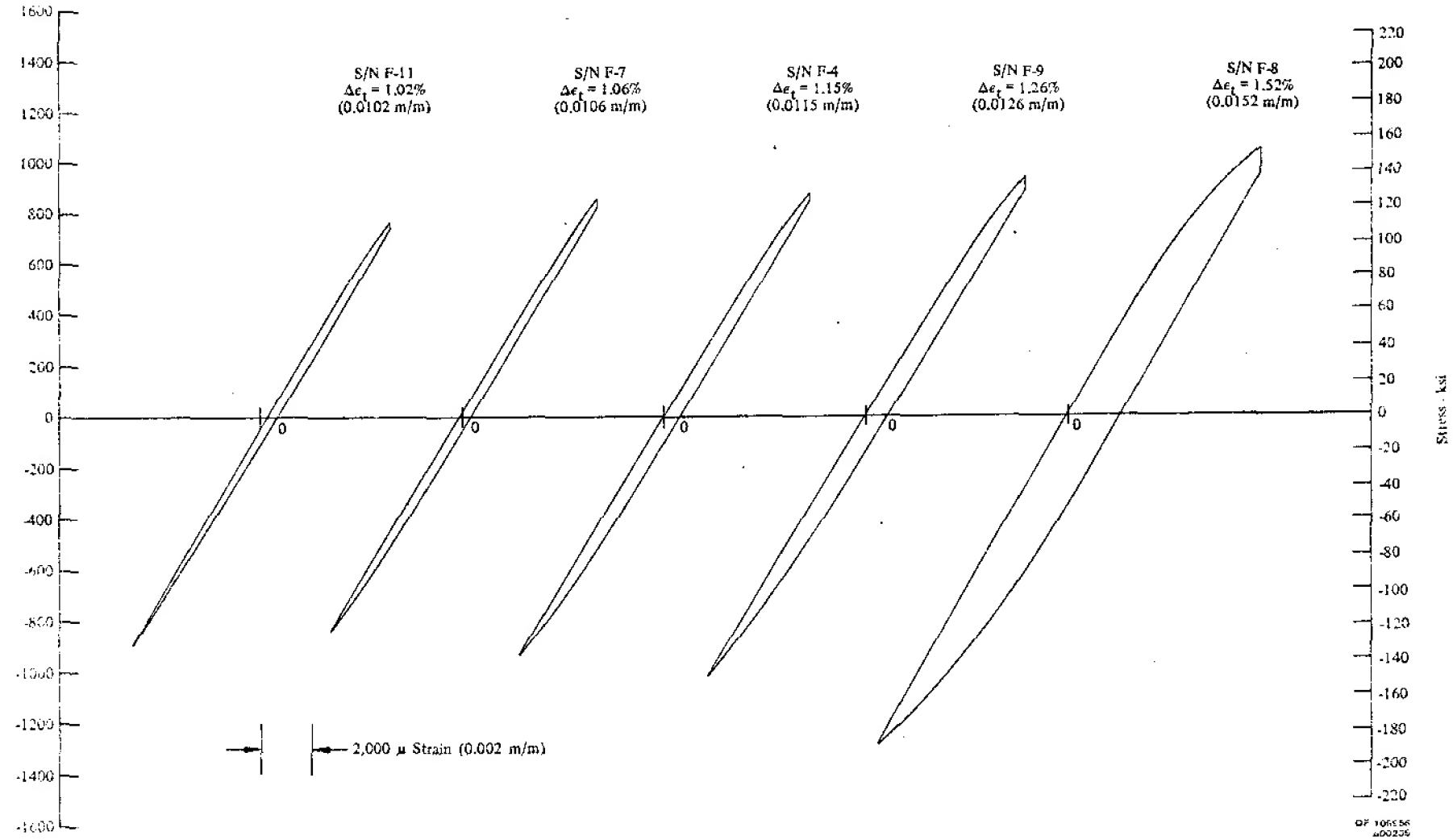

Figure 23. Typical Hysteresis Loops, HIP MERL 76 Dwell Tests

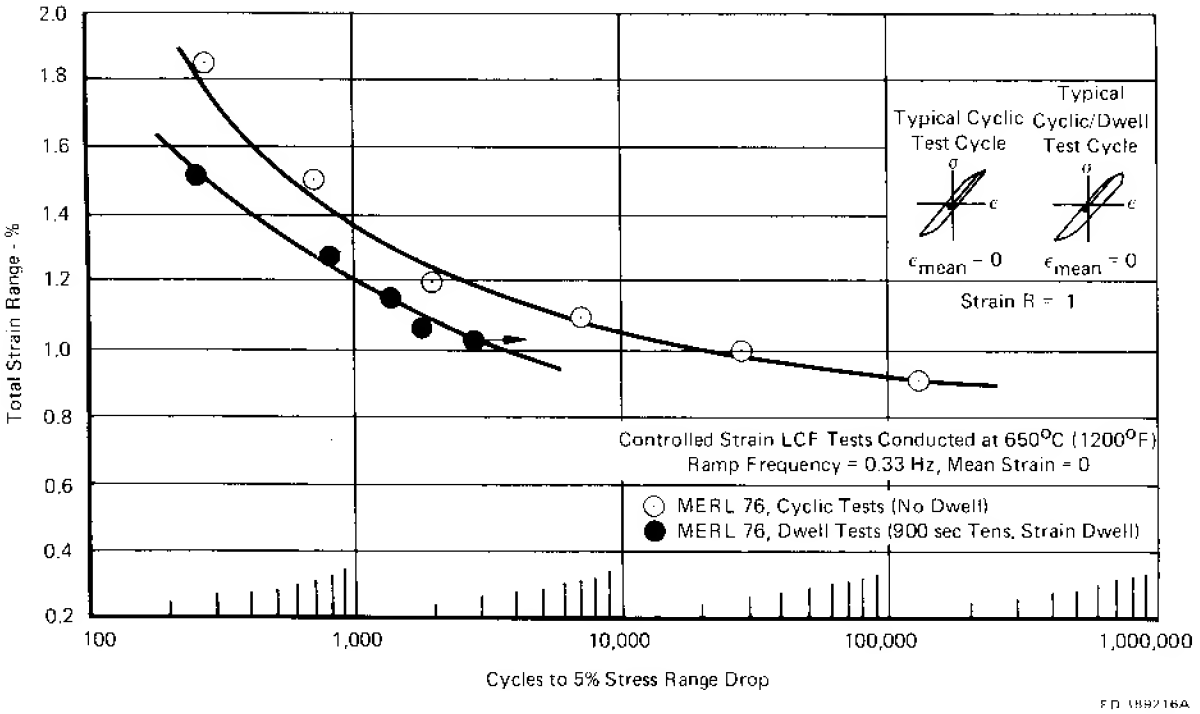

Figure 24. Strain Control LCF Results for HIP MERL 76 (N_5 Life)

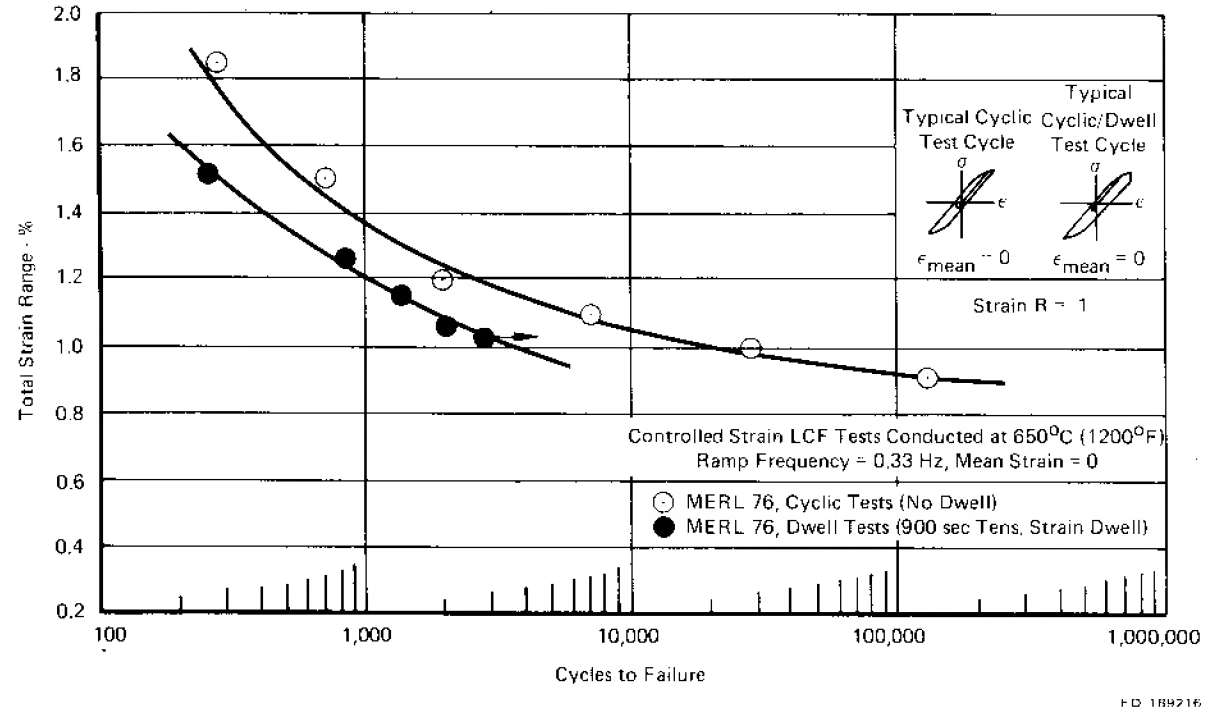

Figure 25. Strain Control LCF Results for HIP MERL 76 (Failure)

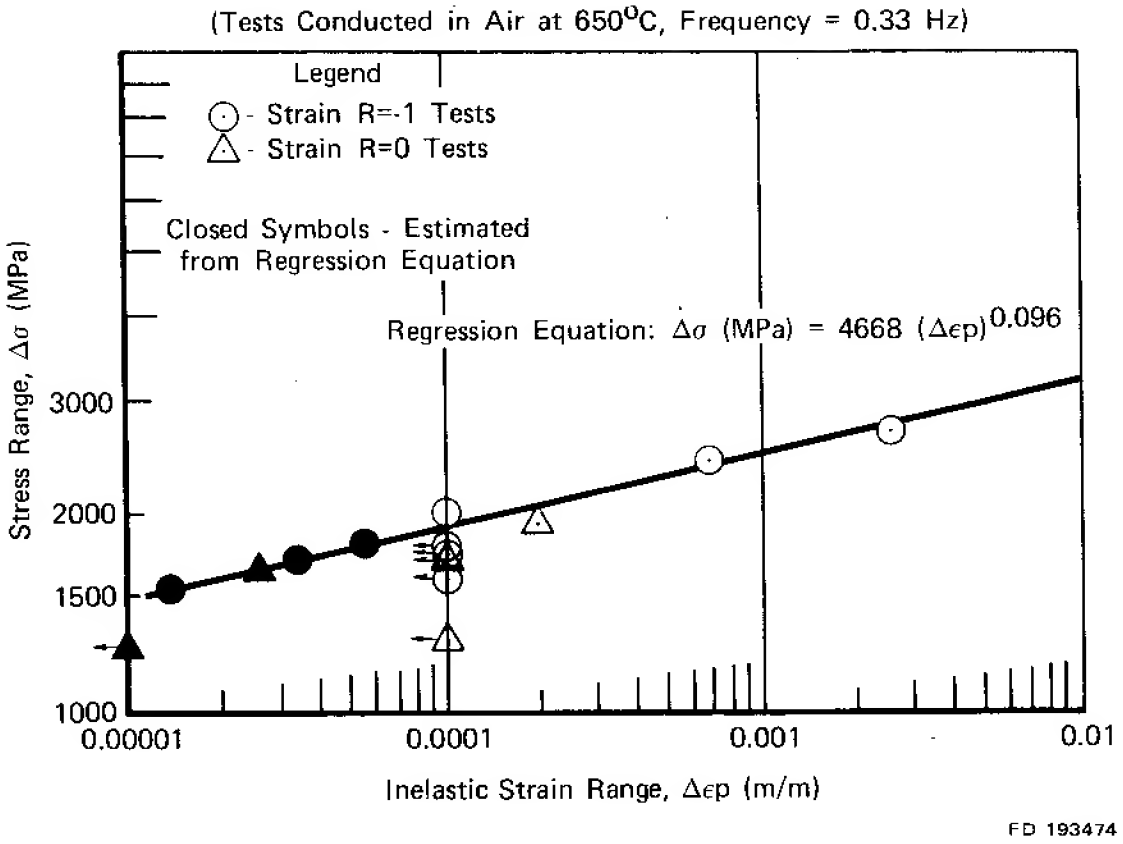

Figure 26. Stress Range vs Inelastic Strain Range for HIP MERL 76

HIP Plus Forged René 95

Seven cyclic tests (0.33 Hz) and four cyclic/dwell tests were performed for this alloy. Three additional tests were run with an all-tensile strain cycle. (See Supplementary discussion.) Data are presented in table 10.

Stress range and mean stress vs life plots are given in figures 27 through 30. Typical stress-strain hysteresis loops appear in figures 31 and 32. Strain range vs life curves are shown in figures 33 and 34.

Fatigue testing of René 95 was also conducted to compare Contractor (P&WA and GE) test results. Data from the previous NASA Contract NAS3-20368[2] with GE appears in table 11 and in figures 35 and 36. The mean curve for the cyclic P&WA data is generally parallel to the mean of the cyclic GE data, however the curves are offset with the P&WA results somewhat greater in cyclic life than the GE data. It must be noted that these curves were generated with a limited quantity of data, and that the variance in the GE data itself is of this order of magnitude.

TABLE 10
CONTROLLED STRAIN LOW-CYCLE FATIGUE RESULTS FOR TURBINE DISK ALLOY 2, HIP PLUS FORGED RENE 95 (P&WA DATA)
Testing Conducted at 650°C (1200°F)

Spec S/N	Type* Test	Strain R Ratio (min/max)	Strain (m/m at $N_f/2$)				Mean Stress at $N_f/2$		Stress Range		Cyclic Stability	Cycles to Failure	
			Range	Elastic	Inelastic	Creep	MPa	ksi	Cycle 1	$N_f/2$		N_s%	N_f
1	Cyclic	-1	0.0150	0.0131	0.0019	0	-37	-5.4	2392 MPa (346.9 ksi)	2299 MPa (333.4 ksi)	Soften	540	595
2	Cyclic	-1	0.0126	0.0119	0.0007	0	-60	-8.8	2176 MPa (315.6 ksi)	2106 MPa (305.5 ksi)	Soften	1,387	1,490
7	Cyclic	-1	0.0116	0.0112	0.0004	0	-23	-3.4	1998 MPa (289.8 ksi)	1951 MPa (283.0 ksi)	Slight Softening	4,617	4,841
11	Cyclic	-1	0.0108	0.0106	0.0002	0	-33	-4.8	1923 MPa (278.9 ksi)	1904 MPa (276.2 ksi)	Stable	19,042	20,502
3	Cyclic	-1	0.0100	0.0098	0.0002	0	5	0.7	1756 MPa (254.9 ksi)	1730 MPa (250.9 ksi)	Stable	29,302	31,729
10	Cyclic	-1	0.0090	0.0090	≤0.0001	0	0	0	1609 MPa (233.3 ksi)	1604 MPa (232.6 ksi)	Stable	—	290,100**
9	Cyclic	-1	0.0199	0.0157	0.0042	0	-31	-4.4	2620 MPa (380.0 ksi)	2707 MPa (392.6 ksi)	Harden	154	187
12	Cyclic/Dwell	-1	0.0126	0.0120	0.0006	0.0002	-28	-4.0	2157 MPa (312.9 ksi)	2125 MPa (308.2 ksi)	Stable	484	495
14	Cyclic/Dwell	-1	0.0115	0.0112	0.0003	0.0001	-52	-7.5	1981 MPa (287.3 ksi)	1987 MPa (288.1 ksi)	Stable	704	749
4	Cyclic/Dwell	-1	0.0131	0.0122	0.0009	0.0002	-57	-8.2	2282 MPa (330.9 ksi)	2202 MPa (319.4 ksi)	Soften	271	285
13	Cyclic/Dwell	-1	0.0099	0.0098	0.0001	<0.0001	9	1.3	1758 MPa (254.9 ksi)	1734 MPa (251.5 ksi)	Stable	5,107	5,144
8	Cyclic	0	0.0124	0.0117	0.0007	0	146	21.2	2022 MPa (293.2 ksi)	2046 MPa (296.7 ksi)	Stable	1,059	1,079
5	Cyclic	0	0.0100	0.0099	0.0001	0	347	50.3	1651 MPa (239.4 ksi)	1709 MPa (247.9 ksi)	Slight Hardening	3,539	4,001
6	Cyclic	0	0.0090	0.0089	≤0.0001	0	367	53.2	1511 MPa (219.1 ksi)	1526 MPa (221.3 ksi)	Stable	45,885	46,479

*— Cyclic tests conducted at 0.33 Hz (20 cpm)

Cyclic/Dwell tests have a 900 sec (15 min) hold time at the maximum tensile strain. Ramp frequency is the same as the cyclic tests.

**— Test discontinued; no indication of failure.

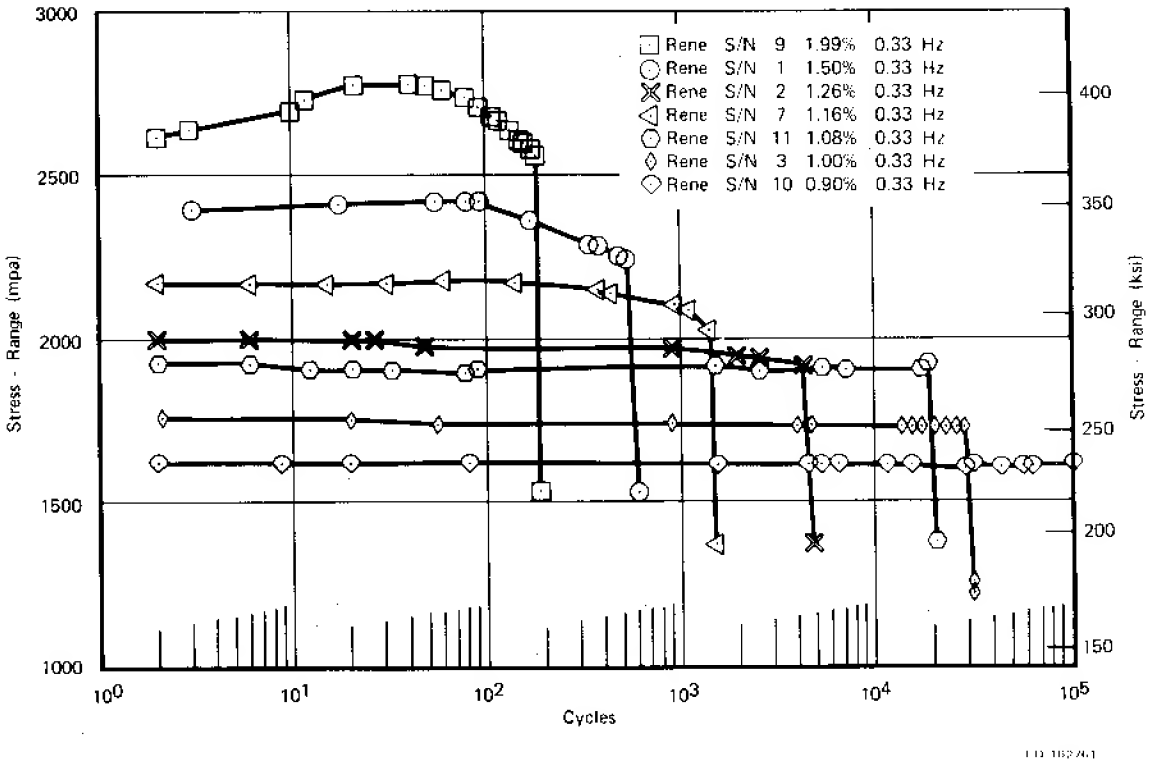

Figure 27. Stress Range vs Cycles for René 95 (0.33 Hz, R_ϵ = -1)

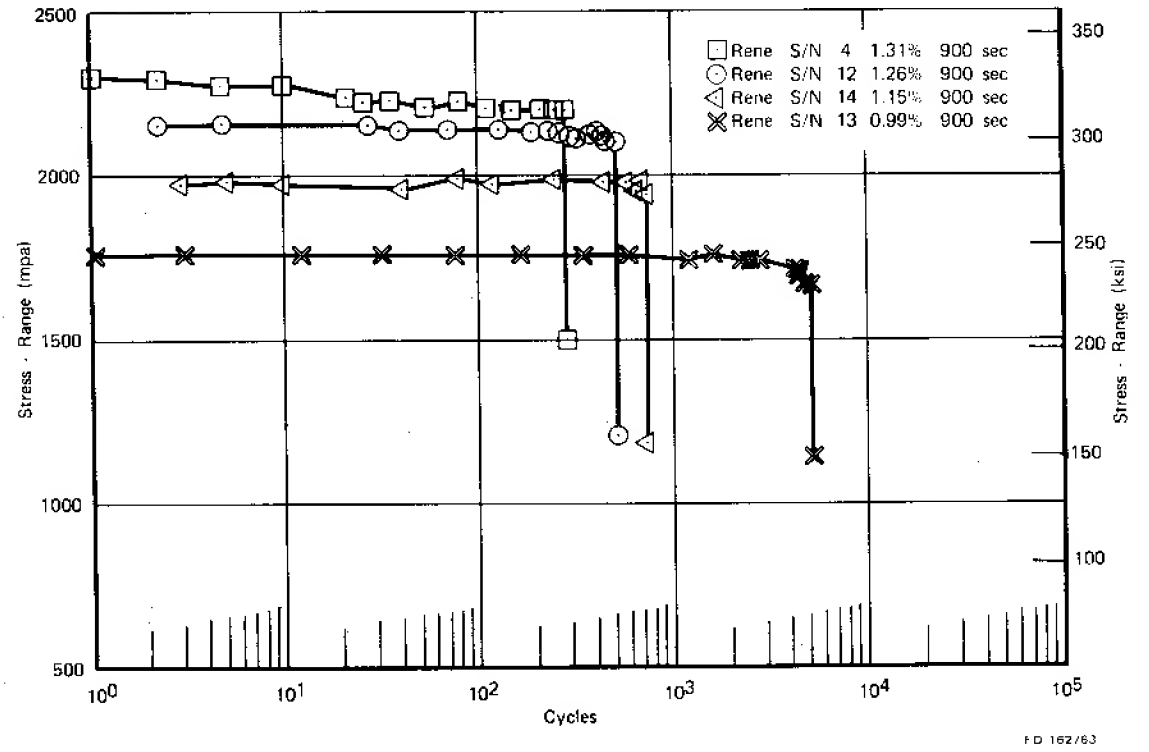

Figure 28. Stress Range vs Cycles for René 95 (900 sec Dwell, R_ϵ = -1)

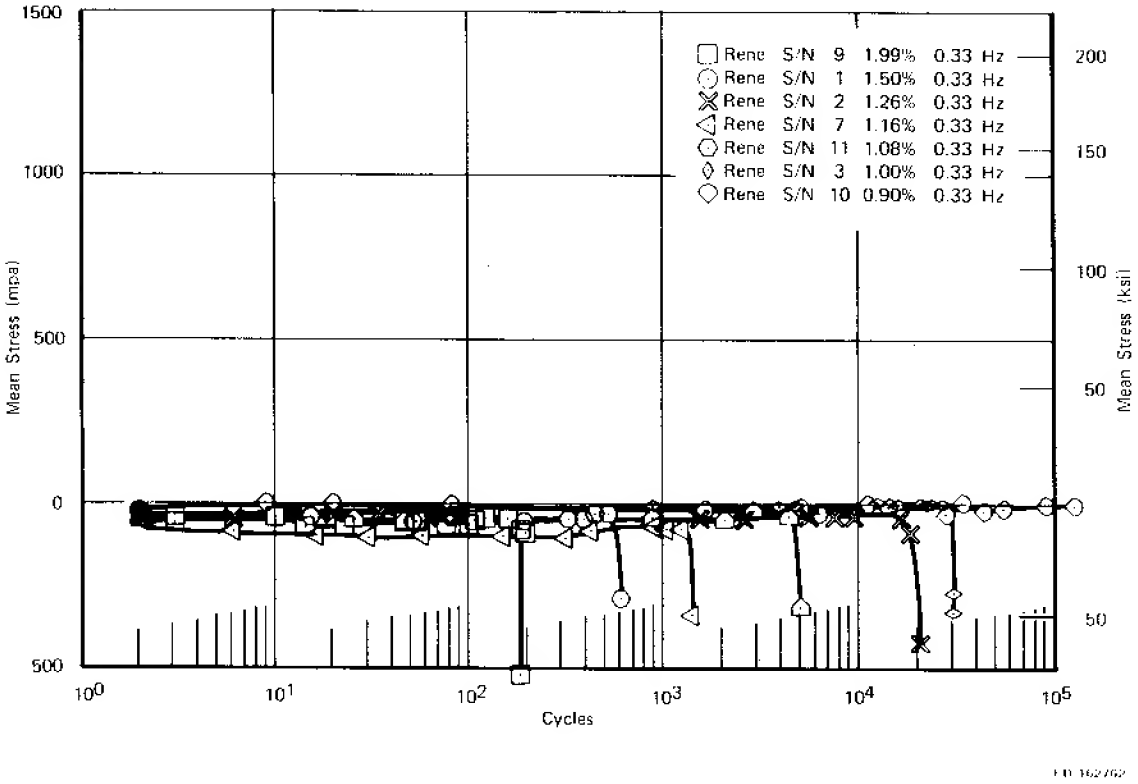

Figure 29. Mean Stress vs Cycles for René 95 (0.33 Hz, R_ϵ = -1)

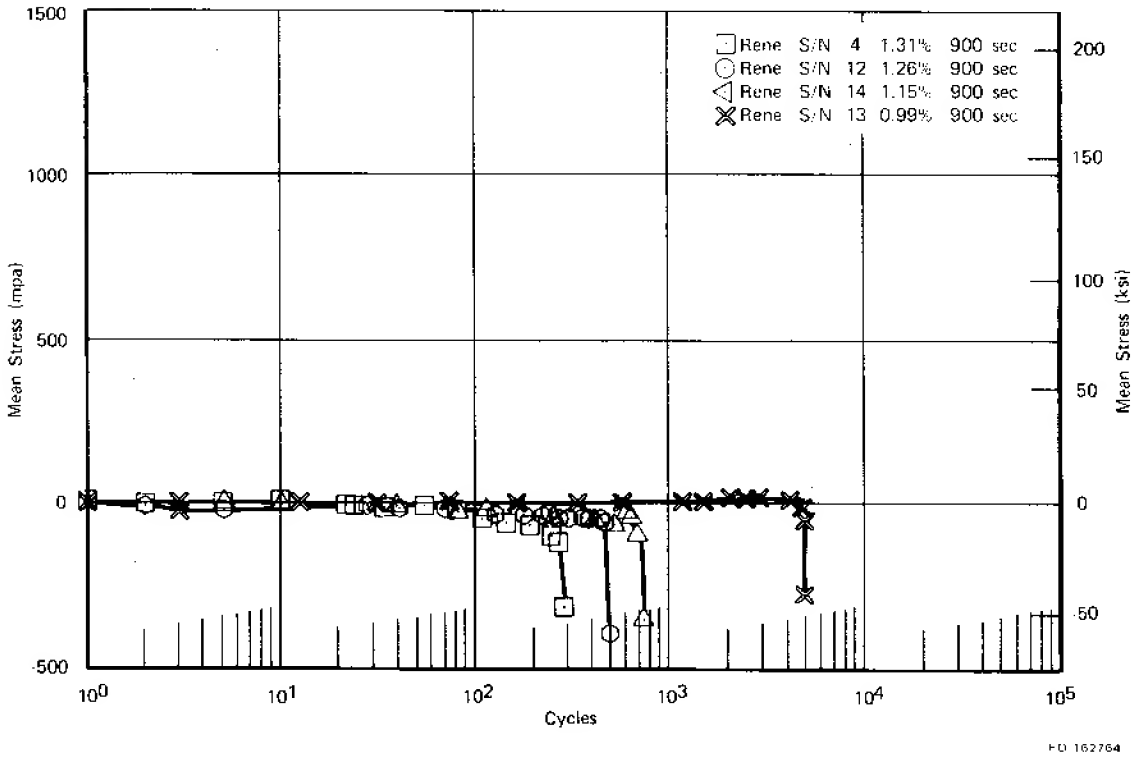

Figure 30. Mean Stress vs Cycles for René 95 (900-sec Dwell, R_ϵ = -1)

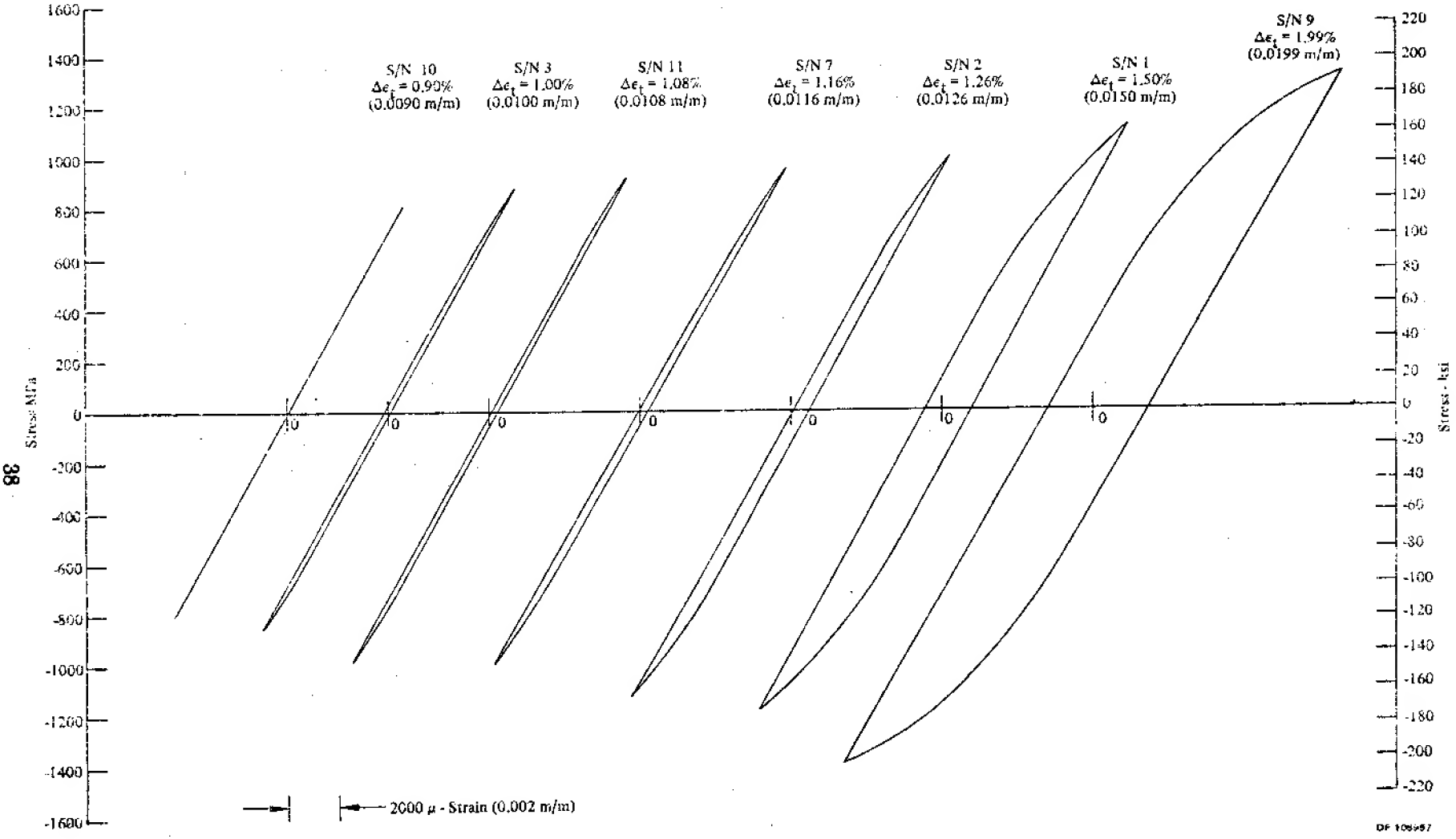

Figure 31. Typical Hysteresis Loops, René 95 Cyclic Tests

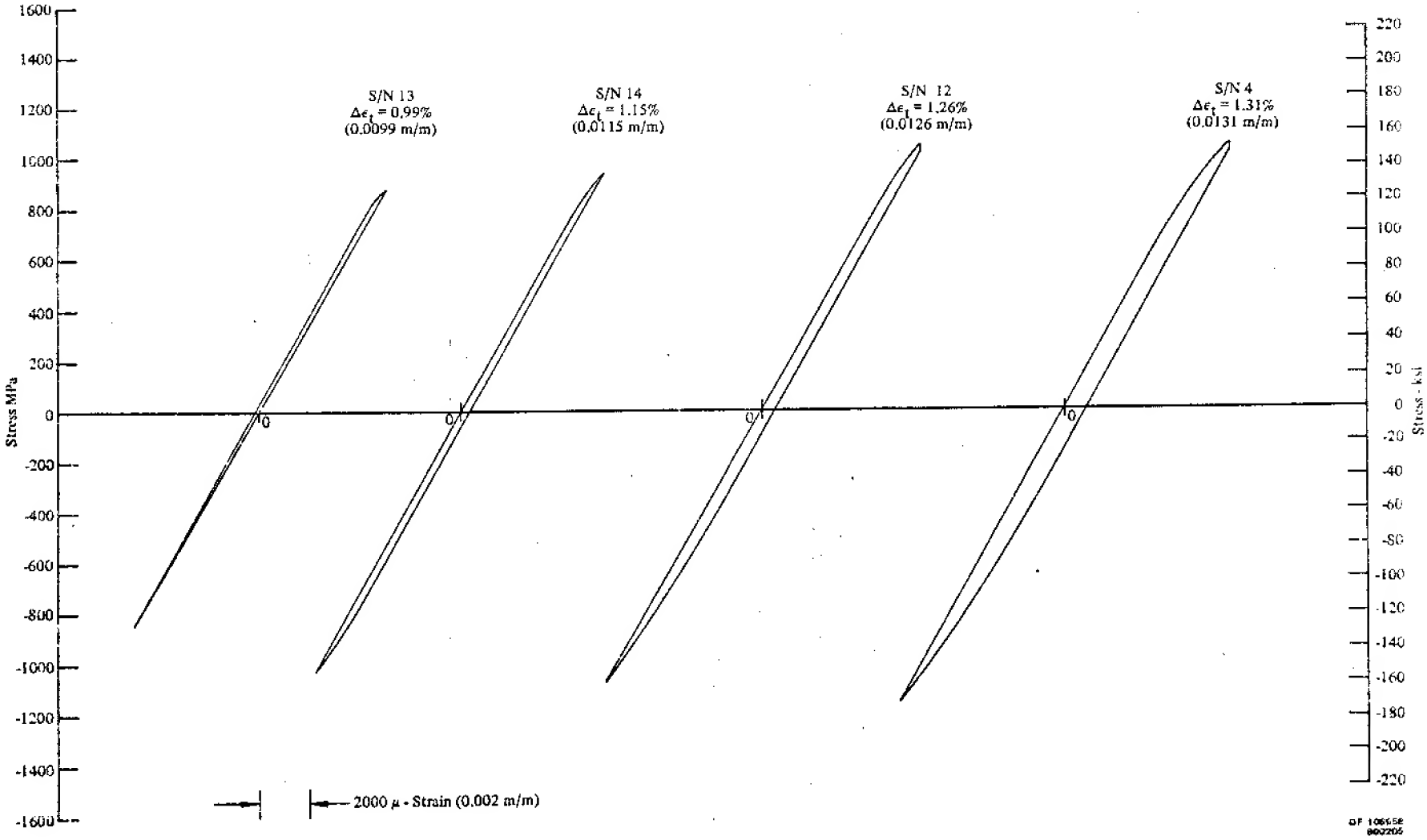

Figure 32. Typical Hysteresis Loops, René 95 Dwell Tests

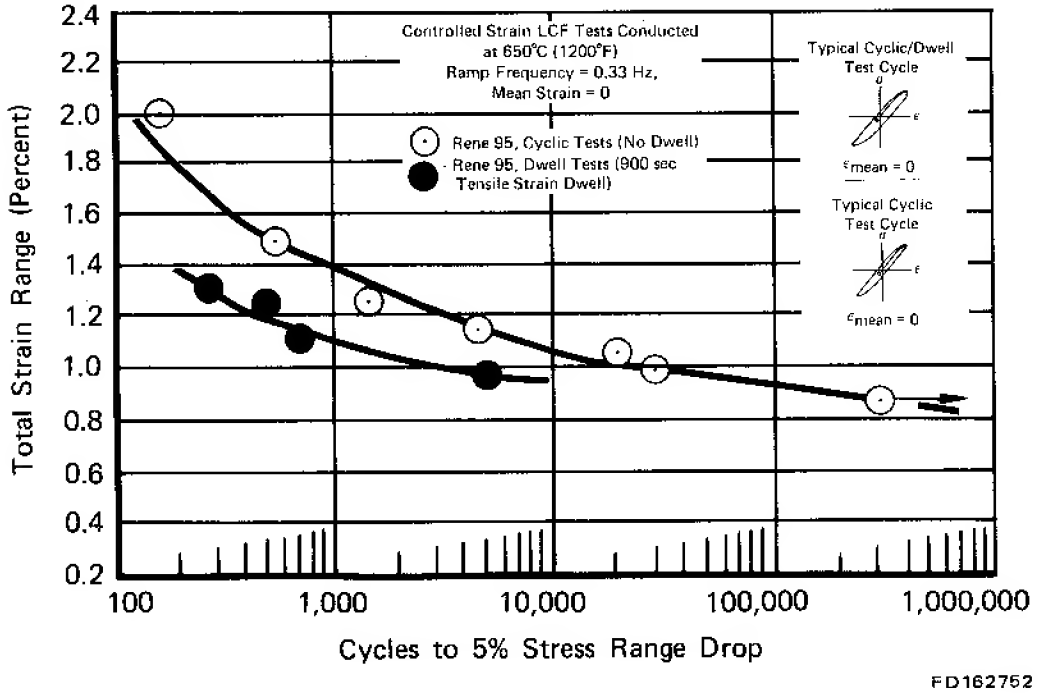

Figure 33. Strain Control LCF Results for Rene 95 (N_5 Life)

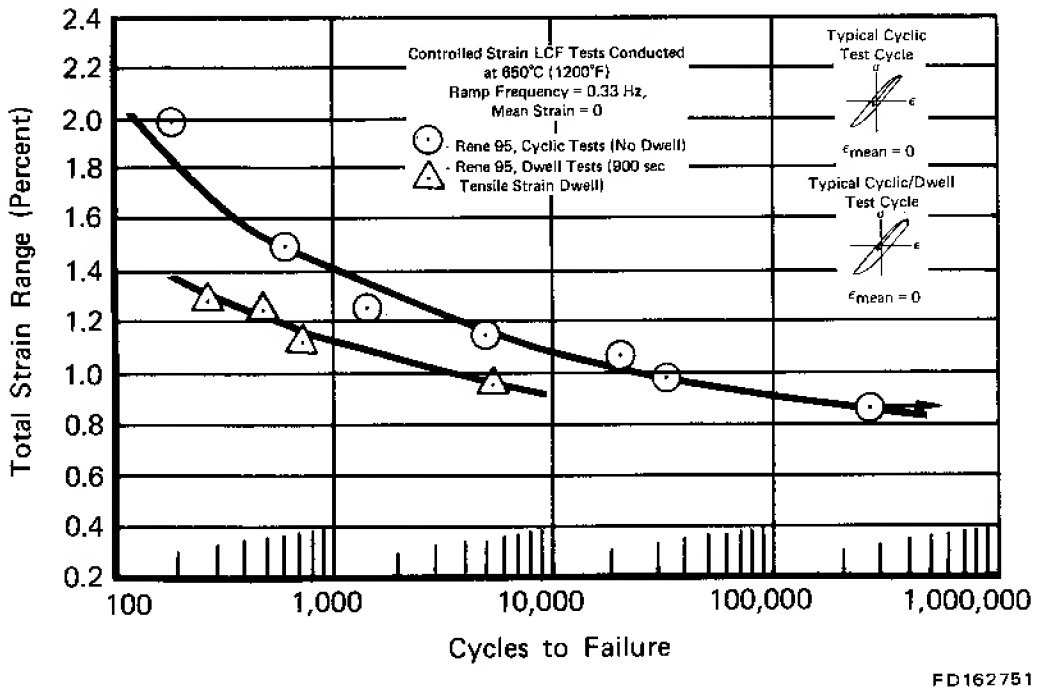

Figure 34. Strain Control LCF Results for Rene 95 (Failure)

TABLE 11
CONTROLLED STRAIN LOW-CYCLE FATIGUE RESULTS FOR TURBINE DISK ALLOY 2, RENÉ 95 HIP PLUS FORGED (GE DATA)[1].
Identification — Cartech Vim Heat No. V91085/Ladish Co. Forging EX091
Triangular Wave, 0.33 Hz (20 cpm)
Test Temperature 650°C (1200°F); R = -1 (A = ∞); Trapezoidal Wave, 15 min Hold Time at the Max Tensile Strain

Spec No.	*Type Test*	*Percent Longitudinal Strain at $N_f/2$*				*Stress Range (P/A), MPa*		*Mean Stress at $N_f/2$, MPa*	*Max Tensile Stress at $N_f/2$, MPa*	*Cycles to Failure*		
		$\Delta\epsilon_e$	$\Delta\epsilon_{in.}$	$\Delta\epsilon_c$	$\Delta\epsilon_t$	N'^{+}	$N_f/2$			N_i*	$N_5^{\approx}$	N_f
II-7	Cont	1.151	0.059	—	1.210	2048	2058	0	1054	1,050	1,180	1,232
II-16	Cont	1.032	0.036	—	1.068	1881	1886	-14	936	4,160	4,450	4,454
II-2	Cont	0.934	0.0279	—	0.962	1729	1707	50	909	9,250	9,250	9,292
II-6	Cont	0.987	0.023	—	1.010	1838	1830	14	918	9,250	10,680	10,680
II-5	Cont	0.970	0.016	—	0.986	1726	1780	32	918	14,200	14,750	14,827
II-8	Cont	0.892	0.028	—	0.920	1632	1625	37	864	16,550	16,900	16,963
II-14	Cont	0.893	0.028	—	0.921	1697	1603	-59	778	84,000	63,000	96,205
NII-9	Hold Time	1.138	0.138	0.016	1.276	2023	2095	-294	914	425	438	446
NII-10	Hold Time	1.176	0.099	0.020	1.275	2096	2091	-158	982	465	520	543
NII-11	(π)Hold Time	0.951	0.056	0.013	1.007	1889	1841	-253	805	690	697	701
NII-12	Hold Time	0.953	0.070	0.013	1.023	1831	1781	-330	728	3,440	3,547	3,547
NII-1	Hold Time	0.891	0.066	0.019	0.957	1861	1768	-104	832	5,060	5,160	5,163

+ N′ — First Cycle
* N_i — Defined as cycles to discernible deviation from stabilized load range
≈ N_5 — Number of cycles to 5% drop in stabilized load range
→ Runout
π Metcut Test

[1]Note — This data has been reproduced from NASA Contract NAS3-20368 Final Report, NASA-CR-159433.[2]

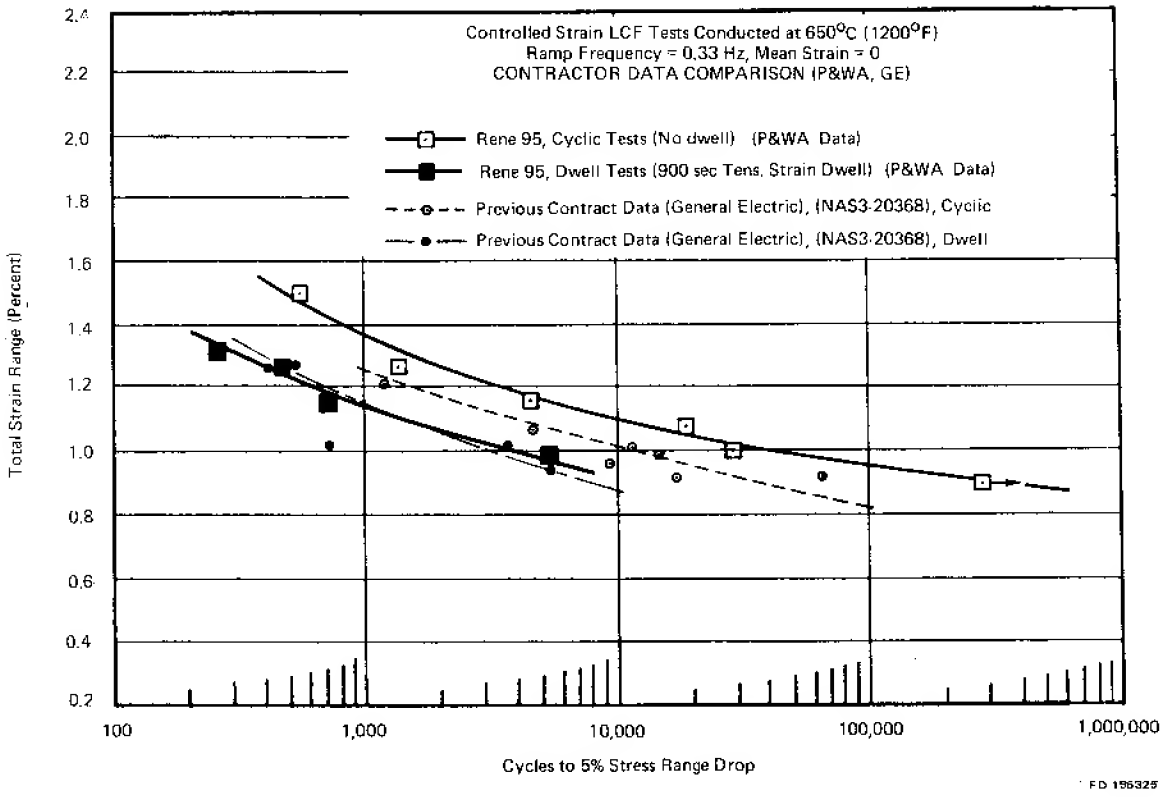

Figure 35. Strain Control LCF Results for René 95 — Contractor Data Comparison (N_5 Life)

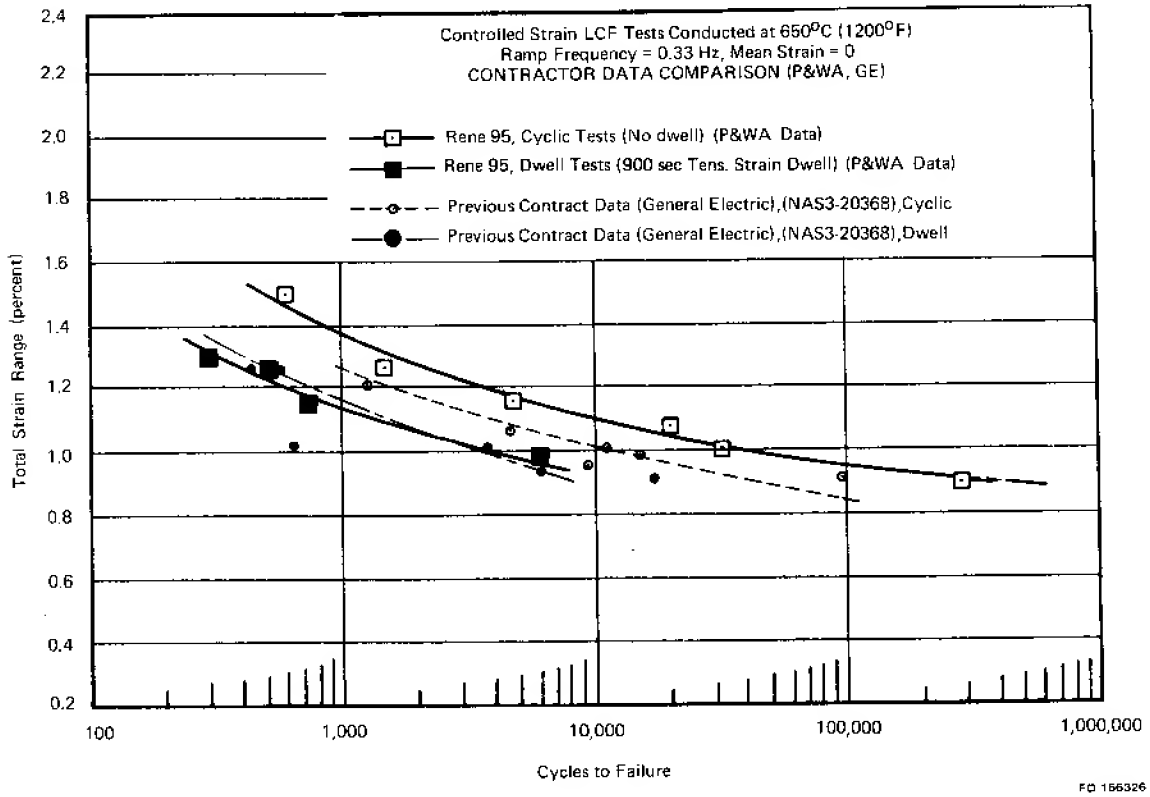

Figure 36. Strain Control LCF Results for René 95 — Contractor Data Comparison (Failure)

For specific tests where the total strain ranges are comparable (between P&WA and GE), both stress ranges and strain components are similar. Figure 37 illustrates the stress vs inelastic strain range behavior for this alloy. The figure includes both P&WA and GE cyclic data, and a strain R comparison for the P&WA data. The P&WA and GE data agree well, except for three GE data points which appear anomalous. This indicates that both P&WA and GE measurements of inelastic strain are reasonably close, and the factor of 2 difference in life is probably attributable to specimen machining and surface preparation. Strain R ratio has little or no effect, as would be expected from the general relationship: $\Delta\sigma = K\epsilon_p^n$ for the stress range ($\Delta\sigma$) and inelastic strain ($\Delta\epsilon_p$).

The cyclic/dwell vs life data from P&WA and GE agree quite well with the exception of one apparently anomalous GE test point. In this case, however, for the tests that are comparable, the stress ranges are similar for given total strain ranges, but the strain components themselves differ. When compared with P&WA data, GE elastic strain components are lower, inelastic strain components are higher, and creep-strain components are similar.

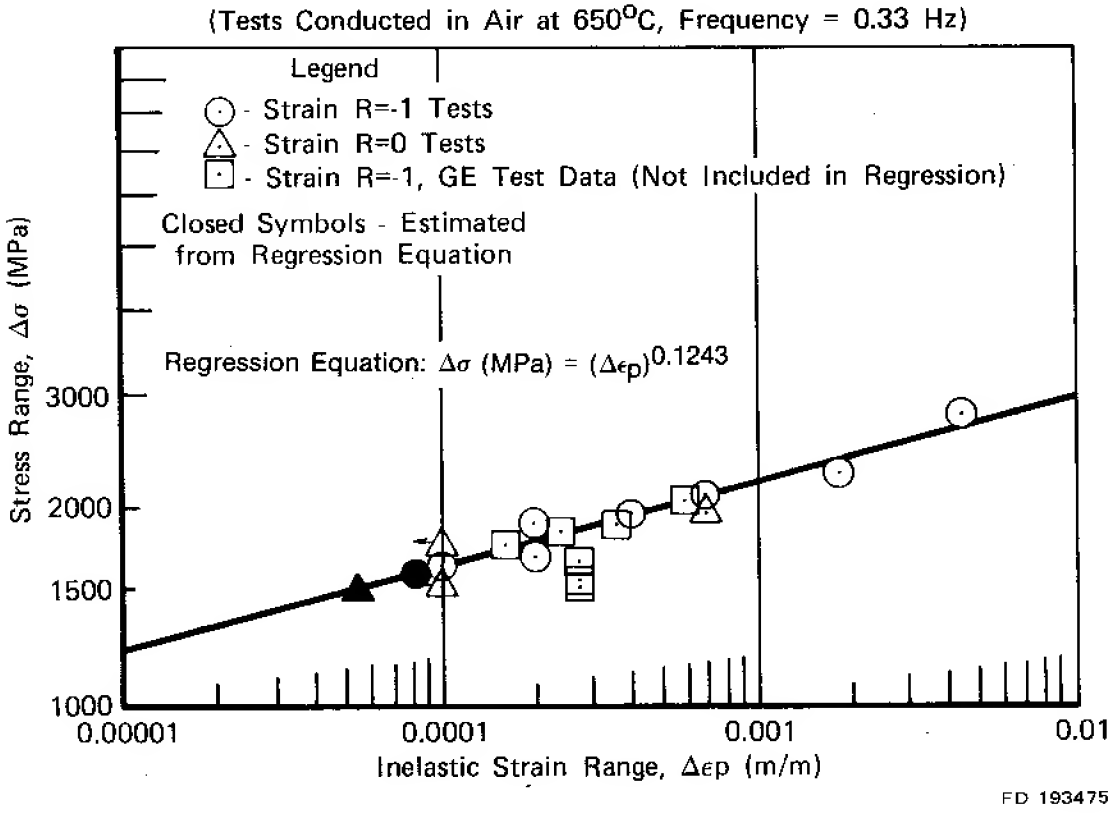

Figure 37. Stress Range vs Inelastic Strain Range for René 95

All-Tensile Strain LCF Tests (Mean Strain = ½ Max Strain, Strain R_ϵ = 0)

All-tensile strain cycle LCF tests were run for wrought Waspaloy and GATORIZED IN 100. These alloys were tested in earlier contract work (NAS3-20367) with a fully reversed strain cycle (R_ϵ = -1). Under actual turbine engine operating conditions, however, the strain cycle for many critical aircraft turbine disk locations can be better simulated with the all-tensile strain LCF cycle. For this reason and to obtain a better understanding of the effect of R_ϵ on LCF life, this test cycle was chosen. Typical hysteresis loops and strain-time waveforms appear in figures 14 and 16.

This LCF cycle induces significant mean stresses into the specimen when running at low strain ranges, and the corresponding LCF life may be substantially reduced. These effects are discussed in more detail in a later section of this report entitled "Effects of Mean Stress and Mean Strain."

The following paragraphs present a discussion of the test results for Waspaloy and GATORIZED IN 100.

Waspaloy

Seven cyclic tests and five cyclic/dwell tests were conducted for this alloy. Table 12 details the test data. The stress range and mean stress vs life plots are shown in Figures 38 through 41. Note in figure 41 that the relaxation of mean stress vs time is nearly a straight line (log-linear) relationship. This could be approximated by a functional relationship of the form $\bar{\sigma}$ = A log t + B, where $\bar{\sigma}$ equals mean stress and t equals time, and with further work could show promise in being integrated into an LCF life prediction model to describe the effect of hold time, mean stress, and strain range on LCF life.

Figures 42 and 43 illustrate typical stress-strain hysteresis loops at half-life. Figures 44 and 45 detail the total strain range vs life curves. These figures indicate that there is no significant difference in LCF life between the cyclic and 900 sec dwell tests below a total strain range of 0.85% at 650°C, and strain R = 0. To confirm the relationship of the cyclic and dwell LCF curves at these conditions an additional cyclic test was run at a similar strain range (~0.90%) as the long life dwell test. This test agreed with the cyclic LCF curve life prediction, and therefore the cyclic and dwell curves do indeed converge at approximately 0.85% strain range. This may be explained in terms of mean stress relaxation. From figure 40, it can be seen that the cyclic tests at the low strain ranges have mean stresses in the 250-350 MPa range which remain essentially constant for the duration of the test. And from figure 41, the mean stresses for the dwell tests relaxed to zero or even compressive in a relatively short time. At the lower strain ranges then, it would be expected that the LCF curves may tend to converge. The cyclic life of the no-dwell tests would be reduced due to the high mean stress, and the cyclic life of the dwell tests would be higher than expected due to mean stress relaxation (both of the above conclusions are made in reference to results for mean stress of zero, mean strain of zero tests). It is interesting to note that the degrading effect of the dwell time is completely offset by the beneficial effect of mean stress relaxation for these dwell tests at low strain ranges.

The stress range vs inelastic strain range relationships for Waspaloy at the R_ϵ = 0 condition tested under this contract and R_ϵ = -1 condition tested under NAS3-20367 are presented in figure 46. The relationship is log-linear.

TABLE 12
CONTROLLED STRAIN LOW-CYCLE FATIGUE RESULTS FOR TURBINE DISK ALLOY 3, WASPALOY
Testing Conducted at 650°C (1200°F)

Spec S N	Type* Test	Strain R Ratio (min max)	Strain (m/m at $N_f/2$) Range	Elastic	Inelastic	Creep	Mean Stress at $N_f/2$ MPa	ksi	Stress Range Cycle 1	$N_f/2$	Cyclic Stability	Cycles to Failure N_s%	N_f
1	Cyclic	0	0.0147	0.0100	0.0047	0	-6	-0.8	1920 MPa (278.4 ksi)	1742 MPa (252.7 ksi)	Soften	753	828
2	Cyclic	0	0.0123	0.0097	0.0026	0	40	5.8	1862 MPa (270.1 ksi)	1696 MPa (246.0 ksi)	Soften	1,021	1,128
4	Cyclic	0	0.0099	0.0089	0.0010	0	86	12.4	1634 MPa (237.0 ksi)	1594 MPa (231.2 ksi)	Slight Softening	2,733	3,025
5	Cyclic	0	0.0079	0.0077	0.0002	0	229	33.2	1387 MPa (201.1 ksi)	1393 MPa (202.0 ksi)	Stable	14,175	15,926
6	Cyclic	0	0.0066	0.0065	<0.0001	0	284	41.2	1154 MPa (167.3 ksi)	1157 MPa (167.8 ksi)	Stable	60,533	62,462
7	Cyclic	0	0.0060	0.0060	<0.0001	0	310	44.9	1069 MPa (155.0 ksi)	1074 MPa (155.8 ksi)	Stable	189,667	195,715
20	Cyclic	0	0.0092	0.0088	0.0004	0	170	24.7	1482 MPa (214.9 ksi)	1476 MPa (214.1 ksi)	Stable	4,012	4,399
9	Cyclic Dwell	0	0.0118	0.0105	0.0013	0.0003	-214	-31.1	1965 MPa (284.9 ksi)	1946 MPa (282.2 ksi)	Stable	862	927
12	Cyclic/Dwell	0	0.0136	0.0112	0.0024	0.0007	-153	-22.2	2063 MPa (299.1 ksi)	2084 MPa (302.2 ksi)	Stable	295	309
10	Cyclic/Dwell	0	0.0099	0.0093	0.0006	0.0001	-76	-11.0	1691 MPa (245.3 ksi)	1676 MPa (243.1 ksi)	Stable	1,870	2,046
17	Cyclic/Dwell	0	0.0152	0.0113	0.0039	0.0009	-150	-21.7	2086 MPa (302.6 ksi)	2145 MPa (311.1 ksi)	Harden	148	160
19	Cyclic Dwell	0	0.0087	0.0083	0.0004	0.0001	-146	-21.2	1476 MPa (214.1 ksi)	1465 MPa (212.5 ksi)	Stable	5,534	5,695

*Cyclic tests conducted at 0.33 Hz (20 cpm).
Cyclic/Dwell tests have a 900 sec (15 min) hold time at the maximum tensile strain. Ramp frequency is the same as the cyclic tests.

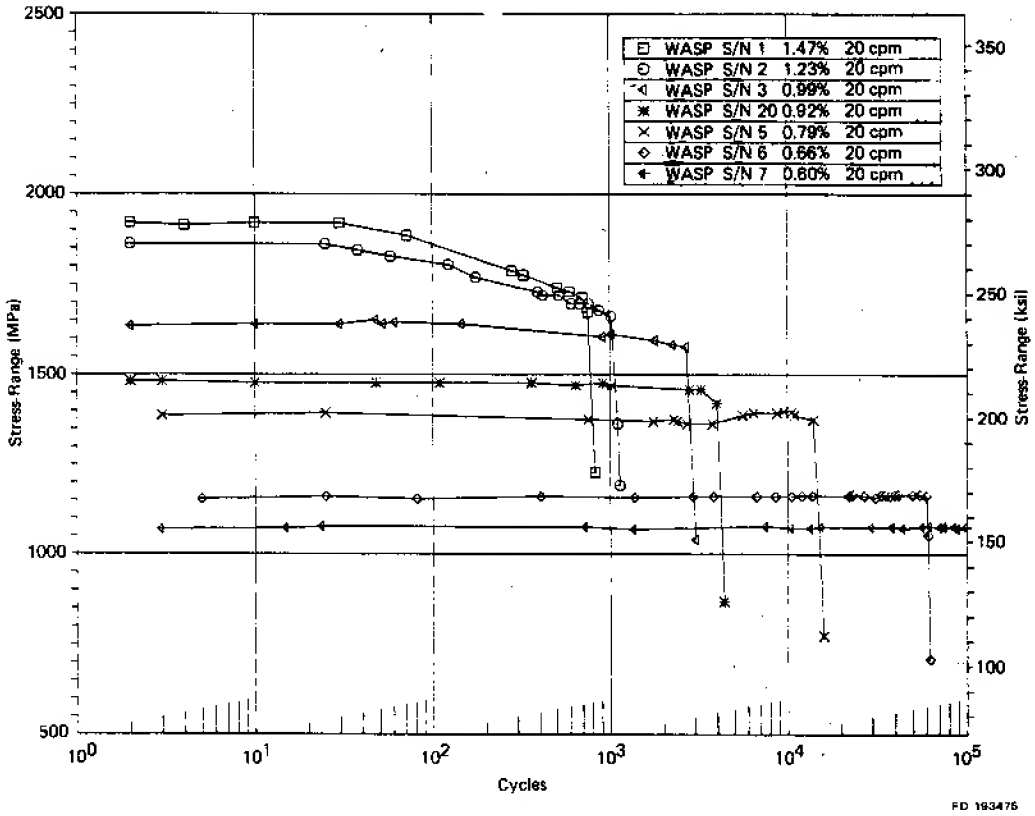

Figure 38. Stress Range vs Cycles for Waspaloy (0.33 Hz, R_ϵ = 0)

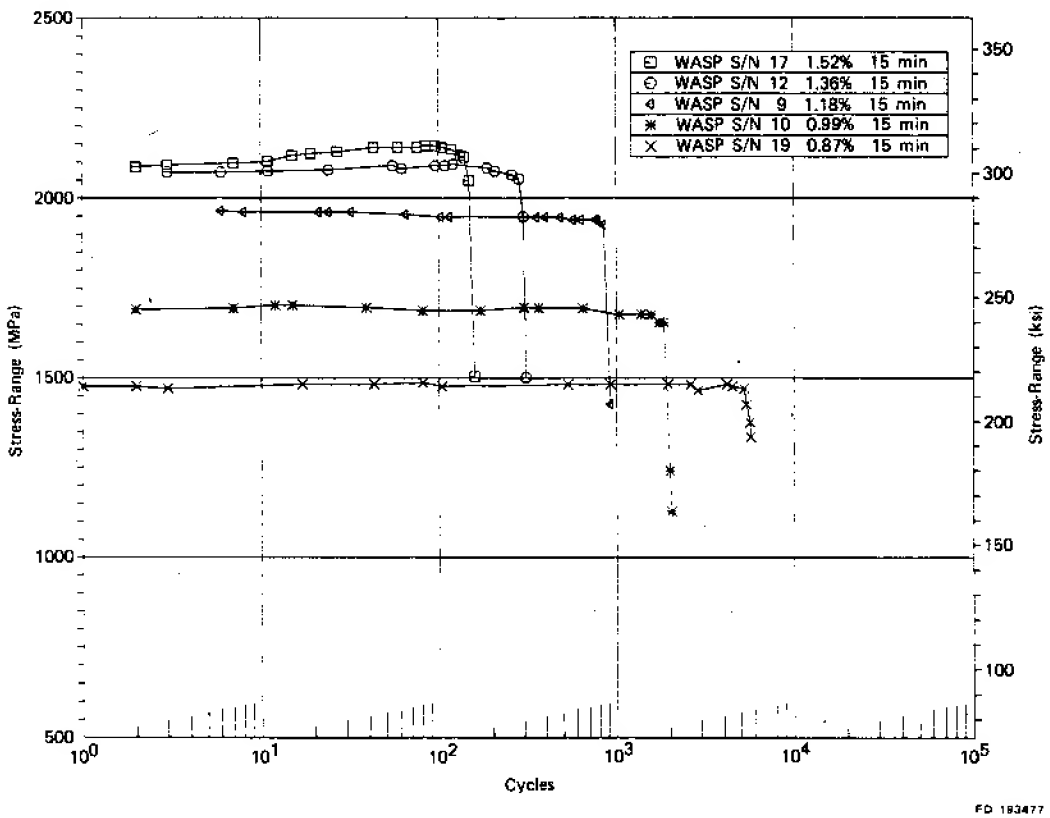

Figure 39. Stress Range vs Cycles for Waspaloy (900-sec Dwell, R_ϵ = 0)

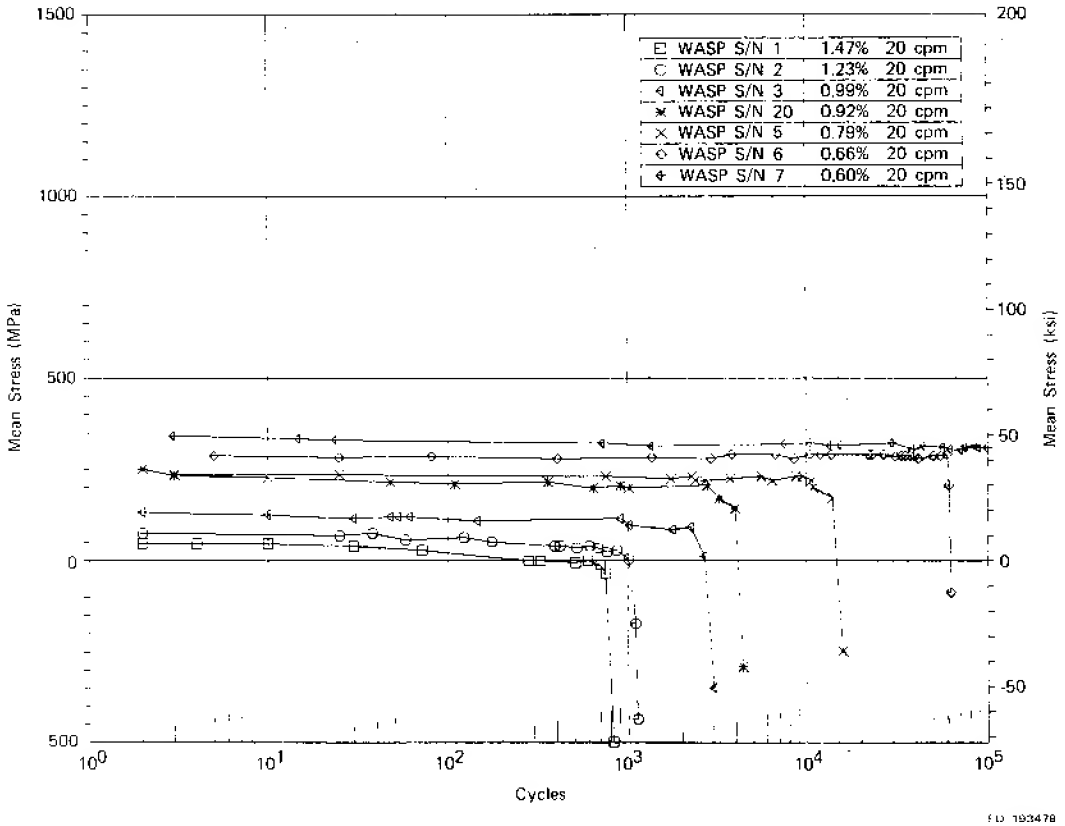

Figure 40. Mean Stress vs Cycles for Waspaloy (0.33 Hz, R_ϵ = 0)

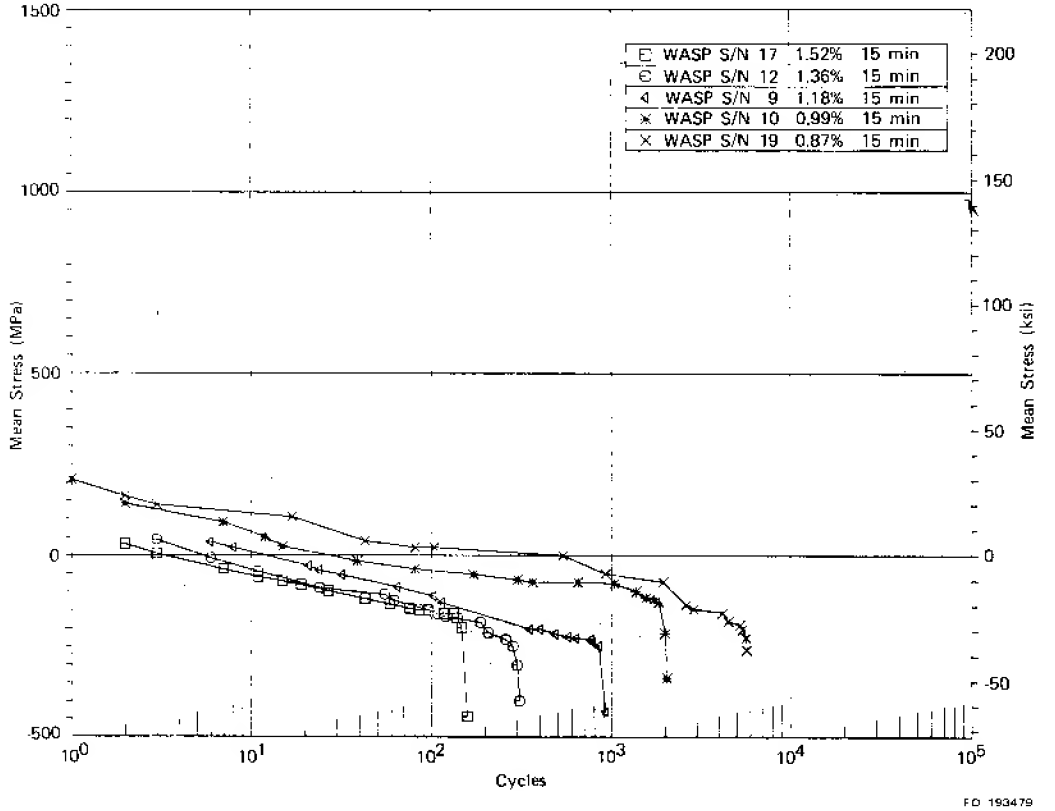

Figure 41. Mean Stress vs Cycles for Waspaloy (900-sec Dwell, R_ϵ = 0)

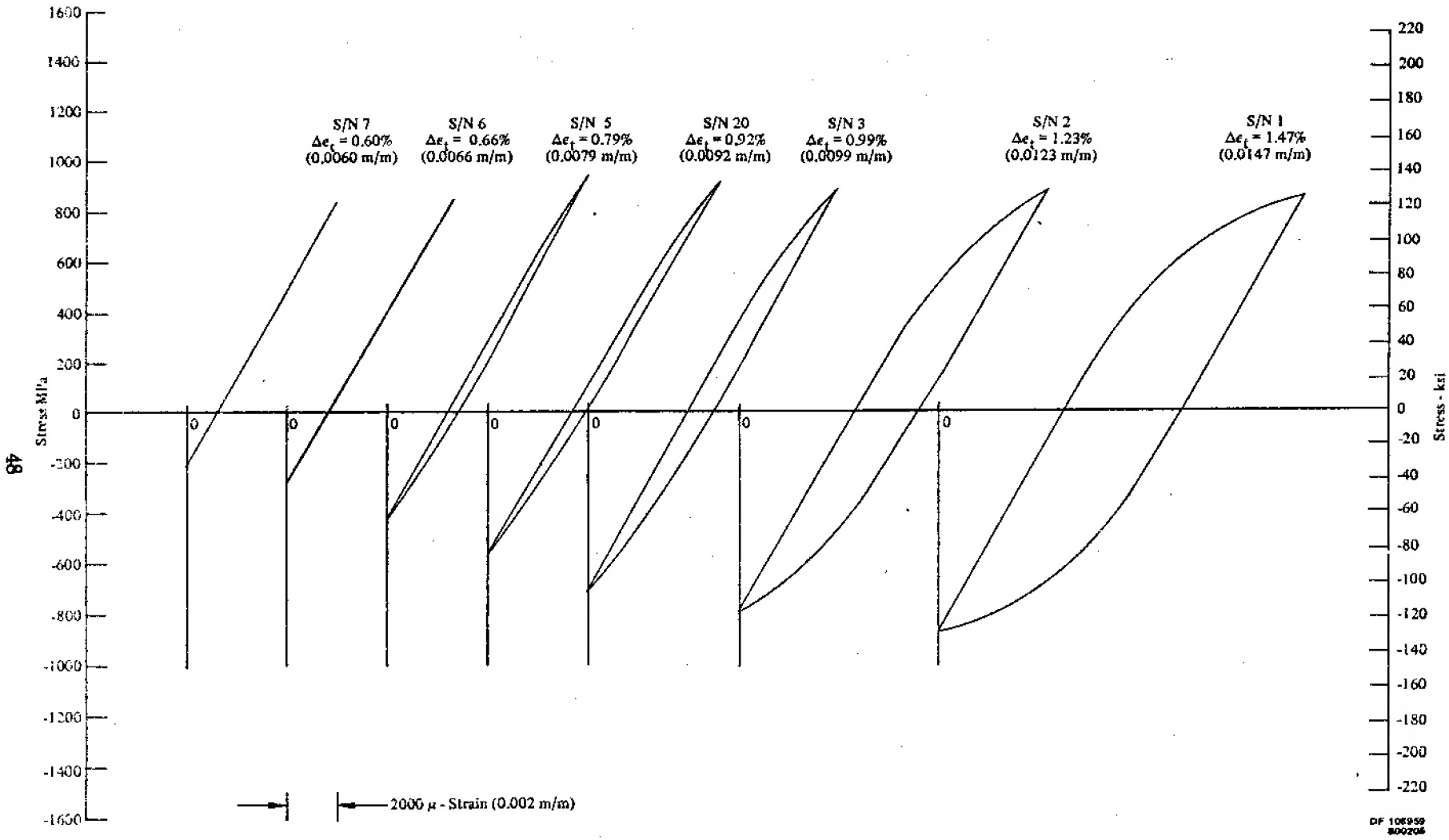

Figure 42. Typical Hysteresis Loops, Waspaloy Cyclic Tests

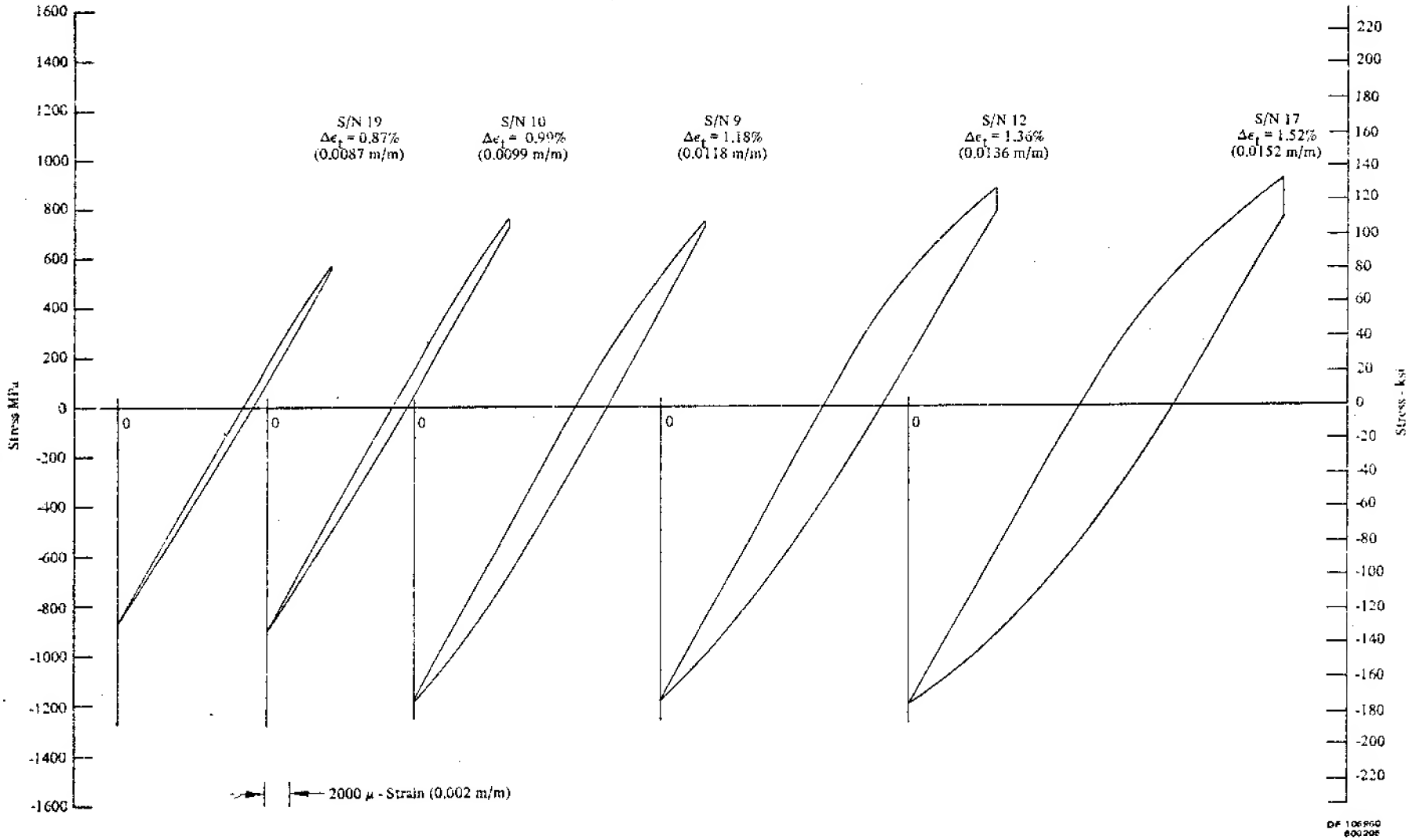

Figure 43. Typical Hysteresis Loops, Waspaloy Dwell Tests

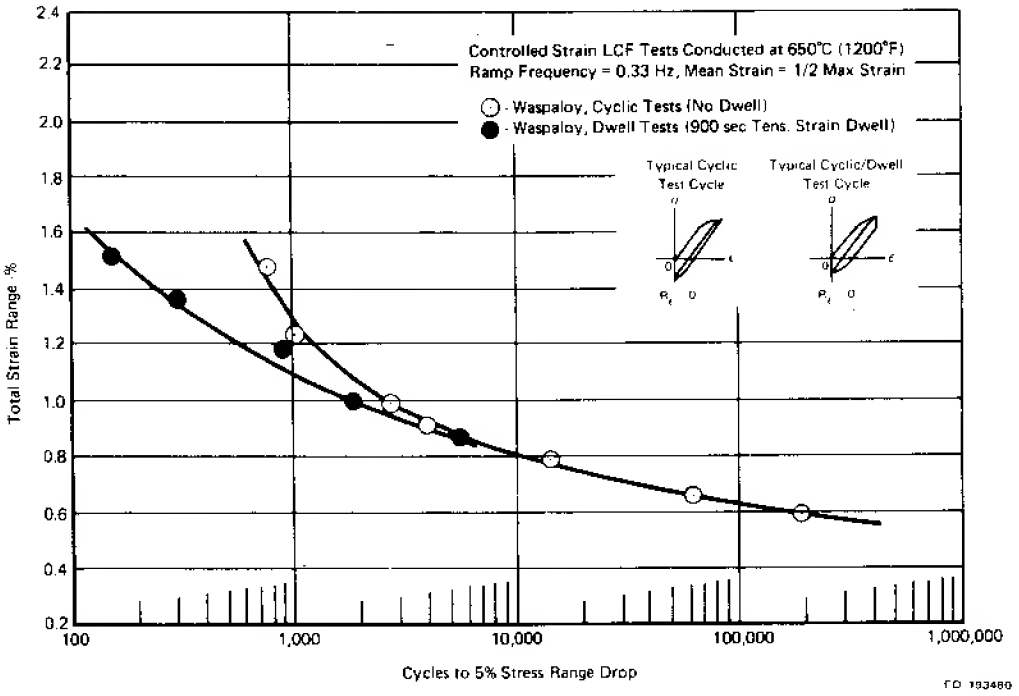

Figure 44. Strain Control LCF Results for Waspaloy (N_5 Life)

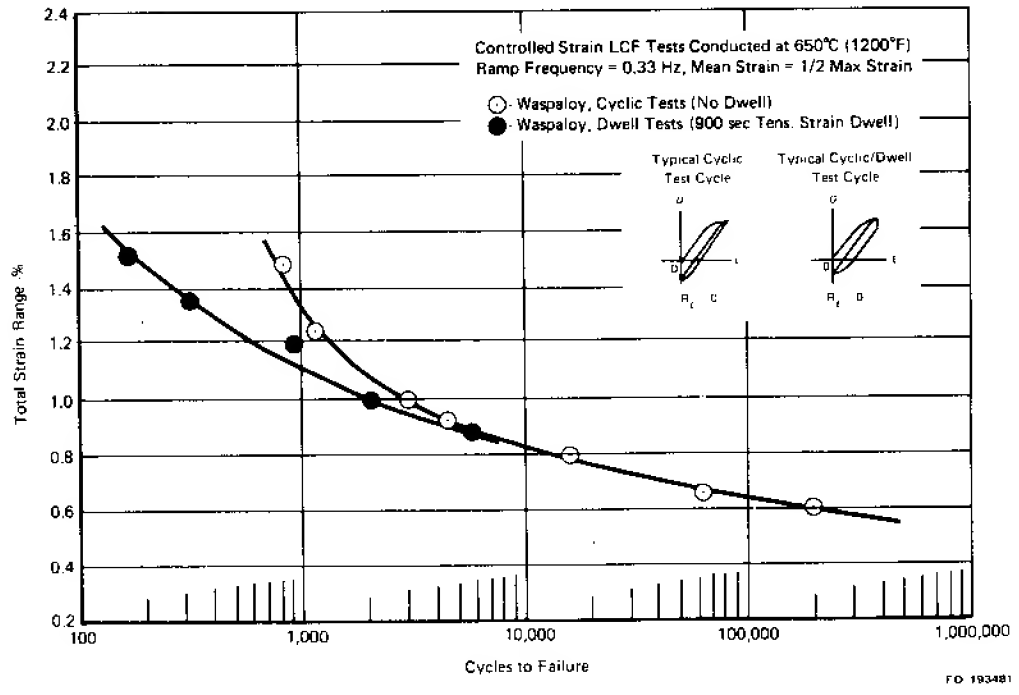

Figure 45. Strain Control LCF Results for Waspaloy (Failure)

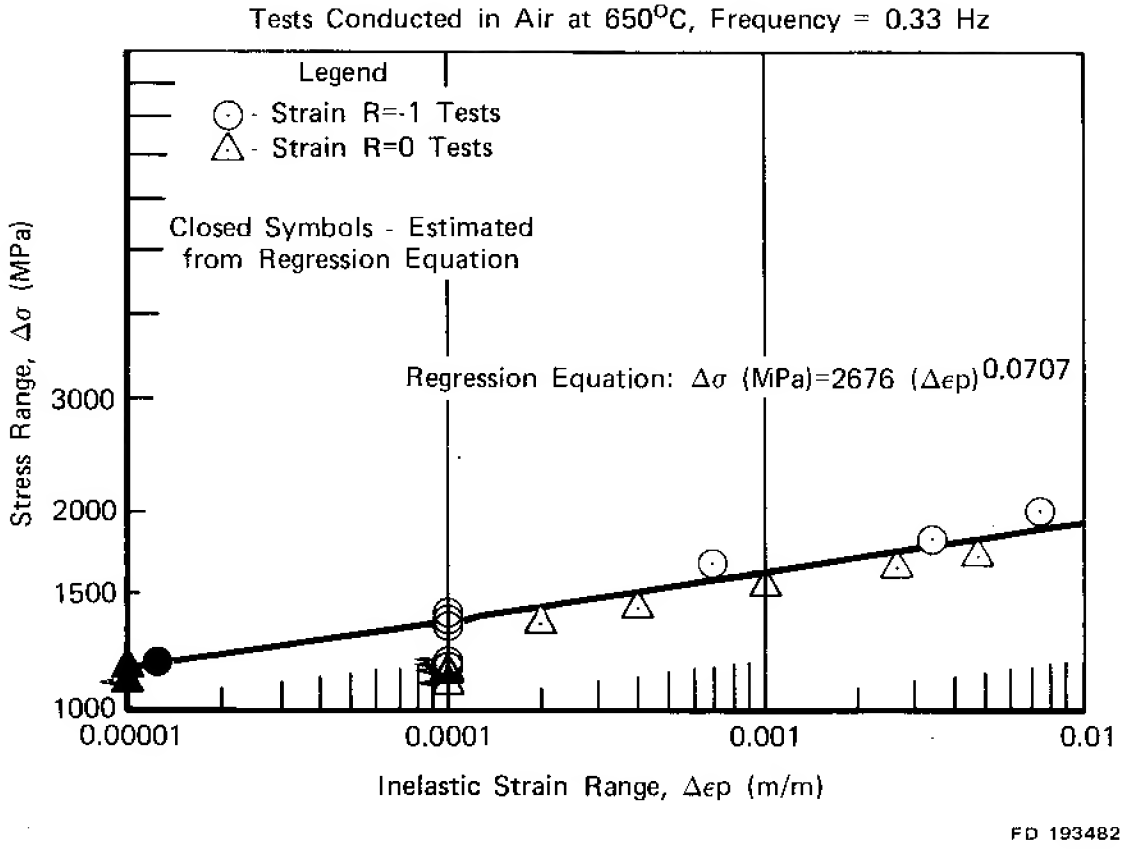

Figure 46. Stress Range vs Inelastic Strain Range for Waspaloy

GATORIZED IN 100

The pancake forging of IN 100 used in this contract (BAQQ-H105-A10) differed from the forging used for IN 100 evaluations tested previously (Heat BAKY-H45-A5) under NAS3-20367. In order to ensure that there were no significant differences in the LCF properties between the two pancakes, several supplementary tests were conducted from the new pancake forging at comparable strain levels with tests run during the previous NASA contract. As can be noted from the data presented in the "Supplementary Tests" section of this report, there was no significant difference in the LCF properties of the two forgings.

Six cyclic tests and four cyclic/dwell tests were conducted using an all-tensile strain cycle. Table 13 lists the test data. Stress range and mean stress vs life plots are shown in figures 47 through 50. Mean stress relaxation (figure 50) for dwell tests of IN 100 also shows a roughly linear decay with log (time) or log (life), as noted with the Waspaloy dwell tests. Mean stress exerts a significant effect on LCF life for both cyclic and cyclic/dwell test conditions.

To further investigate this mean stress vs life phenomenon, supplementary strain control LCF tests were conducted where the mean stresses were held constant. This work is discussed further in a later section of this report entitled "Effect of Mean Stress and Mean Strain."

Figures 51 and 52 illustrate typical stress-strain hysteresis loops at the specimen half-life. Figures 53 and 54 present total strain vs life curves.

Stress range vs inelastic strain data for IN 100 is plotted in figure 55. Both $R_\epsilon = 0$ and $R_\epsilon = -1$ (tested previously) are included. R_ϵ has little or no effect on the stress range vs inelastic strain relationship.

Supplementary Testing

Supplementary tests were conducted under this contract to resolve special problems and questions which arose during the progress of testing. These supplemental tests investigated four areas of concern:

1. Forging to forging LCF property variations (in IN 100 and NASA IIB-7 pancake forgings)
2. High strain range tests for 5 alloys tested previously under NAS3-20367
3. Effects of strain R ratio (for HIP MERL 76, René 95, Waspaloy, IN 100, and NASA IIB-7 materials)
4. Effect of mean stress on LCF life (IN 100).

The latter two items are dealt with in the following section entitled "Effect of Mean Stress and Mean Strain." A discussion of the first two items appears in the following paragraphs.

Forging to Forging Low-Cycle Fatigue Studies

Four strain control LCF tests of alloy 4, GATORIZED IN 100, were conducted using a completely reversed strain cycle (mean strain = 0), as shown in figures 13 and 15. The initial tests of this alloy were run at comparable strain ranges with the tests run under Contract NAS3-20367 to assure that there were no significant differences in the LCF properties of the pancake forging used in this contract (Heat BAQQ-H105-A10) and the pancake forging tested previously (Heat BAKY-H45-A5).

TABLE 13
CONTROLLED STRAIN LOW-CYCLE FATIGUE RESULTS FOR TURBINE DISK ALLOY, GATORIZED® IN 100
Testing Conducted at 650°C (1200°F)

Spec	Type*	Strain R Ratio	Strain (m/m at $N_f/2$)				Mean Stress at $N_f/2$		Stress Range		Cyclic	Cycles to Failure	
S/N	Test	(min/max)	Range	Elastic	Inelastic	Creep	MPa	ksi	Cycle 1	$N_f/2$	Stability	$N_5\%$	N_f
4	Cyclic	−1	0.0147	0.0134	0.0013	0	−2	−0.3	2291 MPa (332.3 ksi)	2377 MPa (344.8 ksi)	Harden	358	412
5	Cyclic	−1	0.0101	0.0100	0.0001	0	−36	−5.2	1796 MPa (260.4 ksi)	1791 MPa (259.7 ksi)	Stable	4,968	5,448
10	Cyclic	−1	0.0090	0.0090	≤0.0001	0	−80	−11.7	1610 MPa (233.5 ksi)	1600 MPa (232.1 ksi)	Stable	52,961	53,363
9	Cyclic/Dwell	−1	0.0124	0.0115	0.0009	0.0002	−38	−5.6	2075 MPa (300.9 ksi)	2065 MPa (299.5 ksi)	Stable	351	375
1	Cyclic	0	0.0144	0.0134	0.0010	0	−74	−10.7	2275 MPa (329.9 ksi)	2321 MPa (336.6 ksi)	Slight Hardening	450	469
2	Cyclic	0	0.0124	0.0121	0.0003	0	161	23.3	1987 MPa (288.2 ksi)	2011 MPa (291.6 ksi)	Stable	905	950
3	Cyclic	0	0.0099	0.0098	0.0001	0	286	41.5	1684 MPa (244.2 ksi)	1660 MPa (240.8 ksi)	Stable	2,989	3,134
6	Cyclic	0	0.0075	0.0075	<0.0001	0	458	66.4	1255 MPa (182.0 ksi)	1255 MPa (182.0 ksi)	Stable	27,135	28,584
7	Cyclic	0	0.0087	0.0086	0.0001	0	339	49.2	1510 MPa (218.9 ksi)	1496 MPa (216.9 ksi)	Stable	6,041	6,342
8	Cyclic	0	0.0065	0.0065	<0.0001	0	476	69.0	1128 MPa (163.6 ksi)	1142 MPa (165.6 ksi)	Stable	88,514	93,686
11	Cyclic/Dwell	0	0.0122	0.0109	0.0013	0.0003	−84	−12.2	1991 MPa (288.8 ksi)	1996 MPa (289.5 ksi)	Stable	310	328
12	Cyclic/Dwell	0	0.0100	0.0097	0.0003	0.0001	56	8.2	1721 MPa (249.6 ksi)	1716 MPa (248.9 ksi)	Stable	775	889
13	Cyclic/Dwell	0	0.0111	0.0105	0.0006	0.0002	9	1.3	1900 MPa (275.6 ksi)	1879 MPa (272.6 ksi)	Stable	333	450
14	Cyclic/Dwell	0	0.0090	0.0088	0.0002	≤0.0001	150	21.8	1566 MPa (227.2 ksi)	1563 MPa (226.7 ksi)	Stable	2,122	2,243

*Cyclic tests conducted at 0.33 Hz (20 cpm).
Cyclic/Dwell tests have a 900 sec (15 min) hold time at the maximum tensile strain. Ramp frequency is the same as the cyclic tests.

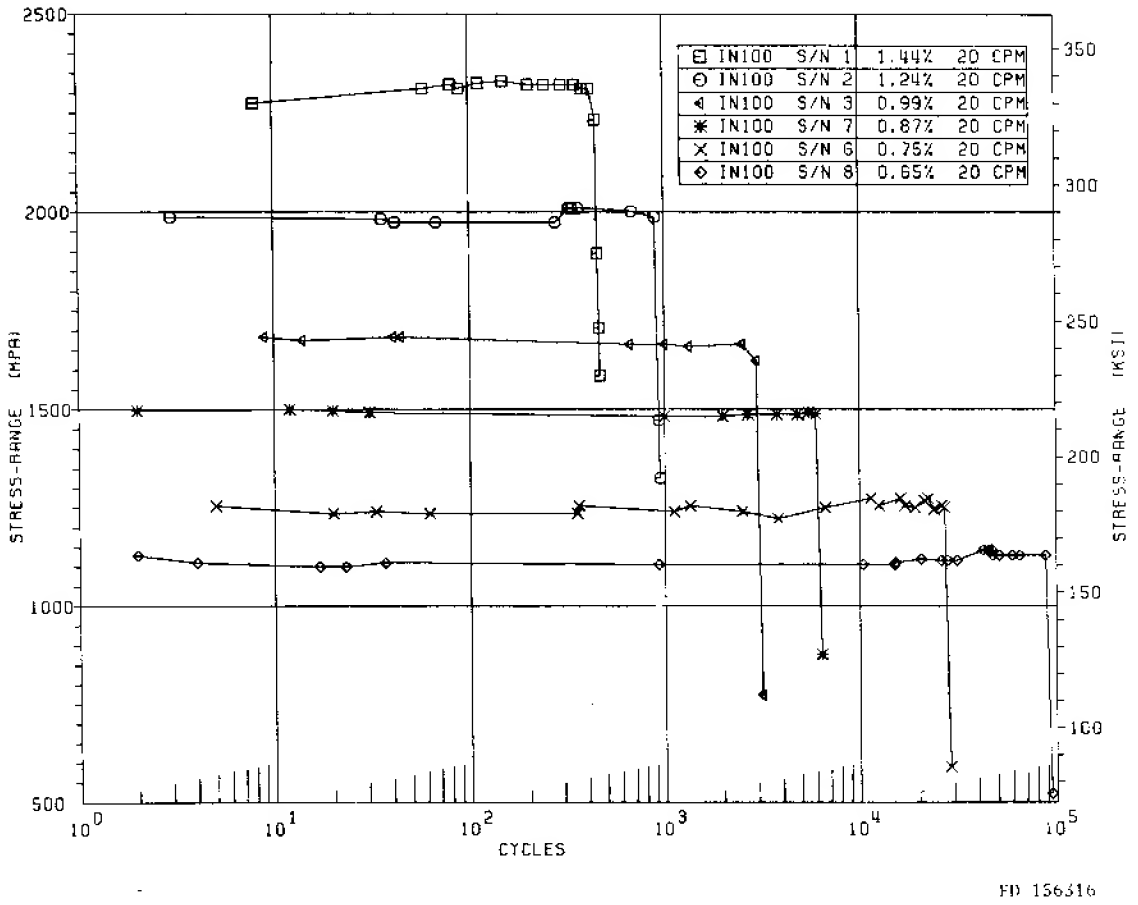

Figure 47. Stress Range vs Cycles for IN 100 (0.33 Hz Tests, R_ϵ = 0)

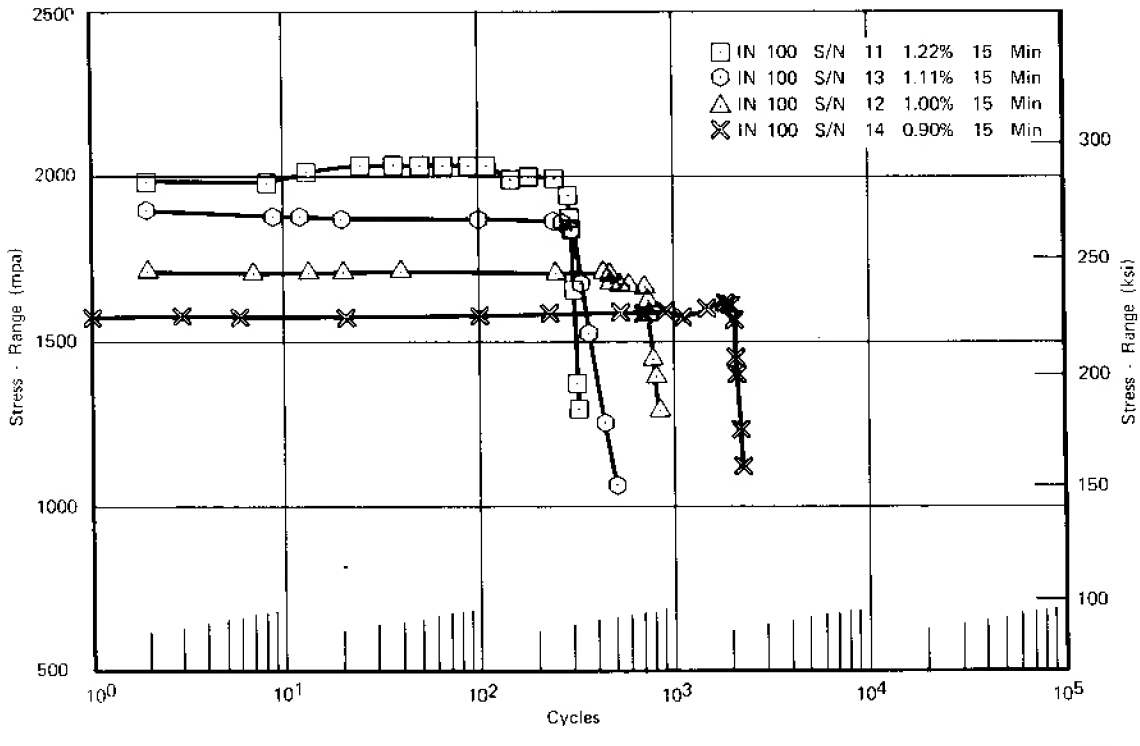

Figure 48. Stress Range vs Cycles for IN 100 (900-sec Dwell, R_ϵ = 0)

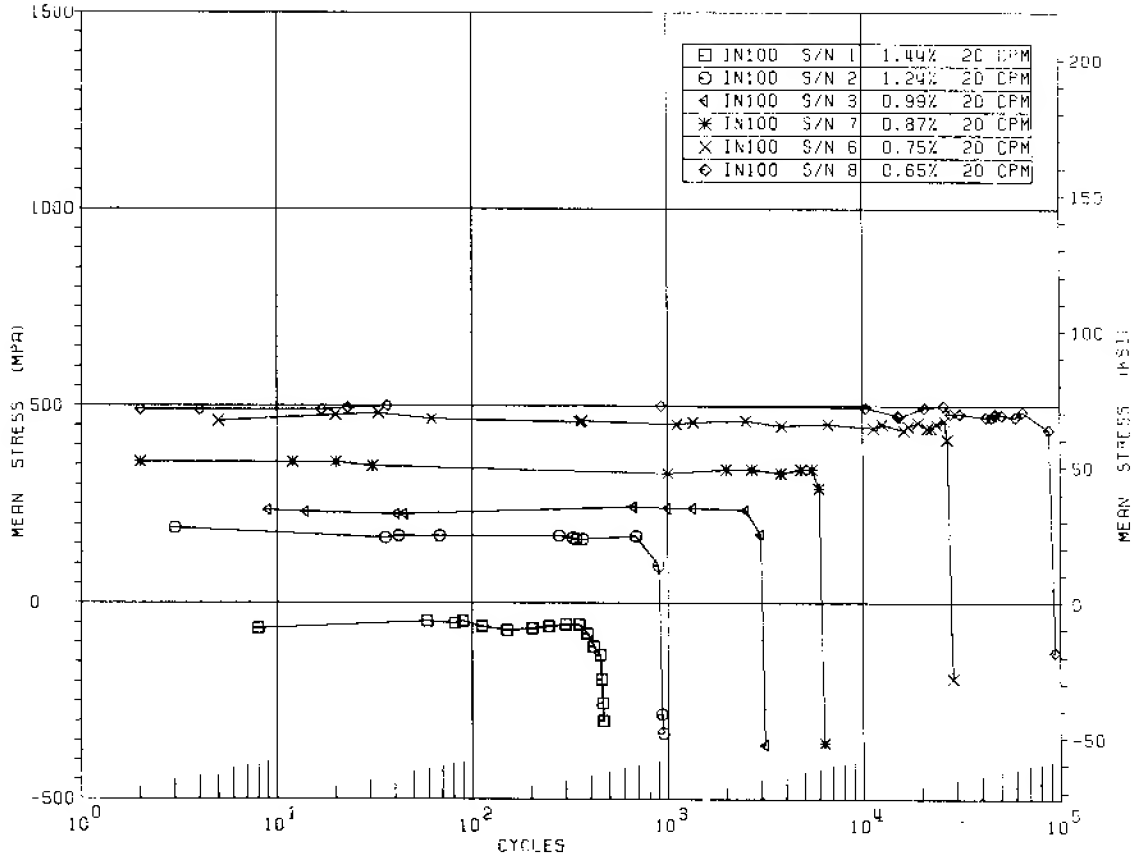

Figure 49. Mean Stress vs Cycles for IN 100 (0.33 Hz Tests, R_ϵ = 0)

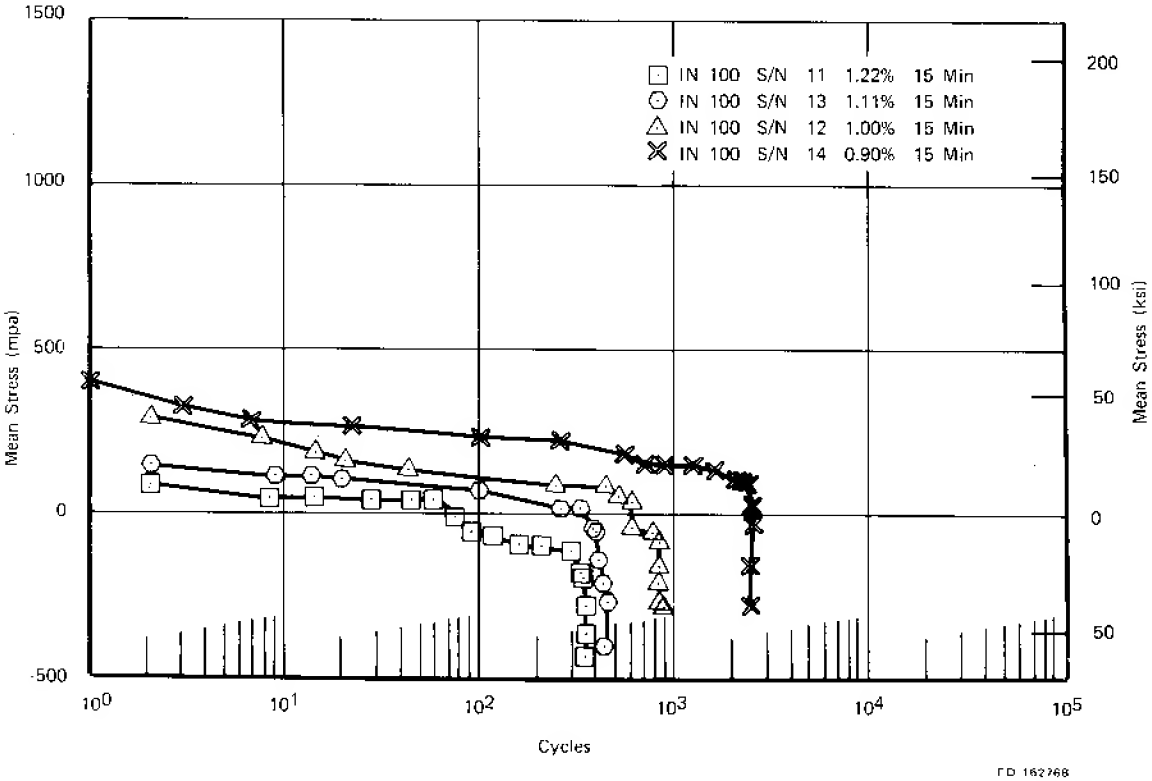

Figure 50. Mean Stress vs Cycles for IN 100 (900-sec Dwell, R_ϵ = 0)

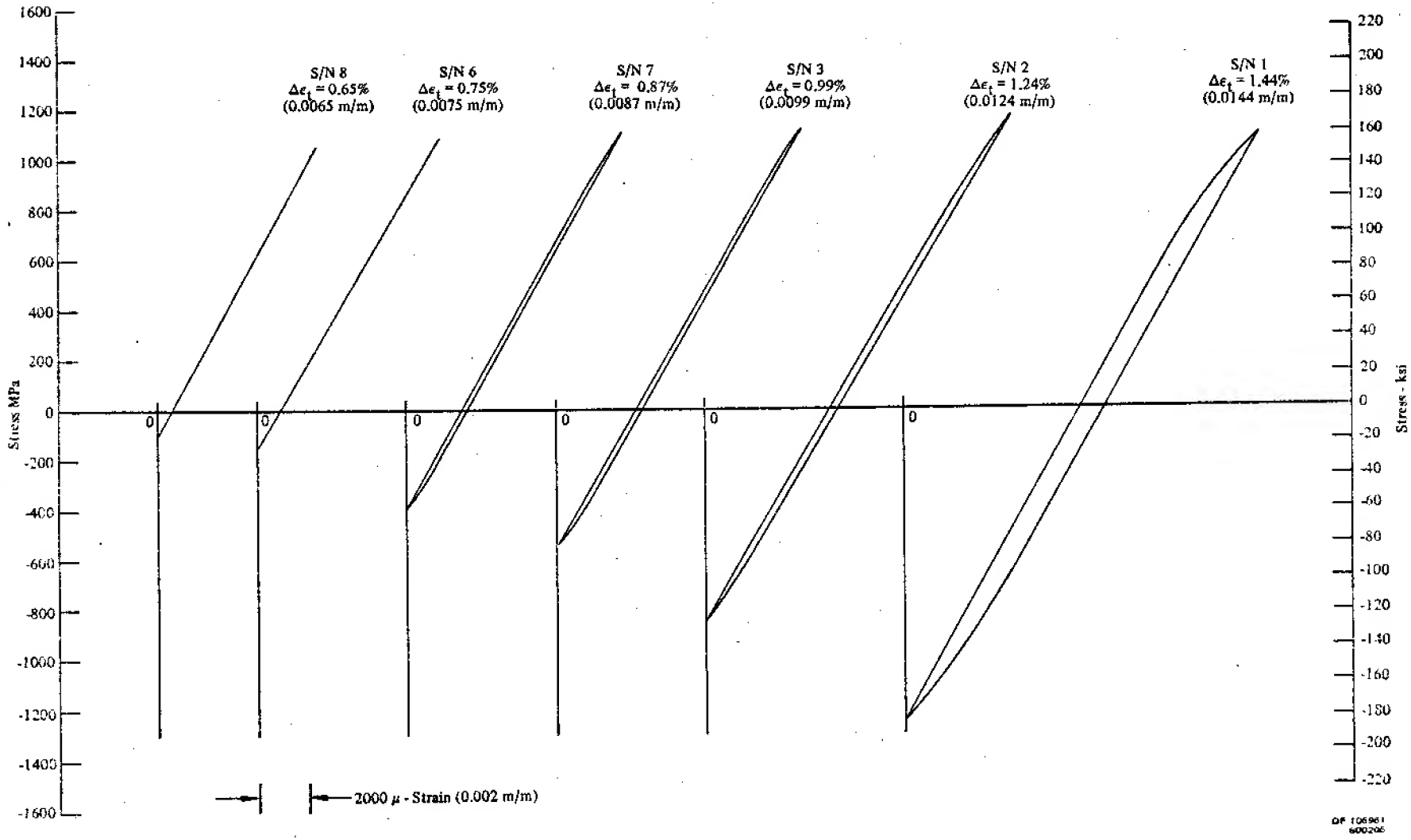

Figure 51. Typical Hysteresis Loops, IN 100 Cyclic Tests

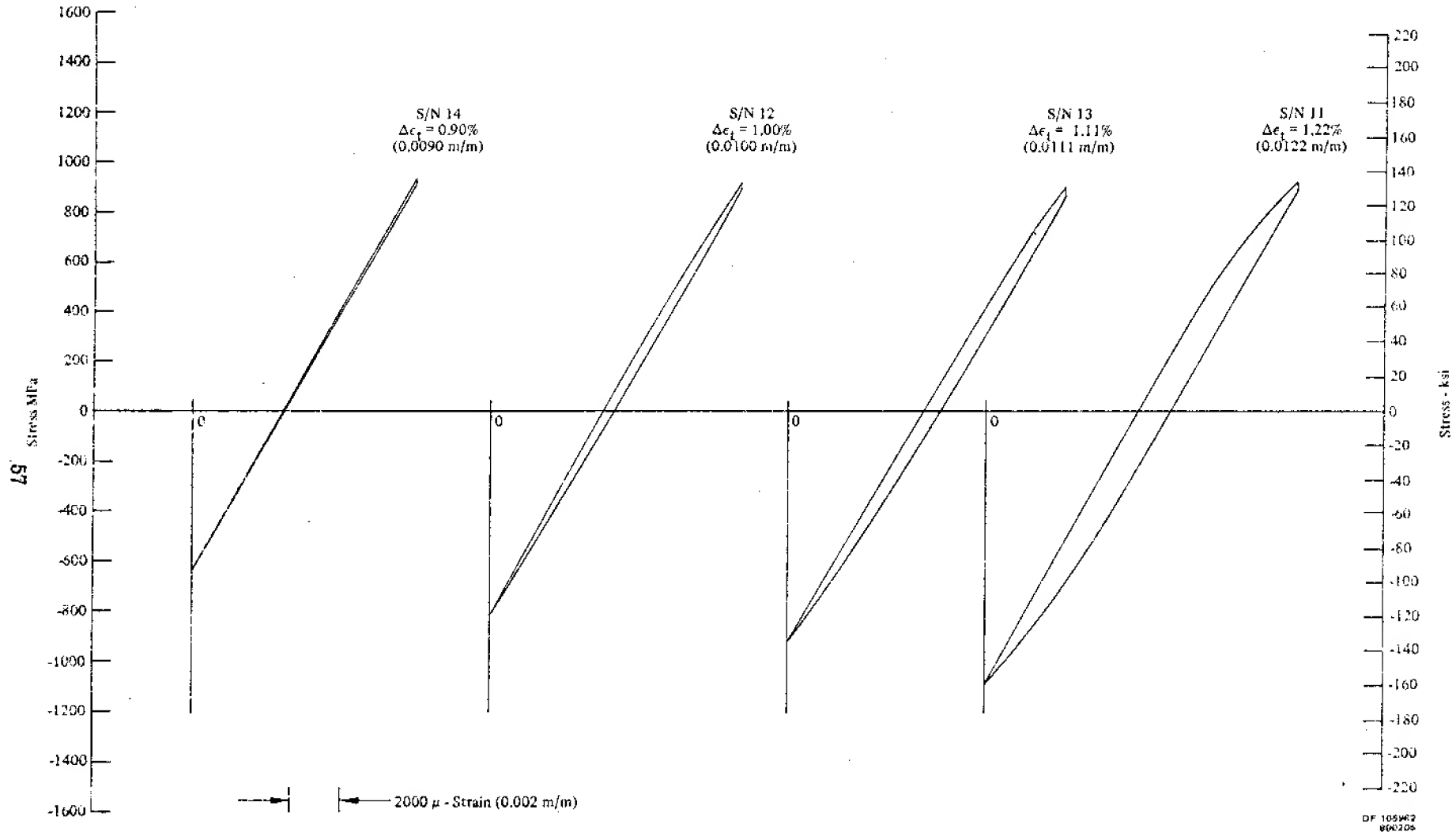

Figure 52. Typical Hysteresis Loops, IN 100 Dwell Tests

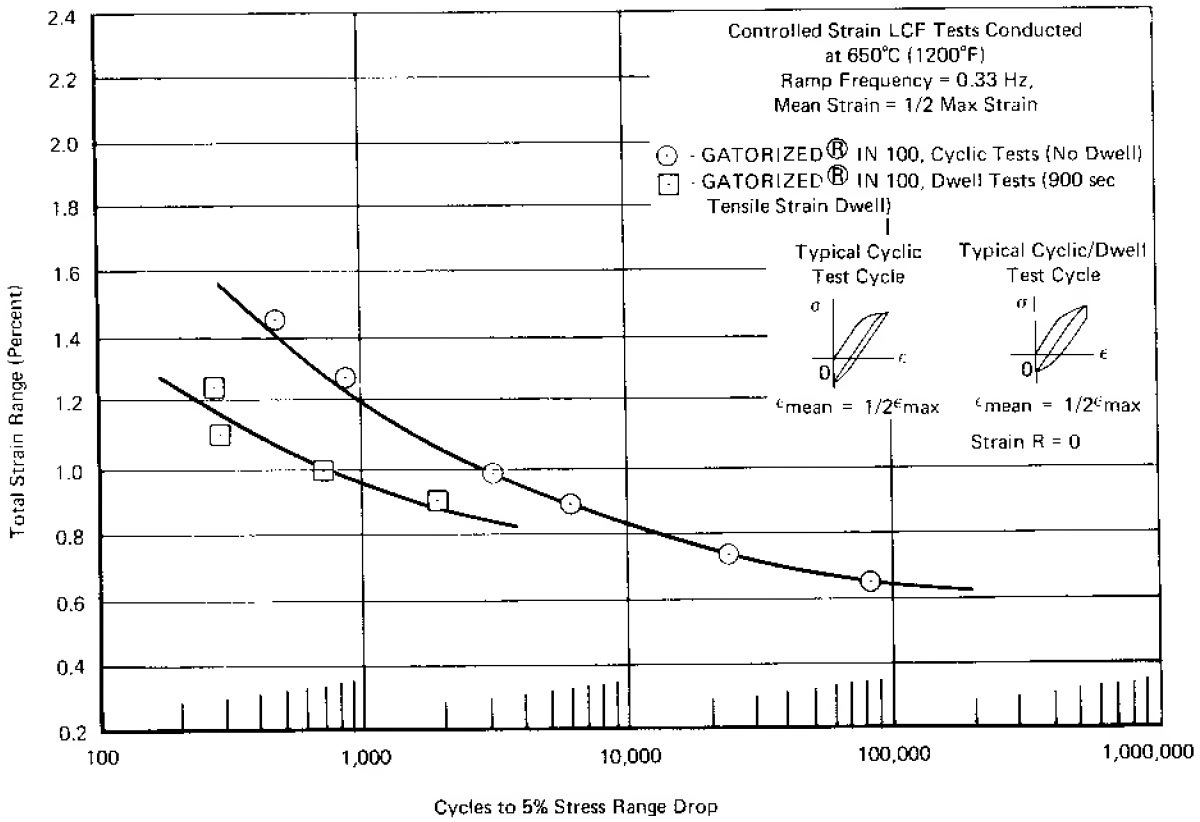

Figure 53. Strain Control LCF Results for GATORIZED® IN 100 (N_5 Life)

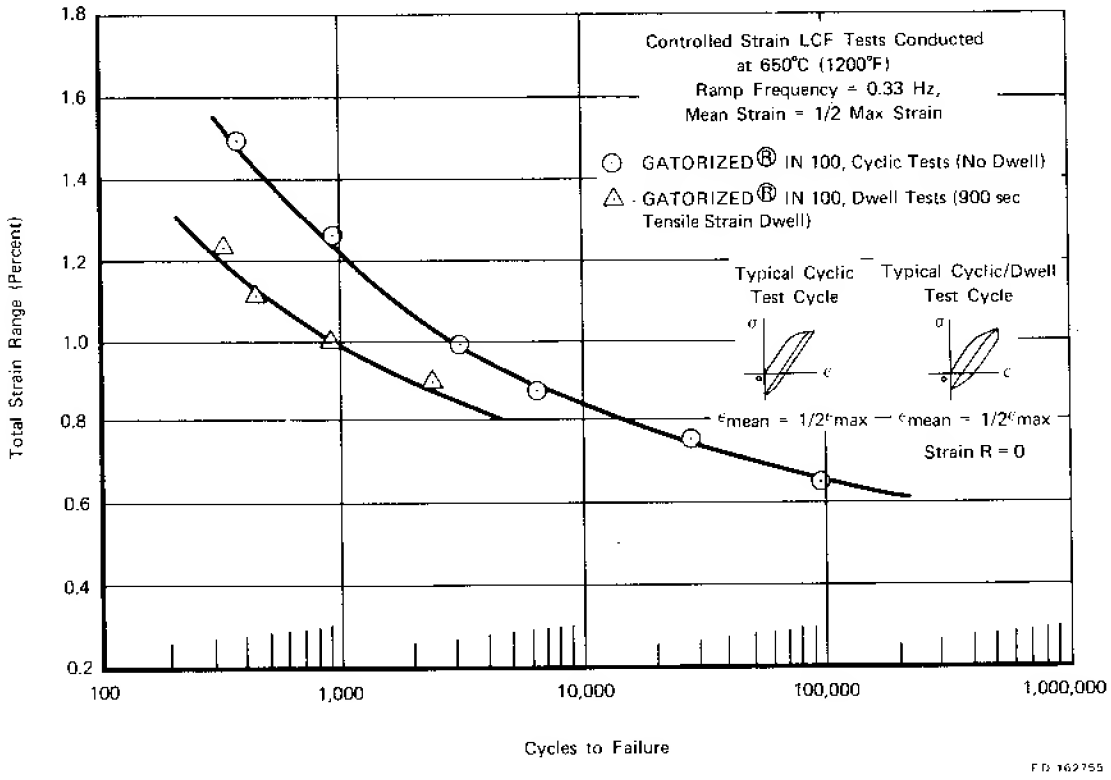

Figure 54. Strain Control LCF Results for GATORIZED® IN 100 (Failure)

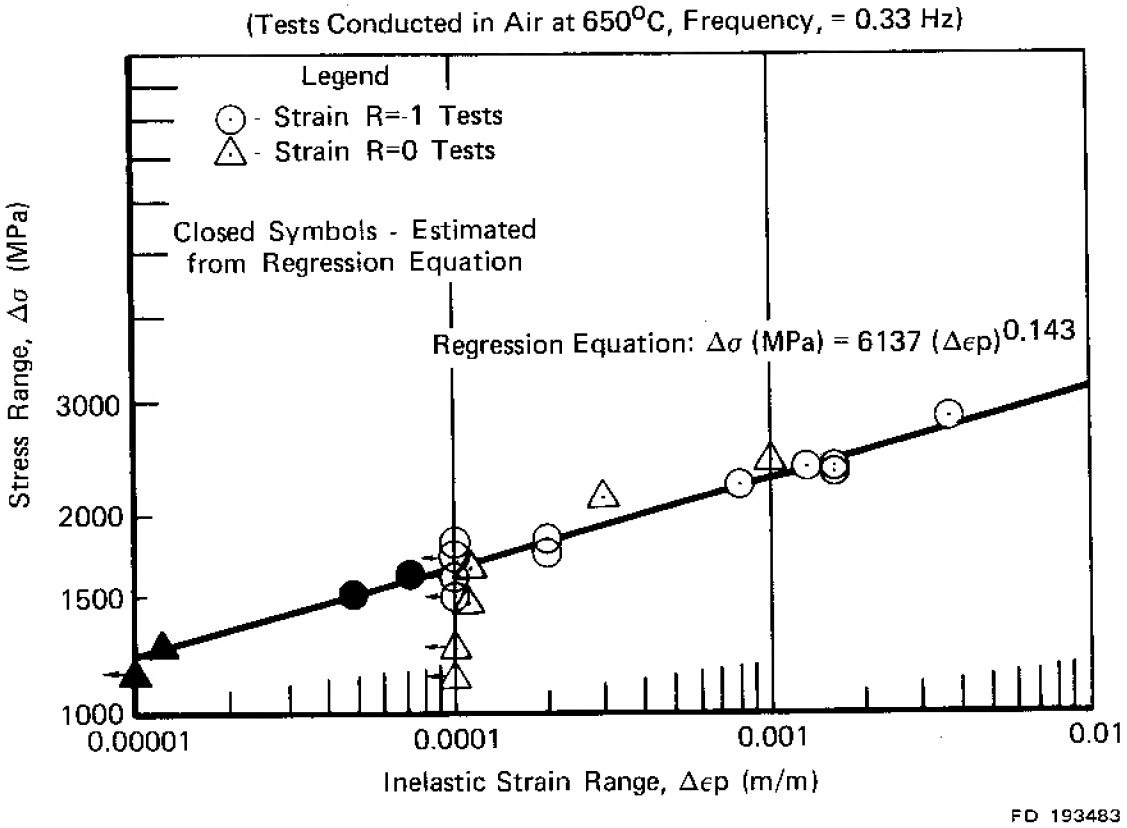

Figure 55. Stress Range vs Inelastic Strain Range for IN 100

Three cyclic tests and one cyclic/dwell test were completed with test results tabulated in table 13. The test data indicate that there were no significant differences in the LCF properties of the two forgings.

Stress range vs cycles for each test was determined from load-strain hysteresis loops generated periodically during the test, as shown in figures 56 and 57 for the cyclic tests and figures 58 and 59 for the cyclic/dwell tests. Test data generated during this program are isolated in figures 56 and 58 and are shown superimposed on previous test data (NAS3-20367) for comparison in figures 57 and 59.

Total strain range vs cycles to 5% stress range drop and cycles to complete separation are detailed in figures 60 and 61. Data from earlier contract work are presented for comparison. It can be observed that there are no significant differences in the LCF properties of the two forgings.

Test specimens had been machined from a cross-roll pancake forging of NASA IIB-7 to study the effect of strain R ratio. This pancake material was forged from a HIP-processed powder billet from heat KR-376 which is the same heat of material used for testing of this alloy under Contract NAS3-20367.

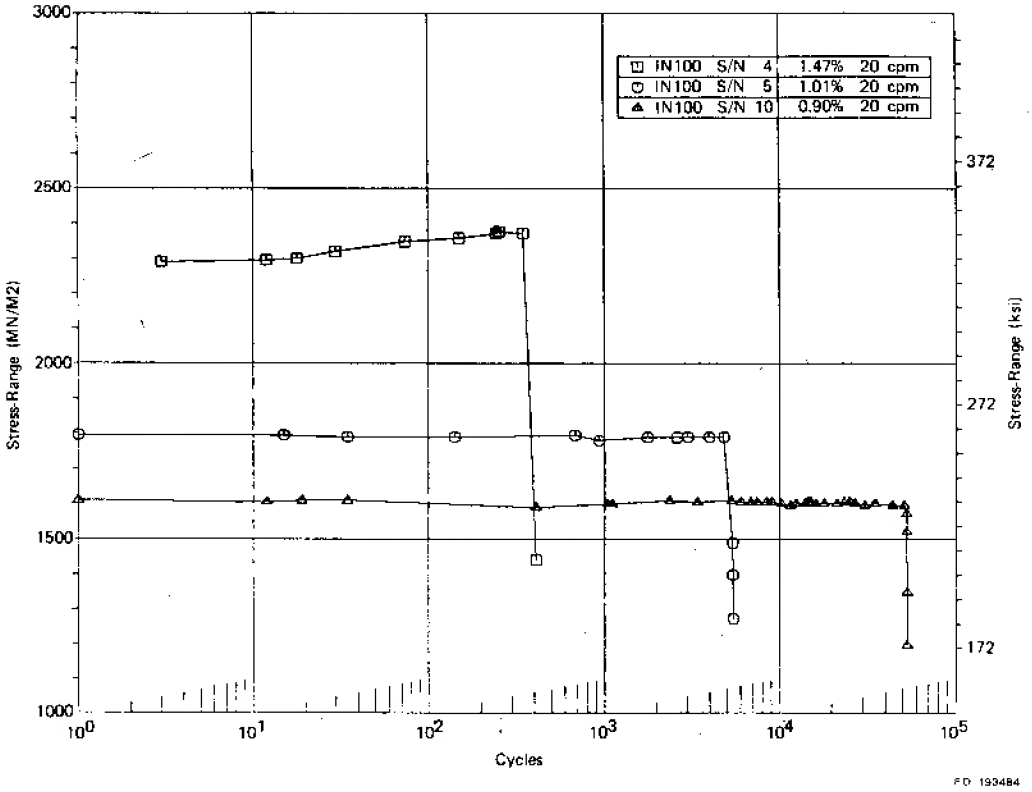

Figure 56. Stress Range vs Cycles for IN 100 (0.33 Hz, R_ϵ = -1)

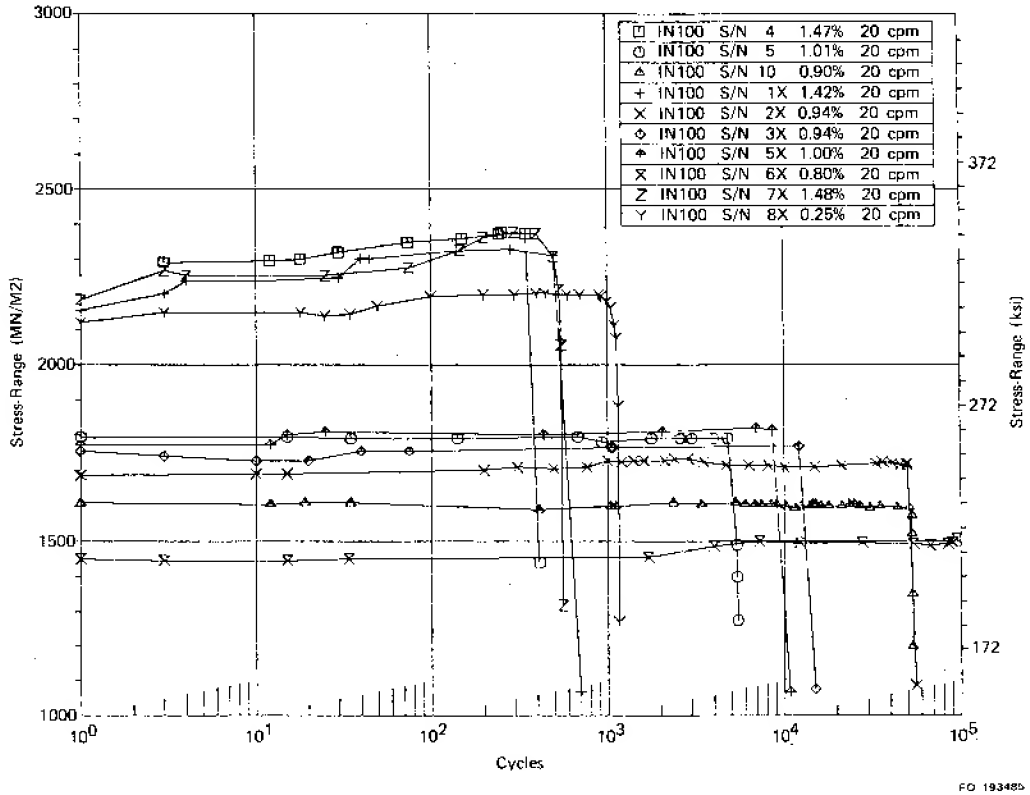

Figure 57. Composite Plot of Stress Range vs Cycles for IN 100 for Comparison with Previous Contract (NAS3-20367) Test Results (0.33 Hz, R_ϵ = -1)

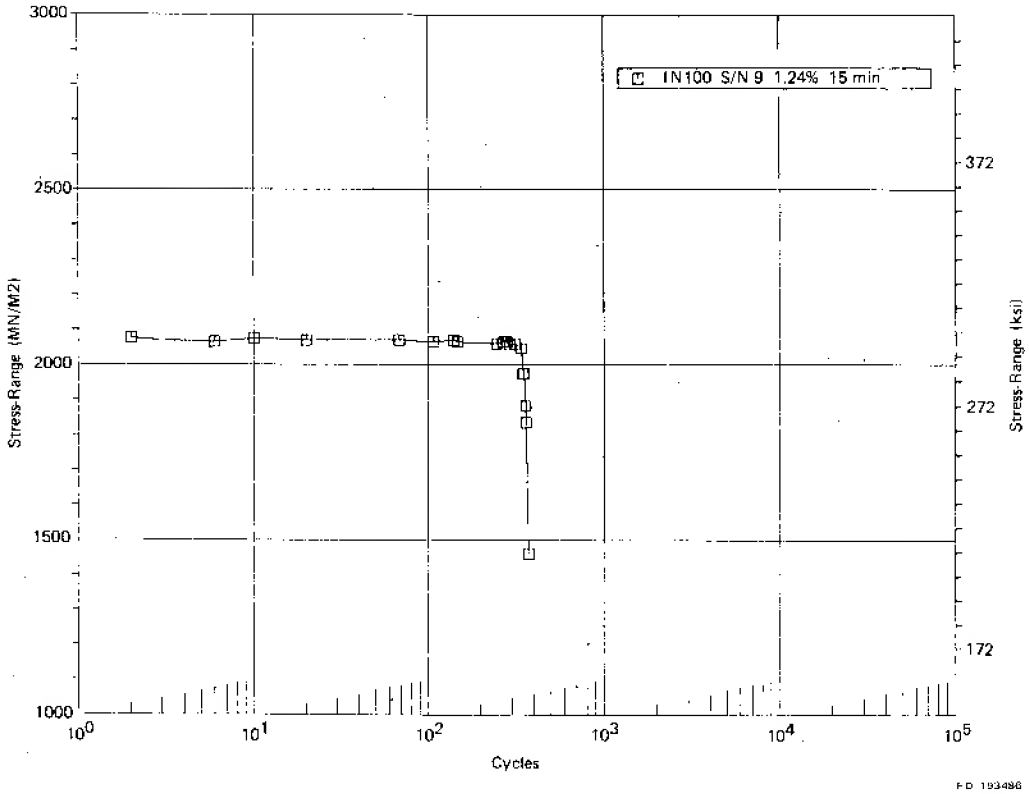

Figure 58. Stress Range vs Cycles for IN 100 (900-sec Dwell, R_ϵ = -1)

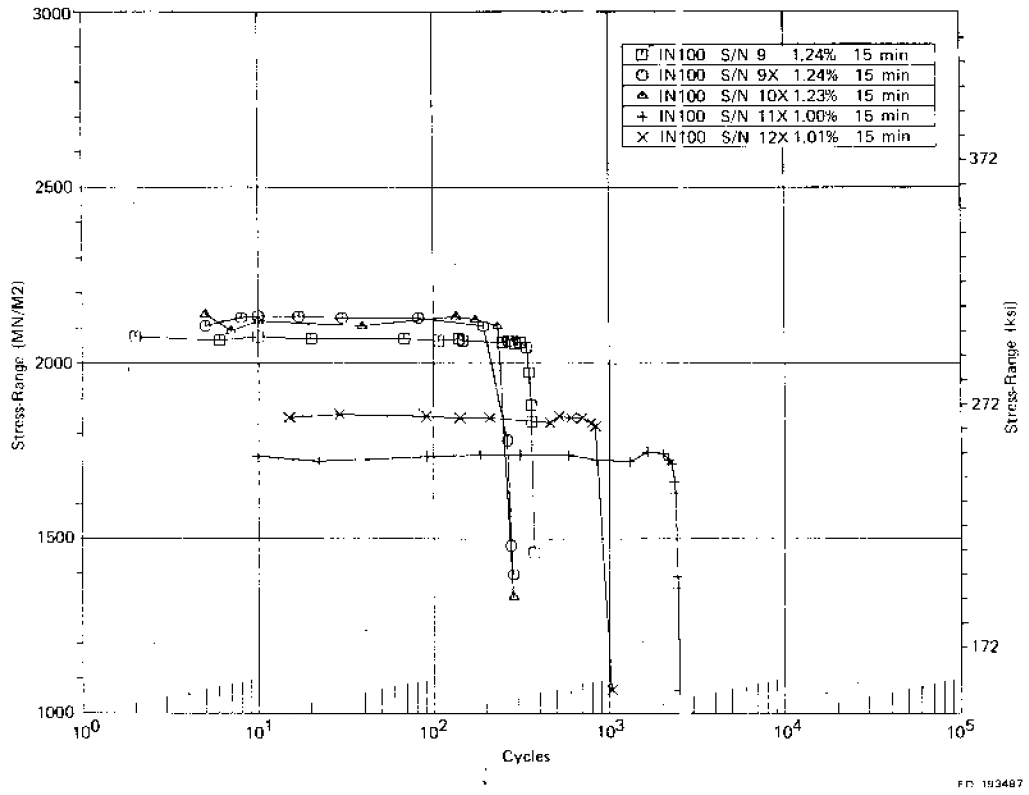

Figure 59. Composite Plot of Stress Range vs Cycles for IN 100 for Comparison with Previous Contract (NAS3-20367) Test Results, (900-sec Dwell, R_ϵ = -1)

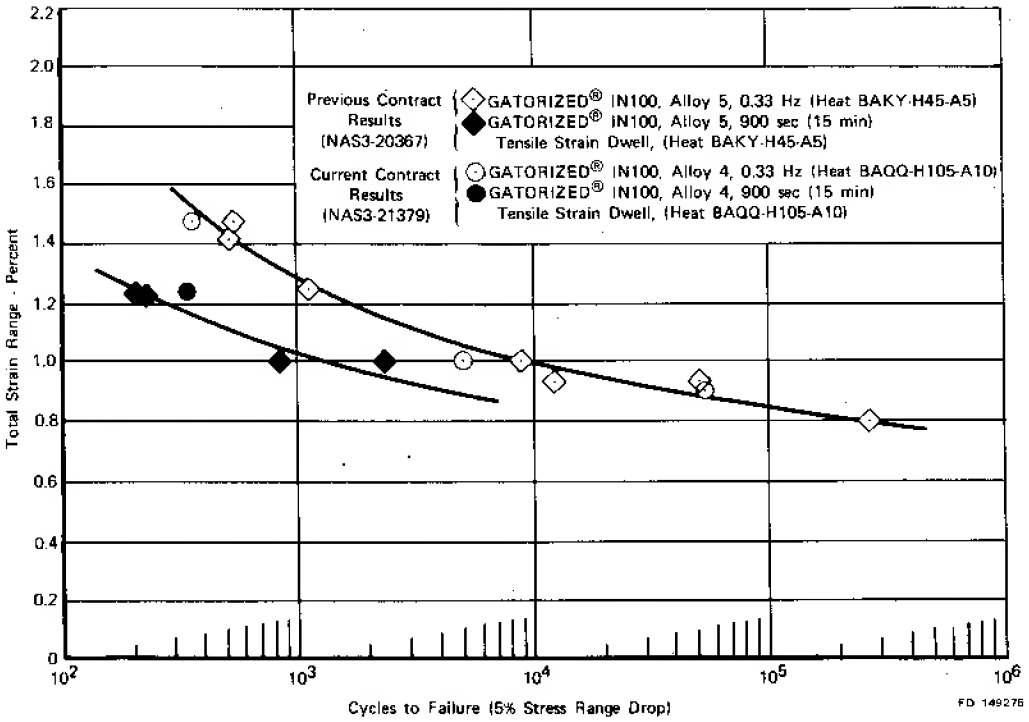

Figure 60. Strain Control LCF Results for Alloy 4, GATORIZED® IN 100, for Comparison with Previously Generated Contract (NAS3-20367) Test Results (R_ϵ = -1, N_5 Life)

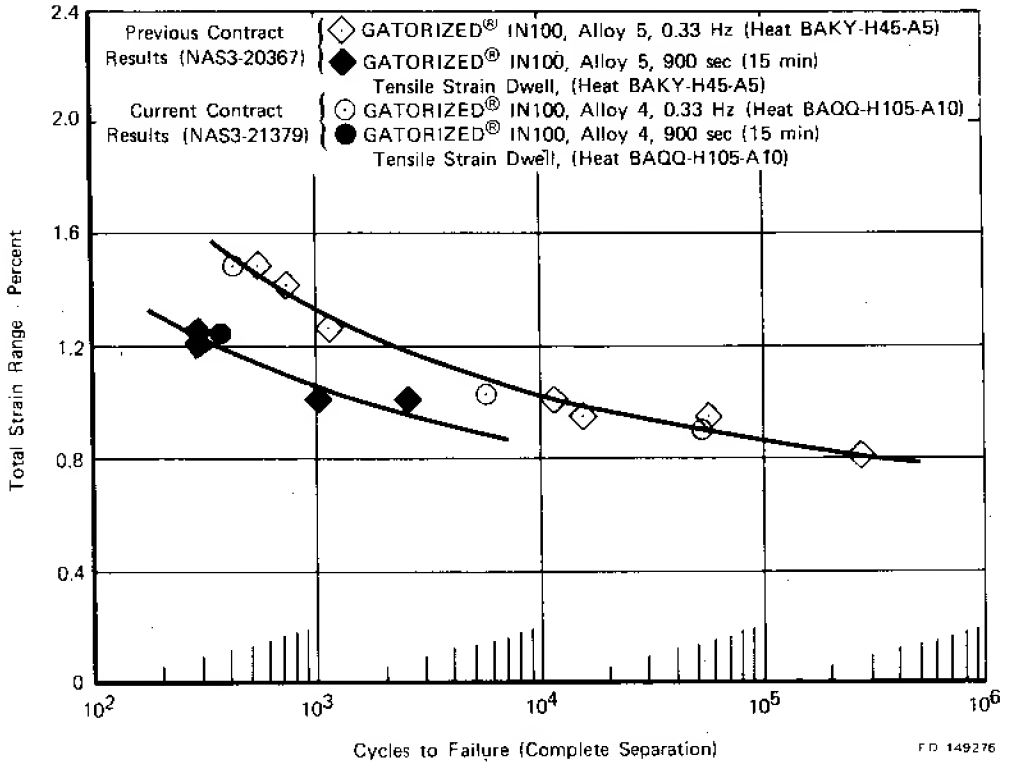

Figure 61. Strain Control LCF Results for Alloy 4, GATORIZED® IN 100, for Comparison with Previously Generated Contract (NAS3-20367) Test Results (R_ϵ = -1, Failure)

Five cyclic tests with a fully reversed strain cycle (strain R = -1) were conducted to determine if there was any billet-to-billet variation between this material and that which was previously tested under Contract NAS3-20367. The data are plotted in figures 62 and 63. The data generally agree; however, there is some divergence at the lower strain ranges. The two test points at approximately 1.0% strain range had much longer LCF life than expected. Upon failure, the fractures were examined and the initiation sites were found to be internal at probable nonmetallic inclusions (see figure 64). It has been experienced with high strength powder alloys that, at low strain ranges, the failures frequently initiate at internal inclusions, and the LCF lives associated with this type fatigue initiation are often longer than normally expected for surface initiations.

Billet-to-billet comparison data were examined statistically with a confidence level of 95%. Differences were found to be insignificant. Stress range and mean stress vs life plots are shown for this testing in figures 65 and 66. The test results for NASA IIB-7 appear in table 14. Subsequent strain R ratio tests were then run and reported in the "Effects of Mean Stress and Mean Strain" section of this report.

High Strain Range Tests

Five tests have been run on the five alloys (one test of each) investigated under the previous NASA contract NAS3-20367. The five alloys were: Waspaloy, wrought Astroloy, NASA IIB-7, HIP Astroloy, and IN 100. Strain ranges under the previous contract were necessarily low in order to generate test data in the long life regime typical of military aircraft engine operating conditions. These tests generally yielded low inelastic strain ranges, and made the inelastic strain vs life regression lines highly dependent on extremely small strain values (less than 0.0001 m/m), which are below the resolution and accuracy of the test equipment. In order to increase confidence in the slopes of these curves ($\Delta\epsilon_i$ vs life), these tests were conducted with high strain ranges ($\Delta\epsilon_t \sim 2.0\%$) and consequently with large inelastic strain ranges ($\Delta\epsilon_i$). The tests were cyclic (0.33 Hz) with a fully-reversed strain-time waveform, as shown in figure 13. Test results are shown in table 15. Data analysis proceeded to reevaluate the strain range vs life curves generated under the earlier contract using this new data. New strain range vs failure life curves for these five alloys are presented in figures 67 through 71. New life equations and coefficients are given in the Alloy Comparison section of this report.

Effects of Mean Stress and Mean Strain

Strain R Ratio Effects

$$R_\epsilon = \frac{\text{minimum strain}}{\text{maximum strain}}$$

Testing of Waspaloy and IN 100 was conducted at $R_\epsilon = 0$ for comparison with earlier work (NAS3-20367) on these same alloys at $R_\epsilon = -1$. In general, strain R ratio imparts little effect at high total strain ranges and large effects at lower strain ranges. At the lower strain ranges, mean stress is generally high. At high strain ranges, mean stress approaches zero. This effect of decreasing mean stress with increasing strain range (for all-tensile strain tests) is shown in figure 72. Note also in this diagram that yield stress is a critical factor in determining at what total strain range the mean stress reduction begins.

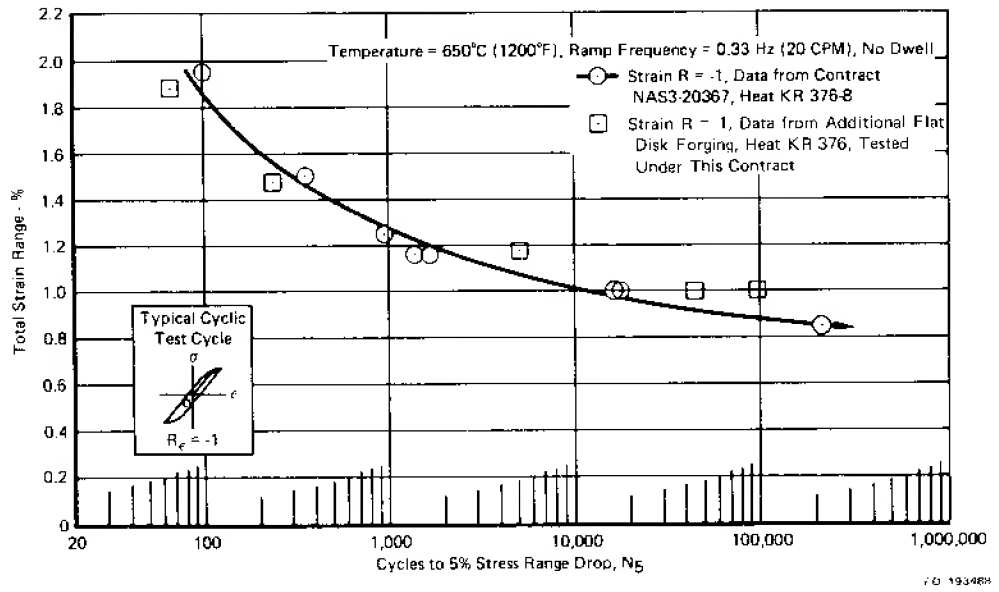

Figure 62. Billet-to-Billet Comparison for Supplementary Strain Control LCF Testing of NASA IIB-7 (N_5 Life)

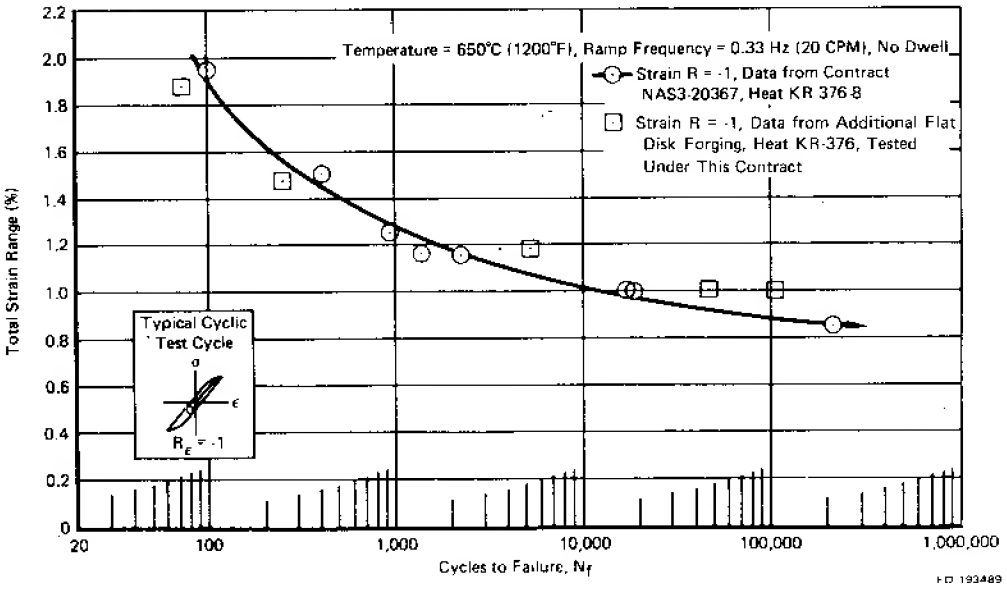

Figure 63. Billet-to-Billet Comparison for Supplementary Strain Control LCF Testing of NASA IIB-7 (Failure)

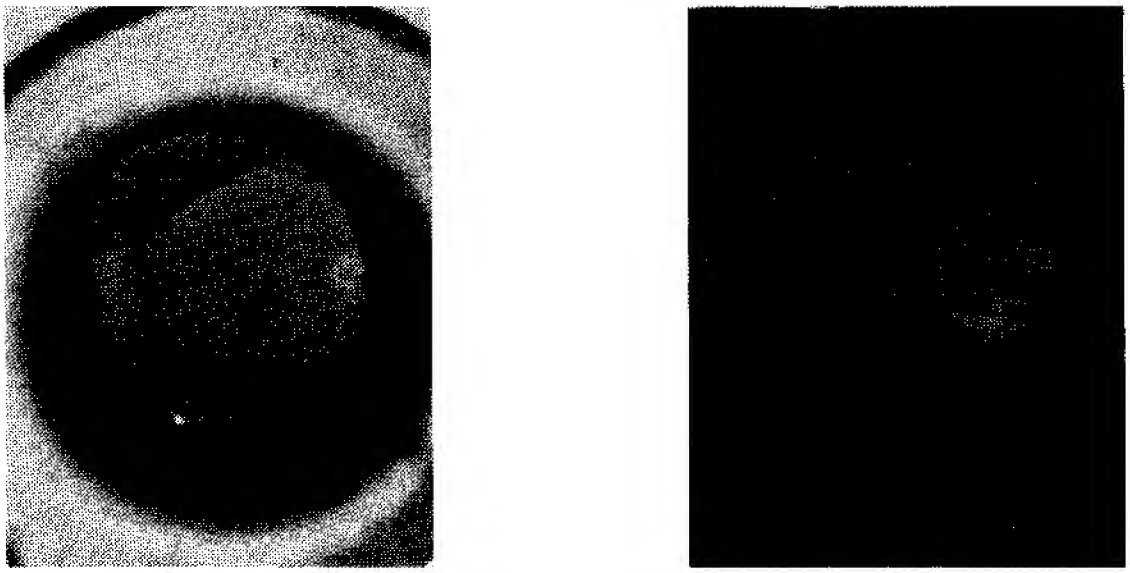

7X 30X

Specimen S/N 3-3, $\Delta\epsilon_t$ = 1.00%, N_f = 104,657 Cycles

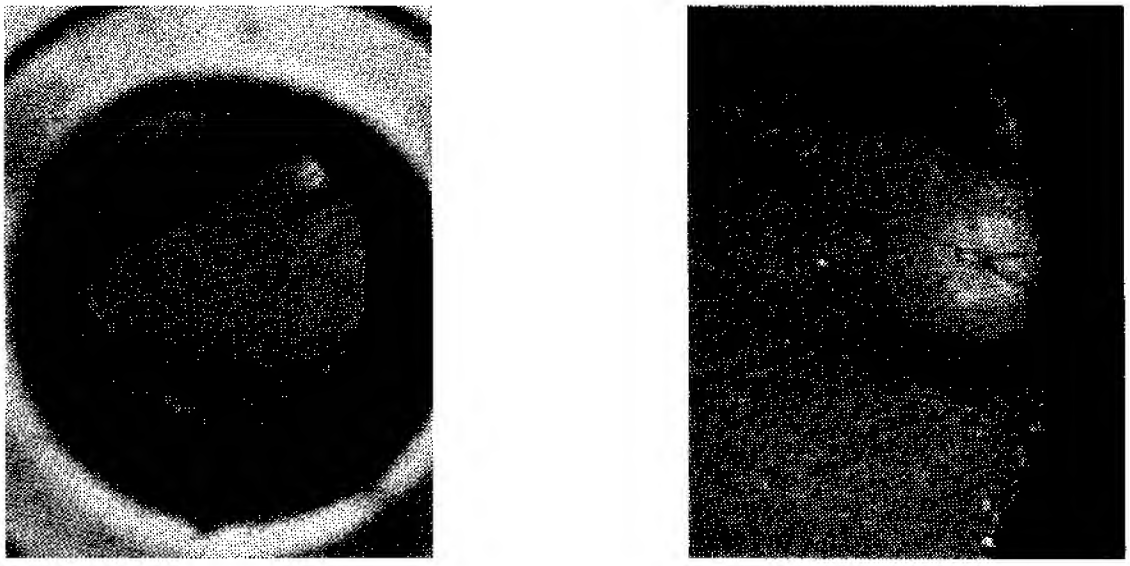

7X 30X

Specimen S/N 3-4, $\Delta\epsilon_t$ = 1.01%, N_f = 46,832 Cycles

FD 193490

Figure 64. Photomacrographs of Fracture Faces on Two NASA IIB-7 LCF Specimens with Failure Sites at Probable Inclusions

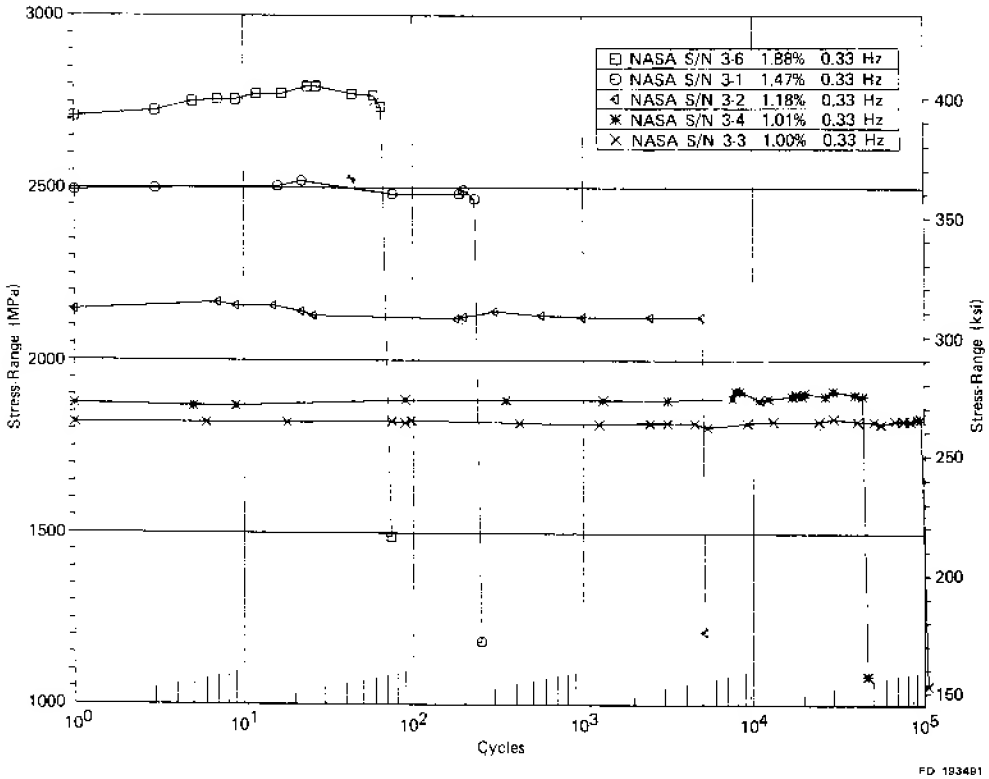

Figure 65. Stress Range vs Cycles for Billet-to-Billet Comparison Supplementary Tests of NASA IIB-7 (0.33 Hz, R_ϵ = -1)

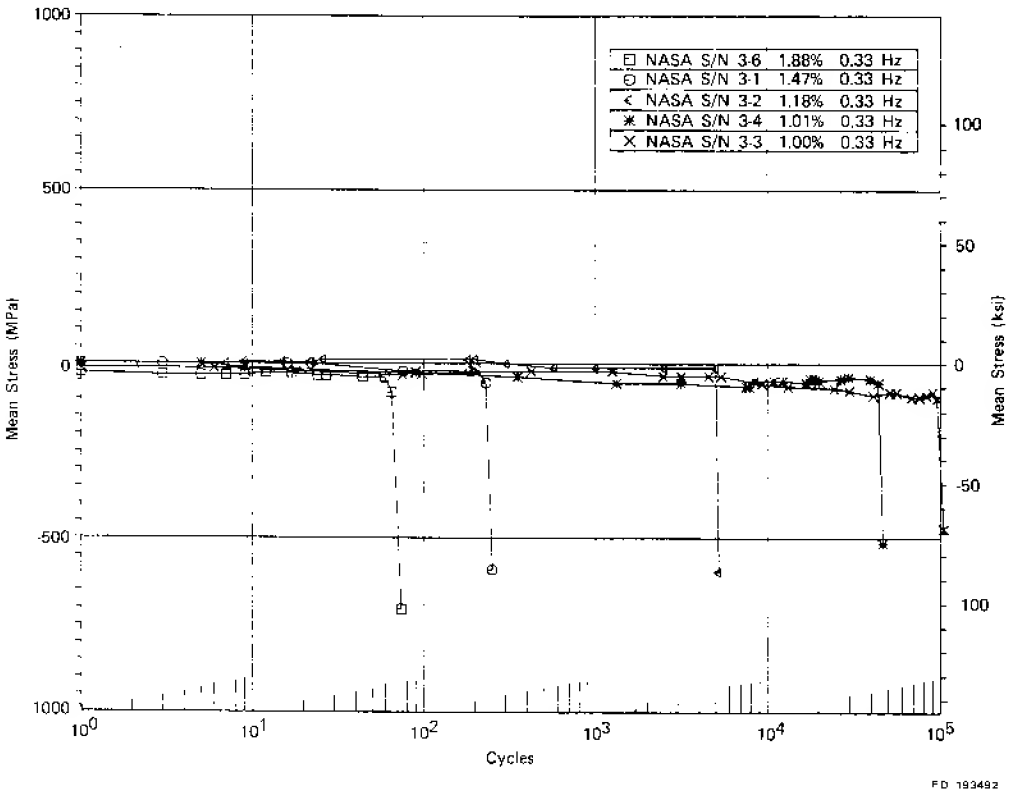

Figure 66. Mean Stress vs Cycles for Billet-to-Billet Comparison Supplementary Tests of NASA IIB-7 (0.33 Hz, R_ϵ = -1)

TABLE 14
CONTROLLED STRAIN LOW-CYCLE FATIGUE TEST RESULTS FOR NASA IIB-7.**
Testing Conducted at 650°C (1200°F)

Spec S/N	Type* Test	Strain R Ratio (min/max)	Strain (m/m at $N_f/2$) Range	Elastic	Inelastic	Creep	Mean Stress at $N_f/2$ MPa	ksi	Stress Range Cycle 1	$N_f/2$	Cyclic Stability	Cycles to Failure $N_5\%$	N_f
3-6	Cyclic	-1	0.0188	0.0157	0.0031	0	33	-4.7	2709 MPa (392.9 ksi)	2795 MPa (405.4 ksi)	Harden	66	74
3-1	Cyclic	-1	0.0147	0.0136	0.0011	0	22	-3.2	2493 MPa (361.6 ksi)	2482 MPa (360.0 ksi)	Stable	232	251
3-2	Cyclic	-1	0.0118	0.0115	0.0003	0	-11	-1.6	2145 MPa (311.1 ksi)	2129 MPa (308.8 ksi)	Stable	5,024	5,216
3-4	Cyclic	-1	0.0101	0.0100	0.0001	0	43	-6.3	1874 MPa (271.9 ksi)	1896 MPa (275.0 ksi)	Stable	44,321	46,832***
3-3	Cyclic	-1	0.0100	0.0099	0.0001	0	-82	-11.9	1841 MPa (267.1 ksi)	1844 MPa (267.4 ksi)	Stable	96,837	104,657***
3-7	Cyclic	0	0.0121	0.0119	0.0002	0	347	50.3	2056 MPa (298.1 ksi)	2080 MPa (301.7 ksi)	Stable	1,645	1,675
3-5	Cyclic	0	0.0099	0.0098	0.0001	0	427	61.9	1852 MPa (268.6 ksi)	1852 MPa (268.6 ksi)	Stable	7,546	8,088***
3-10	Cyclic	0	0.0080	0.0079	<0.0001	0	550	79.7	1414 MPa (205.1 ksi)	1419 MPa (205.8 ksi)	Stable	10,848	11,530***
3-9	Cyclic	0	0.0070	0.0070	<0.0001	0	493	71.4	1261 MPa (182.9 ksi)	1256 MPa (182.1 ksi)	Stable	134,765	148,253***

*Cyclic tests conducted at 0.33 Hz (20 cpm)

**Supplementary tests to determine strain R ratio effects, material taken from a cross-rolled pancake, heat KR-376.

***Failure initiated at an internal inclusion or void.

TABLE 15

CONTROLLED STRAIN LOW-CYCLE FATIGUE RESULTS FOR SUPPLEMENTARY HIGH STRAIN RANGE TESTS CONDUCTED WITH ALLOYS INVESTIGATED UNDER NAS3-20367

Alloy	Spec S/N	Type* Test	Strain R Ratio (min/max)	Strain (m/m at $N_f/2$)				Mean Stress at $N_f/2$		Stress Range		Cyclic Stability	Cycles to Failure	
				Range	Elastic	Inelastic	Creep	MPa	ksi	Cycle 1	$N_f/2$		$N_5\%$	N_f
Waspaloy	11	Cyclic	-1	0.0193	0.0117	0.0076	0	-17	-2.5	2112 MPa (306.3 ksi)	2027 MPa (294.0 ksi)	Soften	320	352
Wrought Astroloy	13A	Cyclic	-1	0.0198	0.0147	0.0051	0	-55	-7.9	2461 MPa (357.0 ksi)	2636 MPa (382.3 ksi)	Harden	173	176
NASA IIB-7	13B	Cyclic	-1	0.0196	0.0159	0.0037	0	-28	-4.1	2856 MPa (414.2 ksi)	2884 MPa (418.3 ksi)	Stable	100	102
HIP Astroloy	CB-16	Cyclic	-1	0.0191	0.0133	0.0058	0	-28	-4.0	2170 MPa (314.8 ksi)	2321 MPa (336.6 ksi)	Harden	248	261
IN 100	13	Cyclic	-1	0.0191	0.0154	0.0037	0	-69	-10.0	2628 MPa (381.1 ksi)	2835 MPa (411.2 ksi)	Harden	140	146

*Cyclic tests conducted at 0.33 Hz (20 cpm), Temperature = 650°C (1200°F).

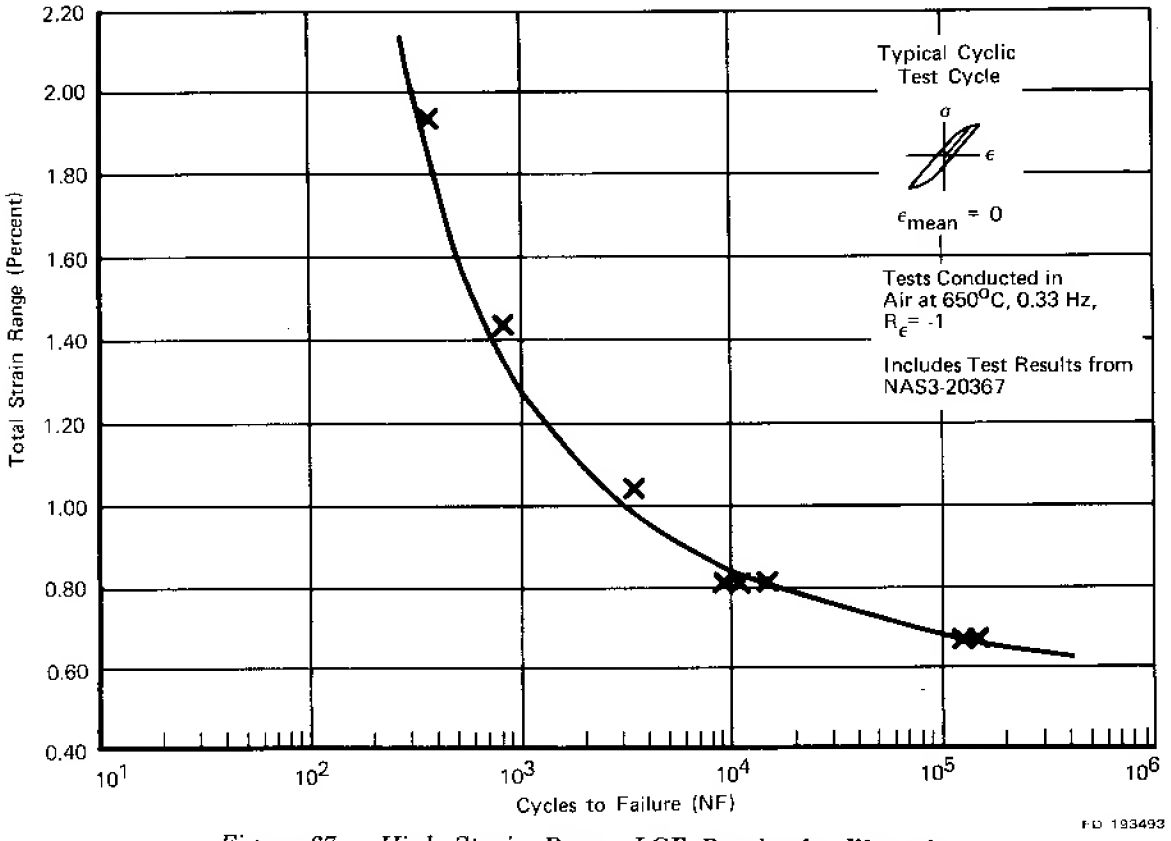

Figure 67. High Strain Range LCF Results for Waspaloy

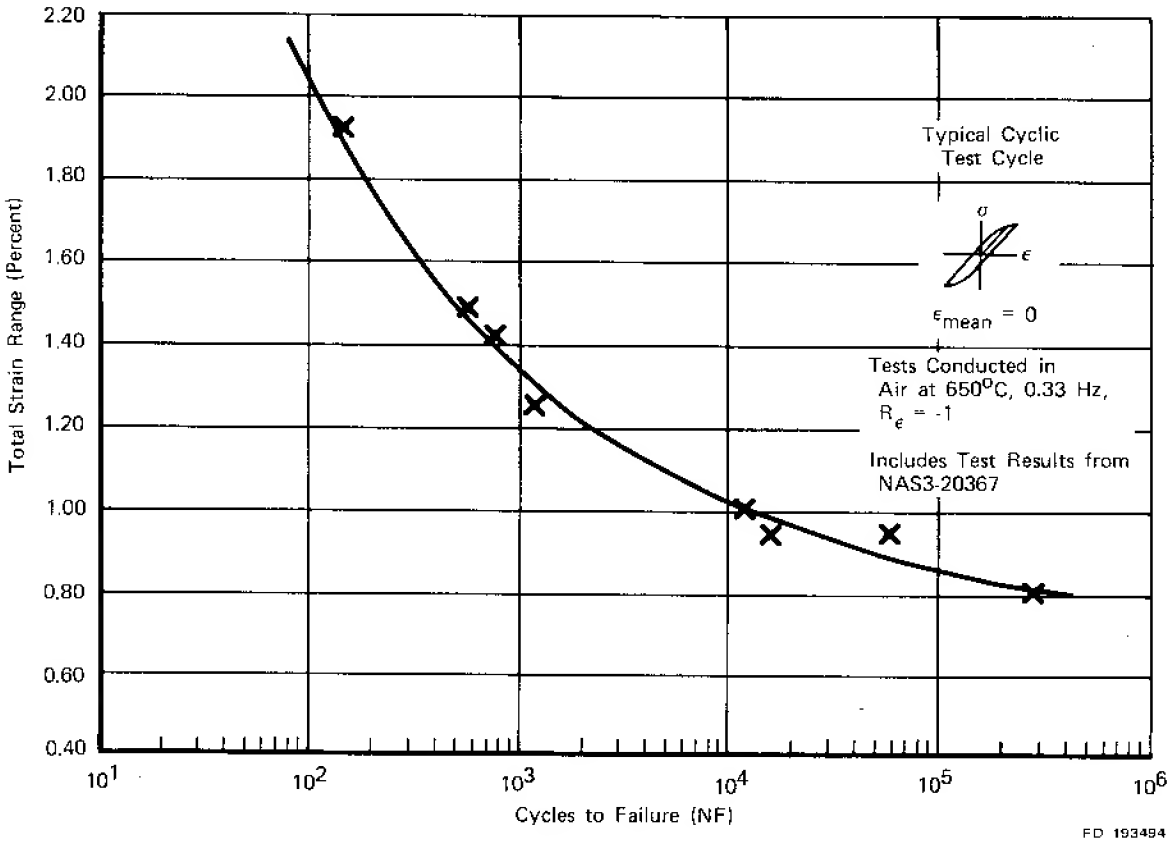

Figure 68. High Strain Range LCF Results for IN 100

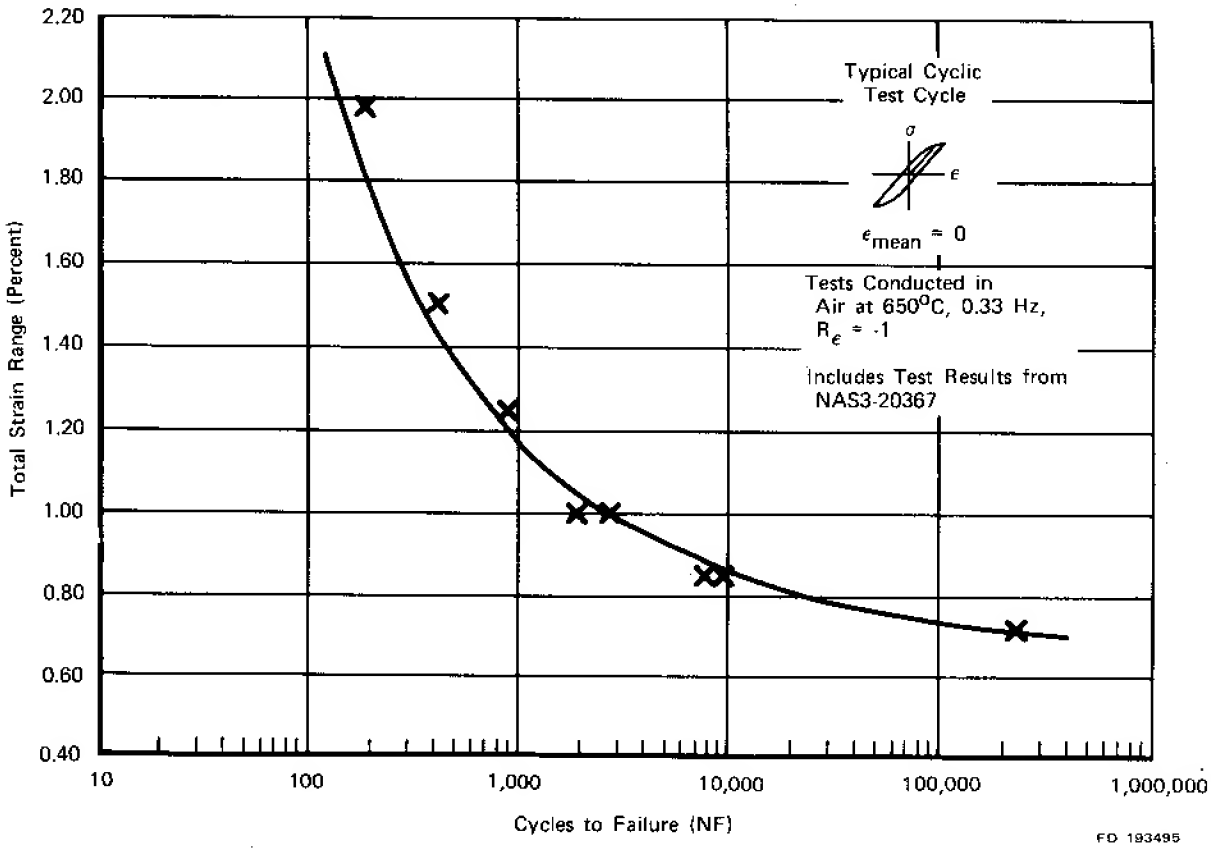

Figure 69. High Strain Range LCF Results for Wrought Astroloy

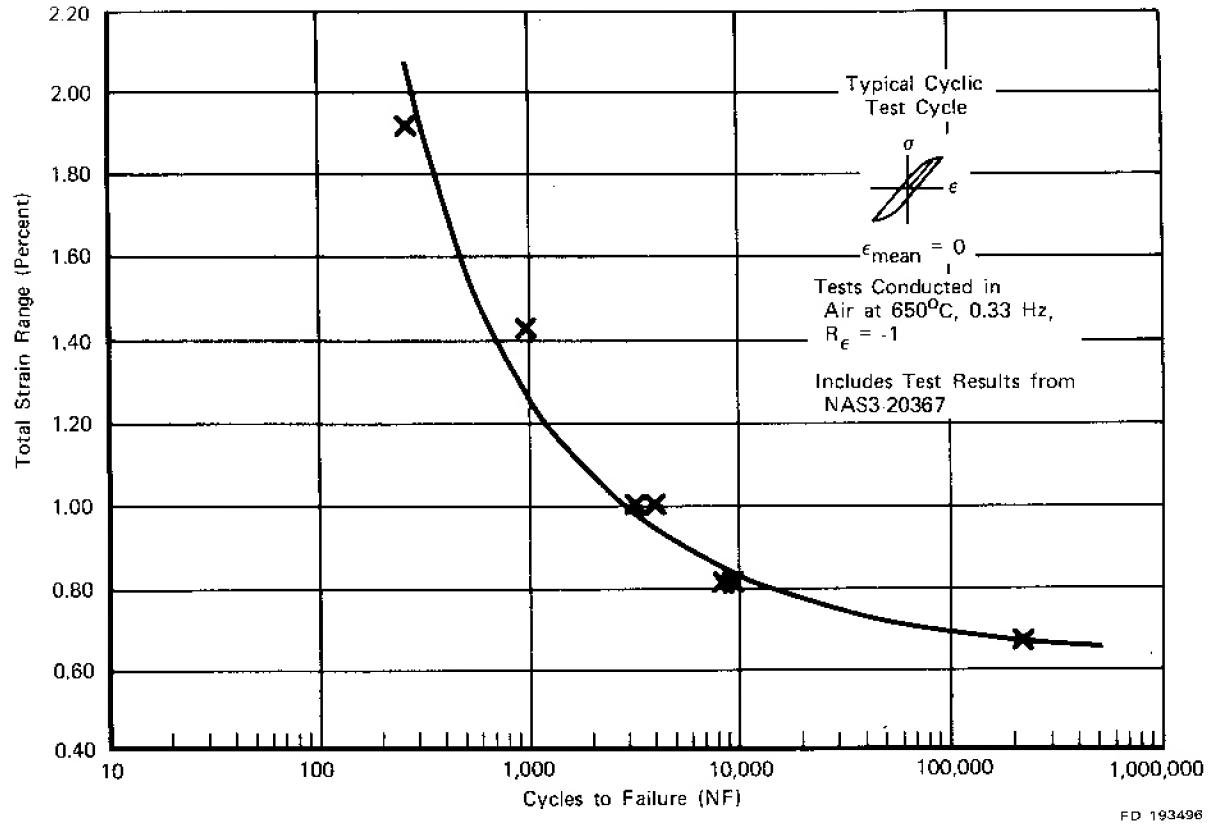

Figure 70. High Strain Range LCF Results for HIP Astroloy

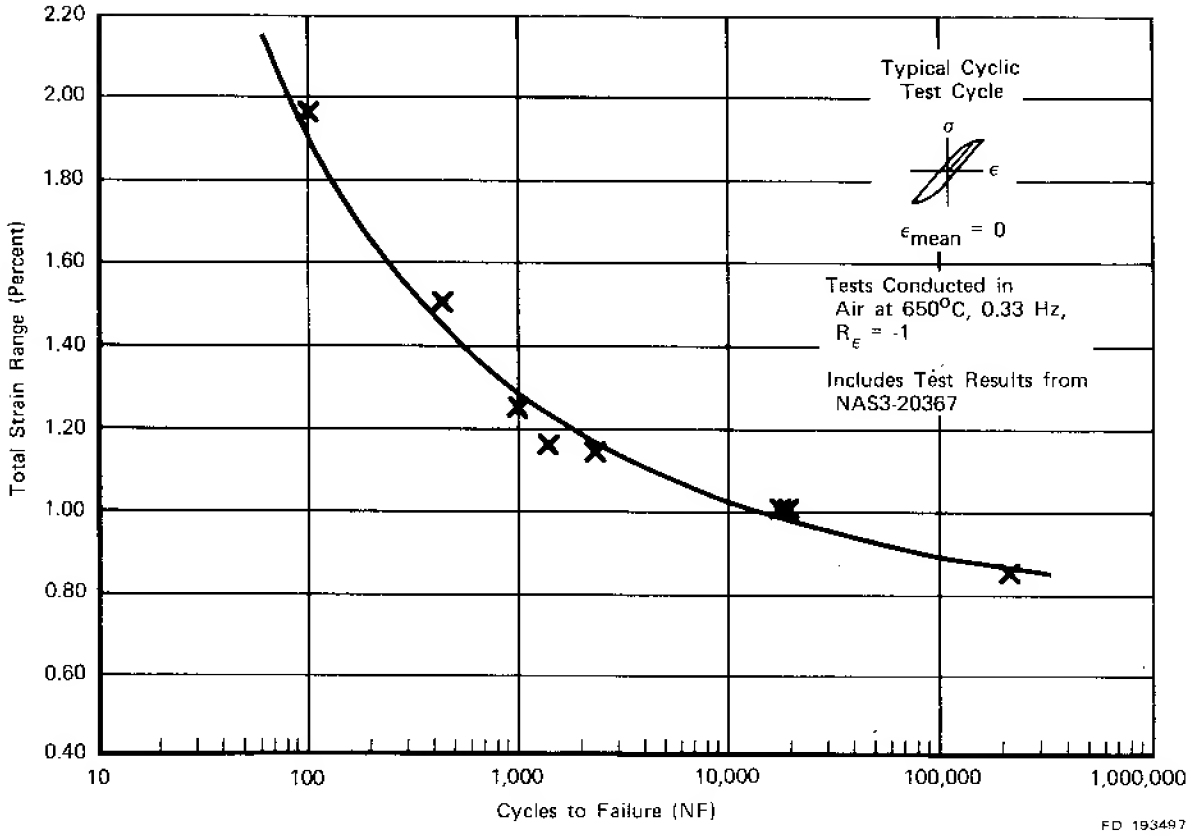

Figure 71. High Strain Range LCF Results for NASA IIB-7

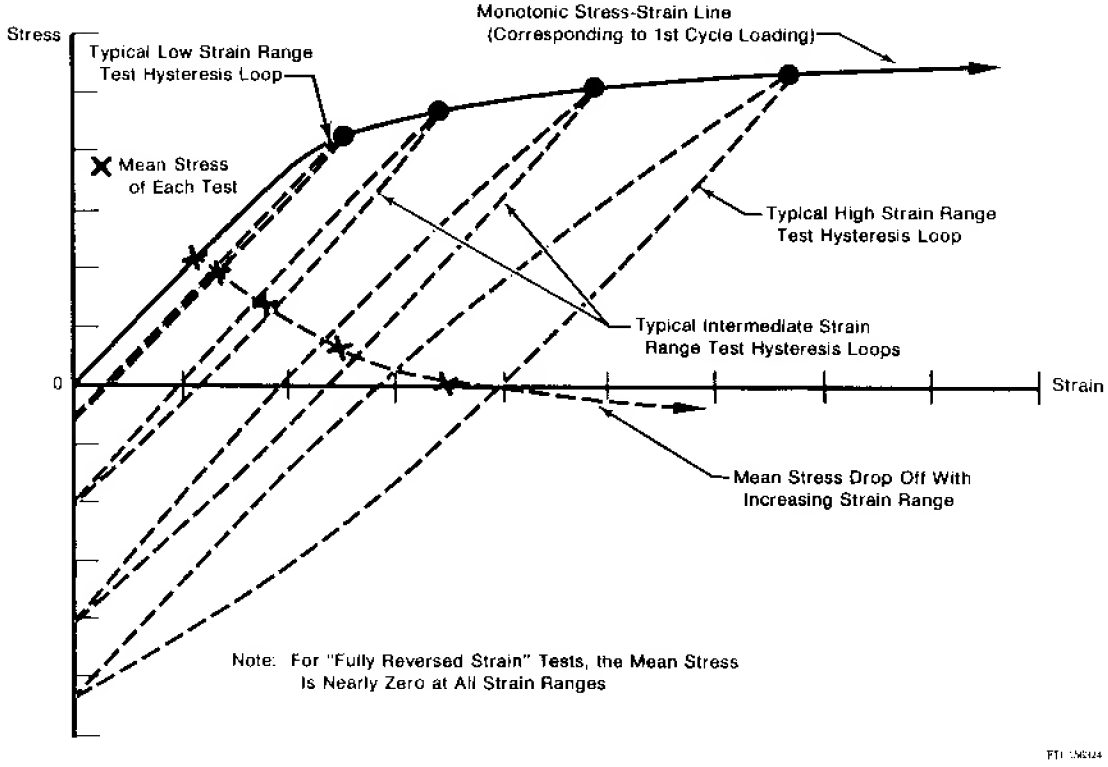

Figure 72. Mean Stress vs Total Strain Range for a Typical Turbine Disk Alloy

Note that for Waspaloy (figure 40) and for IN 100 (figure 49) at the high strain ranges, the mean stresses are near zero due to large first cycle yielding (and similar to mean stress data taken from fully reversed strain tests conducted in the previous Contract NAS3-20367). At the lower strain ranges, the mean stresses significantly deviate from zero (in the 300-500 MPa range). The effect is not as great for Waspaloy due to its lower yield strength (hence lower mean stress at similar strain ranges when compared with IN 100) and the generally flatter monotonic stress-strain curve shape.

Data for Waspaloy from the previous NASA Contract NAS3-20367 with P&WA is presented for comparison with current contract testing in figures 73 and 74. These figures show the effect that mean strain and mean stress have on LCF life. It can be seen in figure 74 that at high strain ranges (where mean stress ~ 0) there is no significant difference between tests run with a fully reversed strain cycle and those with an all-tensile strain cycle. However, at the lower strain ranges (less than 0.7%, with mean stresses > 300 MPa) the effect of mean strain becomes evident. This same phenomenon is observed more clearly with IN 100. Dwell tests for Waspaloy do not exhibit any clear behavior of this type, possibly due to rapid mean stress relaxation and, hence, longer than expected life for the $R_\epsilon = 0$ tests or possibly due to the limited quantity of tests used to define the curves.

Data from current testing and previous contract work with IN 100 are presented in figures 75 and 76. For the high strain range tests, the effect of mean strain is not significant. However, at low strains (with corresponding high mean stresses) the differences in LCF properties between test runs with $R_\epsilon = -1$ and tests with $R_\epsilon = 0$ are significant. Dwell tests for IN 100 exhibit similar behavior.

In addition to expressions for cyclic strain ranges, mean stress (rather than mean strain) appears to be the critical parameter for LCF life predictions for these alloys.

Three supplementary tests have been performed to examine the effect of R_ϵ on LCF life for HIP MERL 76. Strain range and mean stress vs life plots are shown in figures 77 and 78. Strain range vs life curves are illustrated in figures 79 and 80. At the higher strain ranges (greater than 1.20%), there appears to be no significant difference in fatigue life. At the lower strain ranges (approximately 0.80%), the LCF life at the all-tensile strain condition exhibits a reduction of one to two orders of magnitude. This effect, due primarily to mean stress, was observed on several other alloys investigated under this contract. The test data appears in table 9.

Three supplementary tests were also run to determine the effect of strain ratio on the LCF life of HIP plus forged René 95. Stress range, mean stress, and strain range vs life plots for these tests are presented in figures 81, 82, and 83, respectively. Strain ratio produced a significant effect on LCF life. An approximate order of magnitude reduction in life occurs at low strain ranges (<0.80%). The long-life test failure initiation site however, was at a probable internal inclusion. This may have contributed to a longer life than anticipated. The entire long life regime for the all tensile strain curve shown in figure 83 is dependent on this one test point and should be viewed with caution. Had the failure initiated at the surface, then it would be expected that an even greater reduction in life would occur due to strain ratio. It would require a number of additional tests to confirm the degree of effect of strain R ratio. Test data appears in table 10.

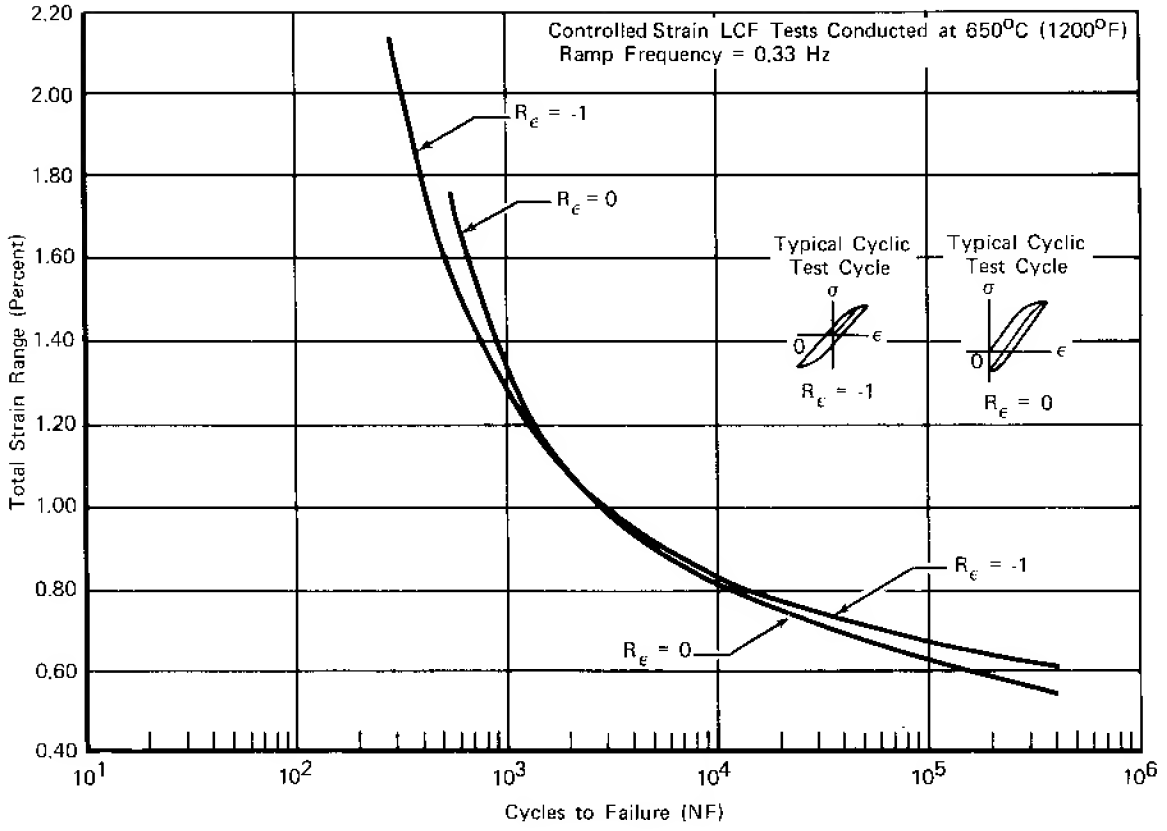

Figure 73. Effect of Strain Ratio on the Cyclic Strain Control LCF Results for Waspaloy

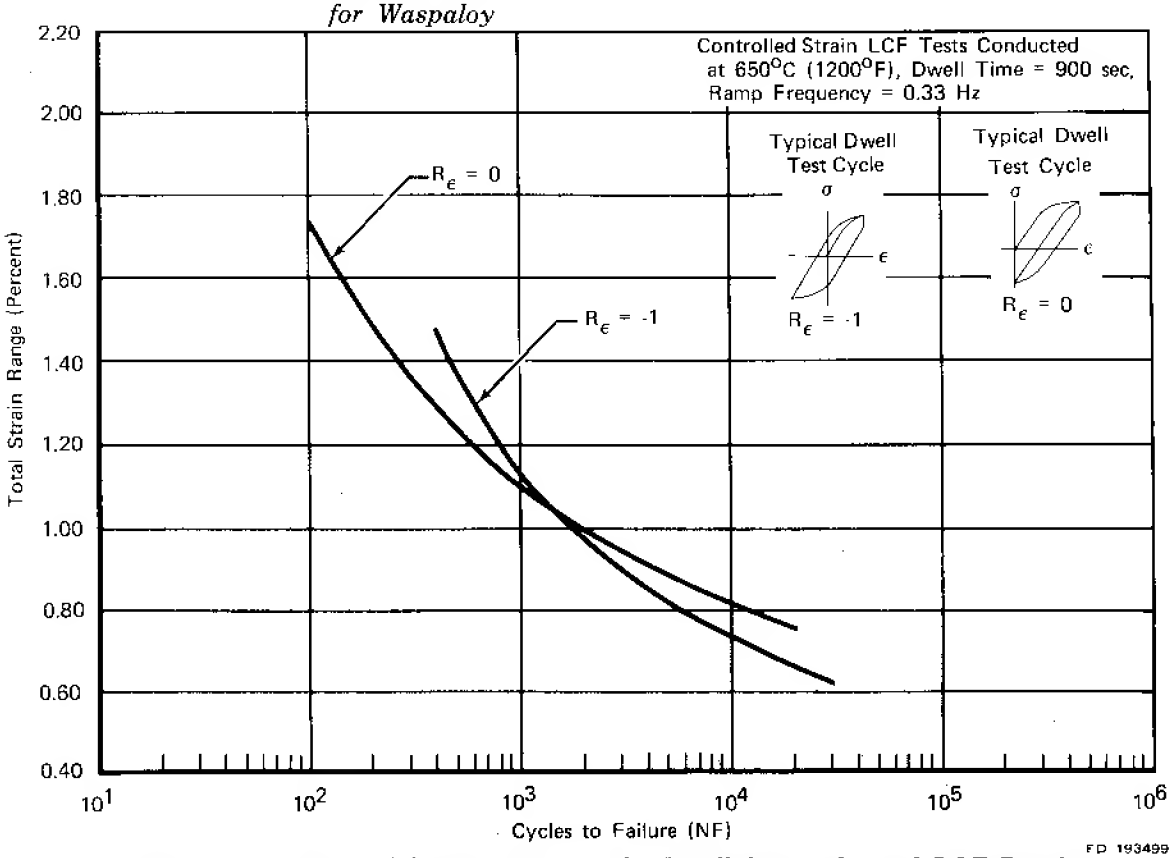

Figure 74. Effect of Strain Ratio on the Dwell Strain Control LCF Results for Waspaloy

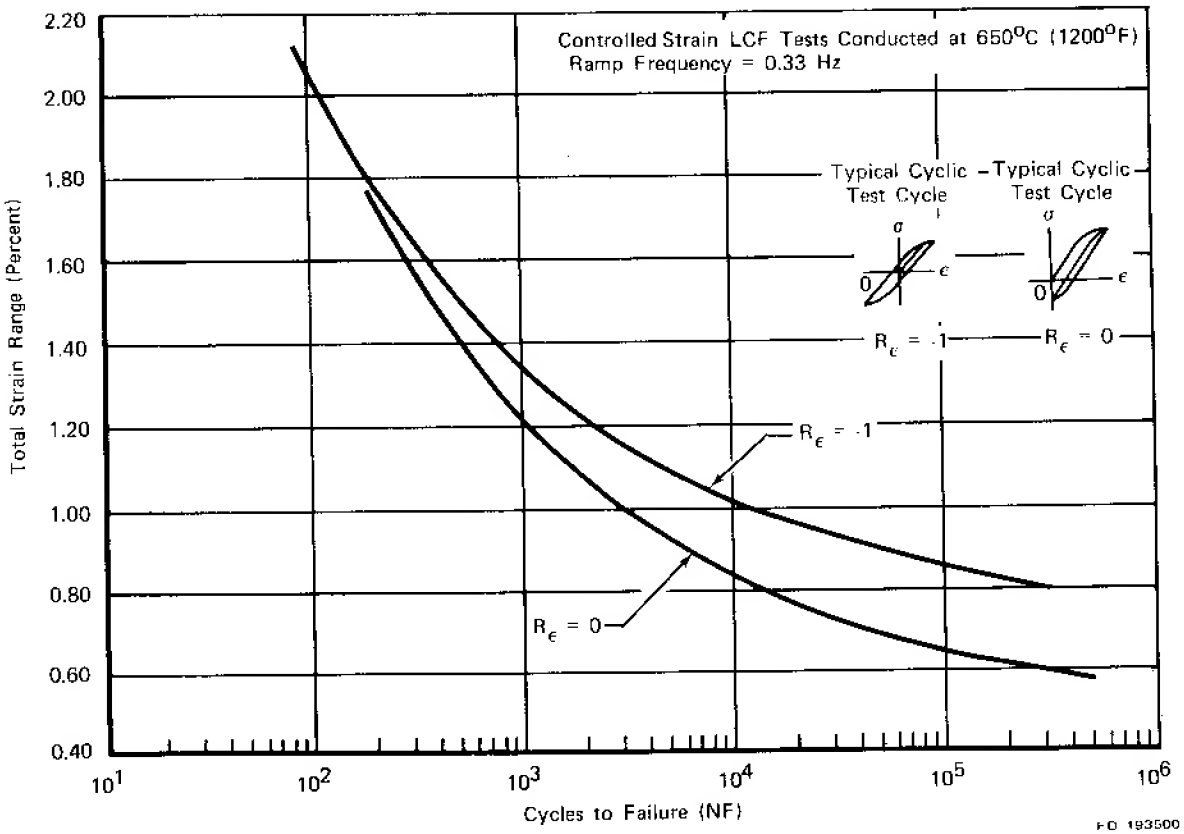

Figure 75. Effect of Strain Ratio on the Cyclic Strain Control LCF Results for IN 100

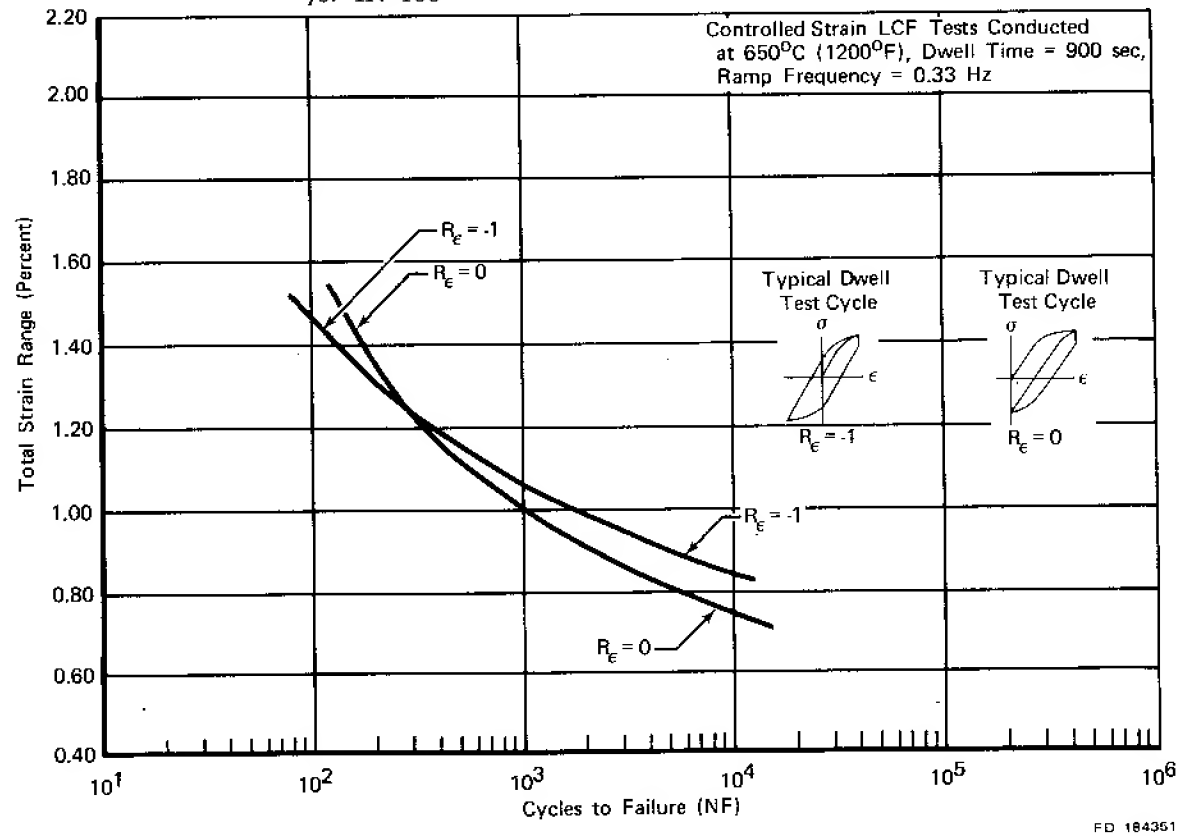

Figure 76. Effect of Strain Ratio on the Dwell Strain Control LCF Results for IN 100

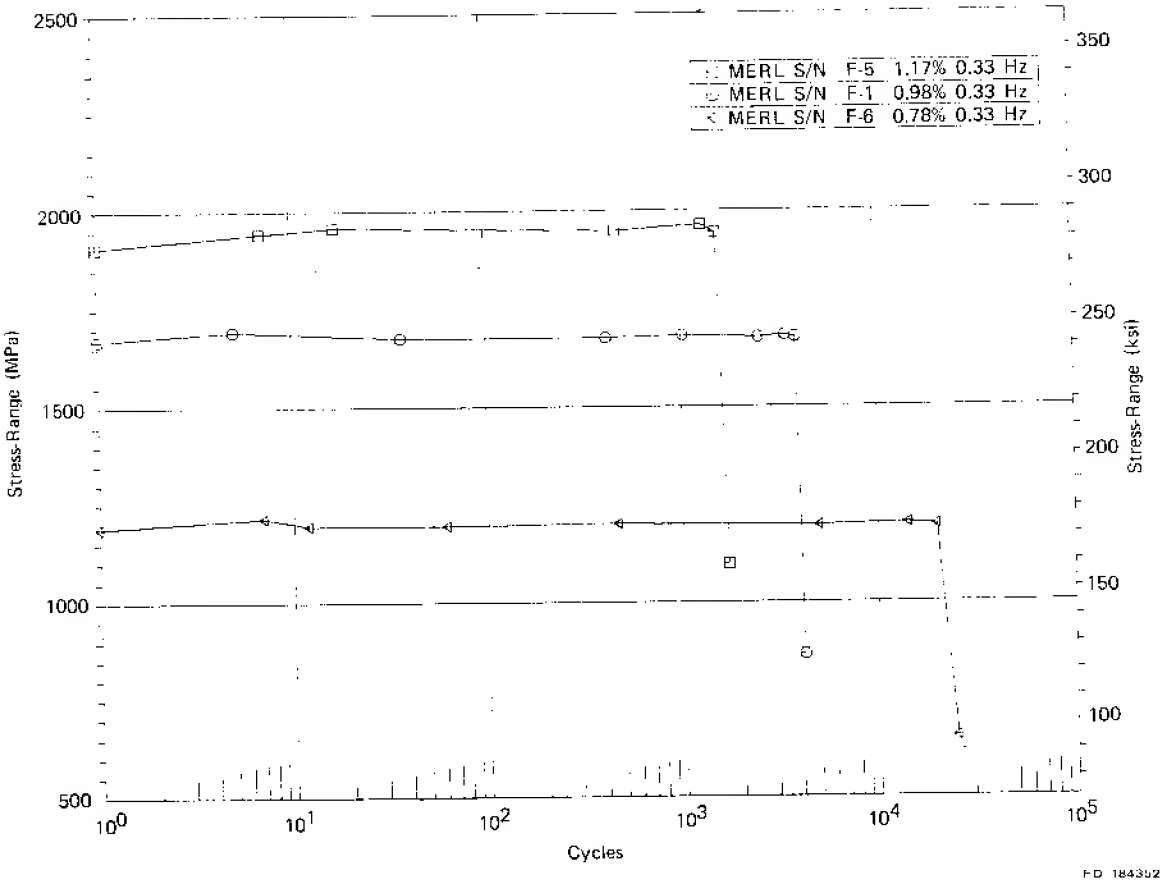

Figure 77. Stress Range vs Cycles for Supplementary Tests of HIP MERL 76 (0.33 Hz, R_ϵ = 0)

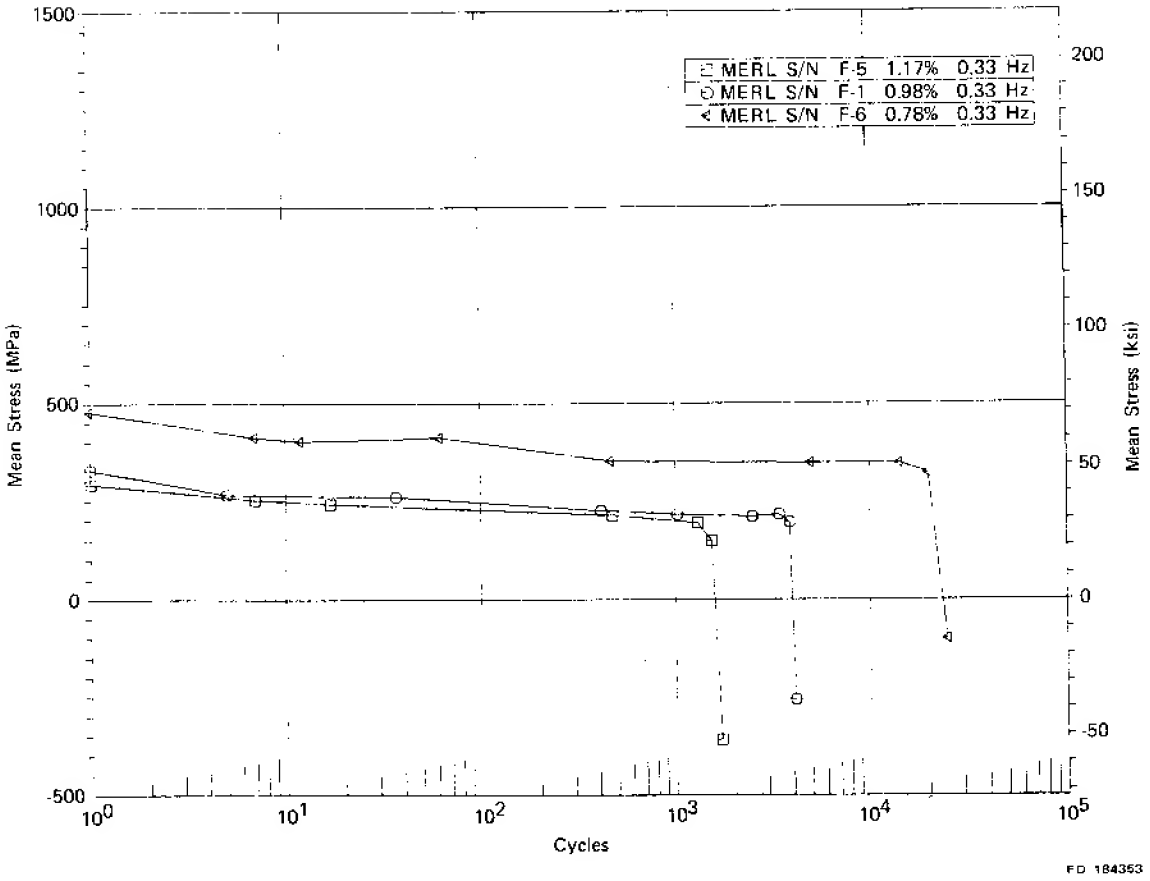

Figure 78. Mean Stress vs Cycles for Supplementary Tests of HIP MERL 76 (0.33 Hz, R_ϵ = 0)

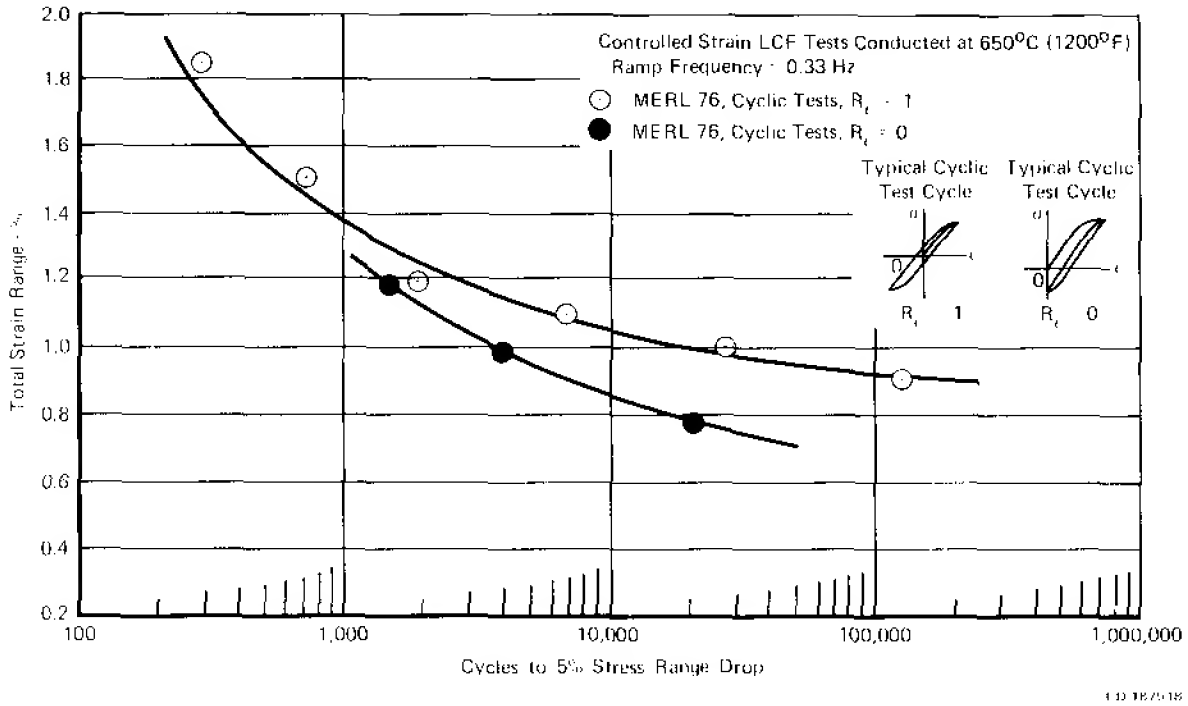

Figure 79. Effect of Strain Ratio on the Strain Control LCF Results for HIP MERL 76 (N_5 life)

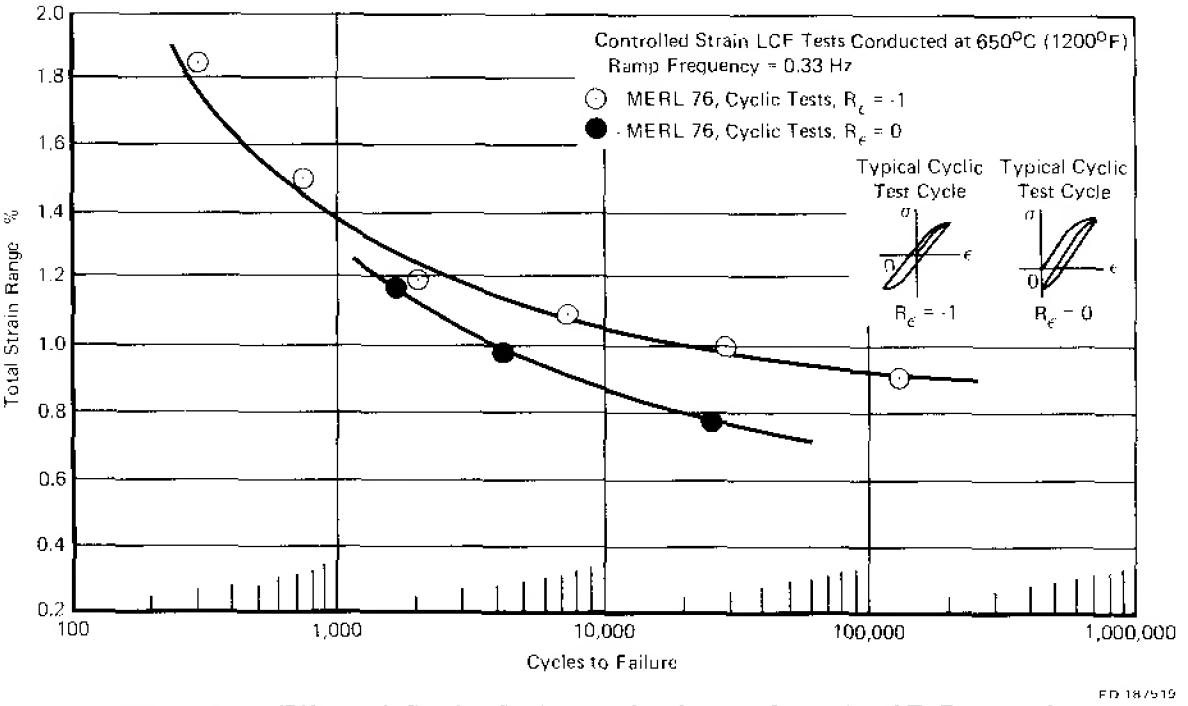

Figure 80. Effect of Strain Ratio on the Strain Control LCF Results for HIP MERL 76 (Failure)

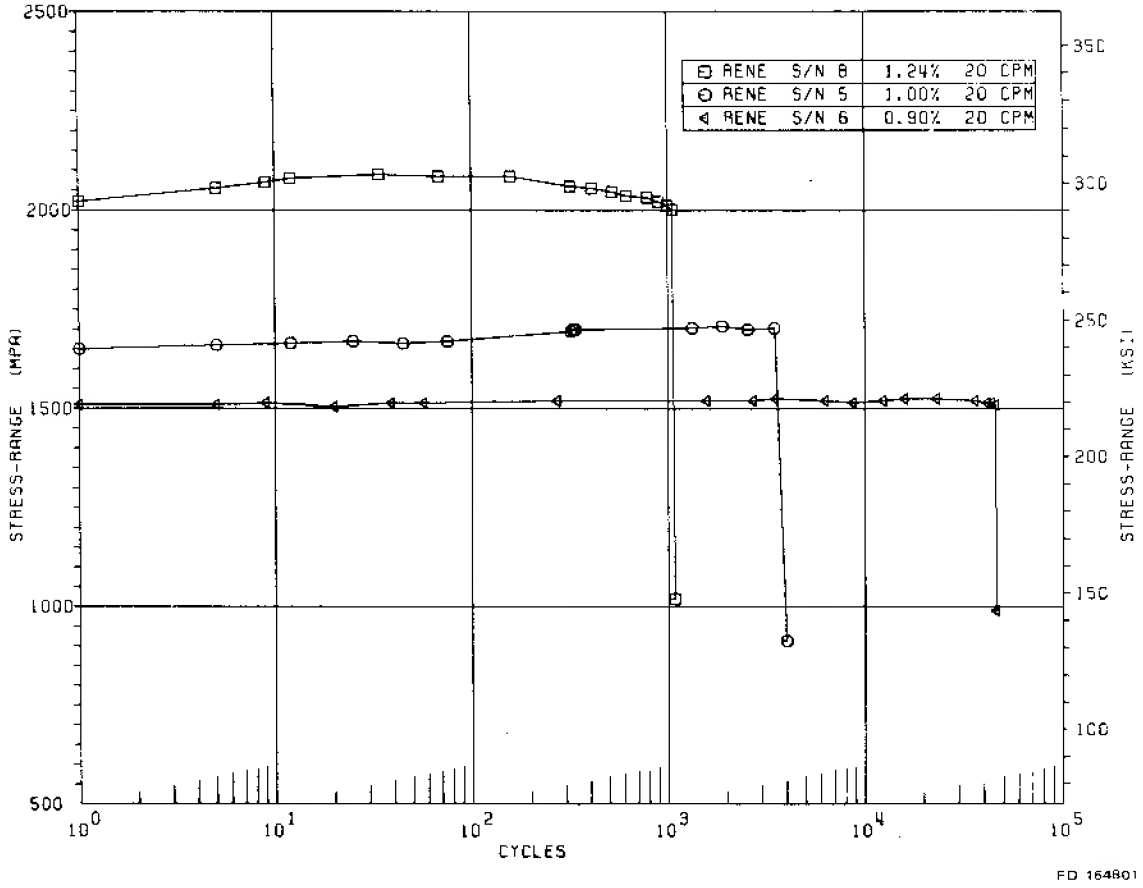

Figure 81. Stress Range vs Cycles for René 95 (0.33 Hz, R_ϵ = 0)

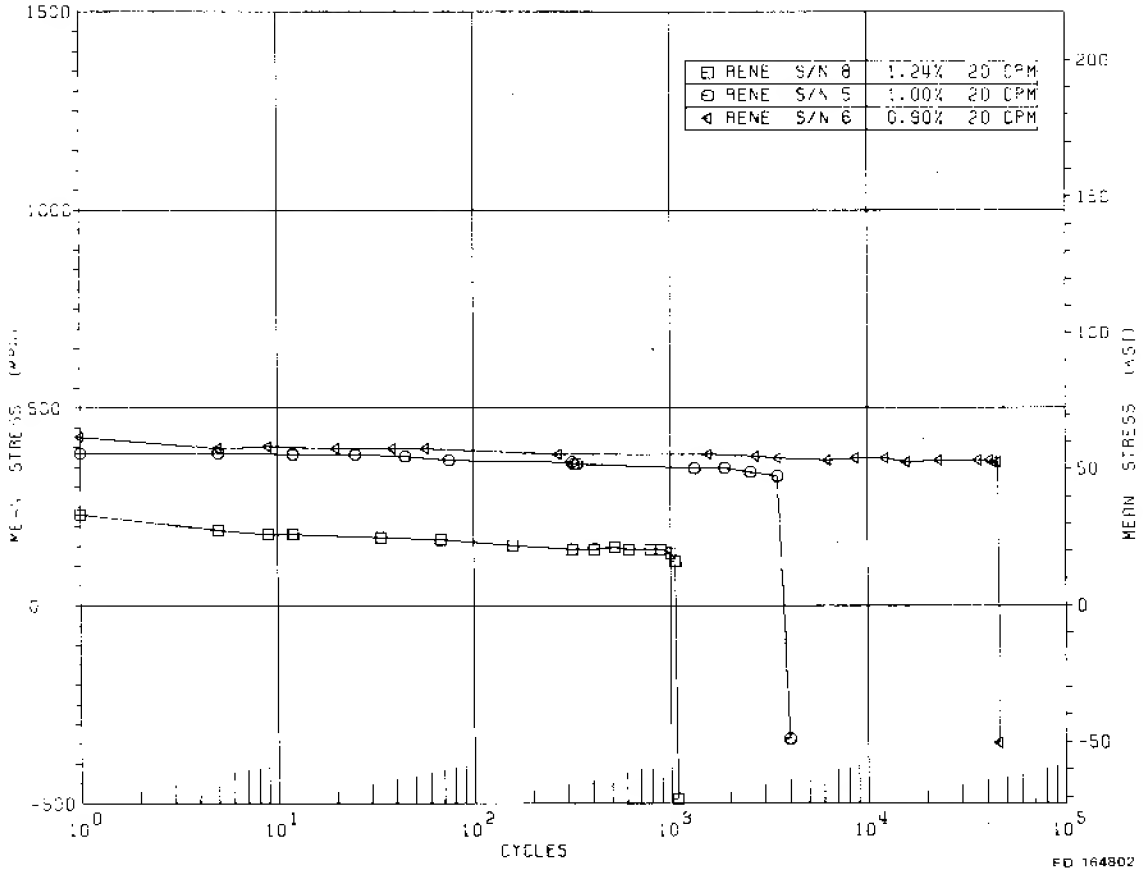

Figure 82. Mean Stress vs Cycles for René 95 (0.33 Hz, R_ϵ = 0)

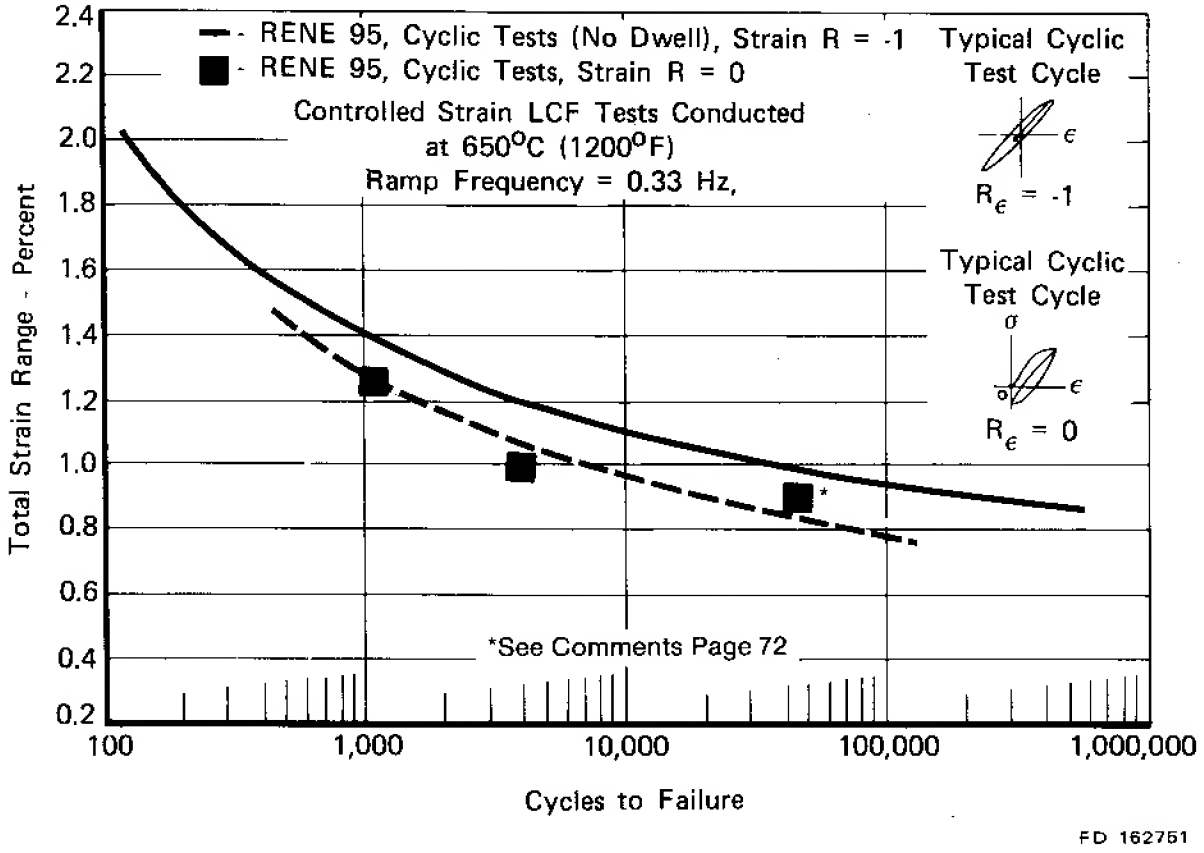

Figure 83. Effect of Strain Ratio on the Strain Control LCF Results for René 95 (Failure)

Four cyclic tests with an all tensile strain cycle (strain R = 0) were conducted to observe strain ratio (R_ϵ) effects for NASA IIB-7. Stress range, mean stress, and strain range vs life results are shown in figures 84 through 87. As was experienced with the other high strength alloys reported previously, there was a significant degradation in life (one to two orders of magnitude) caused by the higher mean stresses encountered with the $R_\epsilon = 0$ testing at the lower strain ranges. At the high strain ranges, the mean stress would approach zero for the strain R = 0 case, and the effect of strain ratio was negligible. Strain ratio produced no effect on the stress range vs inelastic strain range behavior, as shown in figure 88. Test data for NASA IIB-7 is given in table 14.

Constant Mean Stress Testing

To further investigate the mean stress vs life phenomenon, five supplementary controlled strain tests were conducted where the mean stresses were held constant. Figure 89 shows a typical hysteresis loop for this type of test. Test results are shown in table 16 and figure 90. These results show that variations in the tensile mean stress cause roughly linear shifts in the basic LCF curve. Compressive mean stresses, however, exert much less influence.

Alloy Comparisons

Fully Reversed Low-Cycle Fatigue Tests ($R_\epsilon = -1$)

Testing under this contract for fully reversed strain control LCF evaluations involved primarily two alloys: HIP MERL 76 and HIP plus forged René 95. In addition, supplementary tests were conducted for each of the five alloys tested under Contract NAS3-20367.

Composite regression curves for all seven alloys at 0.33 Hz are compared in figures 91 and 92. Table 17 lists the mean curve equations and coefficients. The general rank order from best to worst at low strain ranges (those which yield approximately 100,000 cycles life) is:

René 95 H + F
HIP MERL 76
NASA IIB-7
IN 100
Wrought Astroloy
HIP Astroloy
Waspaloy

This ranking is in general agreement with the rank order by tensile strength (highest to lowest) listed below:

NASA IIB-7
René 95 H + F
HIP MERL 76
Wrought Astroloy
IN 100
Waspaloy
HIP Astroloy

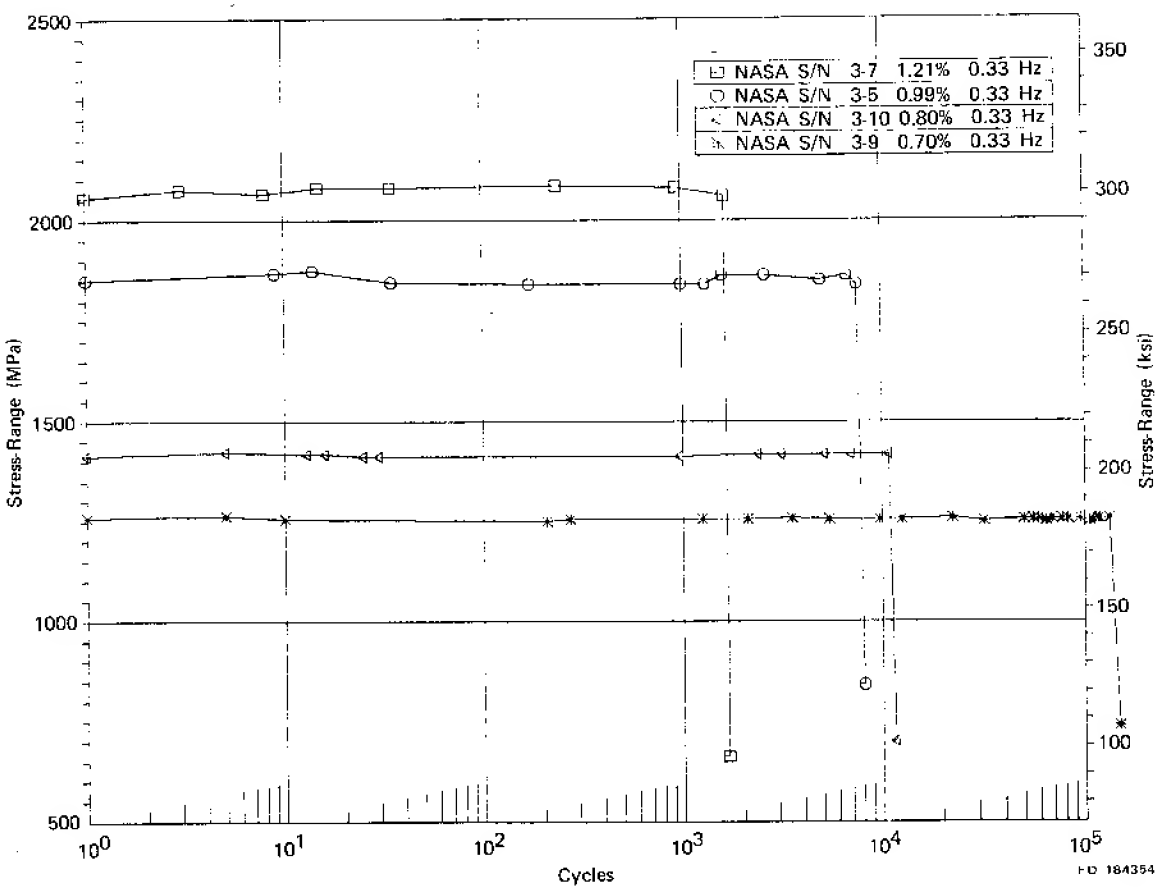

Figure 84. Stress Range vs Cycles for Supplementary Tests of NASA IIB-7 (0.33 Hz, R_ϵ = 0)

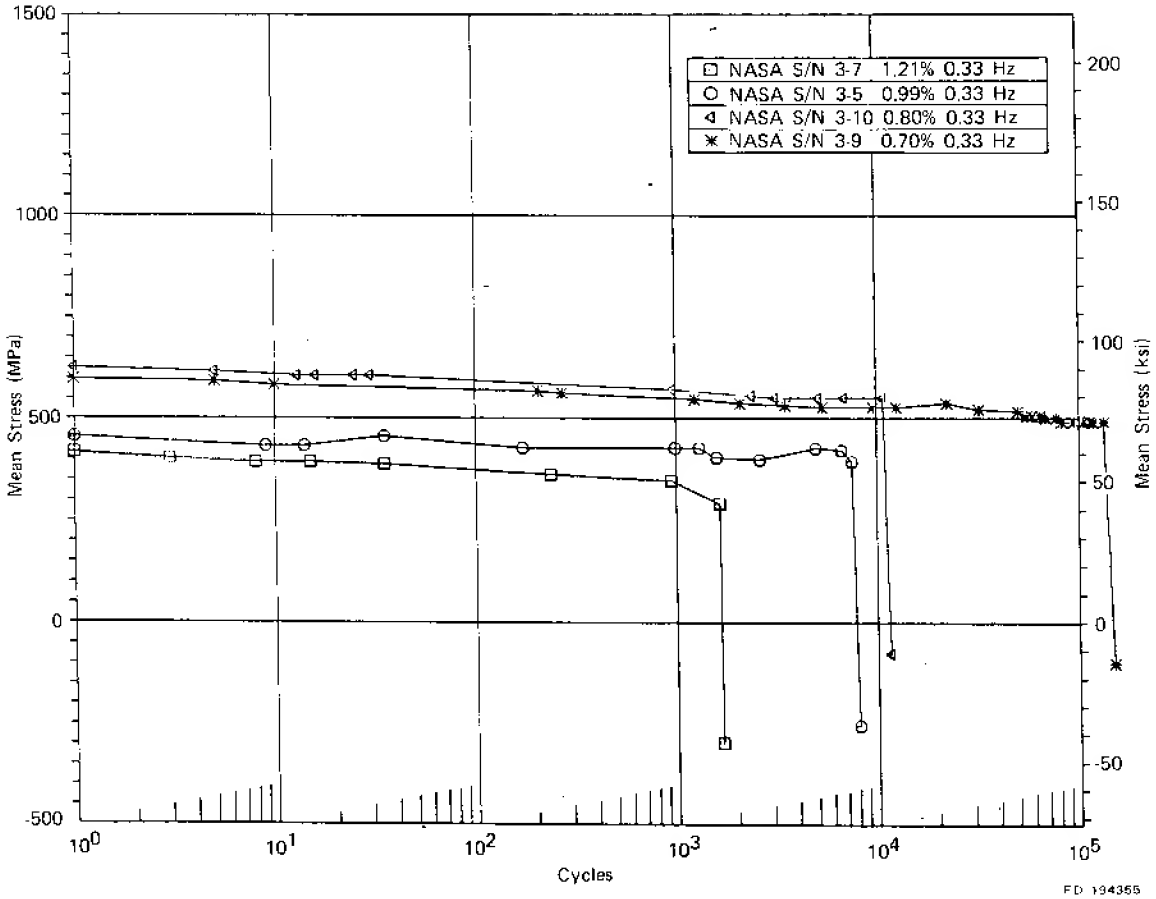

Figure 85. Mean Stress vs Cycles for Supplementary Tests of NASA IIB-7 (0.33 Hz, R_ϵ = 0)

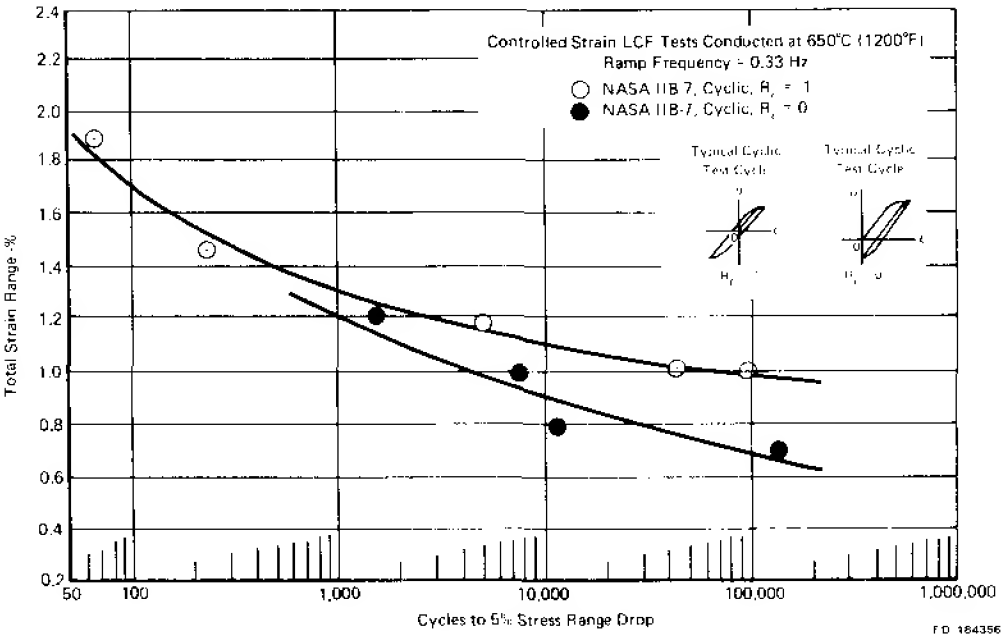

Figure 86. Effect of Strain Ratio on the Strain Control LCF Results for NASA IIB-7 (N_5 Life)

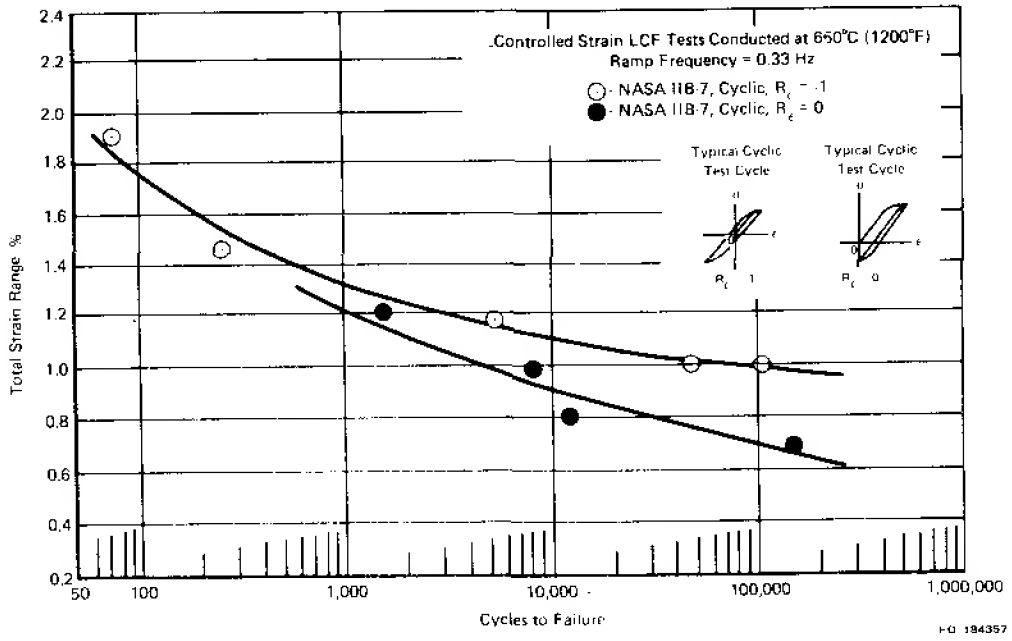

Figure 87. Effect of Strain Ratio on the Strain Control LCF Results for NASA IIB-7 (Failure)

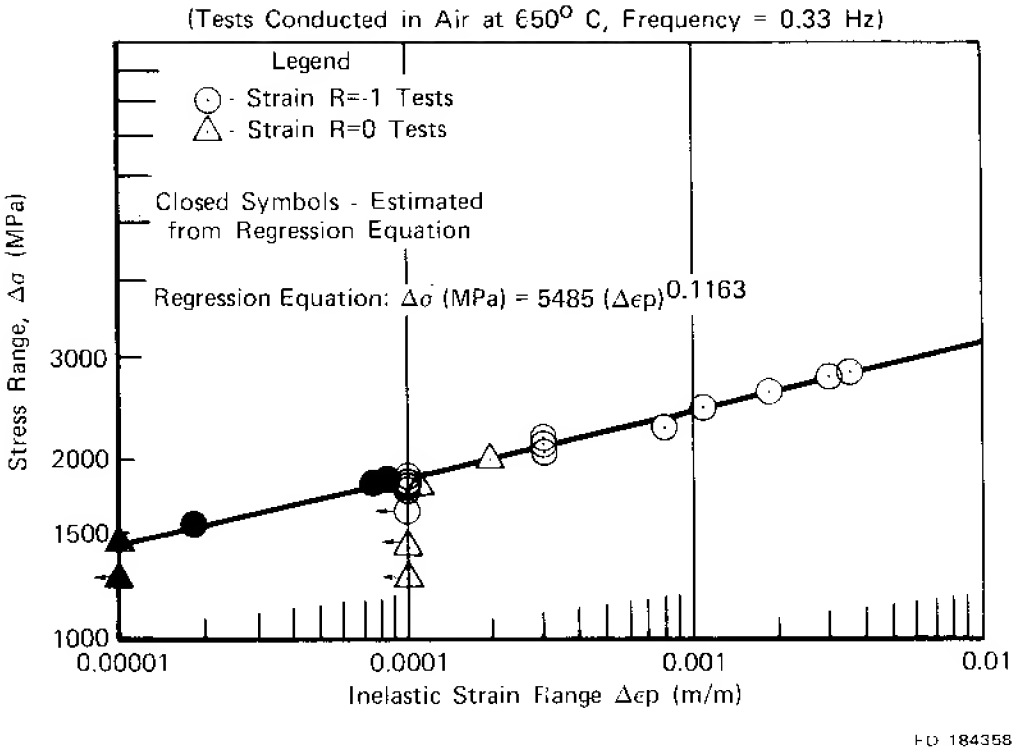

Figure 88. Stress Range vs Inelastic Strain Range for NASA IIB-7

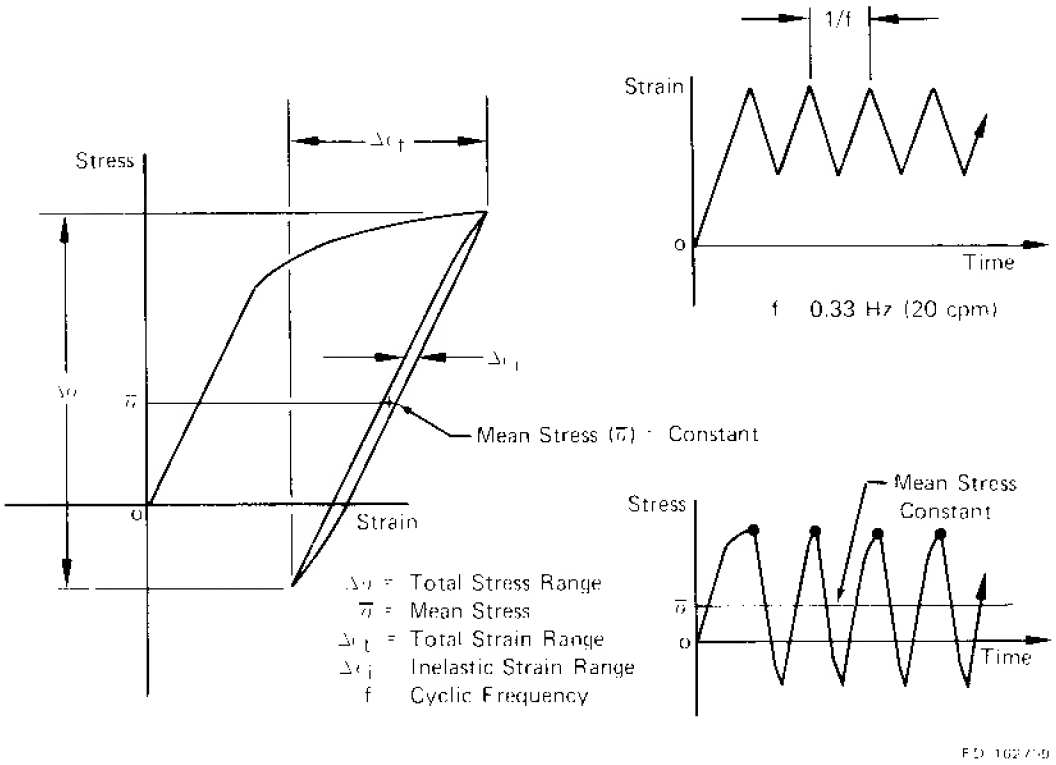

Figure 89. Typical Strain Control LCF Test with Mean Stress Held Constant

TABLE 16
CONTROLLED STRAIN LOW-CYCLE FATIGUE TESTS WITH CONSTANT MEAN STRESS FOR IN 100
Testing Conducted in Air at 650°C (1200°F). Frequency = 0.33 Hz (20 cpm)

Spec S/N	*Strain R (min/max)*	*Mean Strain (m/m at cycle 1)*	*Strain (m/m at $N_f/2$)*				*Mean Stress at $N_f/2$*		*Stress Range*		*Cycles to Failure*
			Range	*Elastic*	*Inelastic*	*Creep*	*MPa*	*ksi*	*Cycle 1*	*$N_f/2$*	
15	0.85	0.0617	0.0097	0.0094	0.0003	0	476	69.0	1669 MPa (242 ksi)	1669 MPa (242 ksi)	785
16	-0.36	0.0019	0.0078	0.0078	<0.0001	0	286	41.5	1379 MPa (200 ksi)	1379 MPa (200 ksi)	26,025
22	3.0	-0.0104	0.0104	0.0102	0.0002	0	-345	-50.0	1862 MPa (270 ksi)	1862 MPa (270 ksi)	12,843
23	1.59	-0.0273	0.0124	0.0119	0.0005	0	-345	-50.0	2069 MPa (300 ksi)	2069 MPa (300 ksi)	2,224
20	1.28	-0.0569	0.0141	0.0132	0.0009	0	-345	-50.0	2319 MPa (336.4 ksi)	2319 MPa (336.4 ksi)	950
[1]8	0	0.0033	0.0065	0.0065	<0.0001	0	476	69.0	1128 MPa (163.6 ksi)	1142 MPa (165.6 ksi)	93,686
[2]3	0	0.0050	0.0099	0.0098	0.0001	0	286	41.5	1684 MPa (244.2 ksi)	1660 MPa (240.8 ksi)	3,134

[1]This data taken from Table 13 and is presented for evaluation with data from specimen No. 15.
[2]This data taken from Table 13 and is presented for evaluation with data from specimen No. 16.

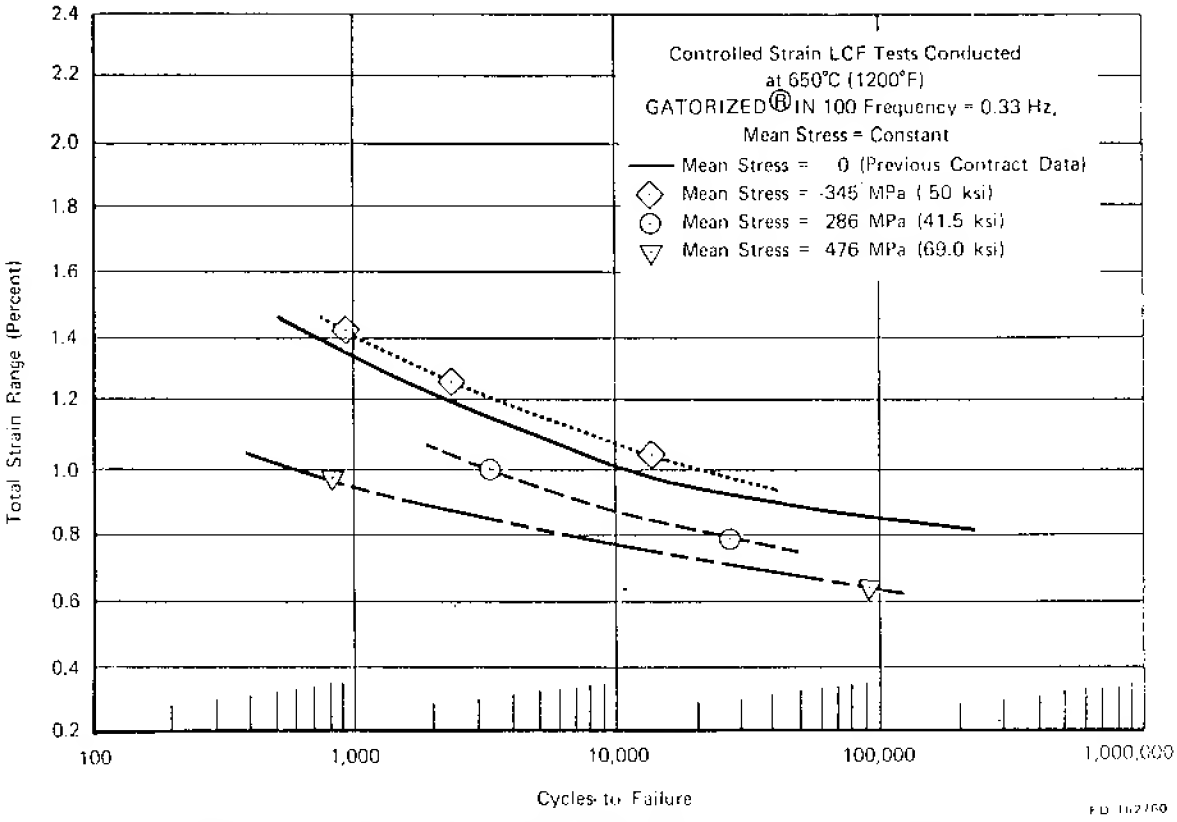

Figure 90. Controlled Strain LCF Tests Conducted at 650°C

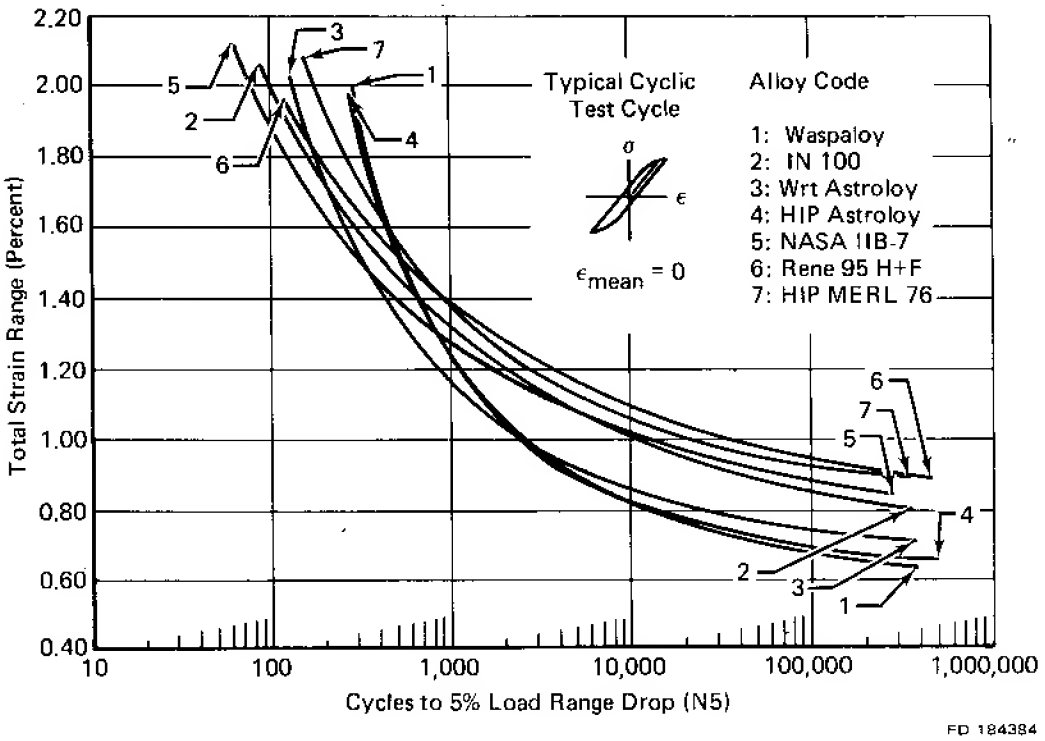

Figure 91. Comparison of Cyclic Strain Control LCF Properties of Seven Alloys Tested Under NAS3-21379 and NAS3-20367 (R_ϵ = -1, 0.33 Hz, N_5 Life)

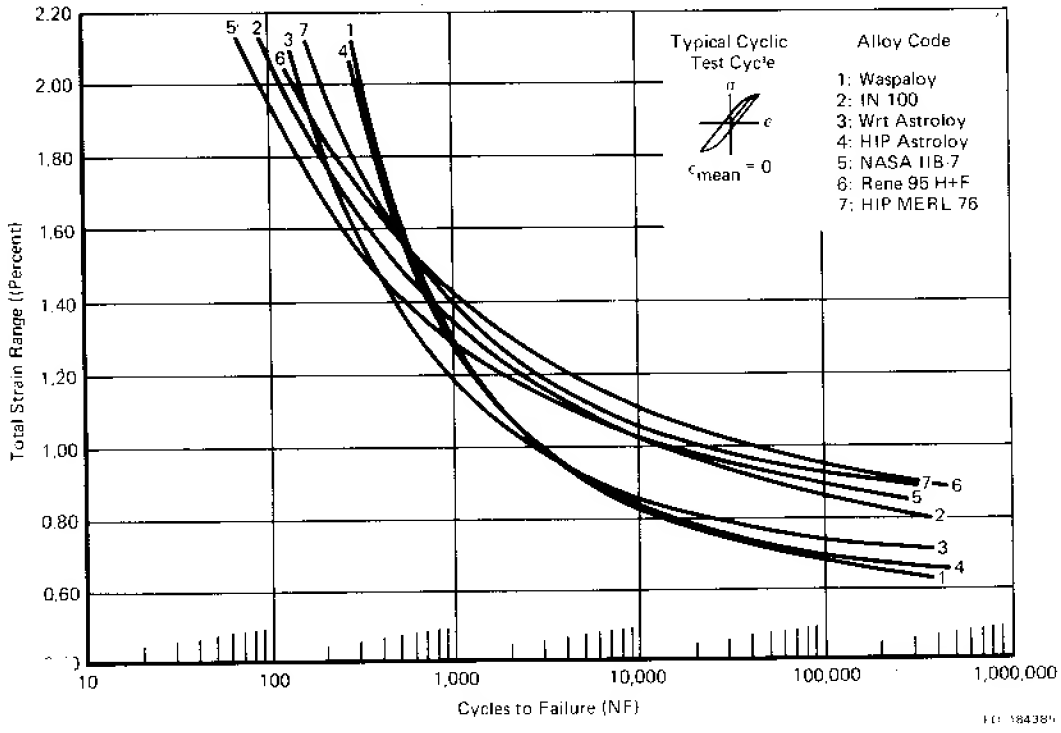

Figure 92. Comparison of Cyclic Strain Control LCF Properties of Seven Alloys Tested Under NAS3-21379 and NAS3-20367 (R_ϵ = -1, 0.33 Hz, Failure)

TABLE 17
MEAN REGRESSION EQUATION COEFFICIENTS FOR
LCF CURVES FOR ALL ALLOYS

Test Temperature = 650°C (1200°F), Cyclic Test Frequency = 0.33 Hz,
Dwell Time = 900 sec at Max Tensile Strain, R = Strain R Ratio (min strain/max strain)
Equations are of the form . . . $TSR = AN^B + CN^D + E$
Where TSR = Total Strain Range (%), and N = Cycles
To Failure (N_f), or to 5% Load Range Drop (N_5)

Alloy	*Mode*	*R*	*N*	*A*	*B*	*C*	*D*	*E*
Waspaloy	Cyclic	0	N_f	936.948	-1.15071	1.93315	-0.0966144	0.0
Waspaloy	Cyclic	0	N_5	741.717	-1.13499	1.89583	-0.0953074	0.0
Waspaloy	Cyclic	-1	N_f	331.304	-1.06045	2.69095	-0.220823	0.469
Waspaloy	Cyclic	-1	N_5	277.18	-1.0543	3.30207	-0.272527	0.536
Waspaloy	Dwell	0	N_f	11.1136	-0.662964	1.92005	-0.0954342	0.0
Waspaloy	Dwell	0	N_5	10.4326	-0.659782	1.90049	-0.0948072	0.0
Waspaloy	Dwell	-1	N_f	174.506	-1.028	2.49034	-0.133992	0.0
Waspaloy	Dwell	-1	N_5	105.453	-0.976823	2.32937	-0.127169	0.0
IN 100	Cyclic	0	N_f	6.47614	-0.742463	5.19399	-0.285168	0.455
IN 100	Cyclic	0	N_5	6.34148	-0.744273	5.15103	-0.285836	0.455
IN 100	Cyclic	-1	N_f	6.13167	-0.585313	2.7693	-0.224129	0.64
IN 100	Cyclic	-1	N_5	5.73815	-0.587497	2.69893	-0.224924	0.64
IN 100	Dwell	0	N_f	40.0167	-1.02353	2.07428	-0.111397	0.0
IN 100	Dwell	0	N_5	31.727	-1.00941	1.97707	-0.106343	0.0
IN 100	Dwell	-1	N_f	5.04254	-0.672029	1.79707	-0.0835582	0.0
IN 100	Dwell	-1	N_5	3.52309	-0.634389	1.71731	-0.0787505	0.0
Wrought Astroloy	Cyclic	-1	N_f	43.1896	-0.911588	4.75333	-0.343688	0.648
Wrought Astroloy	Cyclic	-1	N_5	41.1255	-0.916571	4.54908	-0.342337	0.648
Wrought Astroloy	Dwell	-1	N_f	27.8907	-0.822963	2.14405	-0.108223	0.0
Wrought Astroloy	Dwell	-1	N_5	17.7961	-0.775867	2.02414	-0.102246	0.0
HIP Astroloy	Cyclic	-1	N_f	224.175	-1.04752	6.32319	-0.369926	0.603
HIP Astroloy	Cyclic	-1	N_5	227.915	-1.06715	6.31806	-0.376058	0.603
HIP Astroloy	Dwell	-1	N_f	33.5797	-0.845435	2.17623	-0.116679	0.0
HIP Astroloy	Dwell	-1	N_5	26.1559	-0.821618	2.10282	-0.113414	0.0
NASA IIB-7	Cyclic	0	N_f	10.735	-0.826323	2.65865	-0.116753	0.0
NASA IIB-7	Cyclic	0	N_5	9.92219	-0.823956	2.63281	-0.116592	0.0
NASA IIB-7	Cyclic	-1	N_f	10.5751	-0.730747	2.20074	-0.205722	0.68
NASA IIB-7	Cyclic	-1	N_5	9.89921	-0.730275	2.1636	-0.205787	0.68
NASA IIB-7	Dwell	-1	N_f	1.13662	-0.482994	1.76866	-0.069406	0.0
NASA IIB-7	Dwell	-1	N_5	0.984671	-0.466046	1.73737	-0.0673532	0.0
René 95 H+F	Cyclic	0	N_f	27.0814	-0.832871	5.9552	-0.399425	0.801
René 95 H+F	Cyclic	0	N_5	21.4514	-0.811924	5.31875	-0.389216	0.801
René 95 H+F	Cyclic	-1	N_f	6.87115	-0.577588	2.30477	-0.204706	0.72
René 95 H+F	Cyclic	-1	N_5	6.22047	-0.582488	2.20082	-0.201343	0.72
René 95 H+F	Dwell	-1	N_f	6.8949	-0.779243	1.93584	-0.0802282	0.0
René 95 H+F	Dwell	-1	N_5	6.34249	-0.770933	1.91887	-0.0793418	0.0
HIP MERL 76	Cyclic	0	N_f	334.444	-1.29965	8.37155	-0.353545	0.546
HIP MERL 76	Cyclic	0	N_5	384.81	-1.33284	6.88222	-0.312189	0.468
HIP MERL 76	Cyclic	-1	N_f	33.9208	-0.949977	5.8441	-0.352211	0.819
HIP MERL 76	Cyclic	-1	N_5	31.765	-0.948028	5.69177	-0.351242	0.819
HIP MERL 76	Dwell	-1	N_f	15.519	-0.775396	2.55542	-0.117991	0.0
HIP MERL 76	Dwell	-1	N_5	14.2086	-0.770022	2.53148	-0.117747	0.0

At the higher strain ranges (approximately 2.0%), the rank order reverses somewhat in accordance with the tensile ductilities:

Waspaloy	
HIP Astroloy	
HIP MERL 76	Rank Order by LCF Life
Wrought Astroloy	(highest to lowest at $\Delta\epsilon_t$ = 2.0%)
René 95 H+F	
IN 100	
NASA IIB-7	

HIP Astroloy	
Wrought Astroloy	
Waspaloy	Rank Order by Tensile Ductility
HIP MERL 76	(highest to lowest)
IN 100	
René 95 H + F	
NASA IIB-7	

Cyclic stress-strain curves were reconstructed from these strain control tests and are presented in figure 93. The curves were obtained by plotting one-half the total stress range vs one-half the total strain range as measured at the specimen half-life ($N_f/2$).

Composite regression curves for all seven alloys tested with the 900-sec dwell at the maximum strain are compared in figures 94 and 95. The mean curve equations and coefficients are given in table 17. The rank order of the alloys at low strain ranges (for 10,000 cycles life) under these test conditions is:

NASA IIB-7
René 95 H + F
HIP MERL 76
IN 100
Wrought Astroloy
HIP Astroloy
Waspaloy

This approximates the cyclic test results, with the exception of NASA IIB-7.

The effect of the 900-sec dwell time on fatigue life varied from alloy to alloy. A comparison of N_5 lives obtained at a total strain range of 1.0% is detailed below:

Alloy	*N_5 Life (0.33 Hz)*	*N_5 Life (900-sec Dwell)*	*Percent Reduction in Life*
Waspaloy	2,580	1,500	42
IN 100	10,050	1,500	85
Wrought Astroloy	2,400	1,700	29
HIP Astroloy	2,450	1,340	45
NASA IIB-7	12,500	4,800	62
René 95 H + F	36,500	4,100	89
HIP MERL 76	19,500	3,200	84

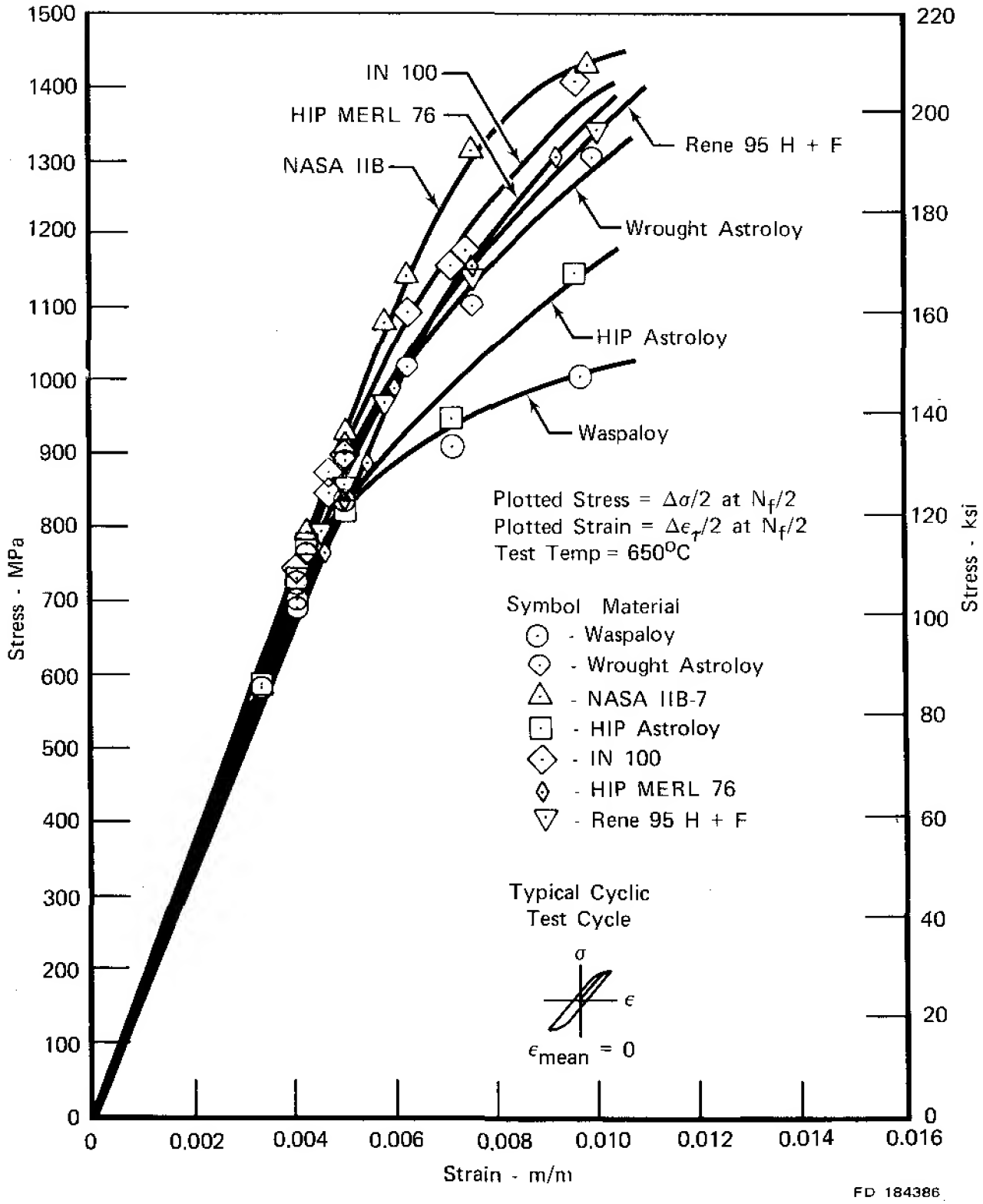

Figure 93. Reconstructed Cyclic Stress-Strain Curves for All Seven Alloys

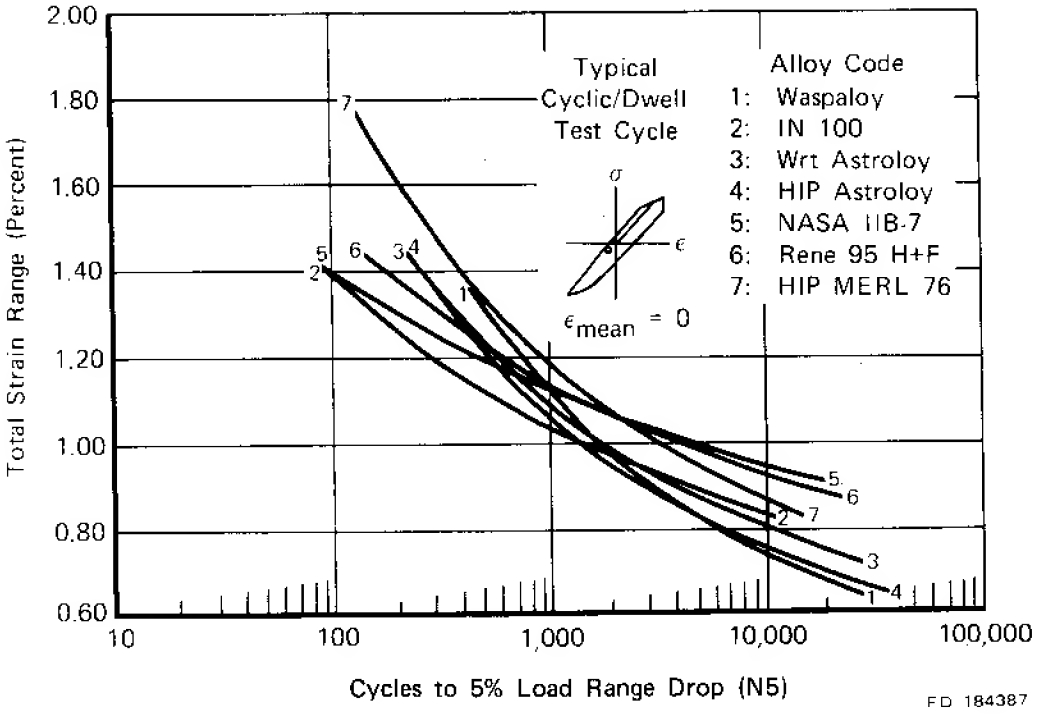

Figure 94. Comparison of Dwell Strain Control LCF Properties of Seven Alloys Tested Under NAS3-21379 and NAS3-20367 (R_ϵ = -1, 900-sec Dwell, N_5 Life)

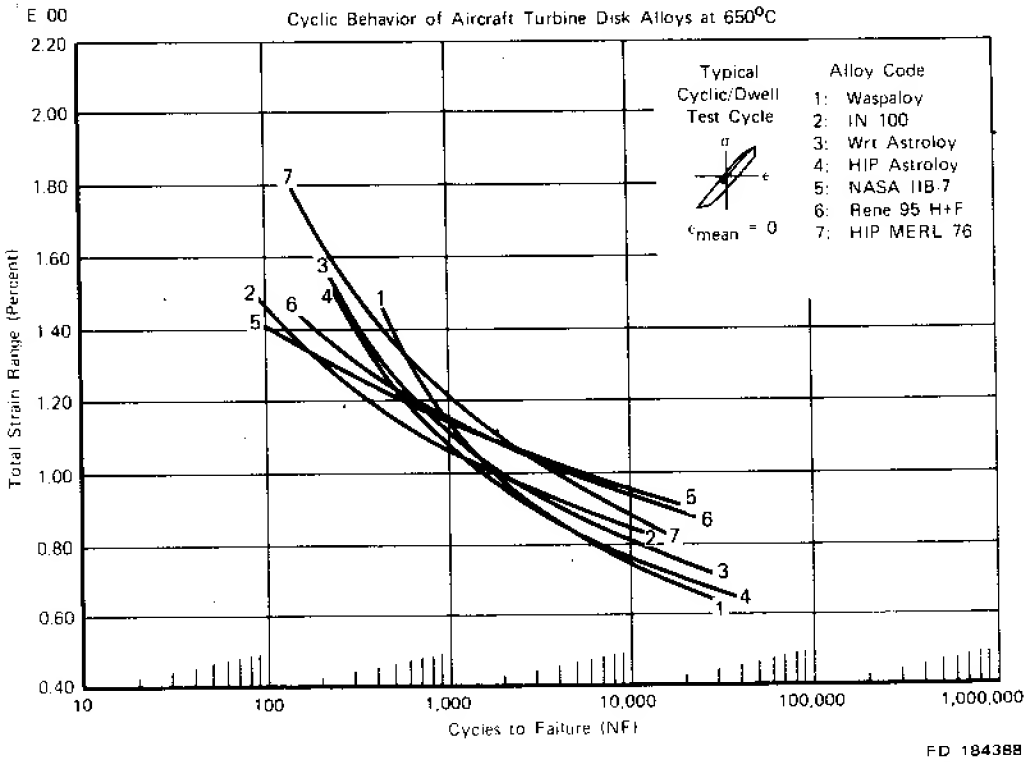

Figure 95. Comparison of Dwell Strain Control LCF Properties of Seven Alloys Tested Under NAS3-21379 and NAS3-20367 (R_ϵ = -1, 900-sec Dwell, Failure)

Wrought Astroloy exhibited the smallest reduction in life (29%) due to the hold time; Waspaloy and HIP Astroloy showed similar reductions at 42 and 45%, respectively. The higher strength alloys produced large reductions with NASA IIB-7 at 62%, followed by HIP MERL 76 (84%), IN 100 (85%), and René 95 H + F (89%).

All-Tensile Strain LCF Tests (R_ϵ = 0)

Testing under this contract for all-tensile strain LCF evaluations involved primarily Waspaloy and IN 100. In addition, several supplementary tests were performed on HIP MERL 76, HIP plus forged René 95, and NASA IIB-7 to evaluate the effect of strain R ratio on these alloys. Testing of this type was conducted to better simulate surface strain behavior at LCF-limited locations of aircraft turbine disks under actual operating conditions.

Composite regression curves for all five alloys at 0.33 Hz are compared in figures 96 and 97. The mean curve equations and coefficients appear in table 17. The rank order of the alloys at low strain ranges (approximately 100,000 cycles life) appears below:

René 95 H + F
NASA IIB-7
HIP MERL 76
IN 100
Waspaloy

Again, this closely approximates the order expected based on relative tensile strength. The only exception is the unusually high life of the René 95 H + F. It should be emphasized that the curve for René 95 H + F in figures 96 and 97 should be viewed with caution (hence it is shown dotted) due to (1) the limited quantity of tests used to generate this curve and (2) as mentioned earlier, the longer life test point where failure initiated at an internal inclusion.

The rank order at higher strain ranges (approximately 1.5%) is:

Waspaloy
HIP MERL 76
René 95 H + F
IN 100
NASA IIB-7

This is identical to the rank order for these alloys for the strain R = -1 tests.

Composite regression curves for the two alloys tested with the 900-sec dwell at the maximum tensile strain are compared in figures 98 and 99. Waspaloy proved superior to IN 100 under these test conditions at all strain ranges.

The percent reduction in N_5 LCF life at 1.0% total strain range due to the 900-sec hold time is given below:

Alloy	*N_5 Life (0.33 Hz)*	*N_5 Life (900-sec Dwell)*	*Percent Reduction in Life*
Waspaloy	2,500	1,900	24
IN 100	2,950	840	72

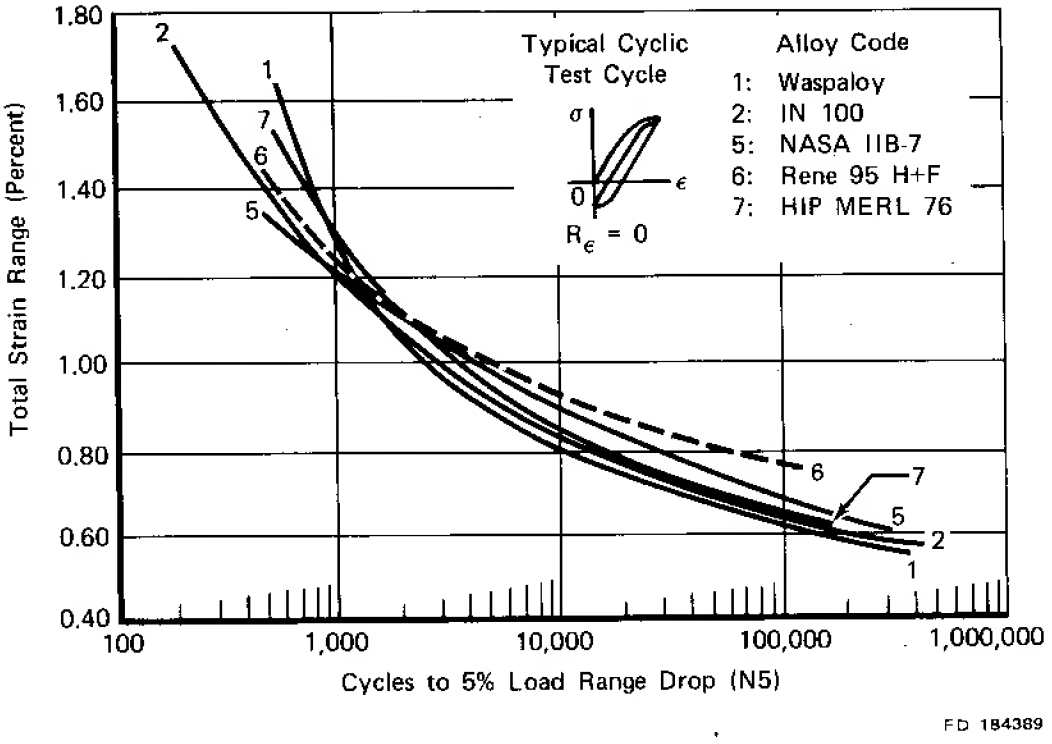

Figure 96. Comparison of Cyclic Strain Control LCF Properties of Five Alloys Tested Under NAS3-21379 (R_ϵ = 0, N_5 Life)

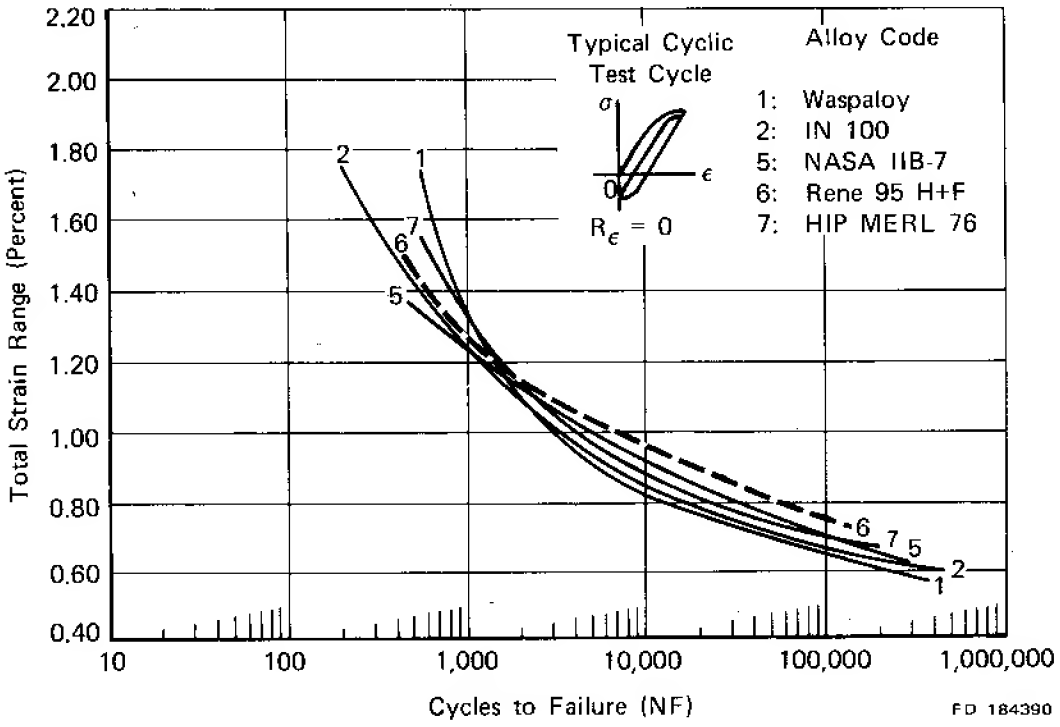

Figure 97. Comparison of Cyclic Strain Control LCF Properties of Five Alloys Tested Under NAS3-21379 (R_ϵ = 0, Failure)

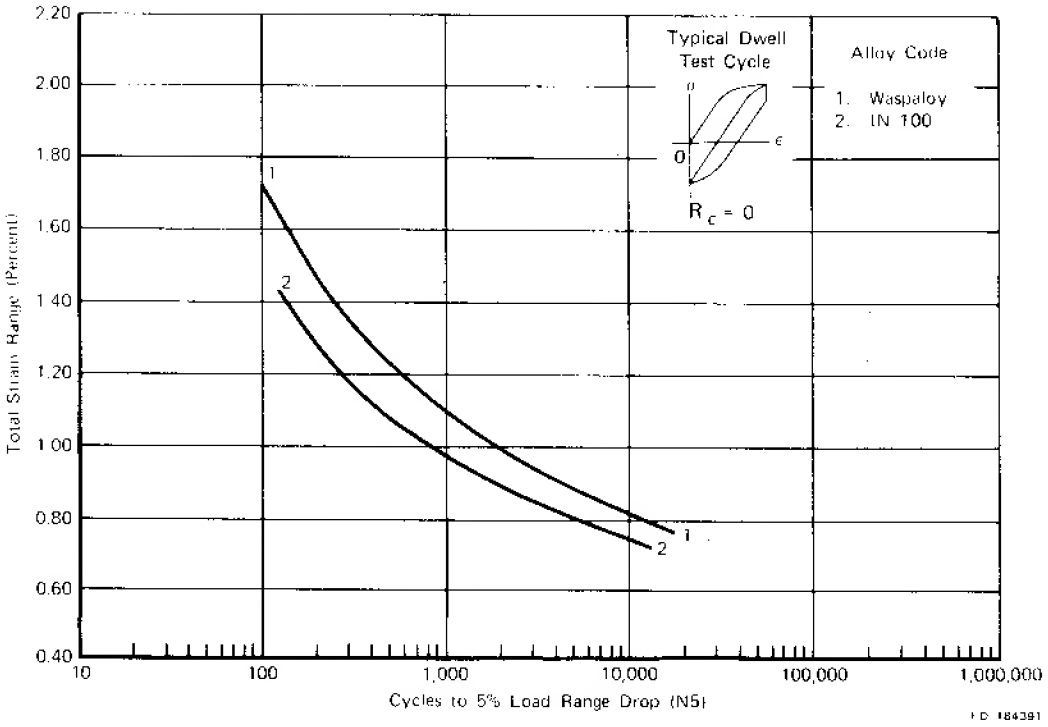

Figure 98. Comparison of Dwell Strain Control LCF Properties of Two Alloys Tested Under NAS3-21379 (R_ϵ = 0, 900-sec Dwell, N_5 Life)

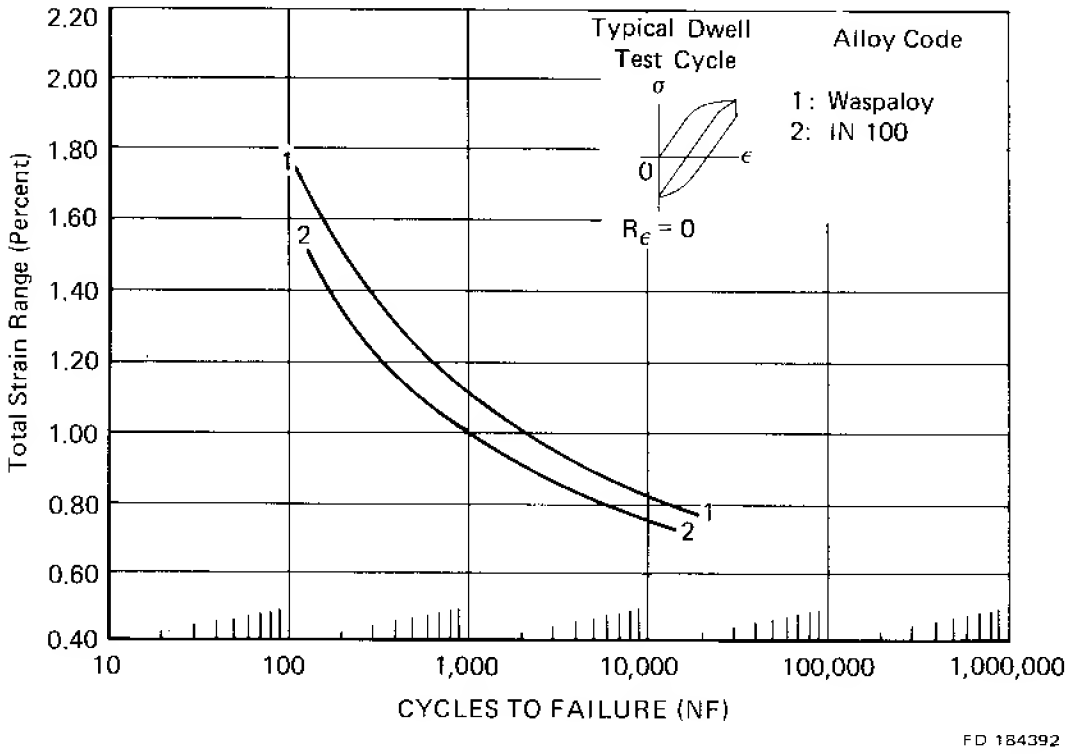

Figure 99. Comparison of Dwell Strain Control LCF Properties of Two Under Alloys Tested NAS3-21379 (R_ϵ = 0, 900-sec Dwell, Failure)

Load-Controlled Crack Growth Testing

Test Methods

Test Specimens

A compact-type (CT) specimen was used in this test program to obtain crack propagation data for each of the alloys. Figures 100 and 101 present the specimen configuration and dimensions. A specimen thickness of 1.270 cm (0.500 in.) was utilized whenever possible. In the case of Waspaloy (Alloy 3), material availability forced the use of 0.635 cm (0.250-in.) thick specimens. In several other instances, material limitations necessitated the use of CT specimens of smaller overall dimensions than shown in figure 101. For those smaller specimens, the dimensional ratios for CT specimens in ASTM-647 were maintained.

Test Procedure

Test specimens were precracked using the procedures outlined in ASTM-399. Precracking was performed at room temperature at a cyclic frequency of 20 Hz.

Crack propagation testing was performed on servohydraulic closed loop test machines operated under load control. Cyclic tests were conducted using triangular load waveforms or triangular waveforms with a hold time at the peak tensile load. Specimen heating was provided by resistance clamshell furnaces.

Crack lengths were measured on both surfaces of the propagation specimen using a traveling microscope. This was facilitated by interrupting the cyclic loading, opening the furnace (allowing the specimen to cool), and applying the mean test load. This procedure held the specimen rigid while increasing crack tip visibility. A high intensity light was used to provide oblique illumination to the crack and further increase crack visibility. In general, crack length measurements were taken at increments no larger than 0.50 mm (0.020 in.). Crack length measurements are considered to be accurate to within ± 0.025 mm (0.001 in.).

All tests were conducted at 650°C (1200°F) with a stress ratio (minimum stress/maximum stress) of 0.05. Table 18 details all crack propagation tests.

Data Analysis Procedure

Two methods were employed to reduce crack length (a) vs cycles (N) data to a more usable form of stress intensity range (ΔK) vs crack growth rate (da/dN). The following paragraphs detail the two data analysis methods.

Direct Secant Method

Crack length (a) vs cycles (N) are not regressed. Discrete values of Δa and ΔN are computed from raw laboratory data. Discrete values of ΔK are calculated using the mean value of crack length over the interval. The expression used to calculate ΔK for a CT specimen is given in ASTM-647. By not smoothing the a - N data, the actual local $\Delta a/\Delta N$ perturbations are observable in the final SINH curve. The idea of plotting instantaneous slopes (da/dN) is not unique[4] and reveals information of a fundamental nature; the observed perturbations may have subtle metallurgical implications.

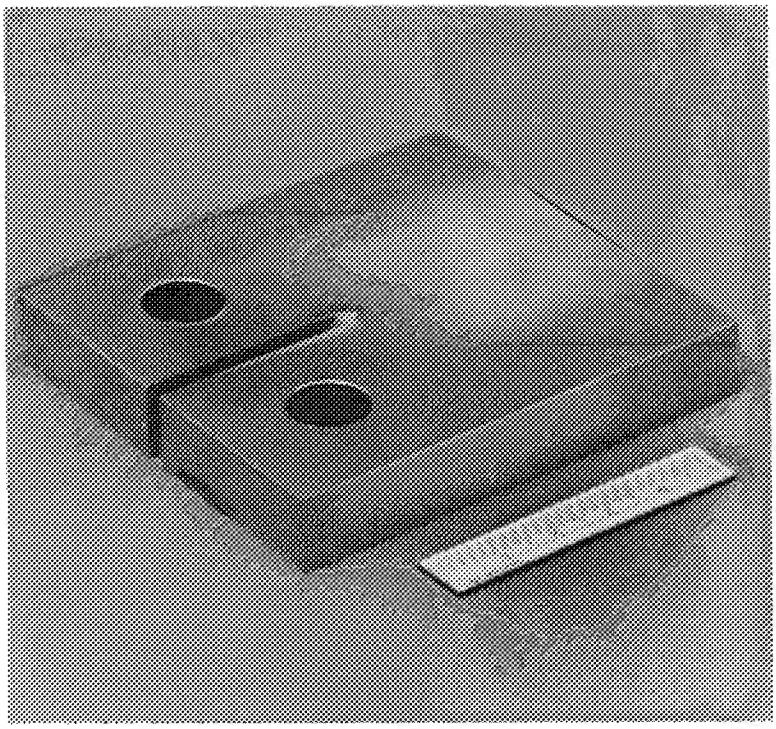

FE 169459

Figure 100. Photograph of Compact Type (ASTM CT) Specimen

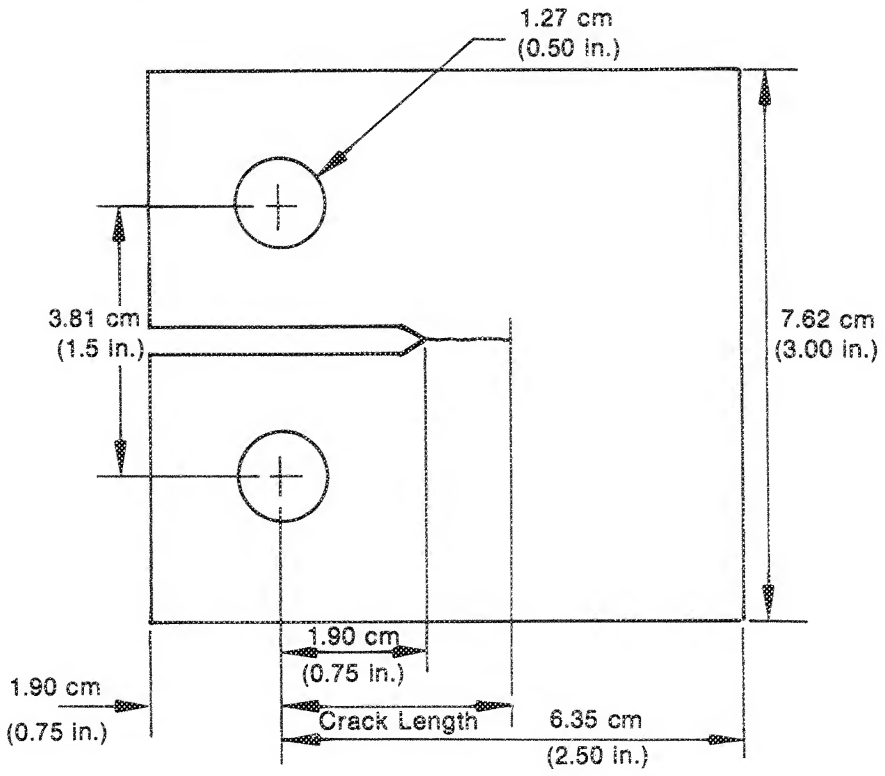

FD 119166

Figure 101. Compact Type (ASTM CT) Specimens

TABLE 18
CRACK PROPAGATION TEST SPECIMEN

Alloy Number	*Material Name*	*Specimen Number*	*Cyclic Frequency*	*Environment*	*Comments*
1	MERL 76	1610	0.33 Hz	Air	
1	MERL 76	1700	0.33 Hz	Air	
1	MERL 76	1701	0.33 Hz	Air	
1	MERL 76	1702	900 sec dwell	Air	
1	MERL 76	1612	900 sec dwell	Air	
1	MERL 76	1608	900 sec dwell	Air	
2	René 95	1398	0.33 Hz	Air	
2	René 95	1400	0.33 Hz	Air	
2	René 95	1403	900 sec dwell	Air	
2	René 95	1589	900 sec dwell	Air	
2	René 95	1590	900 sec dwell	Air	
2	René 95	1616	900 sec dwell	Air	GE specimen config.
3	Waspaloy	1367	0.33 Hz	Argon	
3	Waspaloy	1368	0.33 Hz	Argon	
4	IN 100	1385	0.33 Hz	Argon	
4	IN 100	1388	0.33 Hz	Argon	
4	IN 100	1389	0.33 Hz	Air	Environment chamber calibration

Note: All specimens tested at 650°C (1200°F), R = 0.05

Seven-Point Sliding Polynomial

The seven-point sliding polynomial is a smoothing function which reduces the amount of scatter observed in da/dN vs ΔK data. This method for computing da/dN involves fitting a second-order polynomial (parabola) to sets of seven successive data points.[5] The equation takes the form for local fit as:

$$\hat{a}_4 = b_0 + b_1 \left[\frac{N_4 - \xi_1}{\xi_2} \right] + b_2 \left[\frac{N_4 - \xi_1}{\xi_2} \right]^2 \quad (1)$$

where:

$$-1 \leq \left[\frac{N_4 - \xi_1}{\xi_2} \right] \leq +1$$

and b_0, b_1, and b_2 are the regression parameters which are determined by the least squares method (that is, minimization of the square of the deviations between observed and fitted values of crack length) over the range a_1 to a_7. The value $\hat{a}_4$ is the fitted value of crack length at N_4. The parameters, $\xi_1 = \frac{1}{2}(N_1 + N_7)$ and $\xi_2 = \frac{1}{2}(N_7 - N_1)$, are used to scale the input data. The crack growth rate at N_4 is obtained directly from the derivative of equation 2 as follows:

$$(da/dN)\hat{a}_4 = \frac{b_1}{\xi_2} + 2\, b_2 (N_4 - \xi_1)/\xi_2^2 \quad (2)$$

The ΔK associated with this da/dN is calculated using the fitted crack length, $\hat{a}_4$. Again, the ΔK expression comes from ASTM-647.

After calculation of da/dN and ΔK using the first seven a vs N data points, another da/dN vs ΔK value is calculated using actual a vs N data points 2 to 8 (renumbered 1 to 7 for use in the equations). The local fit is moved along the data one point at a time until the last seven points are used in the calculation. Since seven points are required for each local fit, the first three and last three points in the data set are lost in the calculations.

The seven-point sliding polynomial method of data reduction was used when sufficient data was available, while the direct secant method was used in all other cases. On da/dN vs ΔK plots, data reduced by the seven-point sliding polynomial method is distinguished by a "7AN" preceding the specimen number. A "100" prefix to the specimen number implies direct secant data reduction.

A computer-drawn plot of actual crack length vs cycles is produced when the da/dN and ΔK calculations are made, allowing the actual data to be scrutinized prior to further analysis. The da/dN vs ΔK data are modeled using the hyperbolic sine equation (described below), and da/dN vs ΔK computer plots are produced.

Hyperbolic Sine Model

Crack propagation under constant amplitude loading conditions is a function of the applied stress intensity range (within the limits of applicability of linear elastic fracture mechanics). The applied stress intensity, ΔK, is the driving force for crack propagation. Many relationships have been developed to correlate observed crack growth rate and stress intensity. Paris[6] presented the simple relationship:

$$da/dn = C(\Delta K)^n \tag{3}$$

where C and n are material constants. At elevated temperatures, however, the crack growth process is a complicated function of stress ratio, temperature, load history, and environment. These dependencies make the general use of equations such as Equation (3), more difficult. A model developed at P&WA/Florida has accurately and efficiently described the effects of stress ratio, cyclic frequency, and temperature on the crack growth characteristics of selected high temperature nickel- and iron-base alloys. The model is based on the hyperbolic sine

$$\log(da/dn) = C_1 \text{ SINH } (C_2(\log \Delta K + C_3)) + C_4 \tag{4}$$

where the coefficients have been shown to be functions of test frequency, stress ratio, and temperature:

C_1 = material constant
$C_2 = f_2 (R, \nu, T)$
$C_3 = f_3 (R, \nu, T)$
$C_4 = f_4 (R, \nu, T)$

The hyperbolic sine equation was selected as the model for the following reasons:

- It exhibits the overall shape of typical da/dN vs ΔK plots obtained over several decades of crack growth rates.

- All or part of the equation may be used to fit data since the SINH has both a concave and a convex half and a nearly linear portion near inflection. Also, the slope at inflection can vary with the fitting constants. (By comparison, the slope of an x^3 model is always zero at inflection.)

- The SINH is not periodic (e.g., trigonometric tangent) nor asymptotic (e.g., tangent, or inverse hyperbolic tangent); therefore, when extrapolation becomes necessary, the SINH behaves well at distances removed from the data, quite unlike most polynominals, periodic, or asymptotic functions.

- This model requires no information other than a, N data. By comparison, some other models in current use require both K_{th} and K_{IC}, in addition to a, N data, to model crack growth behavior. Both K_{th} and K_{IC} are difficult to obtain experimentally; K_{th} because of the extremely small crack growth measurements necessary, and K_{IC} because of gross plasticity at the crack tip encountered in fracture-toughness testing at elevated temperatures.

The hyperbolic sine is defined as

$$y = \text{SINH } x = \frac{e^x - e^{-x}}{2} \tag{5}$$

and when presented on Cartesian coordinates, it appears as shown in figure 102. The function is zero at $x = 0$ and has its inflection there.

The introduction of the four regression coefficients, C_1 through C_4, permits relocation of the point of inflection and scaling of both axes. In the equation

$$(y - C_4) = \text{SINH } (x + C_3), \tag{6}$$

C_3 establishes the horizontal location of the hyperbolic sine point of inflection and C_4 locates its vertical position.

To scale the axes, C_1 and C_2 are introduced

$$\frac{(y - C_4)}{C_1} = \text{SINH } (C_2 (x + C_3)) \tag{7}$$

which can be rewritten as

$$y = C_1 \text{ SINH } (C_2 (x + C_3)) + C_4 \tag{8}$$

of which equation 4 is a special case where $y = \log (da/dN)$ and $x = \log (\Delta K)$. Note that C_3 has units of $\log (\Delta K)$ and C_4 has units of $\log (da/dN)$; C_1 and C_2 are dimensionless and can be conceptualized as stretching the curve vertically and horizontally, respectively. Experience indicates that, for a given material, C_1 can be fixed without adversely affecting model flexibility.[7]

Once the coefficients for the hyperbolic sine equation have been established by regression analysis, the equation can be used to estimate crack propagation rates for any given level of stress intensity range at the temperature, frequency, and stress ratio under examination.

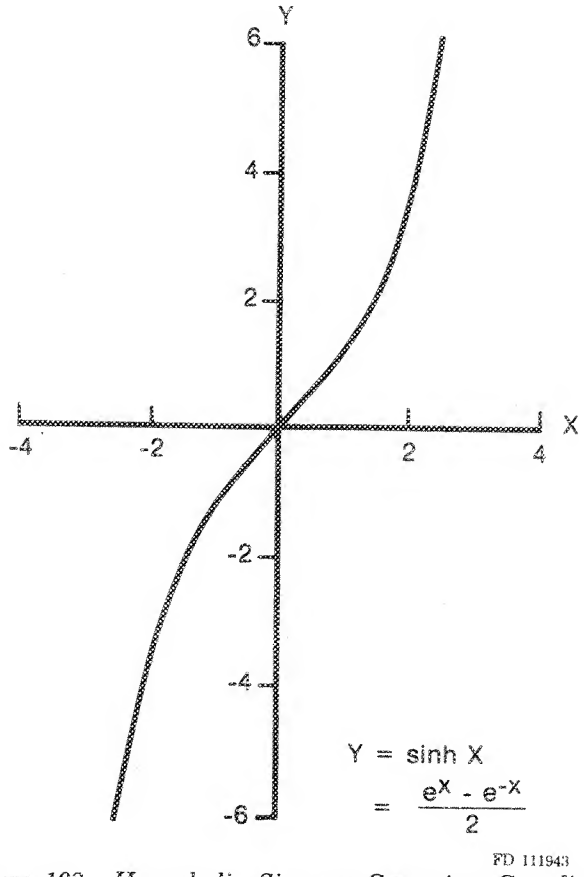

Figure 102. Hyperbolic Sine on Cartesian Coordinates

Limitations of Linear Elastic Fracture Mechanics

A fundamental assumption implicit in the use of the data analysis procedure detailed above involves the applicability of linear elastic fracture mechanics (LEFM) for each of the alloys tested. Consideration of nonlinear fracture mechanics was beyond the scope of this current contract. A brief examination of this LEFM assumption is presented in the following paragraphs.

The presence of a crack in a stressed component necessitates redistribution of stresses around the crack. The stress intensity factor is a parameter that reflects this redistribution and is a function of nominal stress, flaw size, and specimen and crack geometries. The concept of stress intensity factor was originally defined for an infinitely sharp crack in a perfectly elastic medium. In most engineering materials, localized plastic deformation occurs due to high stresses at the crack tip, and it is this deformation that gives the material resistance to crack propagation.

The degree of brittleness of a material (and the limit to the applicability of linear elastic fracture mechanics) is directly related to the type of stress redistribution process that occurs at the crack tip. In the high temperature fatigue process, this redistribution of stress is expected to depend on the relative degree of elastic, plastic, creep, and chemical work expended at the crack. In a completely brittle material, relaxation of the crack tip stress field is negligible, and simple reinitiation of a stopped crack is sufficient to promote complete fracture. The absolute limit to the applicability of fracture mechanics is general yielding.

The usefulness of LEFM depends on a uniparametrical relationship between crack growth rate and the stress intensity factor. Crack tip inelasticity, due to material response at elevated temperatures, can preclude general utility of K as the correlative parameter.

Under these considerations, tests should be designed such that the crack tip experiences sufficient geometric constraint and/or environmental embrittlement as to render da/dN vs ΔK relationships independent of specimen geometry (e.g., thickness).

Alloy Comparisons

Two alloys, HIP MERL 76 (Alloy 1) and HIP plus forged René 95 (Alloy 2), were tested in air at 650°C (1200°F) and R = 0.05. Two frequencies were tested for each alloy: 0.33 Hz (20 cpm) and 900-sec dwell at maximum tensile load. A minimum of two specimens of each alloy were tested at each condition.

Figures 103 and 104 depict crack growth rate curves at 0.33 Hz for HIP MERL 76 and René 95, respectively. Figure 105 is a composite plot showing how these two alloys compare with the five alloys tested under NASA Contract NAS3-20367.[1] As illustrated by figure 105, René 95 exhibited the fastest crack growth for a given ΔK level. HIP MERL 76 also showed a relatively fast crack growth rate at approximately the same rate as NASA IIB-7 and IN 100. A rank ordering of all seven alloys based on crack growth rate from lowest growth rate to highest is presented below:

Waspaloy
HIP Astroloy
Wrought Astroloy
IN 100
HIP MERL 76
NASA IIB-7
René 95 H + F

Table 19 lists the hyperbolic sine coefficients for each alloy tested at 0.33 Hz.

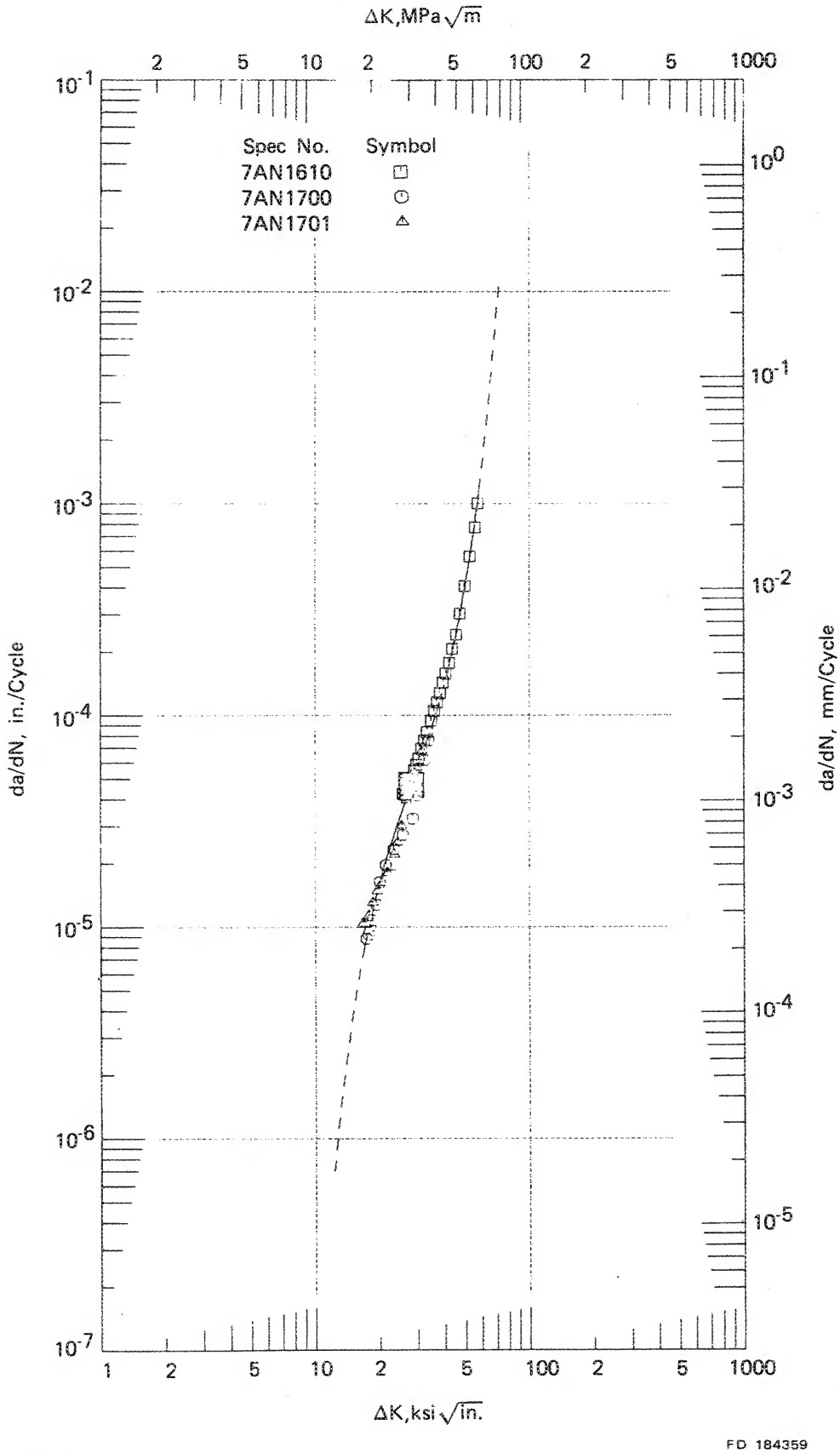

Figure 103. Crack Growth Results for MERL 76 Tested at 0.33 Hz

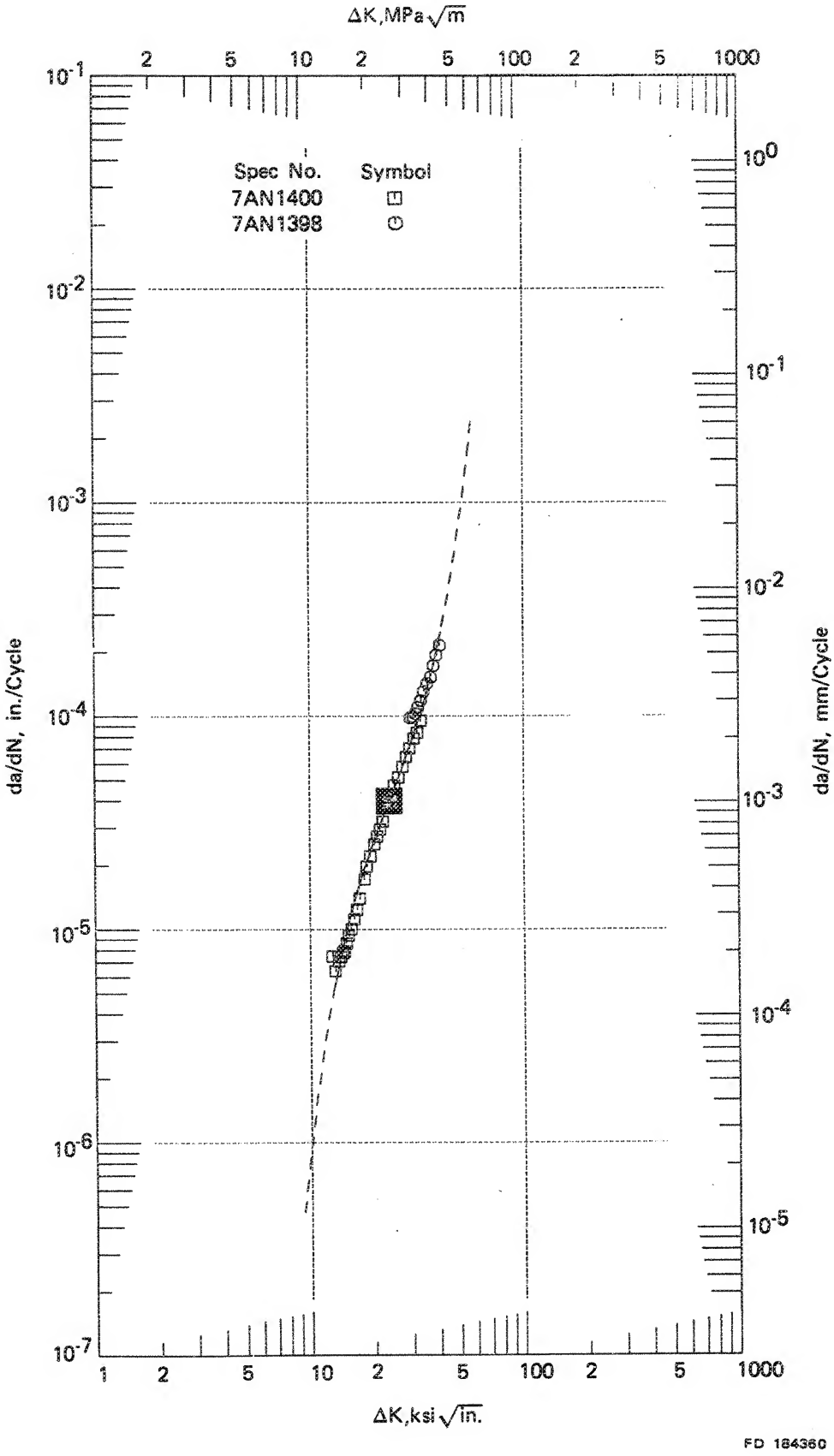

Figure 104. Crack Growth Results for René 95 Tested at 0.33 Hz

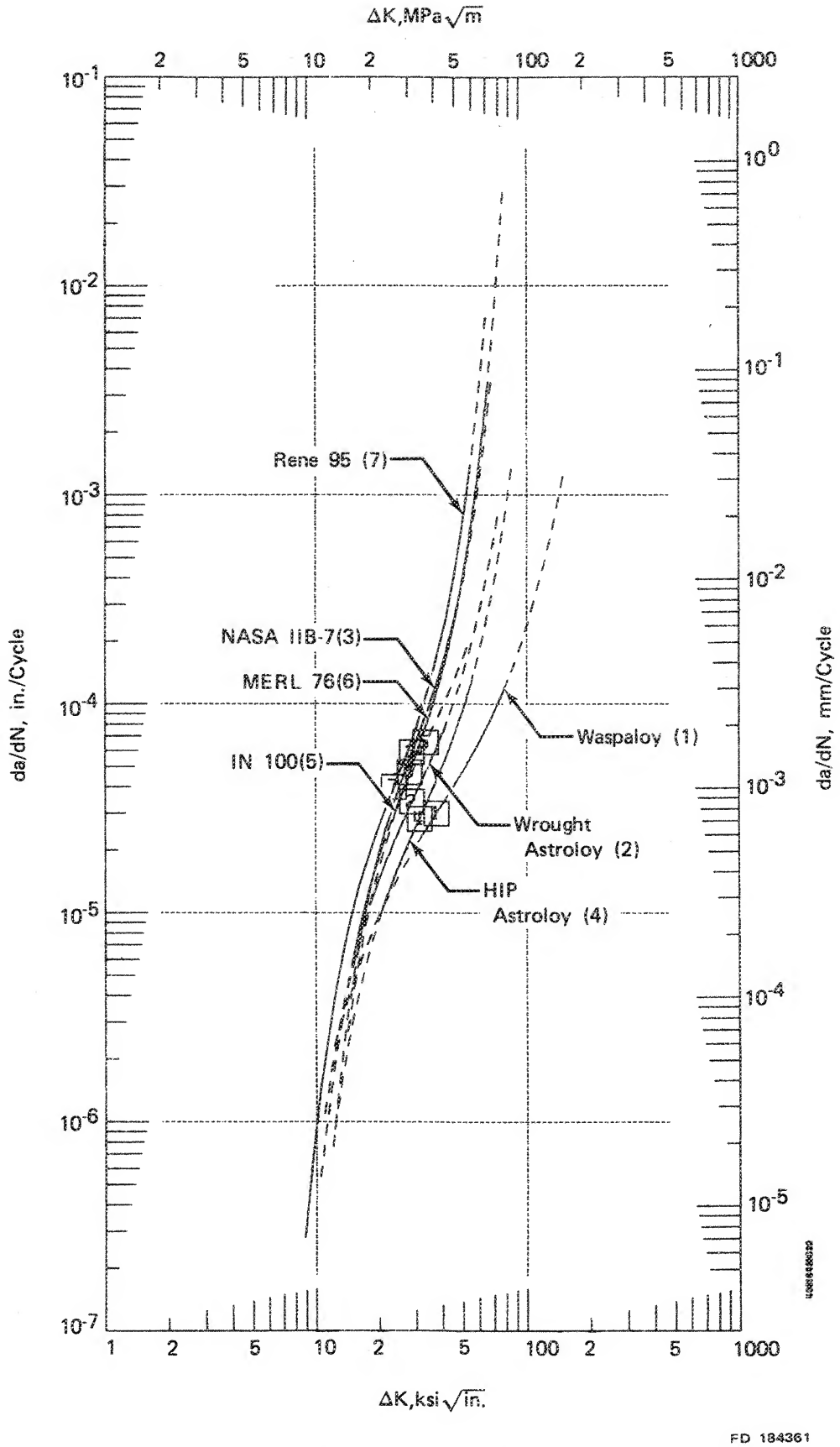

Figure 105. Composite Plot of all Seven Alloys Tested at 0.33 Hz

TABLE 19
HYPERBOLIC SINE COEFFICIENTS FOR ALLOYS TESTED AT 0.33 Hz IN AIR

$Y = C1 \times \sinh (C2 \times (X + C3)) + C4$
Where, Y = Log (da/dN) and X = Log (ΔK)

Curve	*C1*	*C2*	*C3*	*C4*	ΔK Range	R^2	*SEE*
1	0.5000	3.1690	-1.5740	-4.5250	(29.36, 80.69)	0.9032	0.1691
2	0.5000	4.3160	-1.4600	-4.4690	(18.08, 41.66)	0.9774	0.0886
3	0.5000	5.3510	-1.4600	-4.2320	(16.28, 48.49)	0.9760	0.0783
4	0.5000	4.4360	-1.4940	-4.5500	(19.85, 55.40)	0.9786	0.0526
5	0.5000	4.2360	-1.5240	-4.1850	(14.71, 21.25)	0.9657	0.0653
6	0.5000	5.5220	-1.4480	-4.3280	(23.12, 63.92)	0.9547	0.1238
7	0.5000	5.1010	-1.3720	-4.3980	(12.40, 49.33)	0.9710	0.1243

Curve	*Spec No.*	*Material*	*Temp*	*Atm*	*Freq*	*R*	*Type*	*Thik*
1	1000730	Waspaloy	1200F	Air	20 cpm	R = 0.05	CT	0.447
2	1000806	Wrought Astroloy	1200F	Air	20 cpm	R = 0.05	CT	0.501
3	1000797	NASA IIB-7	1200F	Air	20 cpm	R = 0.05	CT	0.500
4	1000726	HIP Astroloy	1200F	Air	20 cpm	R = 0.05	CT	0.420
5	1000710	IN 100	1200F	Air	20 cpm	R = 0.05	CT	0.826
6	1001610	MERL-76	1200F	Air	20 cpm	R = 0.05	CT	0.5015
7	1001400	René 95	1200F	Air	20 cpm	R = 0.05	CT	0.499

One aspect of the cyclic crack growth rate testing of HIP MERL 76 requires further discussion. As indicated by figure 106, one of the four HIP MERL 76 specimens (S/N 1607) tested at 0.33 Hz displayed a slower crack growth rate for a given ΔK. A review of parameters for specimen 1607 reveals that the specimen was run at a lower net section stress than the other three specimens. Note that specimens 1700 and 1701 were smaller CT's than specimens 1607 and 1610, but this should not affect crack growth rates.

Microstructural examination of the material tested, as shown in figure 107, shows a significant number of visible prior powder particle boundaries. Examination of several fracture surfaces indicated that a crack propagates through these at low stress levels, and around them at higher stress levels, as shown in figures 108 and 109.

A comparison of the fracture surfaces of specimens 1607 and 1610 at approximately the same ΔK appears in figures 110 and 111. Apparently, a difference exists in the fracture mechanism of the prior powder particles, and/or their boundaries. This difference may account for the variation in observed crack growth rates, and warrants further investigation.

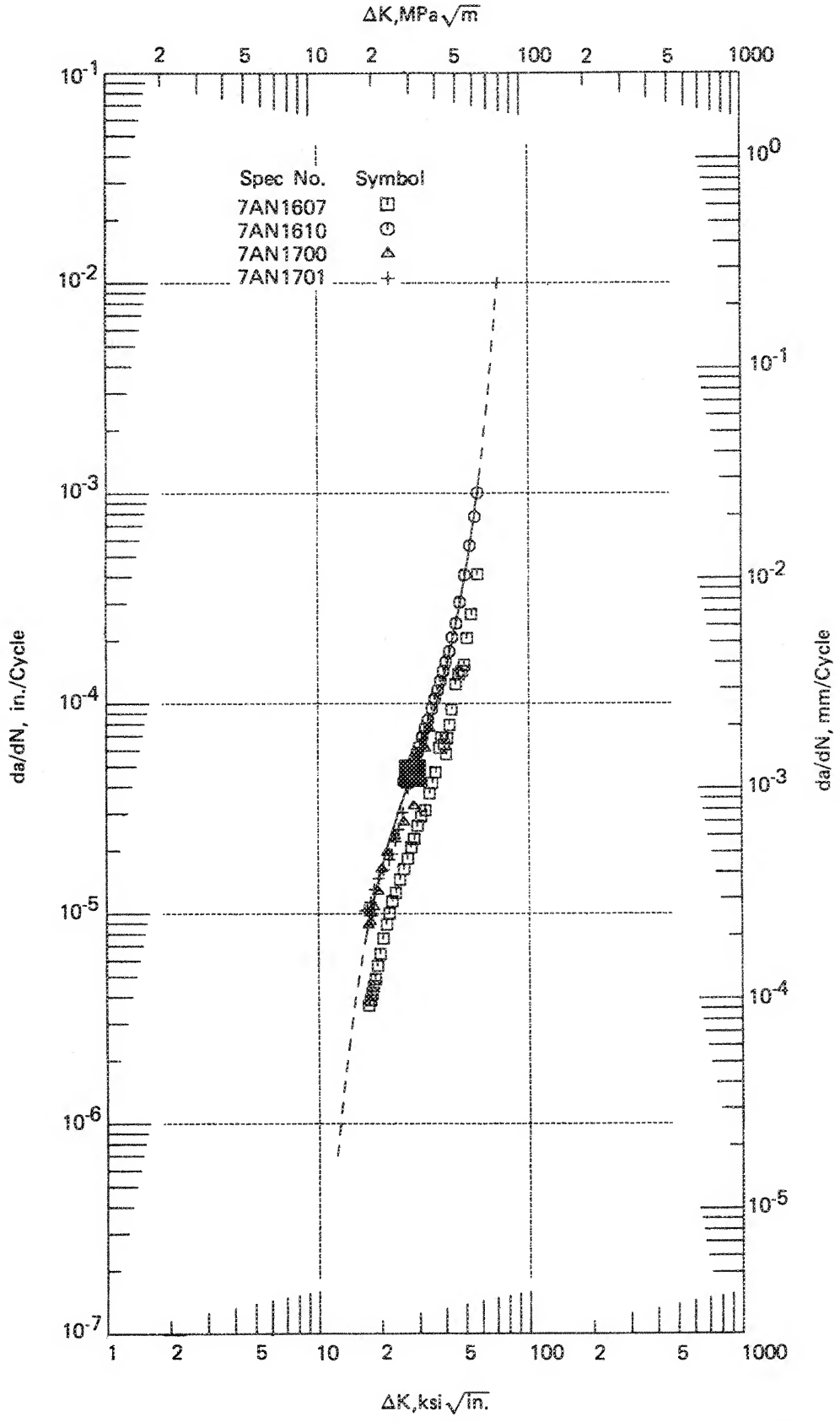

Figure 106. MERL 76 Tested at 0.33 Hz, Showing Apparent Change in Crack Growth Rate for Specimen 1607

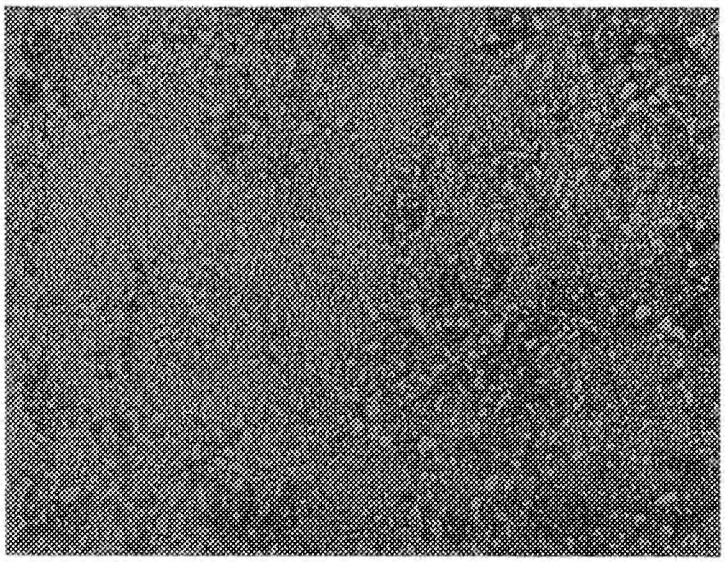

MAG 1000X

FD 184363

Figure 107. Optical Micrograph of Typical Microstructure of HIP MERL 76

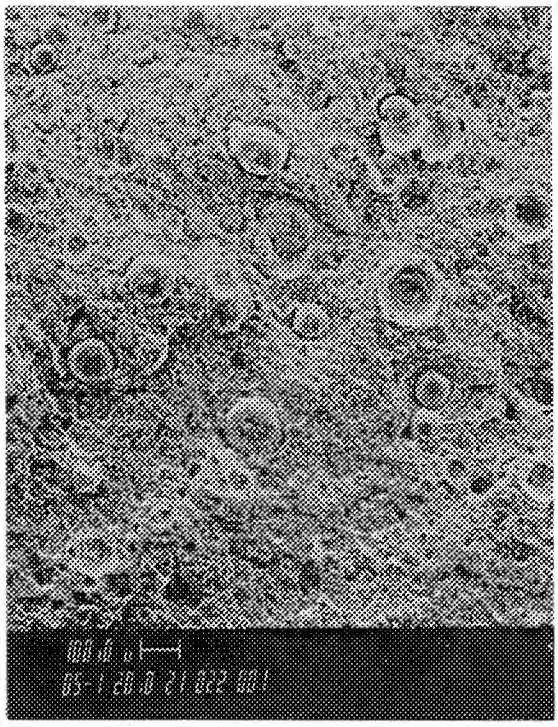

50X

FD 184364

Figure 108. SEM Fractograph of the HIP MERL 76 Fast Fracture Region (High Net Section Stress)

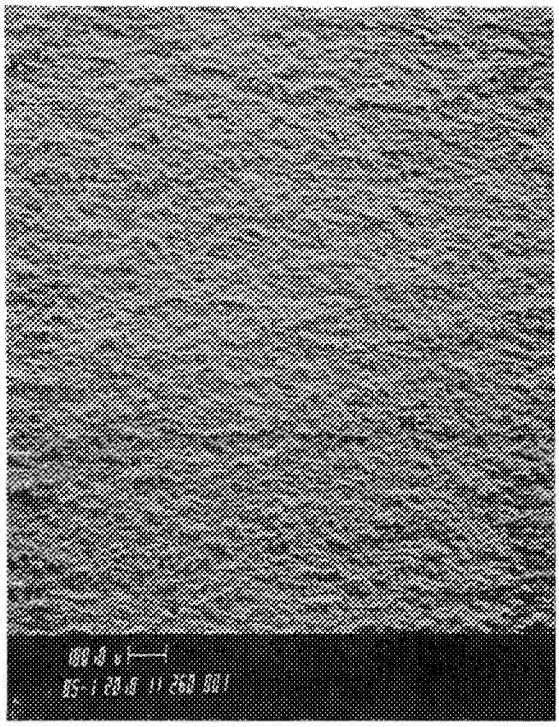

50X

FD 184365

Figure 109. SEM Fractograph of HIP MERL 76 Precrack Region (Low Net Section Stress)

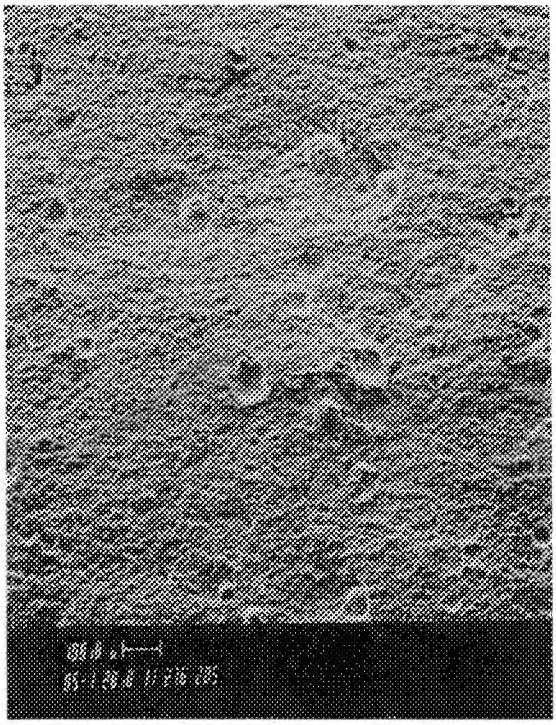

50X

FD 184366

Figure 110. SEM Fractograph of HIP MERL 76, Specimen 1610, Fracture Surface at $\Delta K = 32.3\ MPa\sqrt{m}$

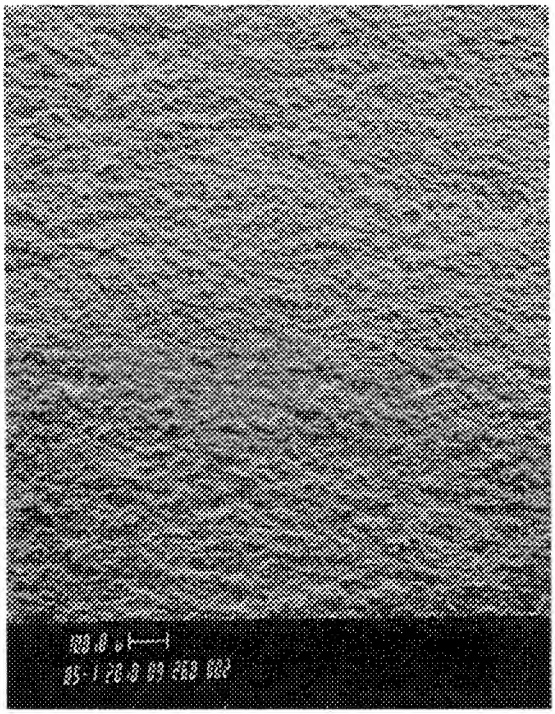

50X

FD 184367

Figure 111. SEM Fractograph of HIP MERL 76, Specimen 1607, Fracture Surface at $\Delta K = 31.5\ MPa\sqrt{m}$

Figures 112 and 113 give the crack growth rate curves for the 900-sec dwell at maximum tensile load for HIP plus forged René 95 and HIP MERL 76, respectively. Figure 114 presents a composite plot showing how these two alloys compare with the five alloys previously tested at the same conditions (NAS3-20367).1 Again, René 95 demonstrates the highest crack growth rate for a given ΔK. Note that the MERL 76 data covers only a limited da/dN range, and that extrapolations beyond that range may be inaccurate. As indicated by figure 114, the alloys generally follow the same trends as the 0.33 Hz data, but the absolute differences in crack growth rates are much larger, as high as two orders of magnitude for René 95 vs Waspaloy. The following listing is a rank ordering of all seven alloys with respect to crack growth rate from lowest to highest growth rate:

Waspaloy
HIP Astroloy
Wrought Astroloy
IN 100
HIP MERL 76
NASA IIB-7
René 95 H+F

Table 20 lists the hyperbolic sine coefficients for each alloy tested with 900-sec dwell at maximum tensile load.

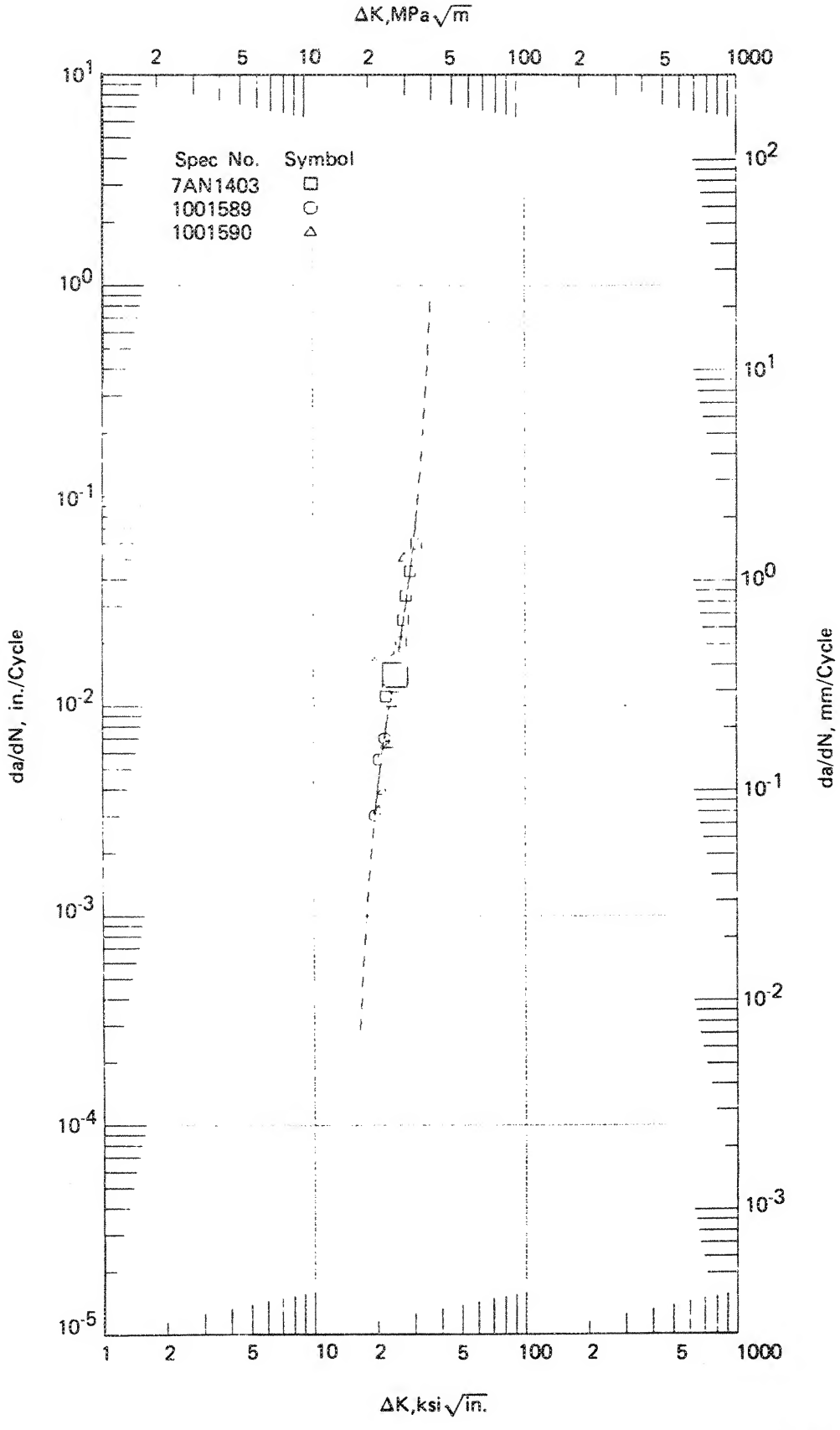

Figure 112. Crack Growth Results for René 95, Tested at 900 sec Dwell

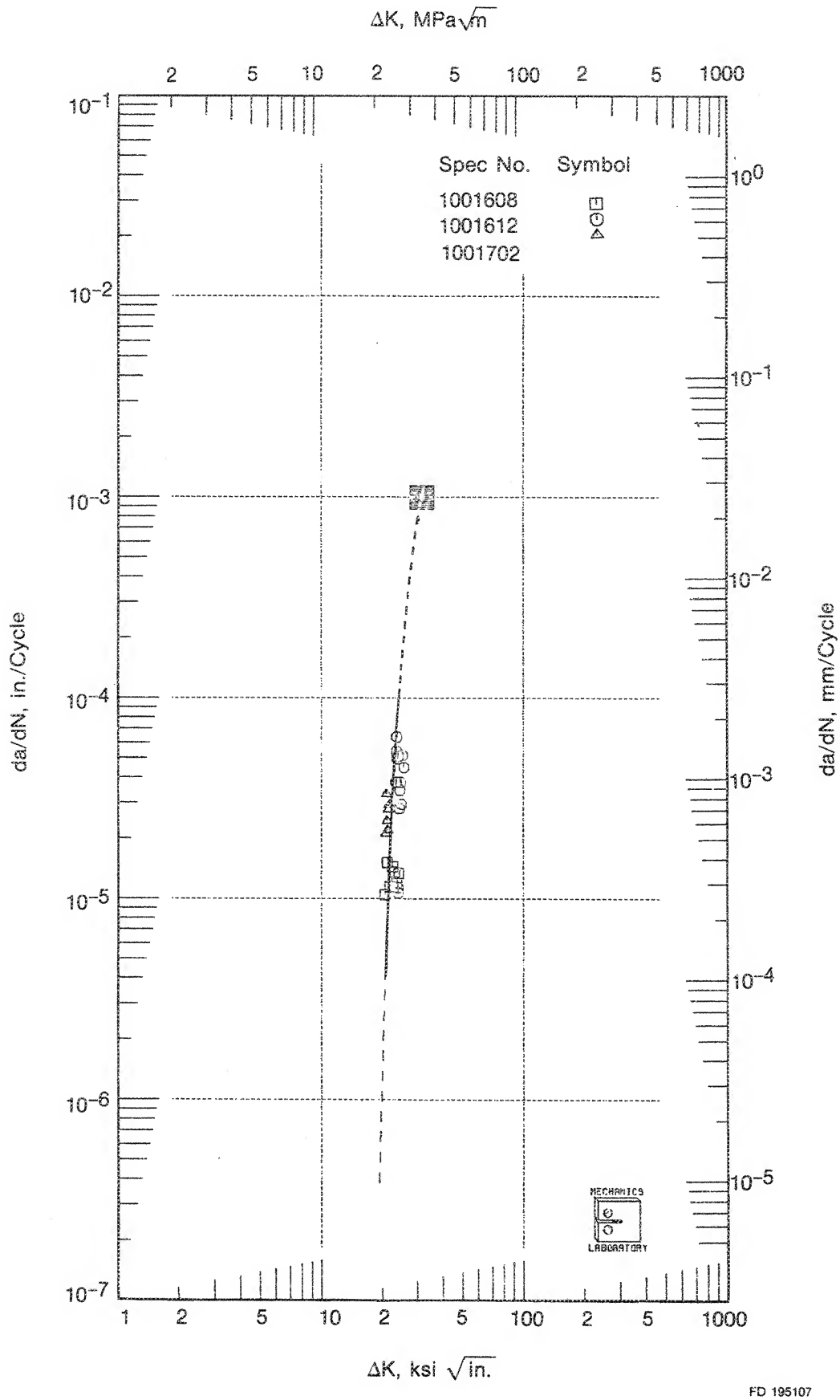

Figure 113. Crack Growth Results for MERL 76, Tested at 900 sec Dwell

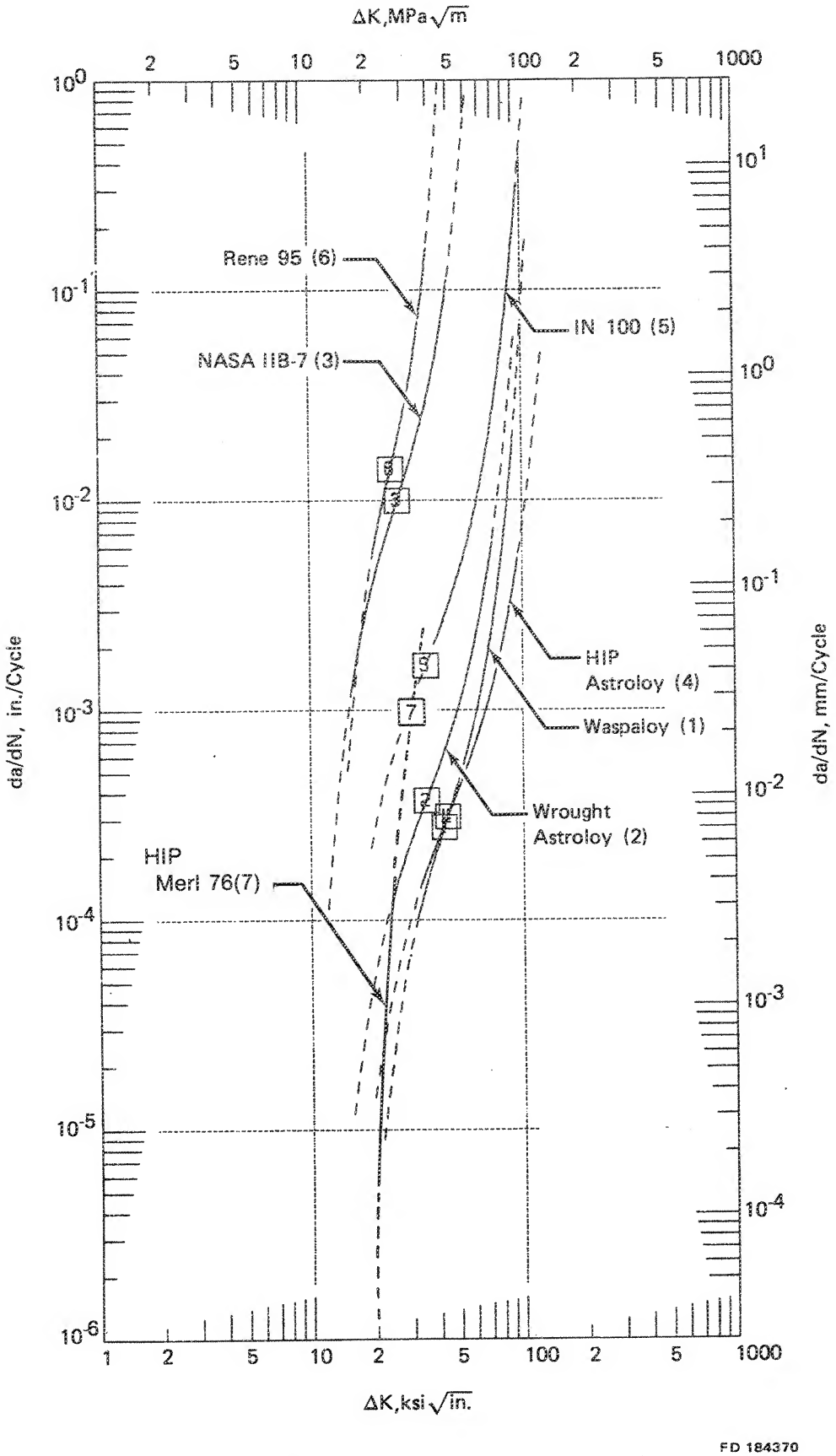

Figure 114. Composite Plot of All Seven Alloys 900-sec Dwell

TABLE 20
HYPERBOLIC SINE COEFFICIENTS FOR ALLOYS TESTED AT
900-sec DWELL IN AN AIR ATMOSPHERE

$Y = C1 \times \sinh (C2 \times (X + C3)) + C4$
Where, Y = Log (da/dN) and X = Log (ΔK)

Curve	*C1*	*C2*	*C3*	*C4*	ΔK Range	R^2	*SEE*
1	0.5000	6.1490	-1.6290	-3.5580	(30.93, 89.51)	0.9443	0.1566
2	0.5000	5.1950	-1.5440	-3.4320	(23.84, 71.39)	0.7815	0.3505
3	0.5000	6.1600	-1.4150	-2.0000	(15.49, 44.80)	0.9390	0.2009
4	0.5000	4.8890	-1.6440	-3.5080	(32.60, 94.11)	0.9363	0.1471
5	0.5000	5.0470	-1.5440	-2.7880	(38.30, 94.84)	0.7635	0.2905
6	0.5000	8.5000	-1.3840	-1.8500	(19.62, 36.01)	0.8216	0.1678
7	0.5000	12.2388	-1.5000	-3.0000	(20.62, 25.59)	0.7520	0.6024

Curve	*Spec No.*	*Material*	*Temp*	*Atm*	*Freq*	*R*	*Type*	*Thik*
1	1000731	Waspaloy	1200F	Air	900 SD	R = 0.05	CT	0.417
2	1000814	Wrought Astroloy	1200F	Air	900 SD	R = 0.05	CT	0.381
3	1000800	NASA IIB-7	1200F	Air	900 SD	R = 0.05	CT	0.500
4	1000728	HIP Astroloy	1200F	Air	900 SD	R = 0.05	CT	0.501
5	10007 5	IN 100	1200F	Air	900 SD	R = 0.05	CT	0.500
6	1001403	René 95	1200F	Air	900 SD	R = 0.05	CT	0.500
7	1001702	HIP MERL 76	1200F	Air	900 SD	R = 0.05	CT	0.503

Test Method Comparison

A comparison of Contractor testing and data analysis procedures was conducted for HIP plus forged René 95 (Alloy 2). Crack propagation tests were conducted at 650°C, R = 0.05, and a frequency of 0.33 Hz. Similar tests were run with a 900-sec dwell at maximum tensile load. The results of these tests were compared to test data derived by General Electric.[2] Testing conducted at P&WA/Florida duplicated the test conditions of temperature, stress ratio, and frequency to produce comparable data. However, each contractor used a different specimen geometry. P&WA used the ASTM CT specimen for all tests, while GE used a K_b bar surface flaw specimen.[2]

The results of the data comparison for 0.33 Hz testing appear in figure 115. This figure shows the crack growth rates obtained with the K_b bar specimen to be approximately a factor of 2 slower than those obtained with the compact specimens.

The results of the data comparison for 900-sec dwell testing appear in figure 116. These data indicate that a considerable difference exists in the crack propagation rates, with the difference increasing as stress intensity increases. Also included in figure 116 is data from a K_b bar specimen that was tested at P&WA in an attempt to resolve the large differences in observed crack growth rates. Unfortunately, no conclusion could be drawn from this limited data. Lack of material precluded further testing of specimens in the K_b bar configuration.

Another possible source of discrepancy in Contractor data lies in the stress intensity solutions utilized in data reduction. The CT specimen is a standard specimen with well-established K solutions, while the K_b bar specimen is a nonstandard surface-flaw specimen. The K solution utilized by GE is given in Reference 2. To establish the validity of that K solution, Sha[8] performed a comparative survey of existing K solutions for surface flaws as applied to the K_b bar specimen geometry. The findings of the survey indicate that the GE K solution corresponds well with other solutions in regions of low net section stress and where bending stresses arising from the presence of a relatively shallow crack are negligible. Considerable deviations occur when the surface crack area becomes large enough, as compared to the gross cross-sectional area of the specimen, to cause high net section stresses (approximately 0.8 σ_{ys}), and when induced bending stresses due to a deep flaw become significant as compared to tensile stresses. At an a/t (crack depth/thickness) ratio of 0.8, induced bending stresses become approximately 30% as high as tensile stresses due to the applied loads. However, this calculated difference in stress due to bending is not of sufficient magnitude to account for the large difference in crack growth rates between the two specimen types in the 900-sec dwell test.

Further testing and analyses are needed in order to reconcile and/or refute the differences in crack growth rates observed in the data presented here.

Controlled Environment Testing

Testing to determine the effect of oxidation on crack growth rate was conducted using Waspaloy (Alloy 3) and IN 100 (Alloy 4). These alloys were selected because they represent extremes in strength, processing technique, and microstructure of turbine disk alloys currently in use. Tests were conducted at 650°C, R = 0.05, and 0.33 Hz for both alloys. Similar tests were conducted utilizing a 900-sec dwell at maximum tensile load. All tests were run in an argon atmosphere in order to minimize oxidation effects on crack growth rates. Data from these tests are compared to tests run at the same conditions in an air atmosphere in order to determine the effects of oxidation on crack growth rates.

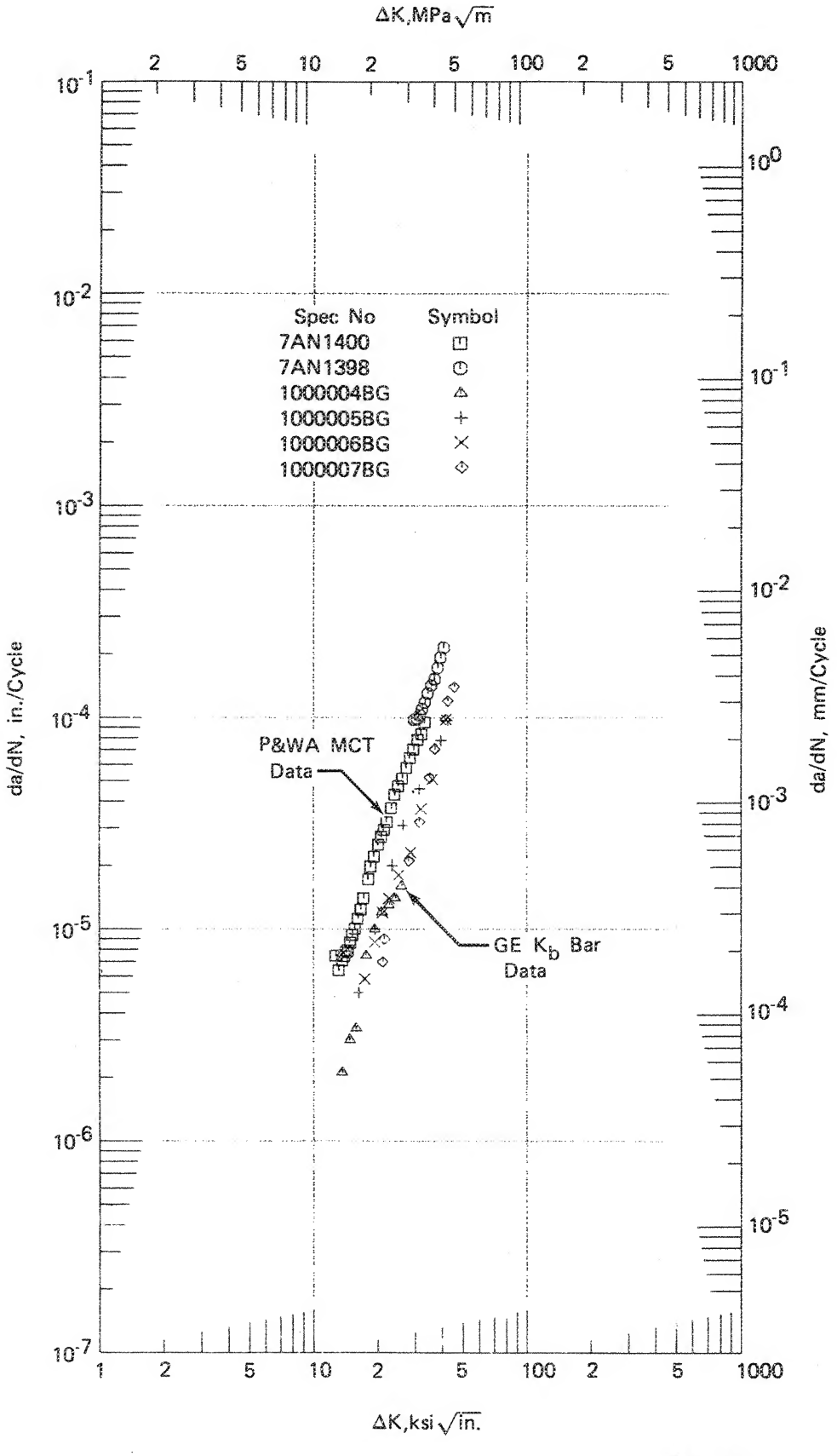

Figure 115. Comparison of P&WA and GE Data — René 95, 0.33 Hz

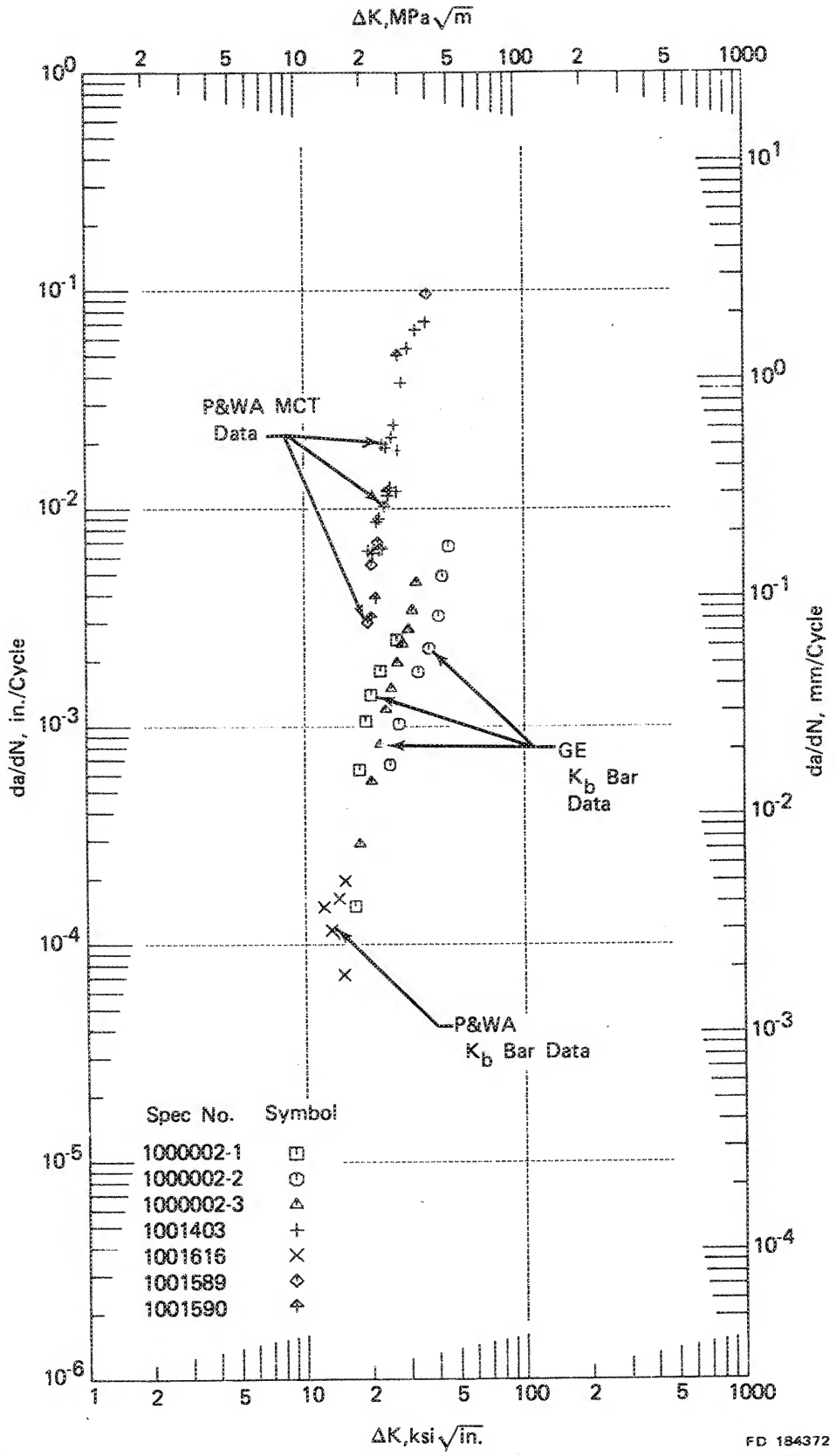

Figure 116. Comparison of P&WA and GE Data — René 95, 900-sec Dwell

Testing in an argon atmosphere required several specialized test procedures. The inert atmosphere was maintained within the environmental chamber depicted in figure 117. To minimize the amount of oxygen remaining, the chamber was evacuated and backfilled with argon a minimum of three times before beginning each test. During testing, argon pressure was maintained at slightly greater than one atmosphere. Specimen heating was provided by external radiant heaters. Crack length readings were obtained by direct optical measurements taken through the glass windows of the chamber.

In the case of IN 100 specimen S/N 1385, heating was provided by a resistance susceptor furnace. In that configuration, crack length was continuously monitored on one side only, since obtaining crack length readings on the second side require complete teardown of the chamber. Complete crack length readings were obtained on both sides of the specimens four times during the course of the test. This awkward test procedure was made necessary by multiple failures of the glass windows in the environment chamber.

Calibration of the environment chamber was accomplished by running an IN 100 test in air in the chamber at 650°C and comparing the results with data from previous experience. Figure 118 details a comparison of the environmental chamber air test results with tests performed under Contract NAS3-20367.[1] Differences in crack growth rates fall within the expected heat-to-heat variations.

The most recent analysis of inhouse argon at P&WA/Florida gave the following specifications for the argon utilized in this test phase:

Water	—	3 ppm
Oxygen	—	5 ppm
Nitrogen	—	20 ppm
Hydrogen	—	3 ppm

Water and oxygen levels were checked at the argon line in the Fracture Mechanics Laboratory and showed slight degradation to:

Water	—	16 ppm
Oxygen	—	5 ppm

It was not feasible to obtain an accurate analysis of gases actually in the environment chamber.

Figures 119 and 120 present comparisons of argon and air data tested at 0.33 Hz for Waspaloy and IN 100, respectively. As indicated in figure 119, there is little difference in crack growth rates for Waspaloy above ΔK value of about 44 MPa$\sqrt{m}$. Below this value, the crack growth rates for the argon environment tests are slightly lower than the air tests. Figure 120 shows a small difference in crack growth rates between IN 100 tested in air and in argon. The data gathered in argon is a factor of 2 to 2.5 times slower than air data up to a ΔK value of about 33 MPa$\sqrt{m}$. The data converge at higher values of ΔK.

Figures 121 and 122 show curve fits and hyperbolic sine coefficients for 0.33 Hz, argon environment tests for Waspaloy and IN 100, respectively.

One possible explanation of the difference in crack growth rates observed in argon at 0.33 Hz is presented by Gell and Leverant.[9] Formation of oxides at the crack tip results in a region depleted of oxide-forming elements. This region will be somewhat weakened and embrittled by the loss of these elements and, thus, subject to relatively easy cracking. If the increment of crack growth per cycle in the absence of oxygen is less than the size of the depleted zone, the crack growth per cycle in the presence of oxygen will be controlled by the size of the depleted zone, resulting in an increased crack growth rate. In terms of intergranular fracture, this process can occur due to preferential grain boundary oxidation.

Cyclic-dwell crack growth tests incorporating a 900-sec hold at maximum load were conducted in an inert environment for both IN 100 and Waspaloy. Results however, were judged to be anomalous and consequently the data are not presented. Causes of the anomalous results are not known, but equipment malfunctions combined with the extreme test conditions of long hold periods, high temperature and discontinuous crack growth are suspected contributors. Further investigations are being conducted to resolve these difficulties.

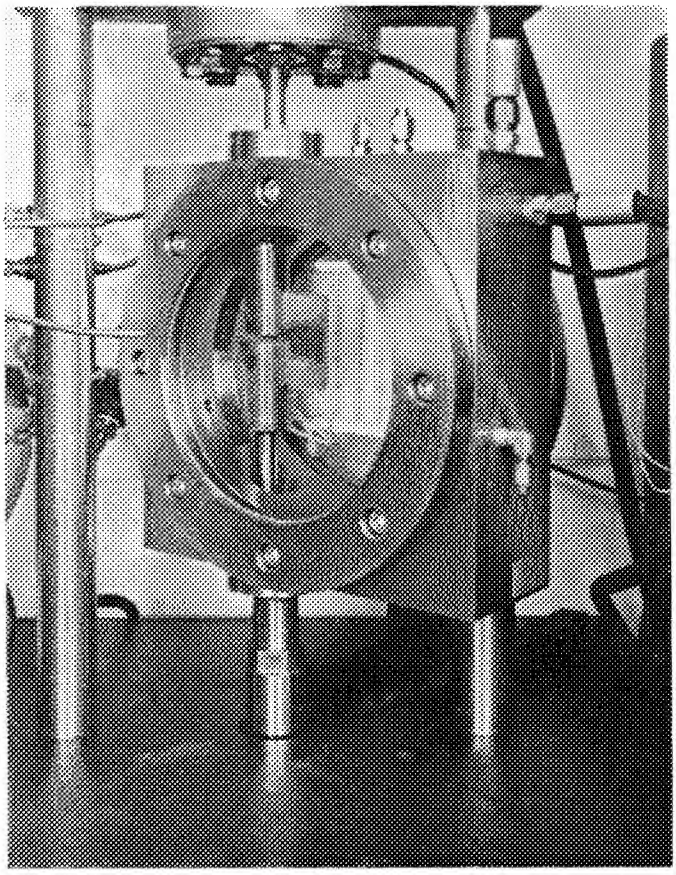

FE 150353

Figure 117. Argon Environment Chamber

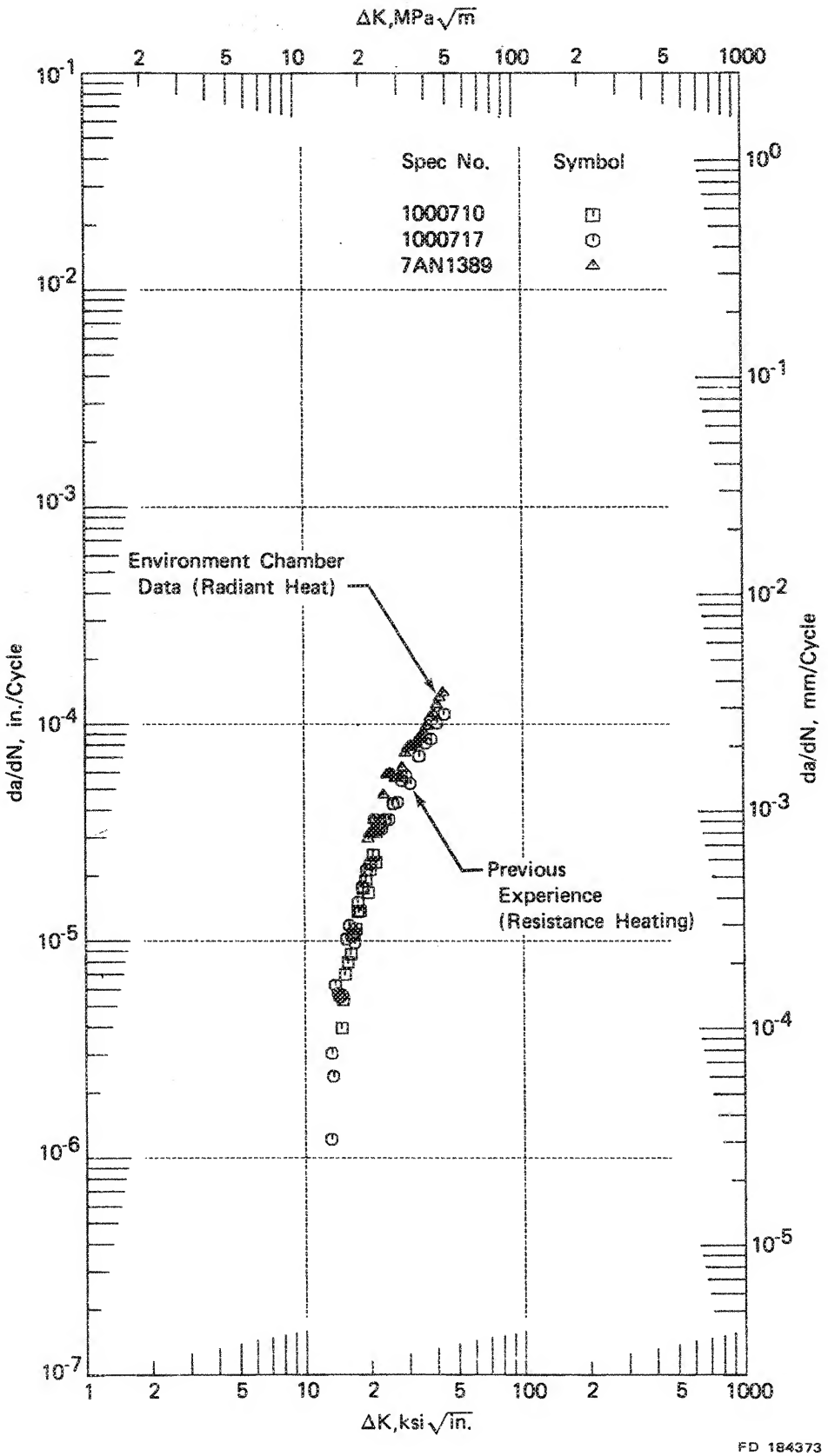

Figure 118. Environmental Chamber Calibration Test Comparison

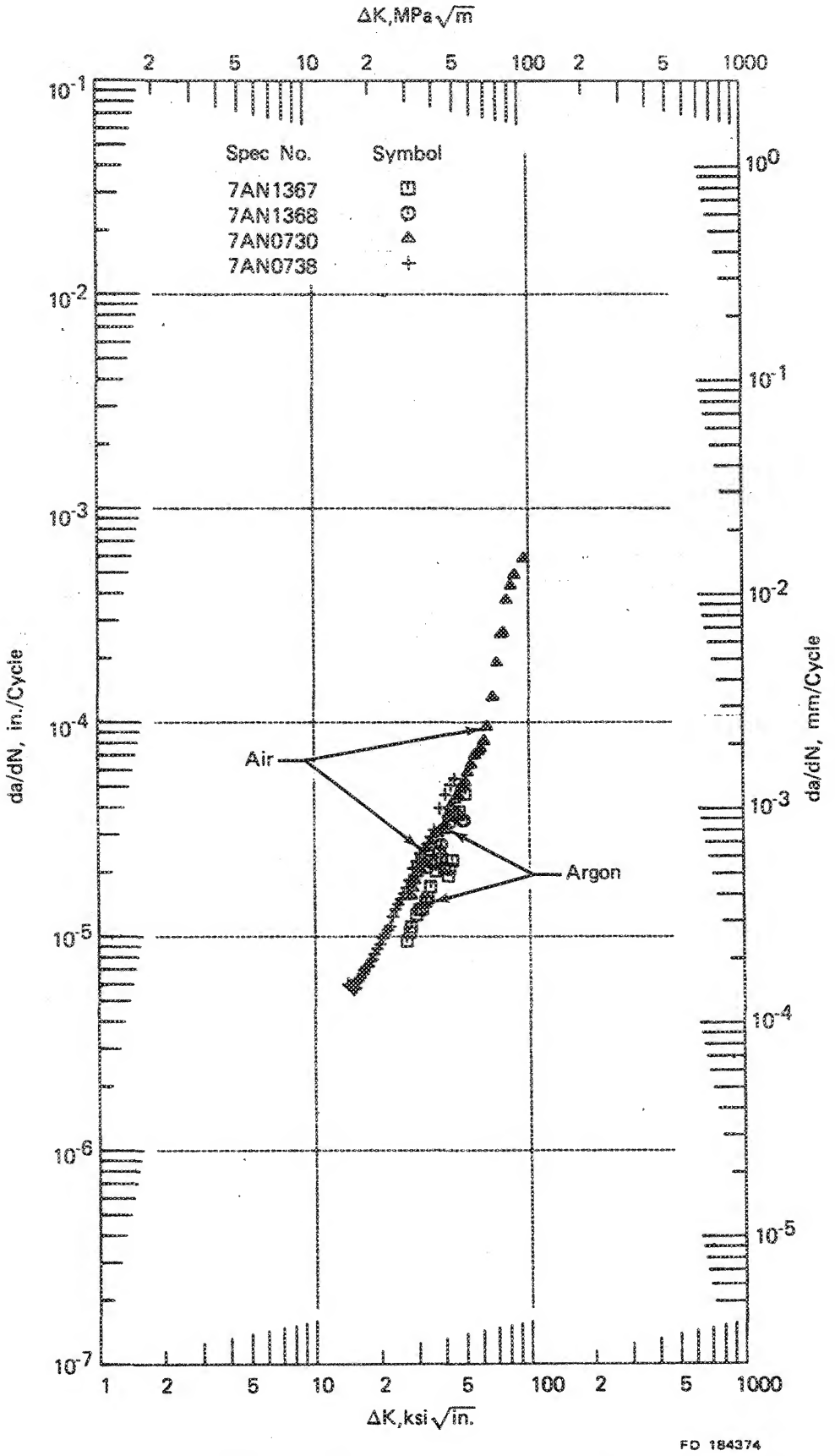

Figure 119. Comparison of Waspaloy Tested in Argon and in Air, 0.33 Hz

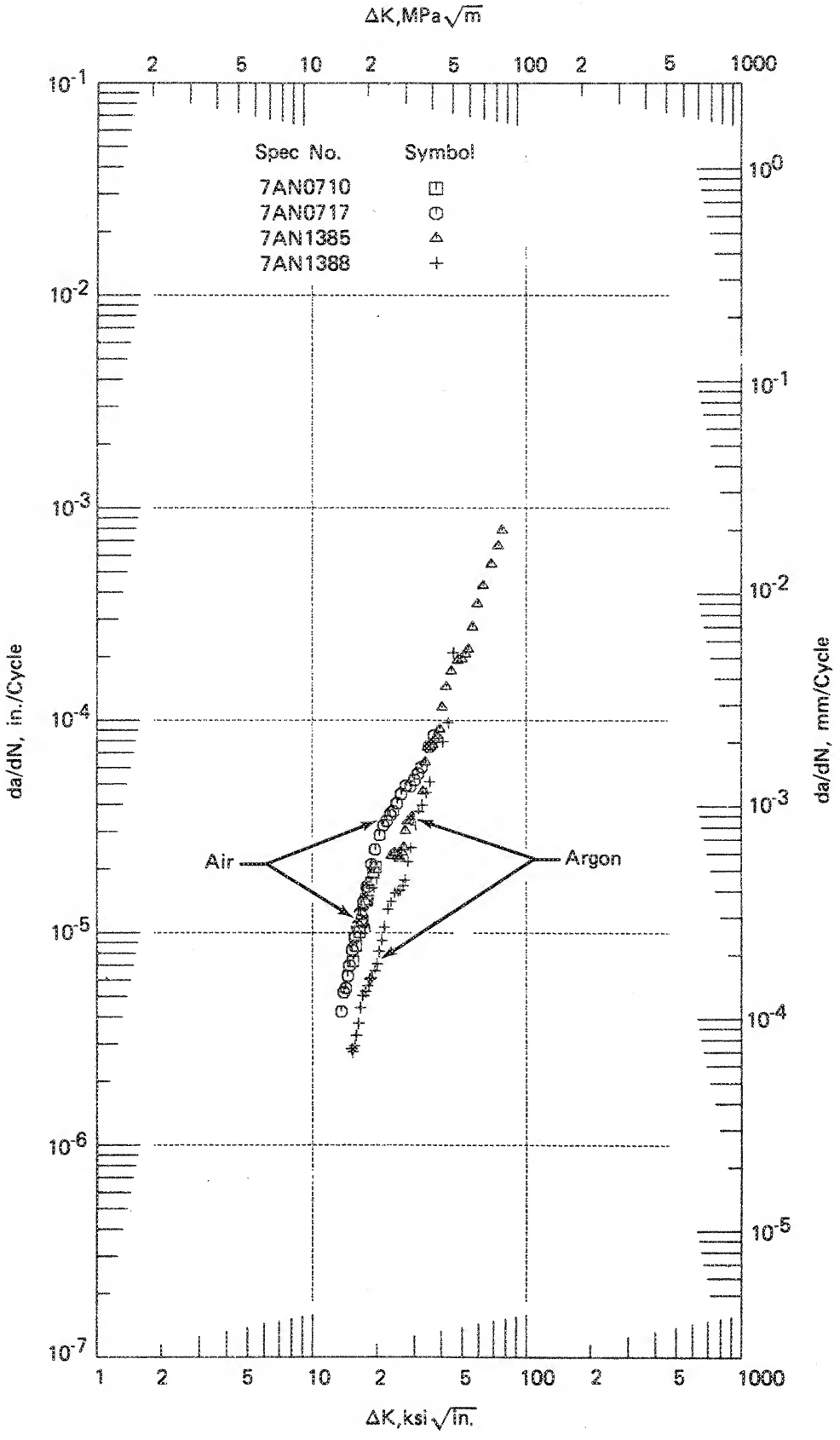

FD 184375

Figure 120. Comparison of IN 100 Tested in Argon and in Air, 0.33 Hz

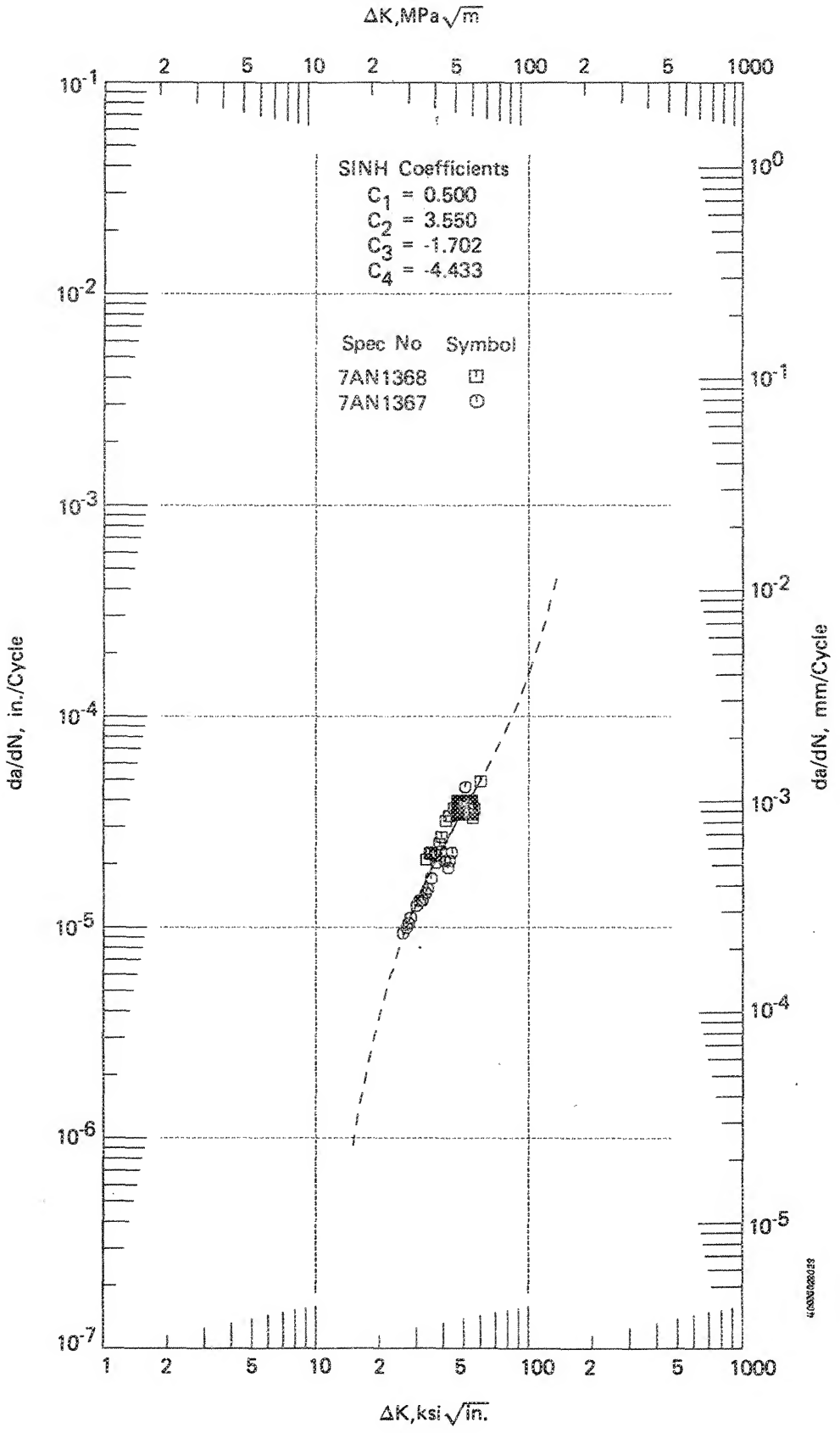

Figure 121. Waspaloy Tested in Argon, 0.33 Hz

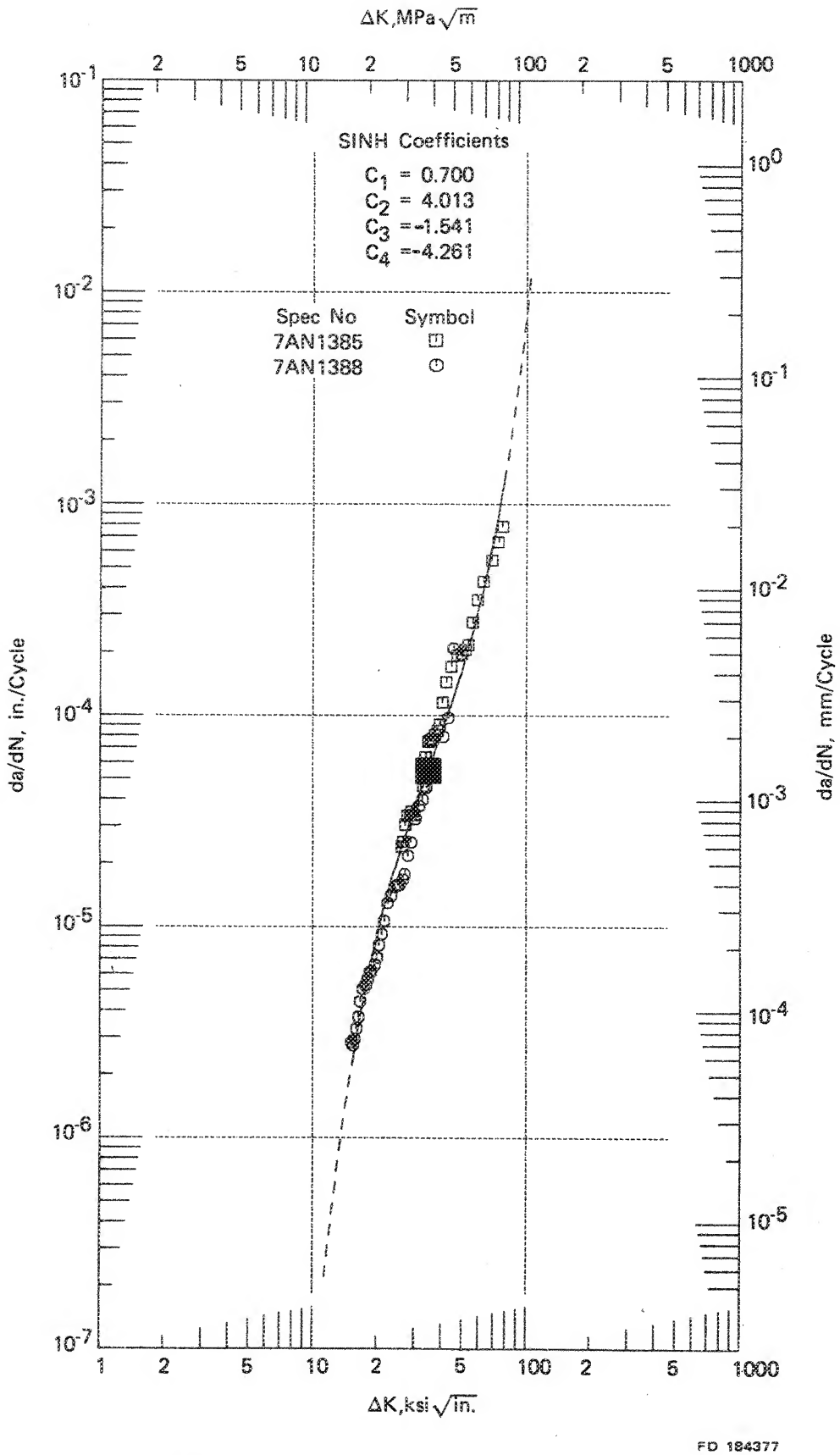

Figure 122. IN 100 Tested in Argon, 0.33 Hz

EVALUATION OF FATIGUE CRACK INITIATION MECHANISMS

General

The cyclic behavior evaluations of turbine disk alloys performed under this and previous contracts[1,2] showed relationships between alloy tensile strengths and fatigue crack initiation and fatigue crack growth behavior. Generally, the higher strength, finer grained alloys exhibited superior crack initiation behavior at strain ranges of interest for turbine disk applications, but showed somewhat faster crack propagation rates than the lower strength, generally coarser grained alloys. Also, the higher strength alloys exhibited a significantly higher degree of degradation due to hold times. Failed strain control test specimens were subjected to fractographic and metallographic examination to determine failure modes for the fatigue crack initiation and early crack propagation stages. The investigation included the relationship of failure mode and relative life to types of cycles (0.33 Hz or 900-sec dwell), grain size, and local microstructure.

Fractographic and metallographic studies were performed on strain control low-cycle fatigue samples test in air at 650°C (1200°F) from the nickel-base turbine disk alloys Waspaloy, wrought Astroloy, NASA IIB-7, HIP-formed Astroloy, GATORIZED® IN 100, HIP plus forged René 95, and HIP MERL 76. Representative high and low strain range cyclic and cyclic/dwell samples from each of the alloys were characterized to determine the mechanisms of crack initiation and propagation. Table 21 presents a detailed listing of the samples. These studies were performed with a high-resolution transmission electron microscope (TEM) using two-step carbon replicas of the fracture and by direct viewing of the fracture with a scanning electron microscope (SEM).

A metallographic section taken through the origin of each sample enabled observation of the microstructure and crack progression. These results were then correlated with those obtained in the fractographic studies.

Fractographic and Metallographic Results

Waspaloy

The high and low strain range cyclic Waspaloy samples (S/N A-2 and A-7) exhibited multiple origins, whereas cyclic/dwell samples (S/N A-11 and A-14) showed single origins, as shown in figure 123. The fracture faces of both cyclic samples showed cleavage at the origin and fatigue striations throughout the remainder of the propagation area, as shown in figure 124, indicating that both initiation and propagation were transgranular. Both cyclic/dwell samples showed heavy oxidation. The low strain range sample (S/N A-14) showed initiation and propagation to be predominantly intergranular, as shown in figure 125. A few isolated facets indicated some evidence of striations. The high strain range sample (S/N A-11) revealed crack initiation to be transgranular as evidenced by cleavage at the very origin and propagation to be predominantly intergranular, as seen in figure 126. As in A-14, a few isolated facets of striations were observed. Metallographic sections taken through each of the origins demonstrated similar results, as seen in figure 127.

Grain structure varied from sample to sample. The cyclic samples (A-2 and A-7) exhibited a coarser grain size (ASTM 3 to 5 with occasional 2) than the cyclic/dwell samples. The high strain range cyclic/dwell sample, A-11, showed a duplexed grain size that was predominantly ASTM 3 to 6 with occasional 1 and 2, with grains ASTM 7 and finer necklaced around the coarse grains. The low strain range cyclic/dwell sample (A-14) had a finer grain size (ASTM 4 to 5 with some 7 and finer) than either the cyclic or high strain range cyclic/dwell sample.

Wrought Astroloy

The high strain range cyclic wrought Astroloy sample (S/N 1A) showed multiple small origins almost completely around the circumference of the sample, whereas all of the other samples had a major origin with one or minor origins, as shown in figure 128. The major origin of the low strain range cyclic sample (S/N 4A) exhibited cleavage at the origin and fatigue striations throughout the remainder of the propagation area, as shown in figure 129. The high strain range cyclic sample shown in figure 129 was smeared at the origin, but showed striations through the propagation area. It appeared that both samples initiated and progressed transgranularly. The high and low strain range cyclic/dwell wrought Astroloy samples showed extremely heavy oxidation, as seen in figure 130. However, both samples (S/N 8A and 10A) appeared to initiate and propagate intergranularly. Metallographic sections taken through each of the origins showed similar results, as seen in figure 131. There were isolated areas of transgranular propagation in the cyclic/dwell samples, possibly through coarser grained areas. The grain structure in all of the samples were duplexed with an ASTM grain size of 4 to 6 necklaced by fine recrystallized grains having an ASTM grain size of 7 to 8.

TABLE 21
CONTROLLED STRAIN LOW-CYCLE FATIGUE SAMPLES
CHARACTERIZED BY FRACTOGRAPHY
Tested in Air at 650°C, 0.33 Hz Ramp Frequency
Mean Strain = 0

Material	*Spec S/N*	*Type[3] Test*	$\Delta\epsilon_T$[1]	N_f[2]
Waspaloy	A-2	Cyclic	1.43	810
Waspaloy	A-7	Cyclic	0.81	10,622
Waspaloy	A-11	Cyclic/Dwell	1.13	1,061
Waspaloy	A-14	Cyclic/Dwell	0.81	3,608
Wrought Astroloy	1A	Cyclic	1.50	400
Wrought Astroloy	4A	Cyclic	0.85	9,350
Wrought Astroloy	8A	Cyclic/Dwell	1.24	516
Wrought Astroloy	10A	Cyclic/Dwell	0.84	8,087
NASA IIB-7	1B	Cyclic	1.50	420
NASA IIB-7	4B	Cyclic	1.00	18,744
NASA IIB-7	9B	Cyclic/Dwell	1.26	254
NASA IIB-7	10B	Cyclic/Dwell	1.01	3,935
HIP-Astroloy	DB-1	Cyclic	1.42	961
HIP-Astroloy	DB-5	Cyclic	0.81	8,901
HIP-Astroloy	DB-10	Cyclic/Dwell	1.23	335
HIP-Astroloy	CB-13	Cyclic/Dwell	0.76	7,780
GATORIZED® IN 100	7	Cyclic	1.48	561
GATORIZED IN 100	3	Cyclic	0.94	15,774
GATORIZED IN 100	9	Cyclic/Dwell	1.24	285
GATORIZED IN 100	11	Cyclic/Dwell	1.00	2,515
HIP Plus Forged René 95	1	Cyclic	1.50	595
HIP Plus Forged René 95	3	Cyclic	1.00	31,729
HIP Plus Forged René 95	4	Cyclic/Dwell	1.31	285
HIP Plus Forged René 95	13	Cyclic/Dwell	0.99	5144
HIP MERL 76	D2	Cyclic	1.84	290
HIP MERL 76	D9	Cyclic	0.91	124,323
HIP MERL 76	F7	Cyclic/Dwell	1.06	2,065
HIP MERL 76	F8	Cyclic/Dwell	1.52	264

[1]Total strain range.
[2]Cycles to failure.
[3]Cyclic/dwell tests incorporated a 900-sec (15 min) hold time at the maximum tensile strain.

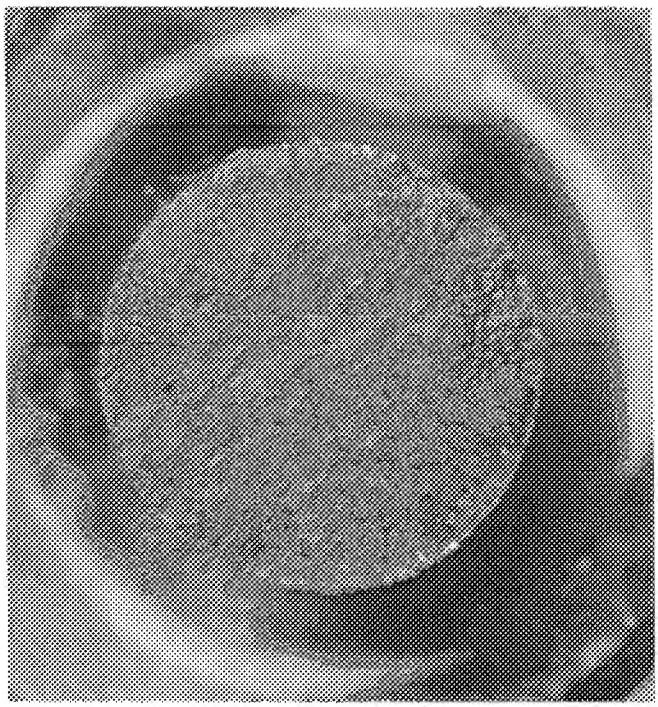

FAL 49583

A

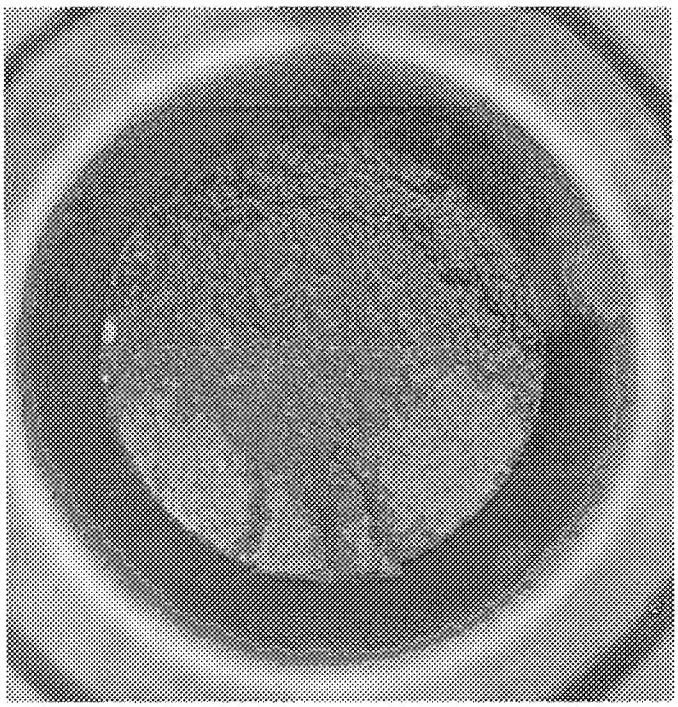

FAL 49584

B

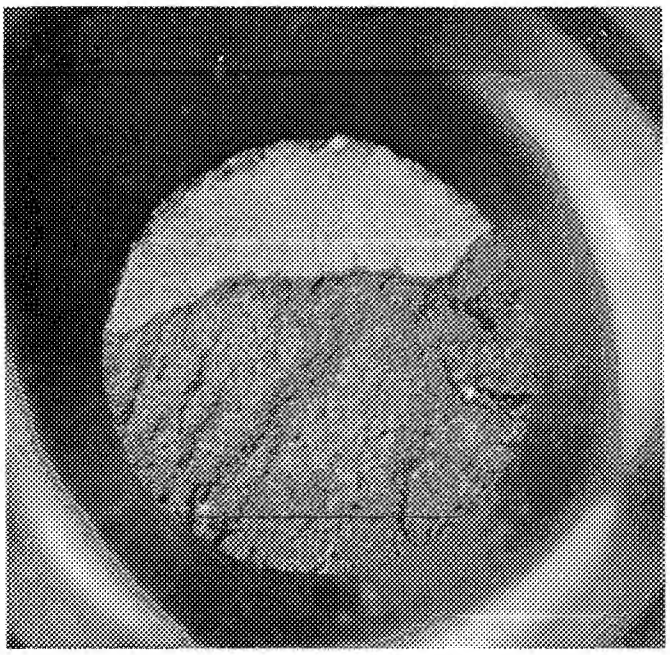

FAL 49585

C

FAL 49586

D

A - S/N A-2, Cyclic, 1.43 $\Delta\epsilon_t$, 810 Cycles

B - S/N A-7, Cyclic, 0.81 $\Delta\epsilon_t$, 10,622 Cycles

C - S/N A-11, Cyclic/Dwell, 1.13 $\Delta\epsilon_t$, 1,061 Cycles

D - S/N A-14, Cyclic/Dwell, 0.81 $\Delta\epsilon_t$, 3,608 Cycles

FD 156331

Figure 123. Waspaloy Strain Control LCF Fracture Faces, Mag 10X

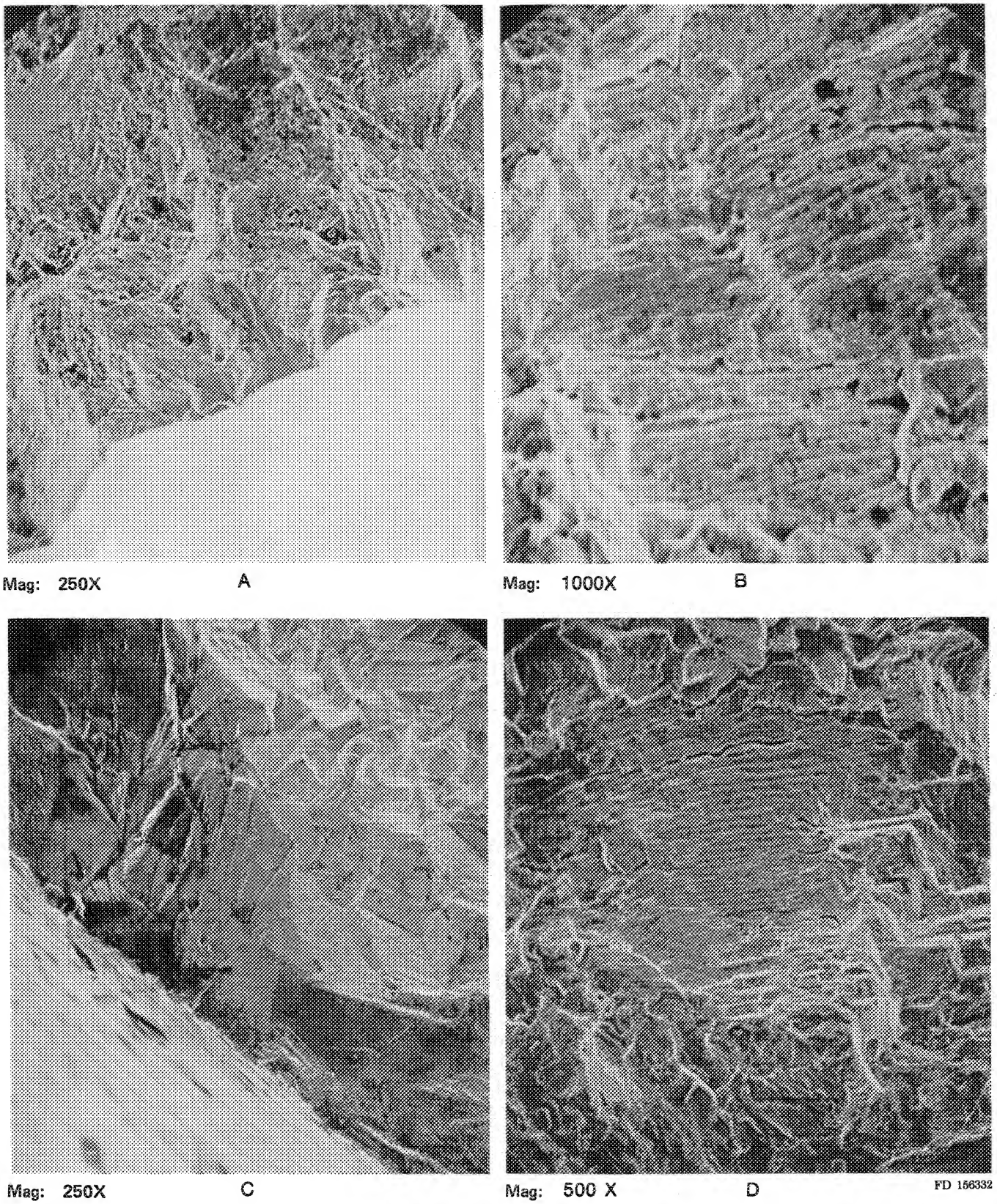

Figure 124. SEM Fractographs of Waspaloy Samples A-2 (Top) and A-7 (Bottom) Showing Cleavage (A and C) at Origin and Fatigue Striations (B and D) Away from Origin

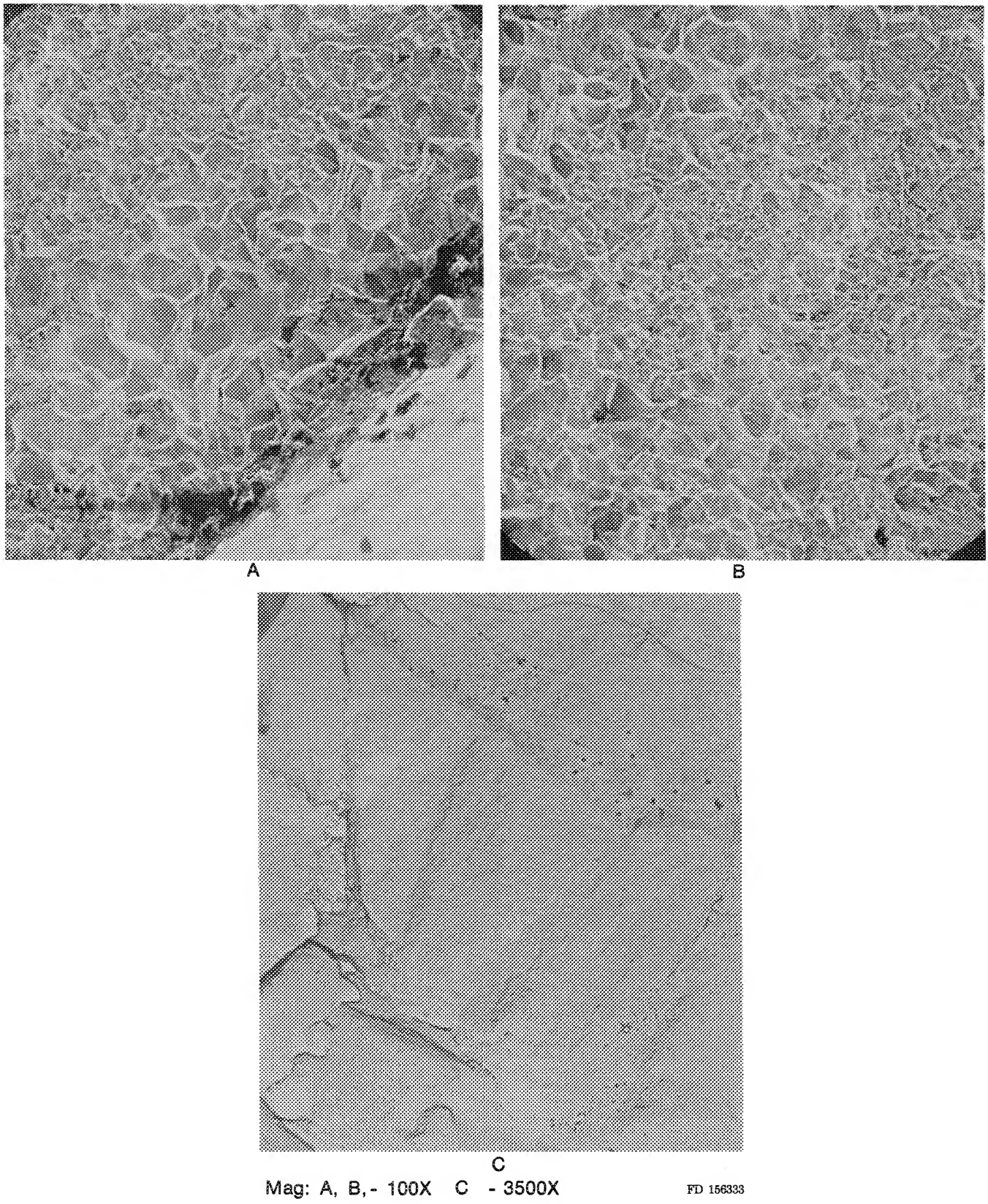

Figure 125. SEM Fractographs of Waspaloy Sample A-14 Showing Intergranular Initiation (A), Propagation (B), and TEM Fractograph (C) Showing Isolated Facet with Remnant Striations

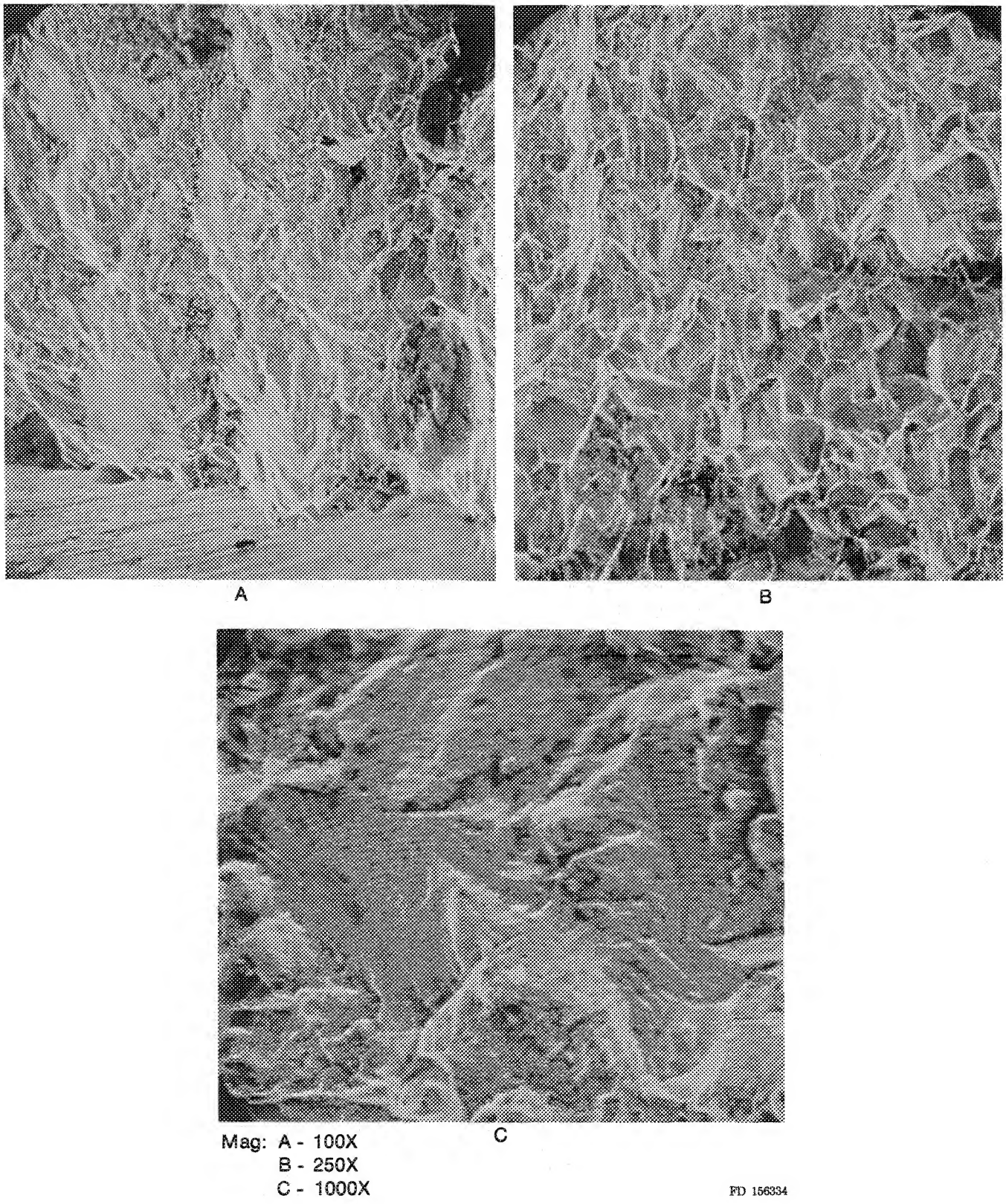

Figure 126. SEM Fractographs of Waspaloy Sample A-11 Showing Cleavage (A) at Origin and Intergranular Propagation (B). Fractograph (C) Shows an Isolated Area of Striations.

A. Sample A-2 Showing Transgranular Initiation and Propagation
B. Sample A-7 Showing Transgranular Initiation and Propagation
C. Sample A-11 Showing Transgranular Initiation and Intergranular Propagation
D. Sample A-14 Showing Intergranular Initiation and Propagation

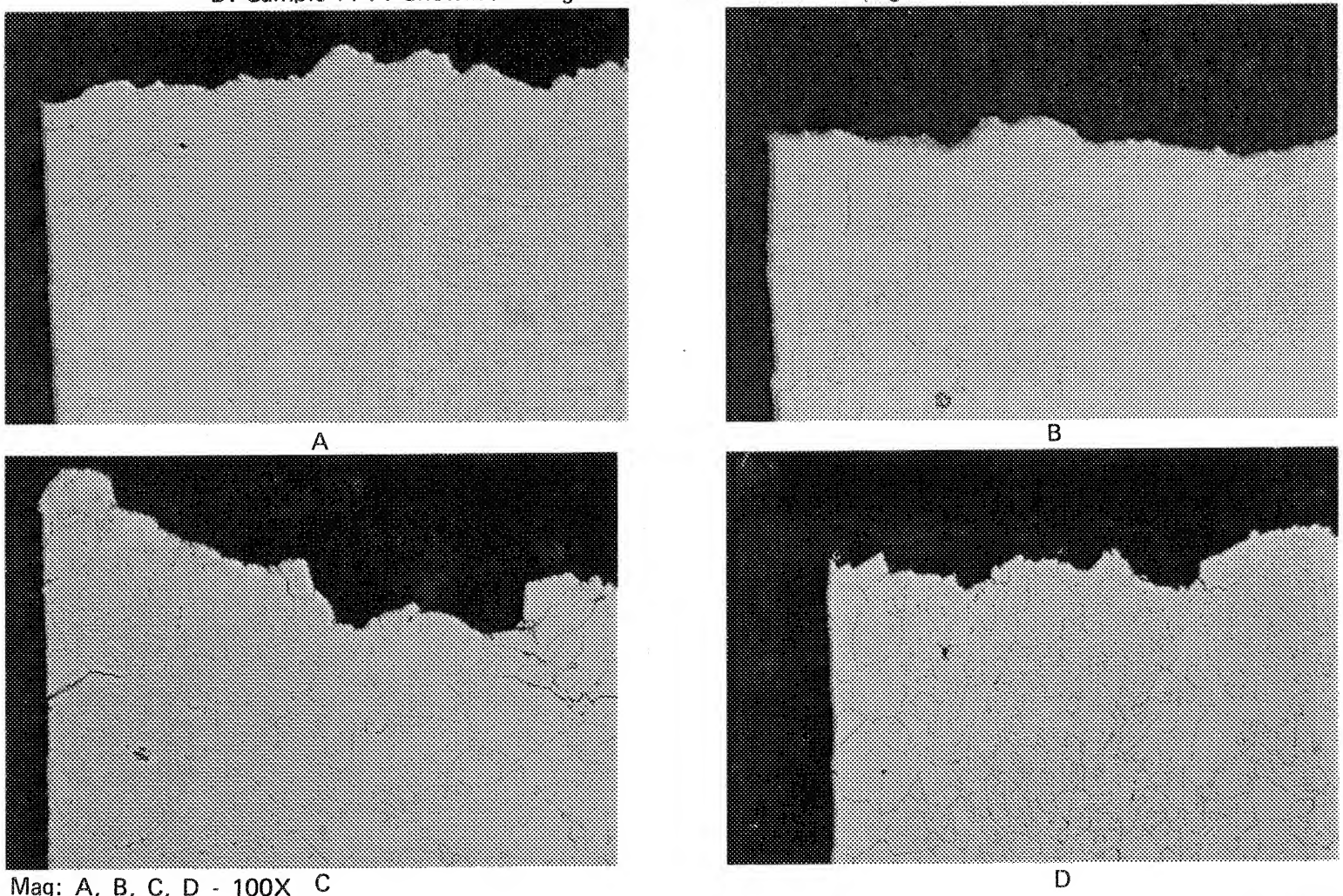

Mag: A, B, C, D - 100X
Etch: Glyceregia

FD 162769
792404

Figure 127. Micrographs Through Origin of Waspaloy Samples

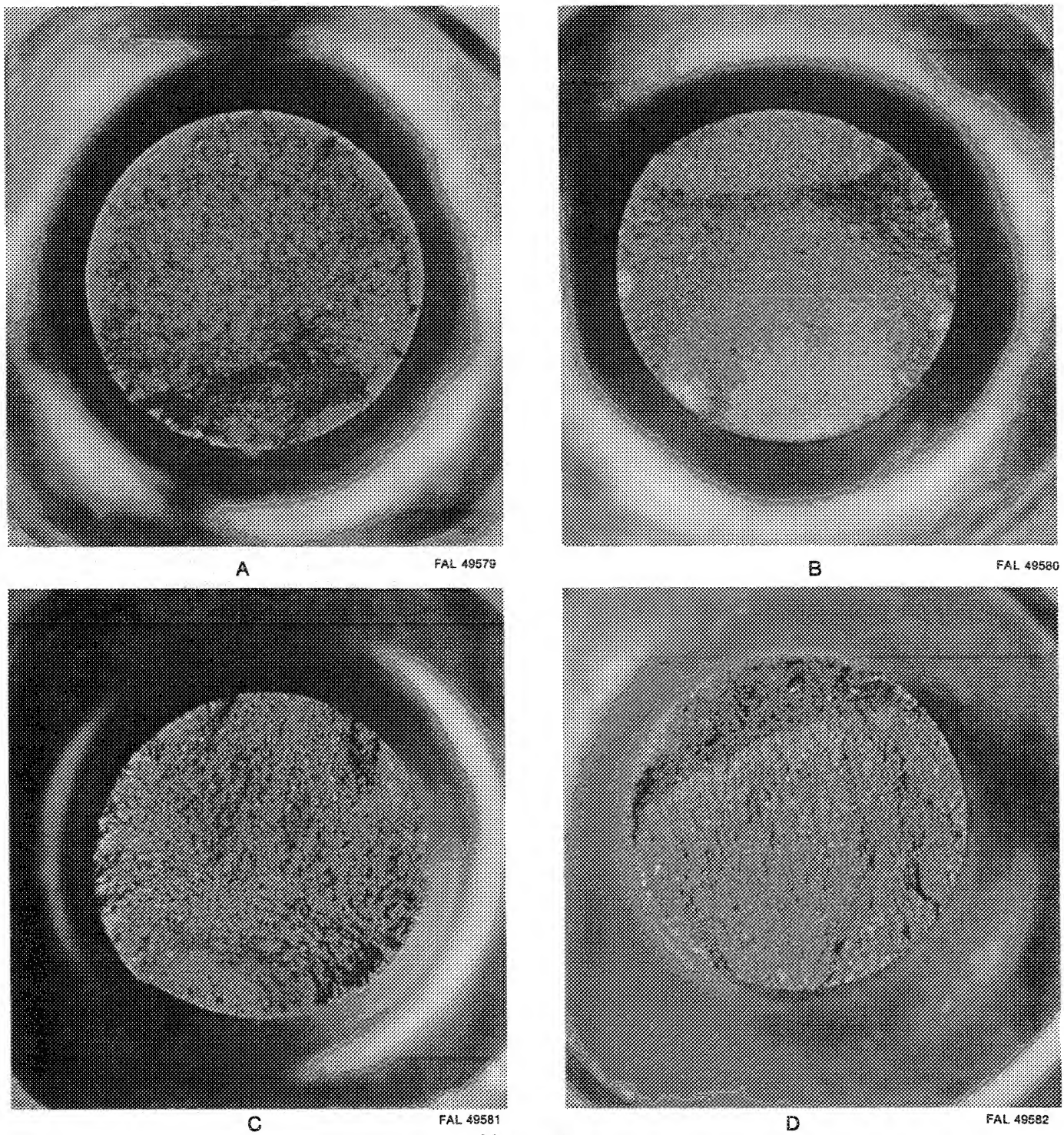

Mag: 10X

A - S/N 1A, Cyclic, 1.5 $\Delta\epsilon_t$, 400 Cycles

B - S/N 4A, Cyclic, 0.85 $\Delta\epsilon_t$, 9350 Cycles

C - S/N 8A, Cyclic/Dwell, 1.24 $\Delta\epsilon_t$, 516 Cycles

D - S/N 10A, Cyclic/Dwell, 0.84 $\Delta\epsilon_t$, 8087 Cycles

FD 156335

Figure 128. Wrought Astroloy Strain Control LCF Fracture Faces

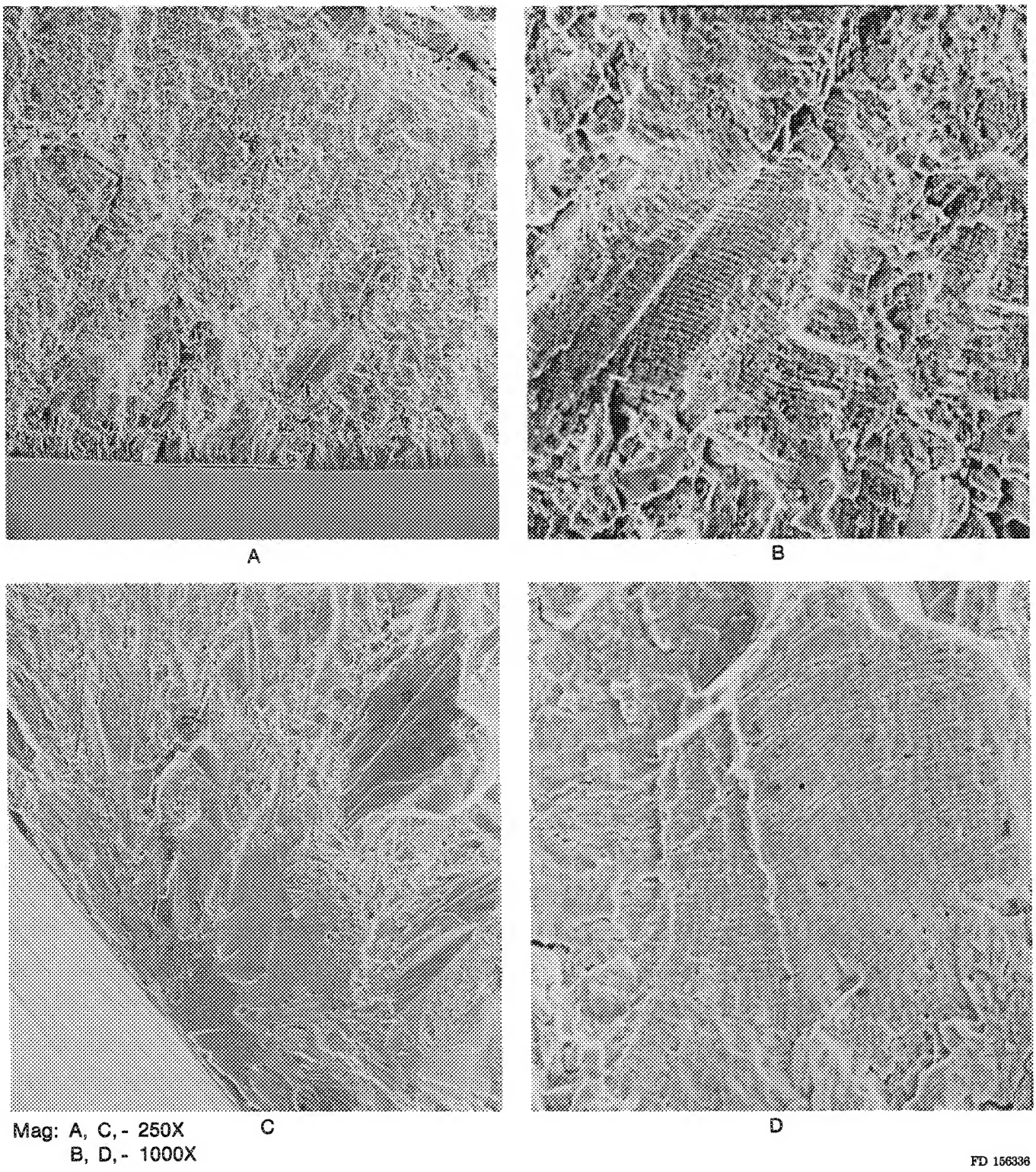

Figure 129. SEM Fractographs of Wrought Astroloy Samples 1A (Top) and 4A (Bottom) Showing Smear (A) and Cleavage (C) at Origin and Fatigue Striations (B and D) Away from Origin

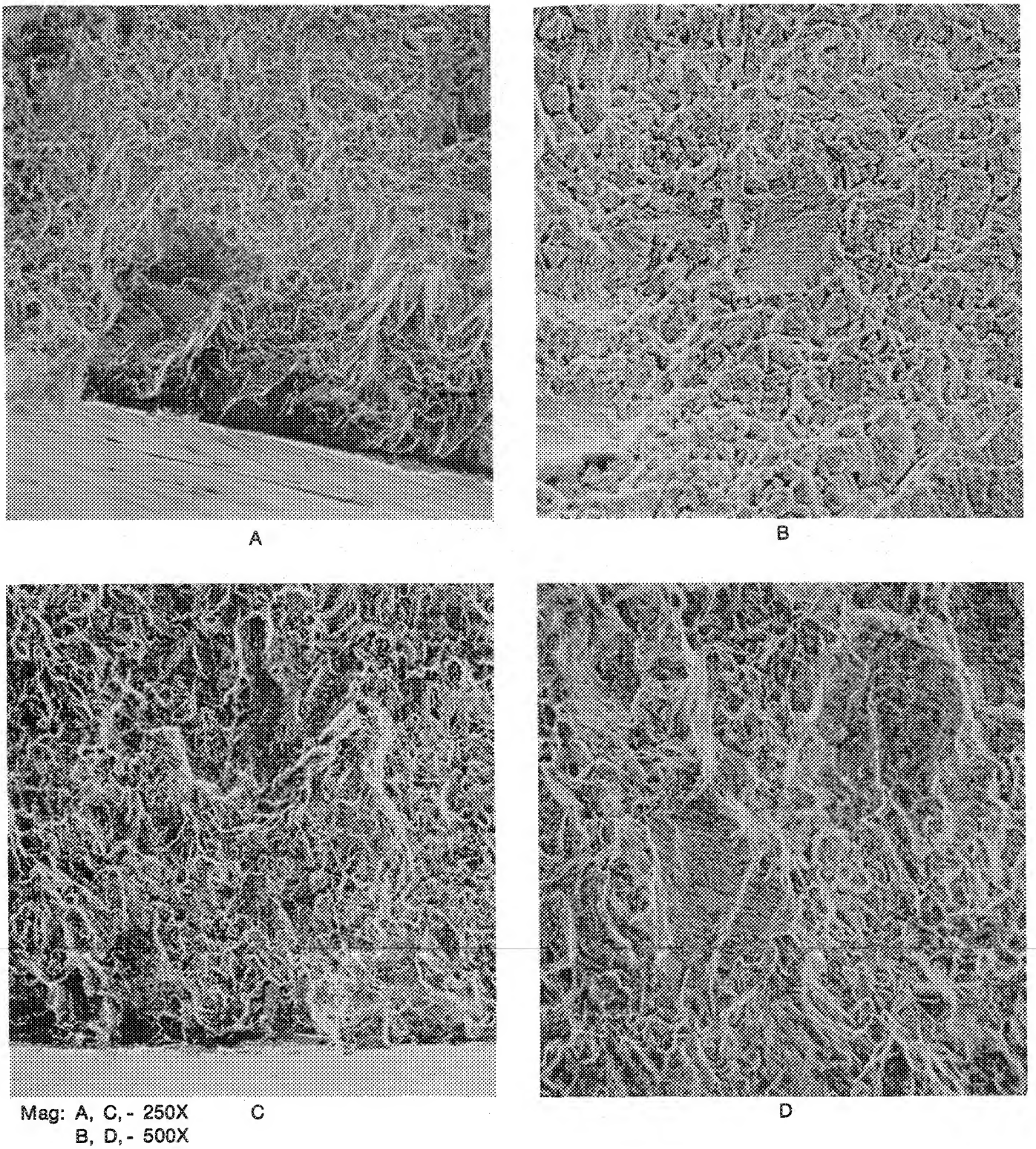

Figure 130. SEM Fractographs Showing Heavily Oxidized Fracture Surfaces of Wrought Astroloy Samples 8A (Top) and 10A (Bottom) with Isolated Patches of Remnant Striations (B and D)

A. Sample 1A Showing Transgranular Initiation and Propagation
B. Sample 4A Showing Transgranular Initiation and Propagation
C. Sample 8A Showing Intergranular Initiation and Propagation
D. Sample 10A Showing Intergranular Initiation and Propagation

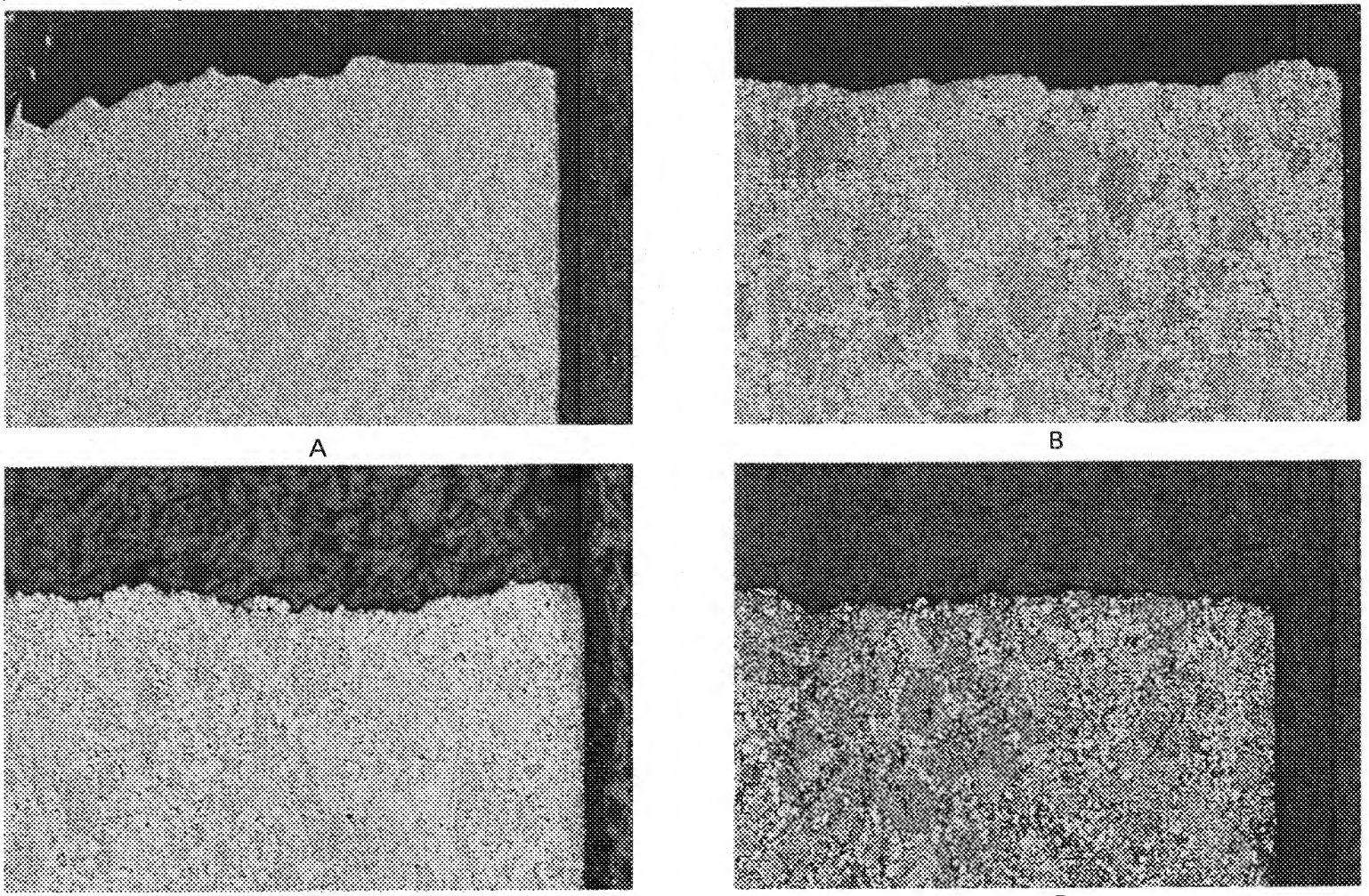

Mag: A, B, C, D - 100X
Etch: Kallings

FD 162771

Figure 131. Micrographs Through Origin of Wrought Astroloy Samples

HIP-Formed Astroloy

The high strain range cyclic HIP-formed Astroloy (S/N DB-1) showed multiple origins around the circumference of the sample, whereas the low strain range cyclic sample had only a single origin, as shown in figure 132. The cyclic/dwell samples exhibited a major origin with one or more minor origins. Figure 133 details the major origin of the low strain range cyclic sample (S/N DB-5) showing cleavage at the origin and fatigue striations throughout the remainder of the propagation area. The high strain range cyclic sample (S/N DB-1) was smeared at the origin, but showed striations through the propagation area. It appeared that both samples initiated and progressed transgranularly. The cyclic/dwell samples (S/N DB-10 and DB-13) exhibited extremely heavy oxidation and smear at the very origin. Figure 134 shows typical fractographs of the fracture faces. Microsections through the origins gave the appearance of intergranular propagation, as shown in figure 135. All of the samples had a recrystallized grain structure with an ASTM grain size of 5 to 7 with occasional 4.

NASA IIB-7

The high strain range cyclic NASA IIB-7 sample (S/N 1B) and the low strain range cyclic/dwell sample (S/N 10B) exhibited two origins, whereas the low strain range cyclic sample (S/N 4B) and the high strain range cyclic/dwell sample (S/N 9B) exhibited single origins, as shown in figure 136. The fracture face of the low and high strain range cyclic samples were too smeared to discern any features. The high and low strain range cyclic/dwell samples showed extreme oxidation. TEM gave some indication that both cyclic/dwell samples propagated intergranularly, as seen in figure 137. The low strain range cyclic sample and the high strain range cyclic/dwell sample both had a small crack through the origin on the fracture surface. All of the samples were fine-grained recrystallized with an ASTM grain size of 12.5 to 13.5.

GATORIZED IN 100

The low and high strain range GATORIZED IN 100 cyclic samples (S/N 3 and 7) had single origins, whereas the cyclic/dwell samples (S/N 9 and 11) had a major origin with one or more minor origins, as shown in figure 138. Both cyclic sample origins were at an aluminum-silicon nonmetallic inclusion, as seen in figure 139. There were no apparent inclusions at the origin of the high strain range cyclic/dwell sample and the low strain range cyclic/dwell sample origin was too smeared to identify features. Both the cyclic and cyclic/dwell samples appeared to have propagated intergranularly, as shown in figures 139 and 140. The high strain range cyclic/dwell sample (S/N 9) also showed some intergranular cracking away from the origin. All of the samples were fine-grained recrystallized with an ASTM grain size of 12.5 to 14.5 with occasional 11.5.

HIP Plus Forged René 95

The high strain range cyclic HIP plus forged René 95 sample (S/N 1) showed multiple origins, whereas the low strain range cyclic and both cyclic/dwell samples had single origins, as shown in figure 141. A machining mark was observed going through two of the multiple origins of the high strain range cyclic sample and through the major origin of the low strain range cyclic sample (S/N 3), as seen in figure 142. Both the high and low strain range cyclic samples (figures 143 and 144, respectively) originated and propagated transgranularly, whereas the high and low strain range cyclic/dwell samples originated and propagated intergranularly (figures 145 and 146, respectively). All of the samples had a grain structure consisting of 60% unrecrystallized grains with the ASTM size of 5 to 6 with occasional 4 necklaced by recrystallized grains finer than 8.

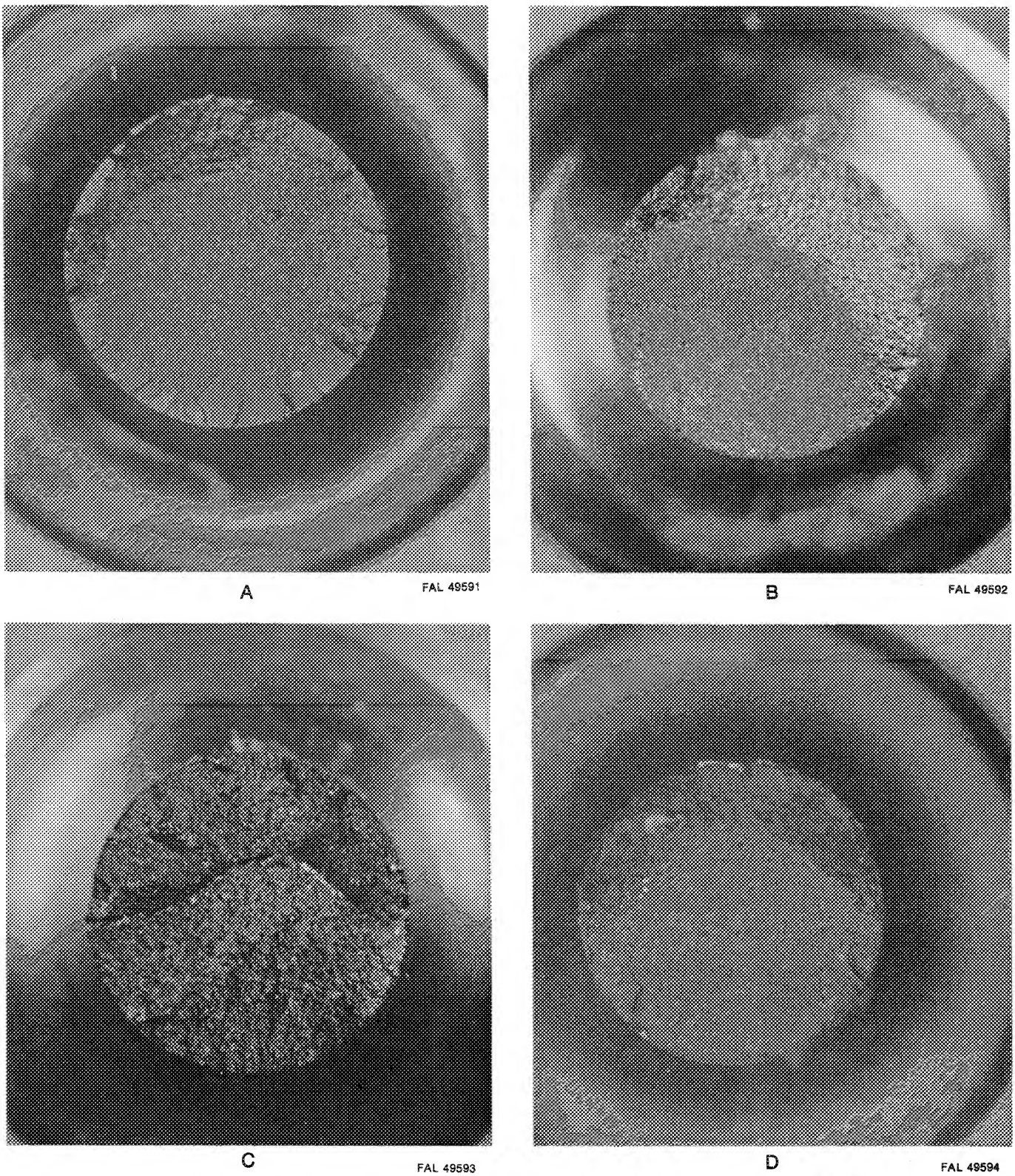

Figure 132. HIP Astroloy Strain Control LCF Fracture Faces, Mag 10X

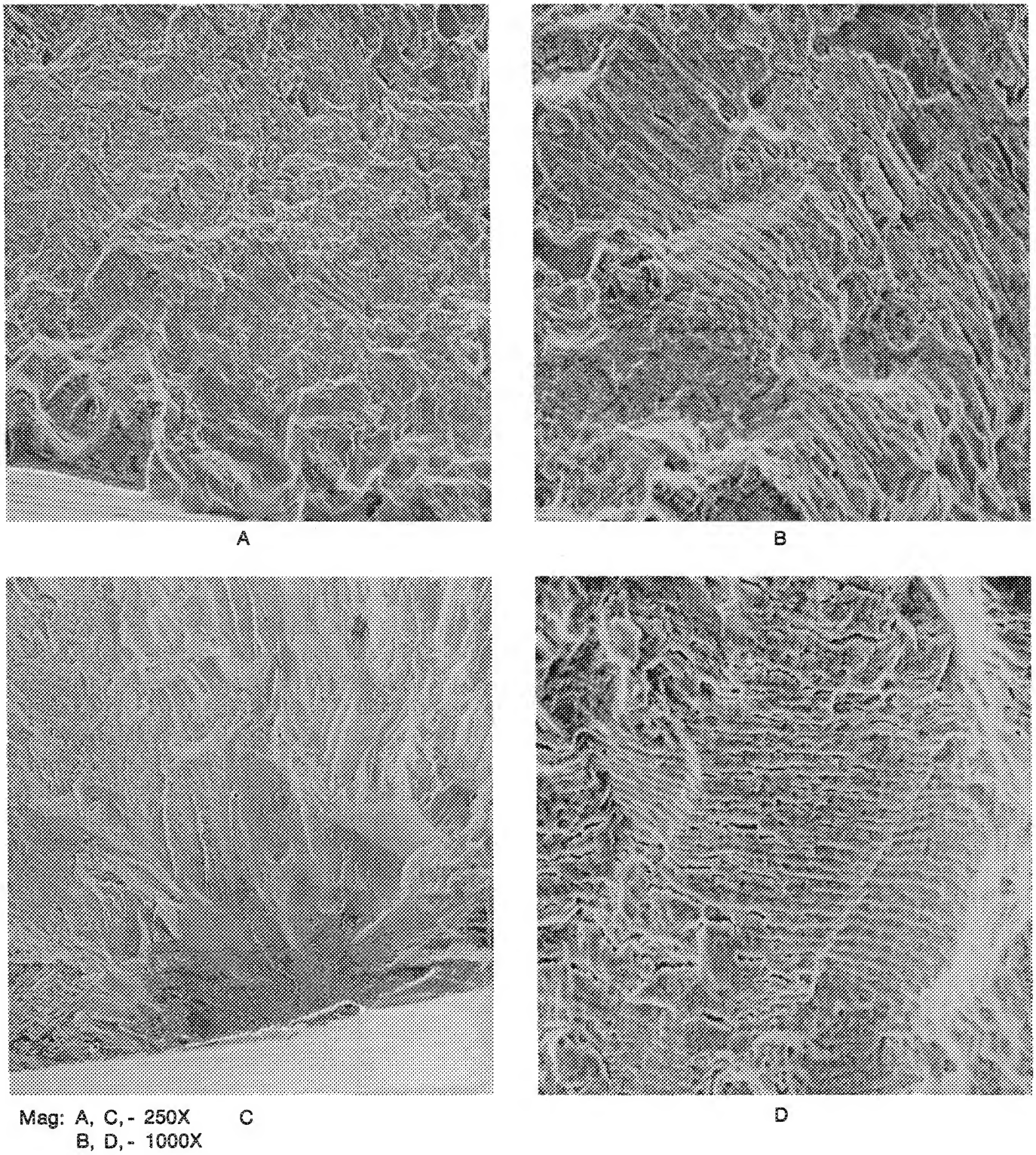

Figure 133. SEM Fractographs of HIP Astroloy Samples DB-1 (Top) and DB-5 (Bottom) Showing Smear (A) and Cleavage (C) at Origin and Fatigue Striations (B and D) Away from Origin

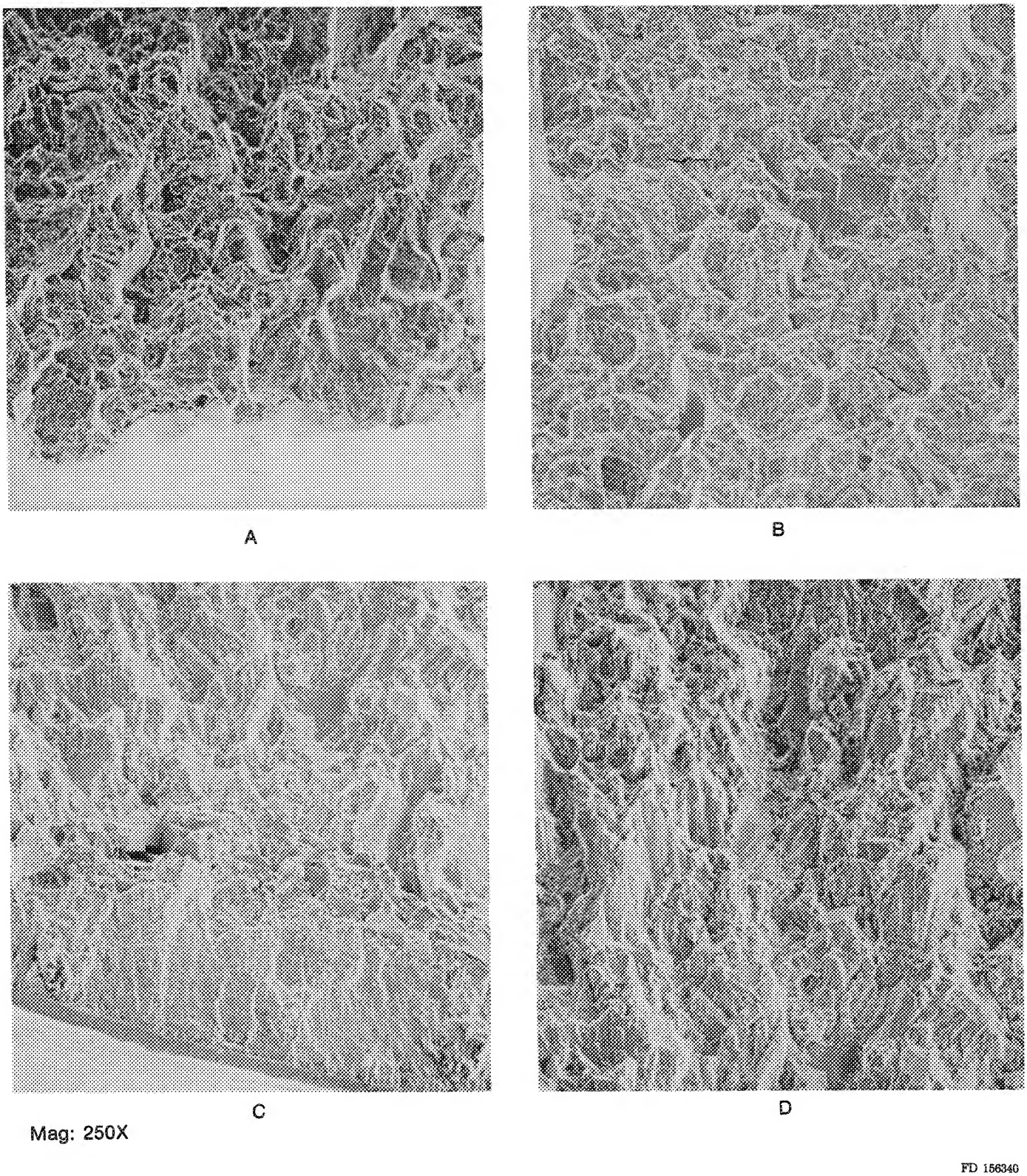

Figure 134. SEM Fractographs of HIP Astroloy Samples DB-10 (Top) and CB-13 (Bottom) Showing Origin (A and C) and Away from Origin (B and D)

A. Sample DB-1 Showing Transgranular Initiation and Propagation
B. Sample DB-5 Showing Transgranular Initiation and Propagation
C. Sample DB-10 Showing Smear at Origin and Intergranular Propagation
D. Sample CB-13 Showing Smear at Origin and Intergranular Propagation

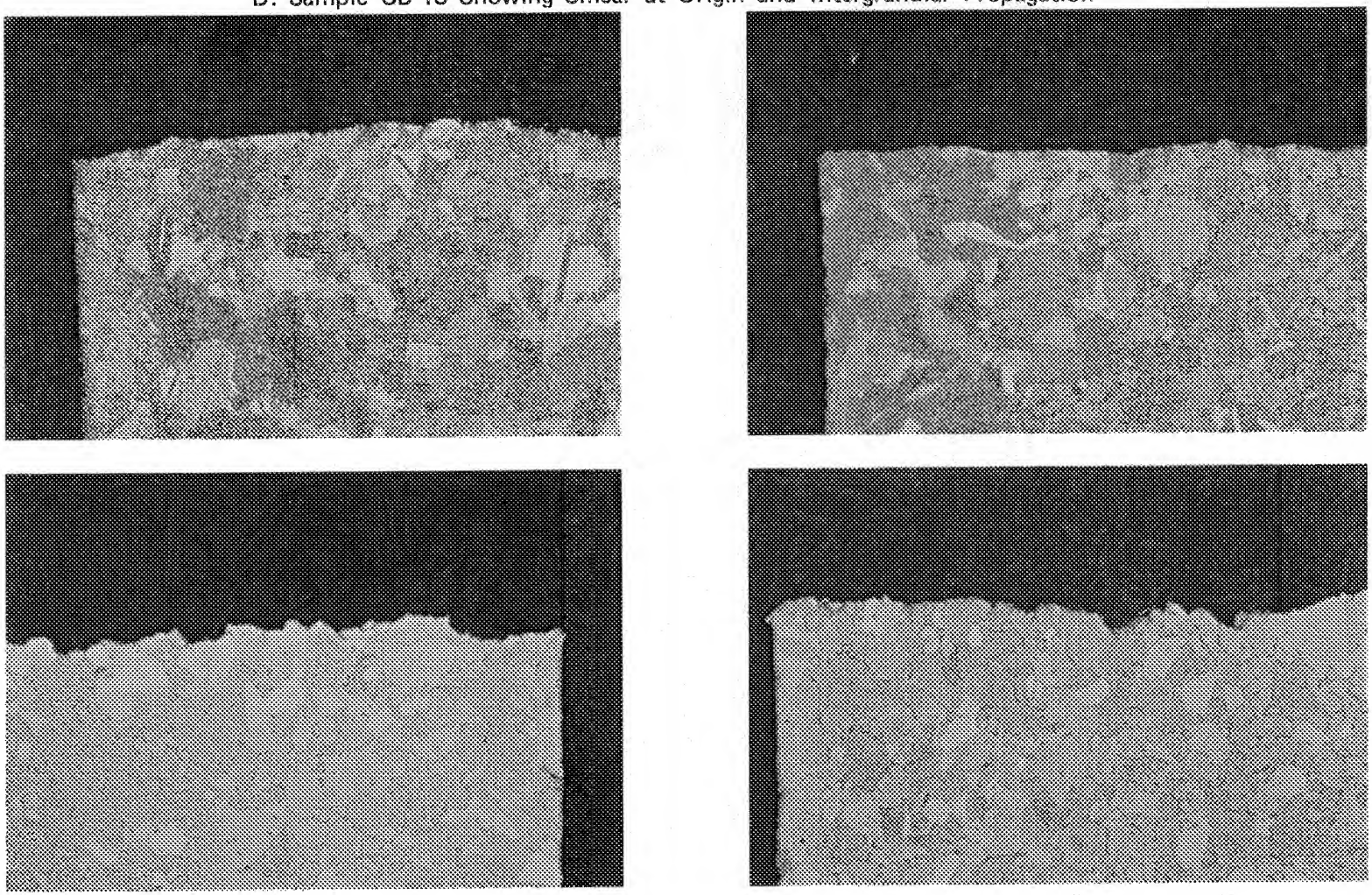

Mag: A, B, C, D - 100X
Etch: Kallings

C

D

FD 162772

Figure 135. Micrographs Through Origin of HIP Astroloy Samples

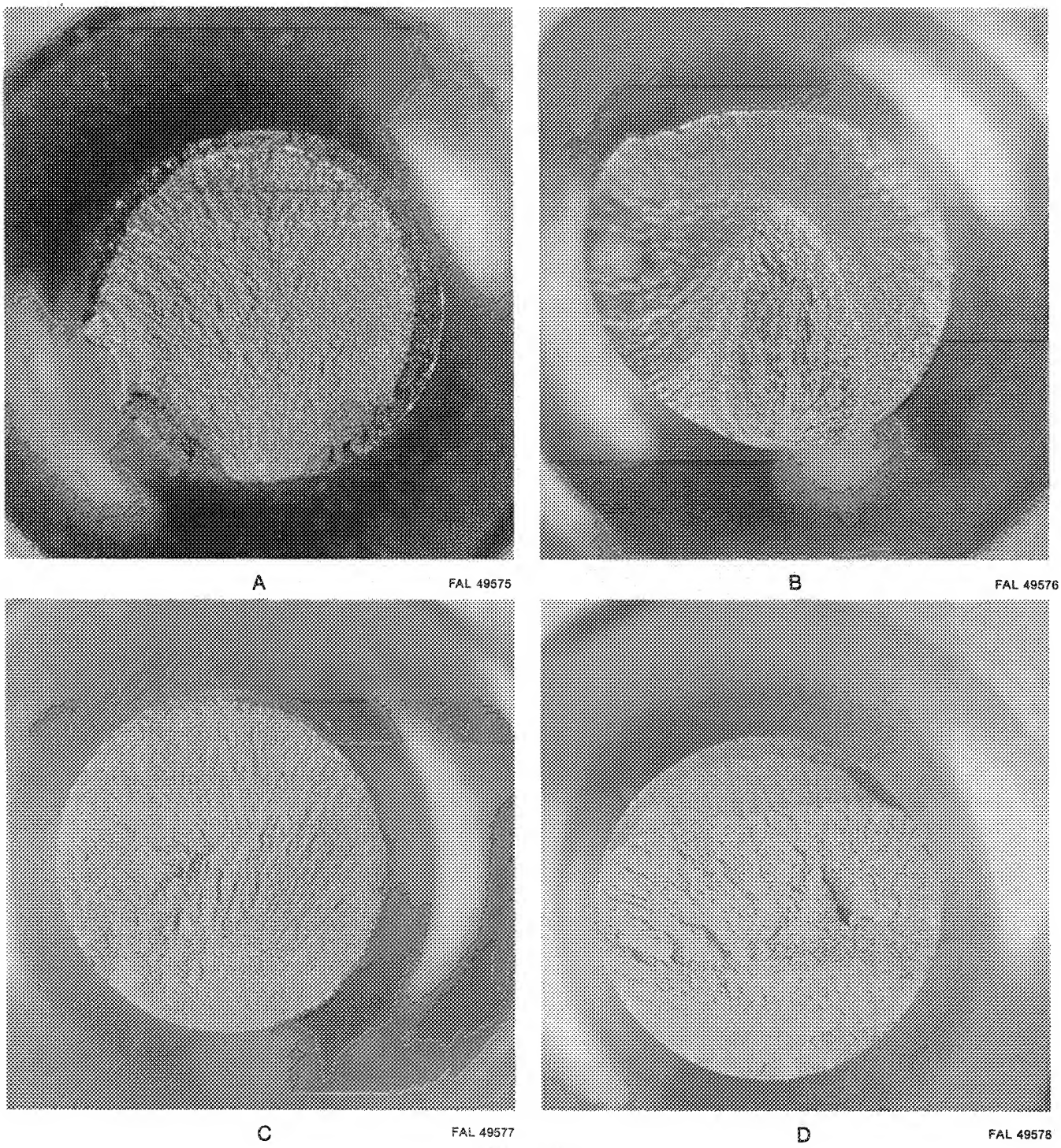

Figure 136. NASA IIB-7 Strain Control LCF Fracture Faces

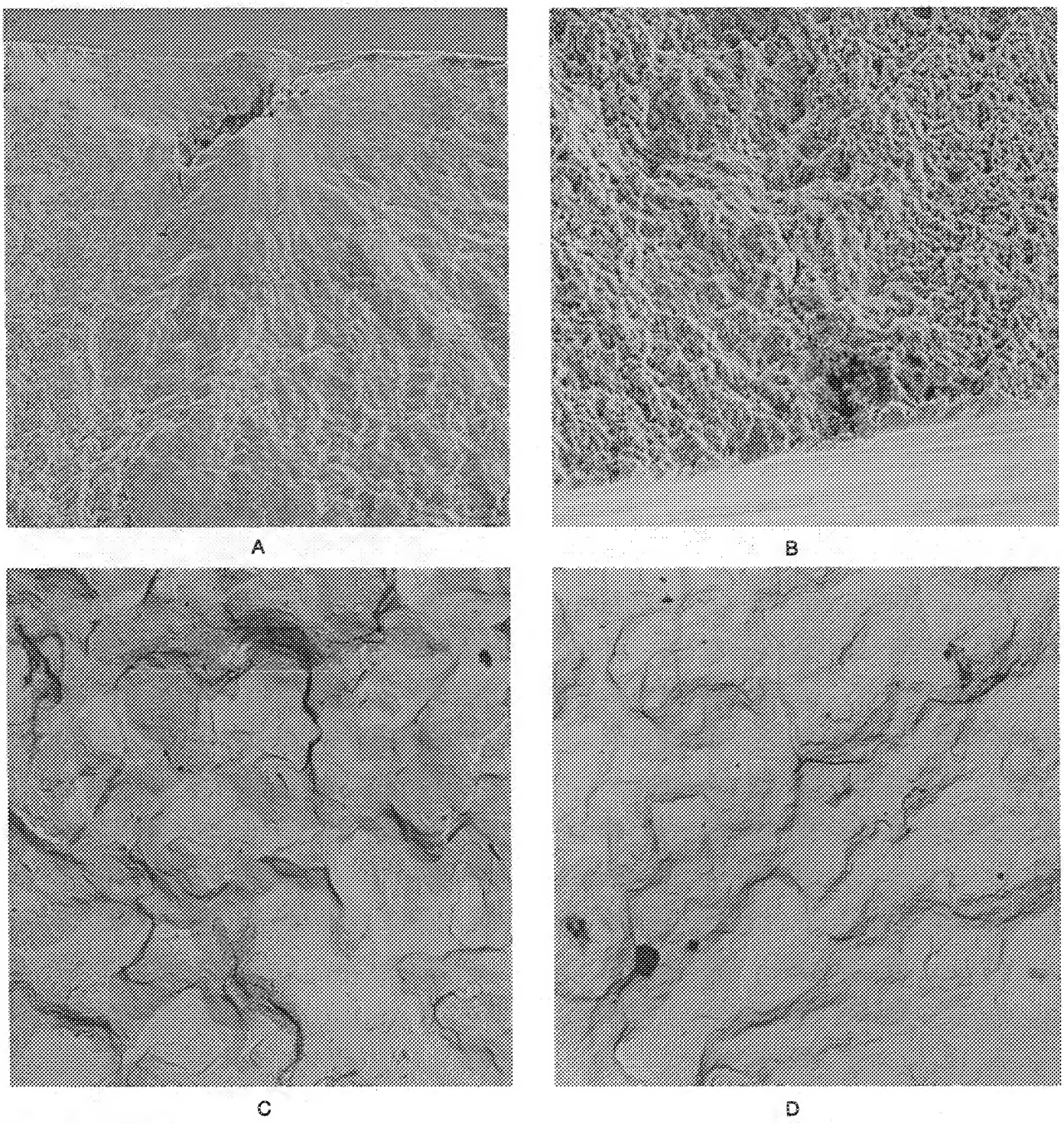

Mag: A,B - 500X
C,D - 3500X

Top: SEM Fractographs Showing Smear and Crack at Origin of Cyclic Sample S/N 4B (A) and Crack Through Origin of Cyclic/Dwell Sample 9B (B)

Bottom: TEM Fractographs Showing Evidence of Intergranular Propagation in Cyclic/Dwell Samples S/N 9B (C) and S/N 10B (D)

FD 156342

Figure 137. Fractographs of NASA IIB-7 Strain Control LCF Fracture Faces

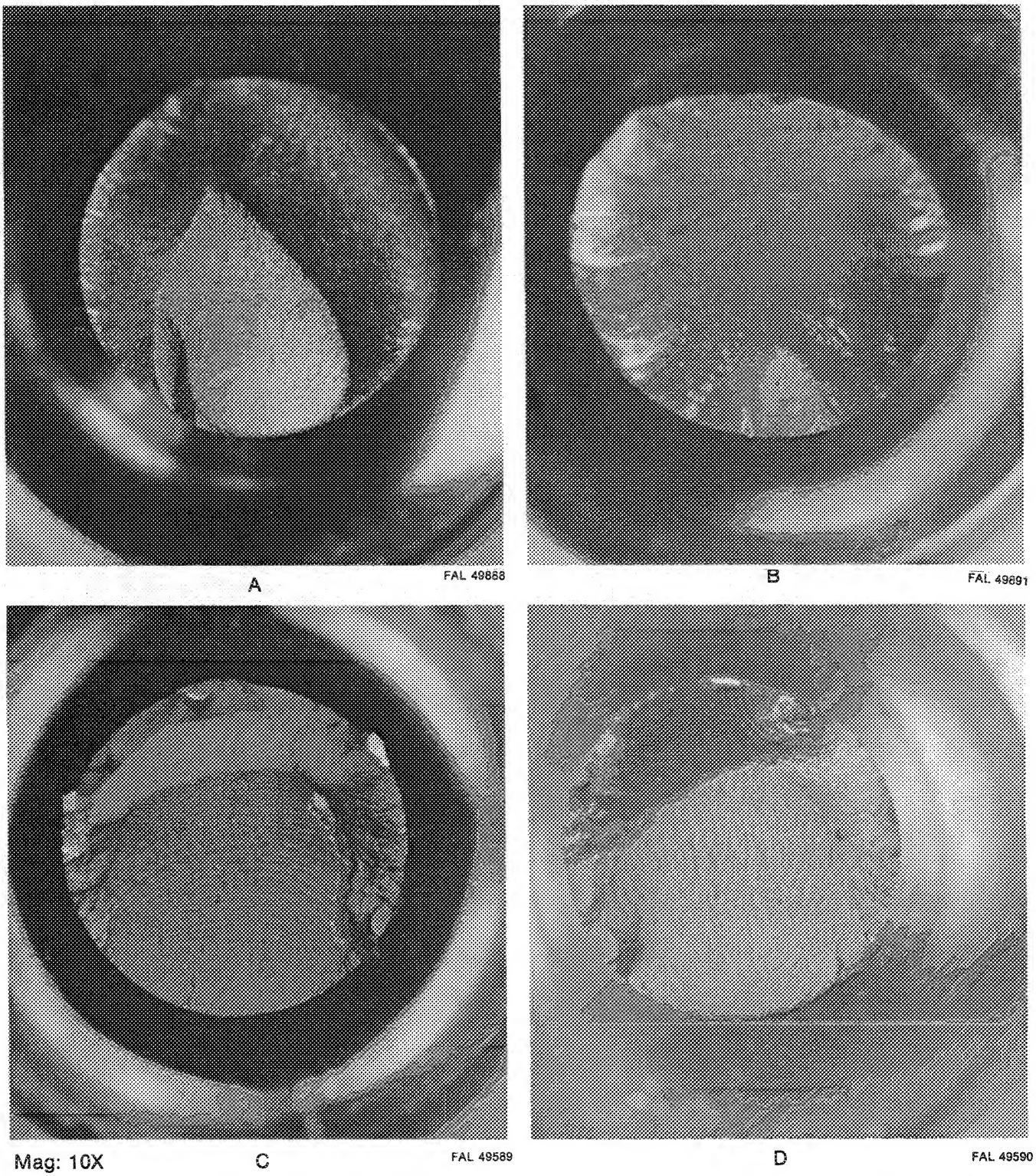

A - S/N 3, Cyclic, 0.94 $\Delta\epsilon_t$, 15,774 Cycles

B - S/N 7, Cyclic, 1.48 $\Delta\epsilon_t$, 561 Cycles

C - S/N 9, Cyclic/Dwell, 1.24 $\Delta\epsilon_t$, 285 Cycles

D - S/N 11, Cyclic/Dwell, 1.00 $\Delta\epsilon_t$, 2,515 Cycles

Figure 138. GATORIZED® IN 100 Strain Control LCF Fracture Faces

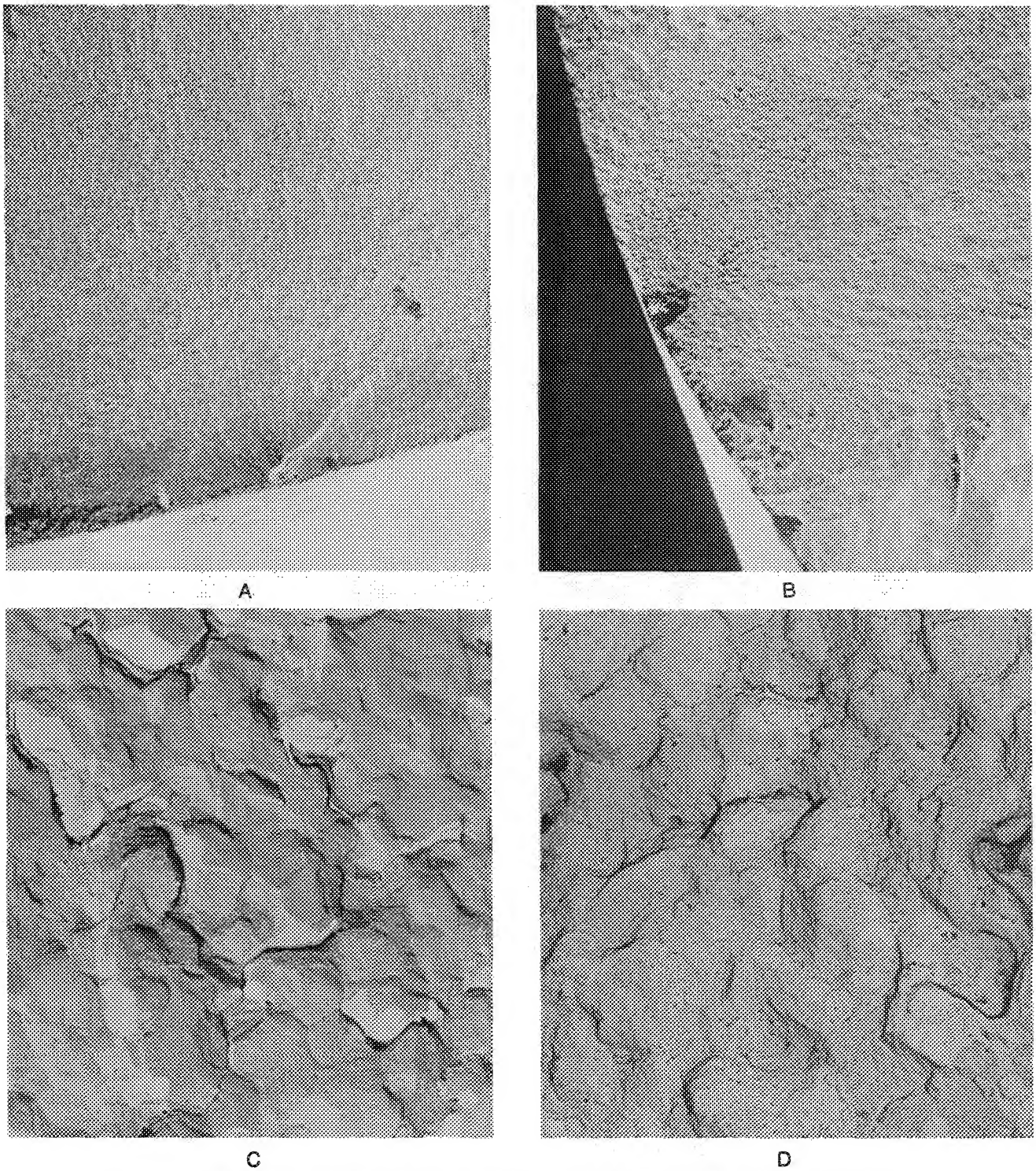

Top: SEM Fractographs from Sample 3 (A) and 7 (B) Showing Area at Origin Containing Nonmetallic Inclusion. Note Heavy Smear on Both Samples

Bottom: TEM Fractographs Showing Evidence of Intergranular Propagation in Cyclic/Dwell Samples of 9 (C) and S/N 11 (D). Note Heavier Oxide on Surface of Sample 11.

FD 156344

Figure 139. Fractographs of GATORIZED® IN 100 Strain Control LCF Fracture Faces

A. Sample 7 Showing Where Non-metallic Inclusion Was Located at Very Origin
B. Sample 7 Showing Typical Fine Grain Size in Gatorized IN 100 Samples
C. Sample 9 Showing Typical Intergranular Propagation IN Gatorized IN 100 Samples

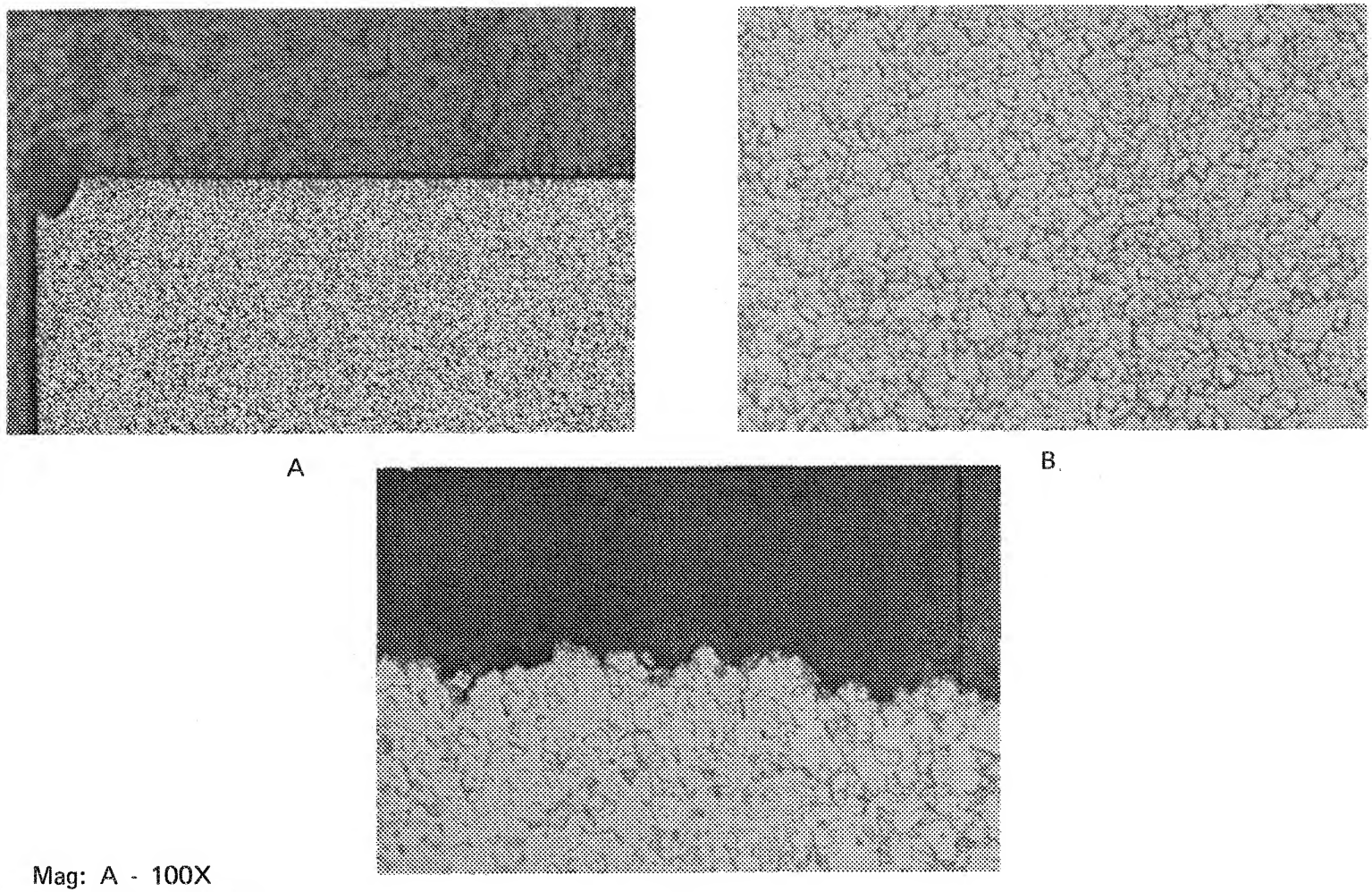

A

B

C

Mag: A - 100X
B, C - 1000X
Etch: Kallings

FD 162770

Figure 140. Microstructure Through Origin of GATORIZED® IN 100

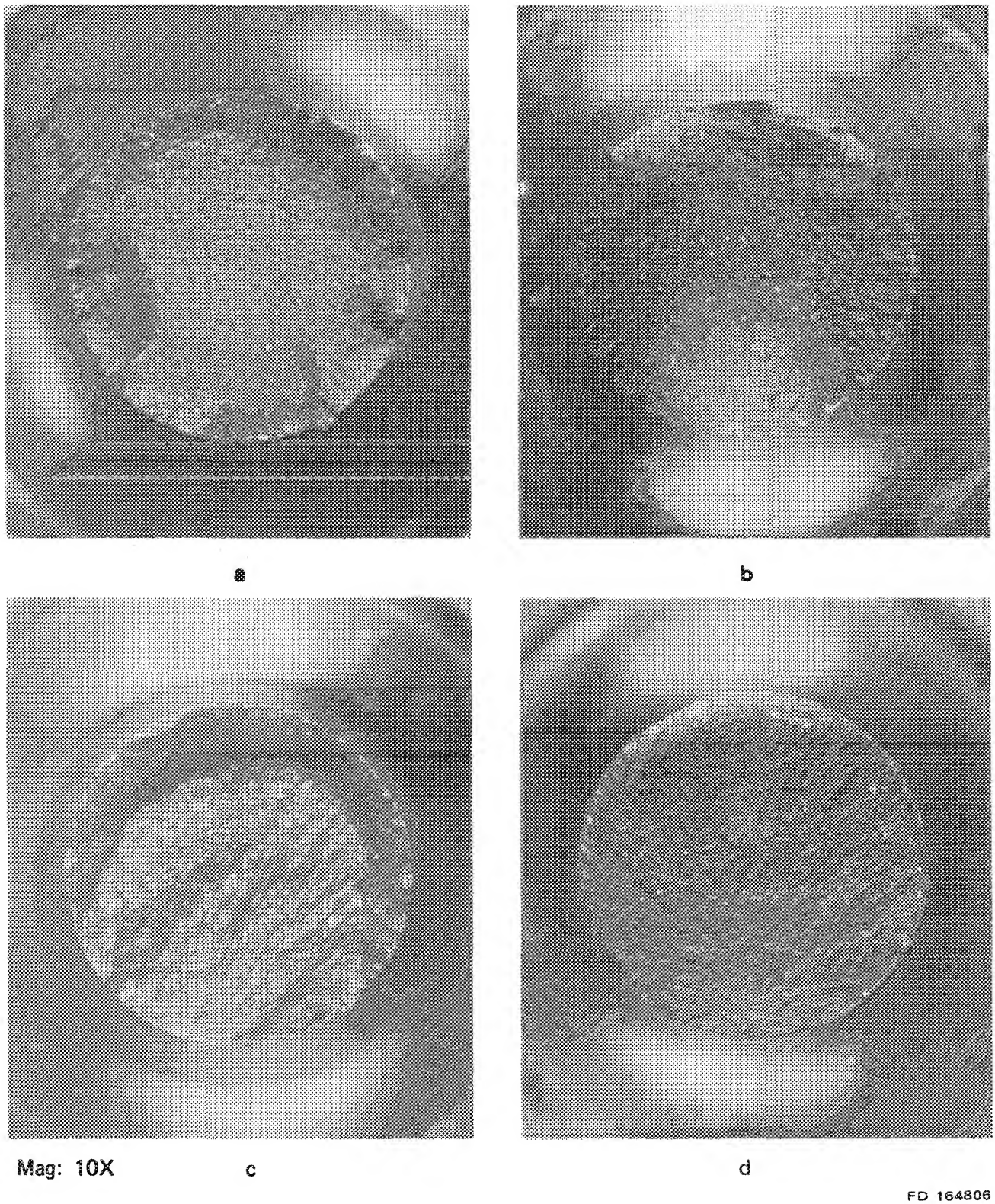

Figure 141. René 95 Strain Controlled LCF Fracture Faces (a) S/N 1, Cyclic, 1.5 $\Delta\epsilon_t$, 593 Cycles, (b) S/N 3, Cyclic, 1.0 $\Delta\epsilon_t$, 31,729 Cycles, (c) S/N 4, Cyclic/Dwell, 1.31 $\Delta\epsilon_t$, 285 Cycles, (d)

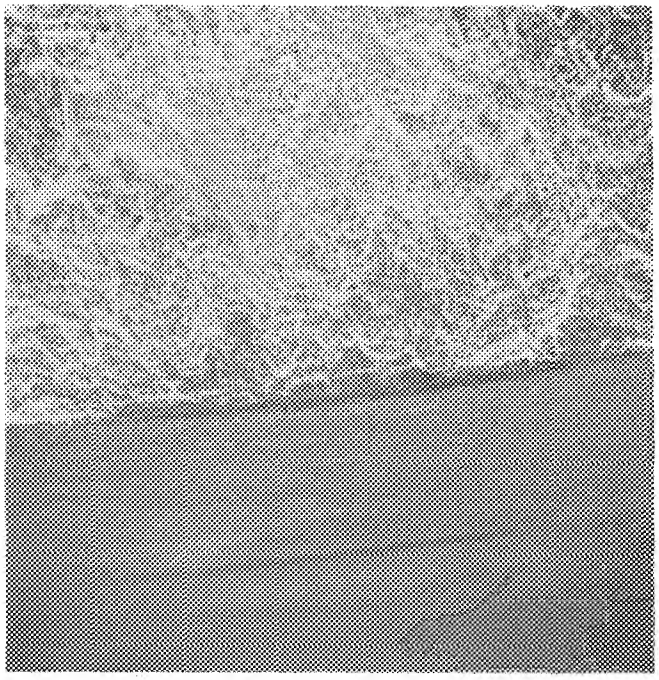

Mag: 250X

a

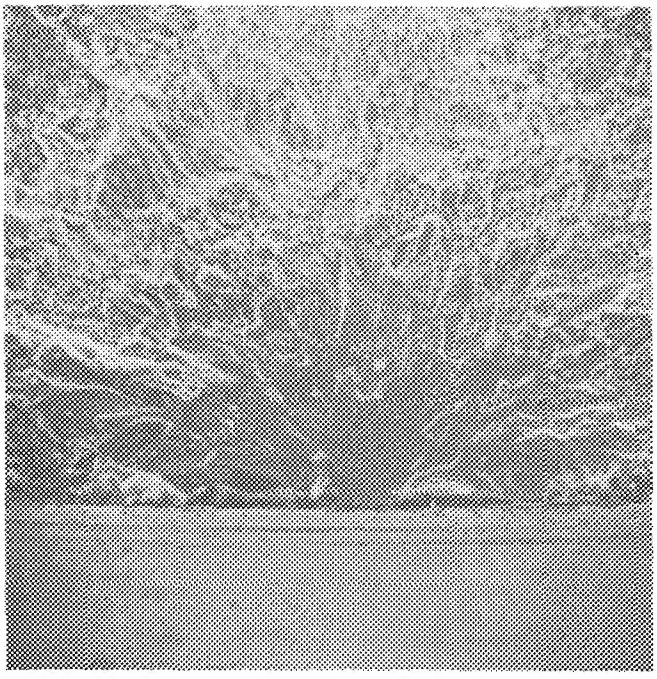

Mag: 250X

b

FD 164807 A

Figure 142. SEM Fractographs of René 95 Samples Showing Machining Groove at Origin

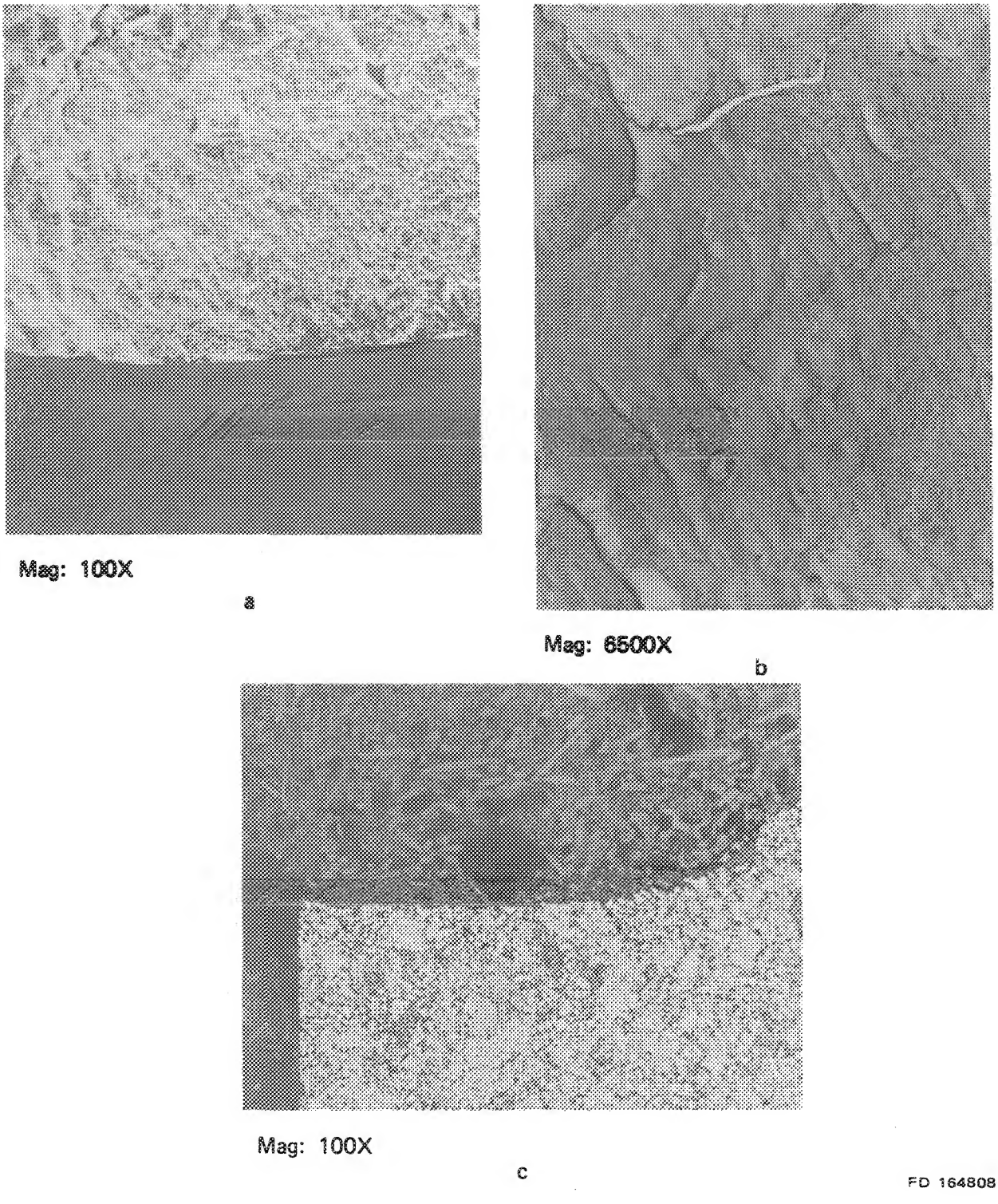

Figure 143. SEM Fractograph (a) TEM Fractograph (b), and Micrograph (c) Through Origin of René 95 Sample S/N 1 Showing Typical Fracture Features and Microstructure

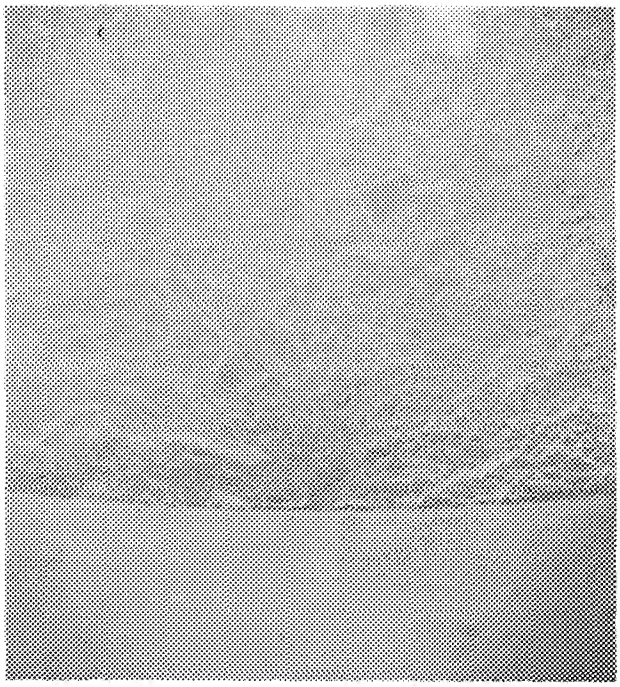

Mag: 100X

a

Mag: 3500X

b

Mag: 100X

c

FD 164809

Figure 144. SEM Fractograph (a), TEM Fractograph (b), and Micrograph (c) Through Origin of René 95 Sample S/N 3 Showing Typical Fracture Features and Microstructure

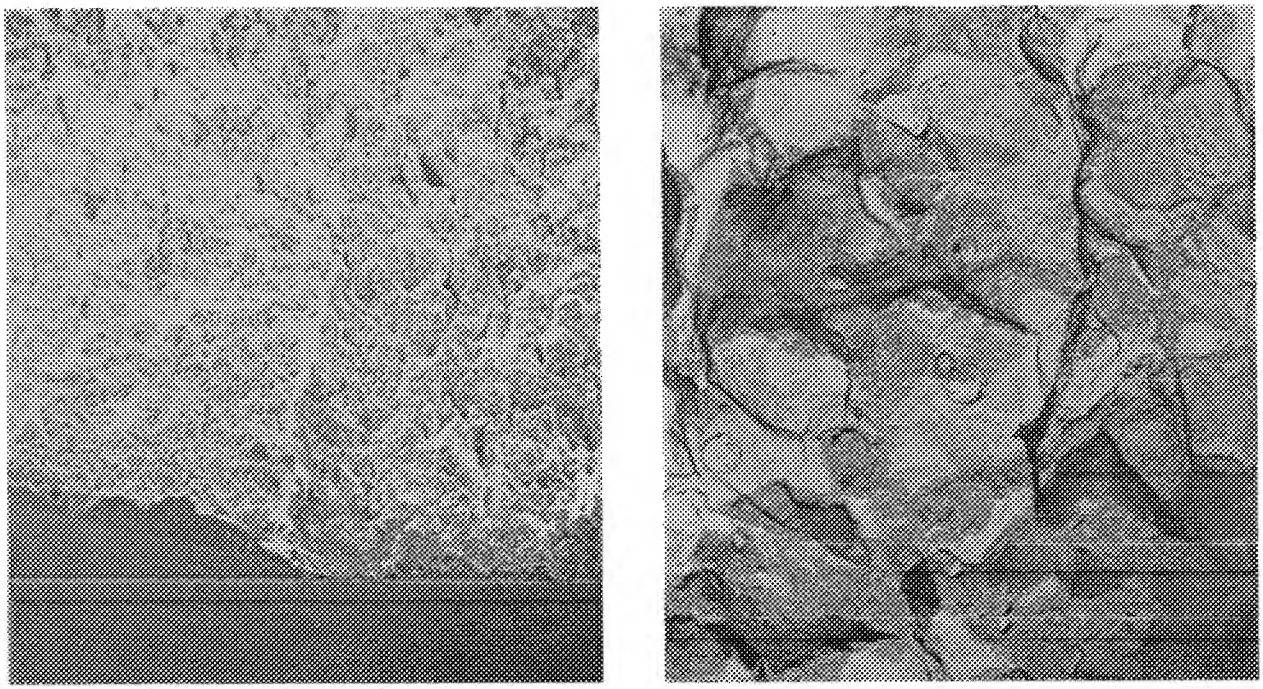

Figure 145. SEM Fractograph (a), TEM Fractograph (b), and Micrograph (c) Through Origin of René 95 Sample S/N 13 Showing Typical Fracture Features and Microstructure

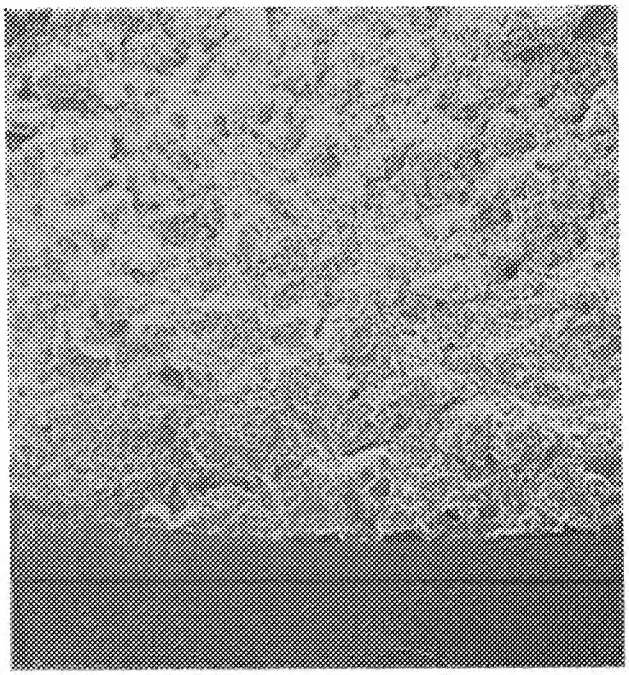

Mag: 100X

a

Mag: 3500X

b

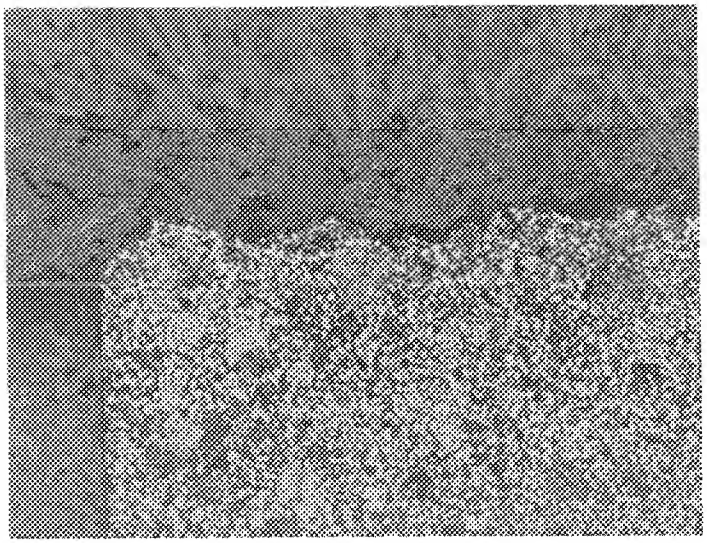

Mag: 100X

c

FD 164811

Figure 146. SEM Fractograph (a), TEM Fractograph (b), and Micrograph (c) Through Origin of René 95 Sample S/N 4 Showing Typical Fracture Features and Microstructure

HIP MERL 76

The high strain range HIP MERL 76 cyclic specimen (S/N F8) and the high strain range cyclic/dwell specimen (S/N D2) had multiple origins around the periphery, as shown in figure 147. The low strain range cyclic and cyclic/dwell samples (S/N F7 and D9) showed single origins. The low strain range cyclic specimen fracture originated at an internal void and propagated transgranularly, as seen in figure 148. The high strain range cyclic specimen fracture originated in voids at the surface or just slightly subsurface, as seen in figure 149, and then propagate transgranularly, as seen in figure 150. The fracture faces of both cyclic/dwell specimens were heavily oxidized. The low strain range specimen fracture appeared to originate and propagate intergranularly from the surface, as seen in figure 151. The high strain range cyclic specimen (S/N F8) fracture showed evidence of origins both at the very surface and at voids just below the surface. The surface origins appear to be intergranular, and propagation was intergranular, as shown in figure 152. All of the samples had an ASTM grain size of 8.5 through 10.5.

Discussion

The fractography and metallography can be summarized as follows:

- Crack initiation in the Waspaloy, wrought Astroloy, HIP-formed Astroloy, and HIP plus forged René 95 *cyclic* samples was transgranular and did not appear to be affected by grain size or structure, based on the limited number of samples reviewed. Crack initiation in the finer-grained HIP MERL 76 and GATORIZED IN 100 started at voids and inclusions, respectively. NASA IIB-7 samples were too smeared at the origin to discern any mode of crack initiation.

- Crack propagation in all of the *cyclic* samples, except the very fine-grained GATORIZED IN 100, was transgranular. The IN 100 samples propagated intergranularly. NASA IIB-7 samples were too smeared to determine any mode of crack propagation.

- Crack initiation in the wrought Astroloy, HIP plus forged René 95, and HIP MERL 76 *cyclic/dwell* samples was intergranular. The origin areas of the HIP-formed Astroloy and GATORIZED IN 100 samples were smeared and the NASA IIB-7 samples were heavily oxidized.

- Crack initiation in the Waspaloy *cyclic/dwell* samples was influenced by grain size. The coarser-grain high strain range sample failed transgranularly, whereas the slightly finer grain low strain range samples failed intergranularly.

- Crack propagation in all of the *cyclic/dwell* specimens was intergranular.

Table 22 summarizes the combined results of the fractographic and metallographic studies.

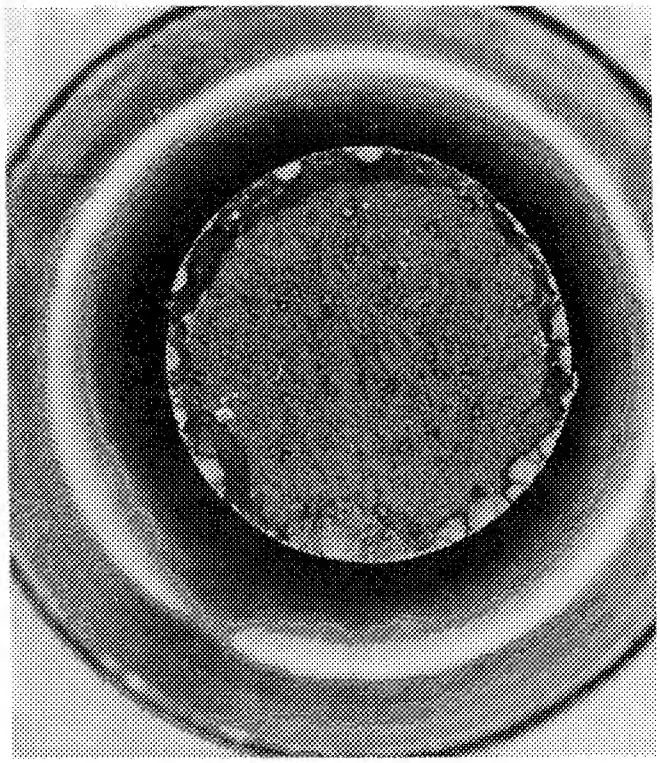

FAL 55795

(a) S/N D2, Cyclic, $1.84\Delta\epsilon_t$, 290 Cycles

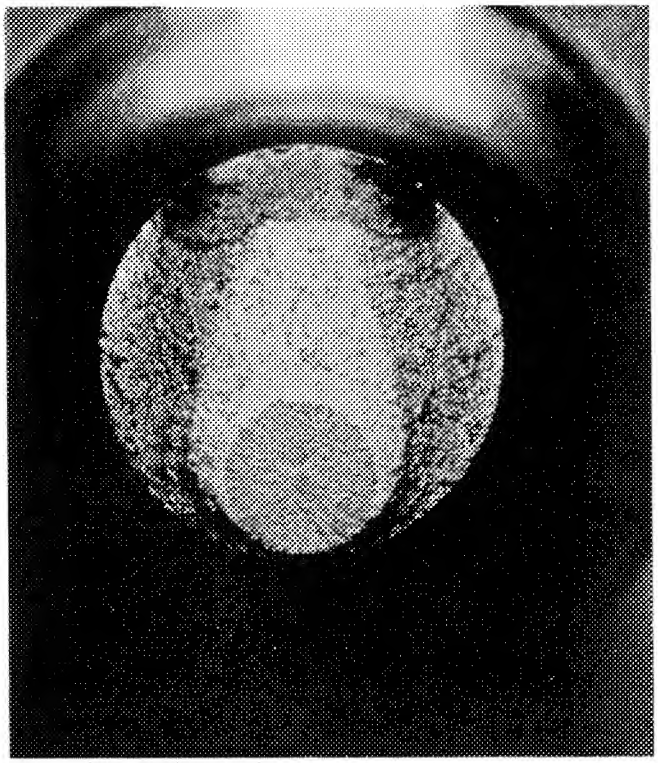

FAL 55796

(b) S/N D9, Cyclic, $0.91\Delta\epsilon_t$, 124,323 Cycles

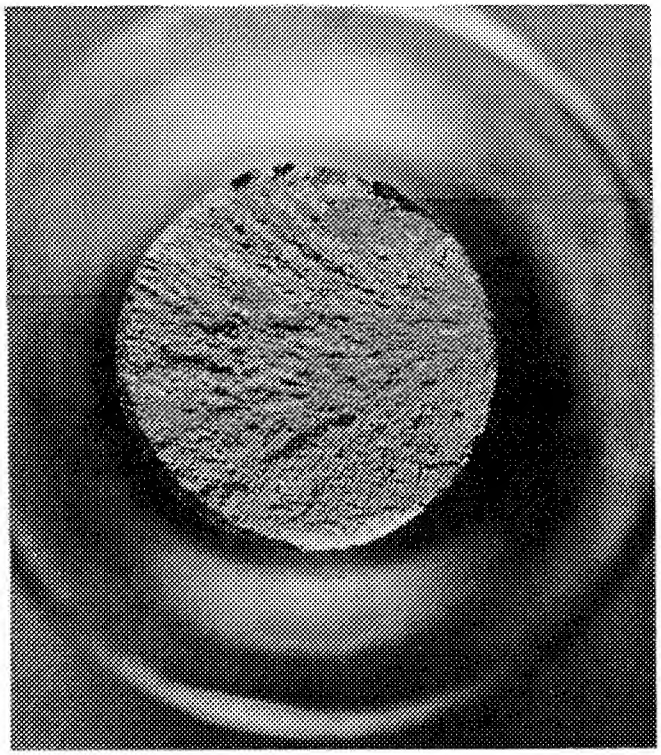

Mag: 10X FAL 56137

(c) S/N F7, Cyclic/Dwell, $1.06\Delta\epsilon_t$, 2,065 Cycles

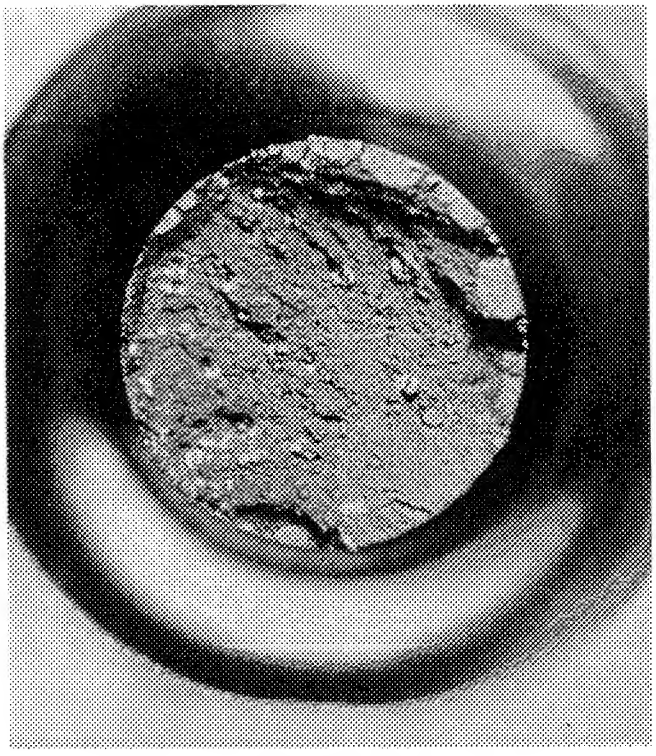

FAL 56132

(d) S/N F8, Cyclic/Dwell, $1.52\Delta\epsilon_t$, 264 Cycles

FD 189352

Figure 147. HIP MERL 76 Strain Control LCF Fracture Face

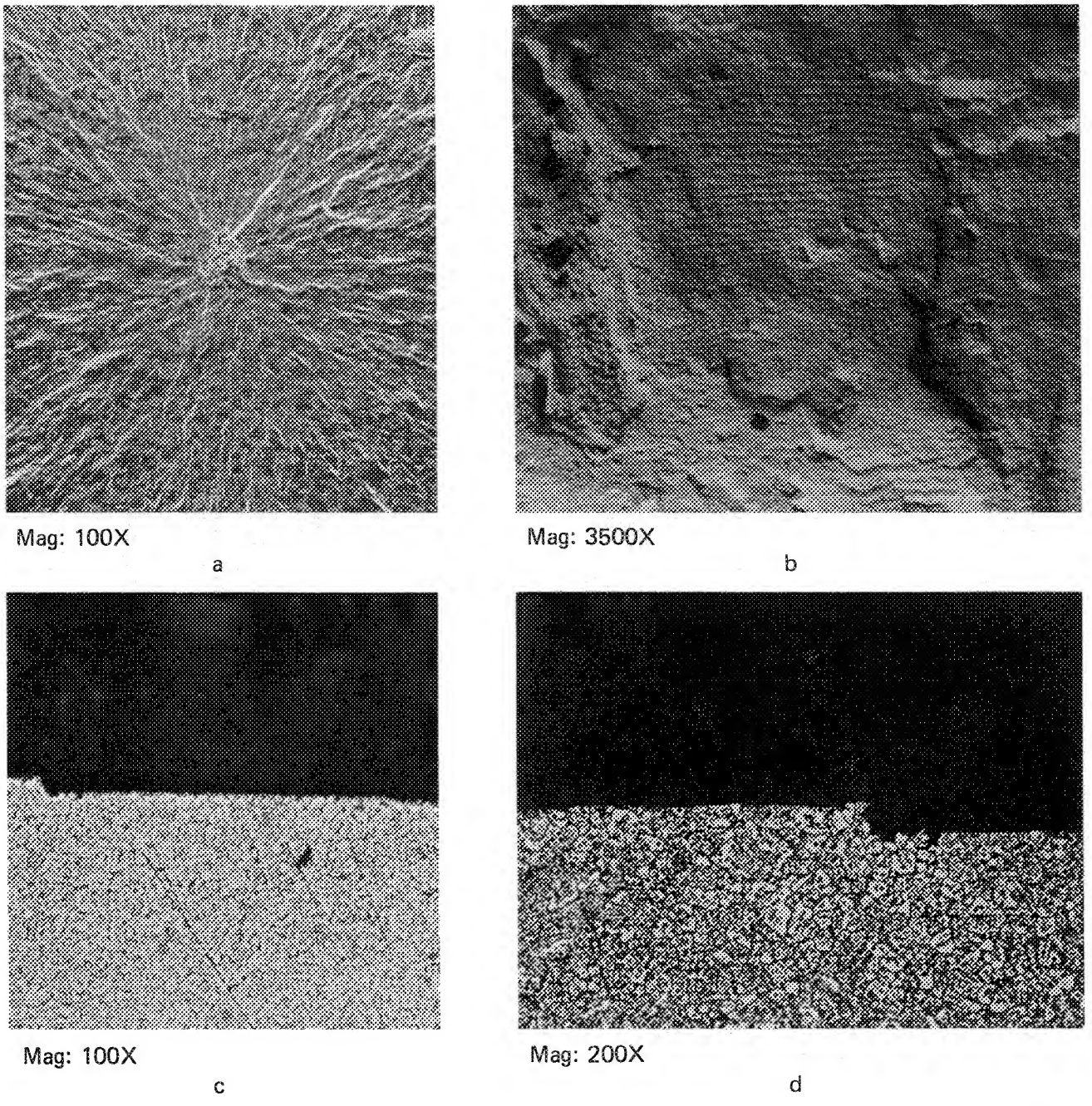

Figure 148. SEM Fractograph (a), TEM Fractograph (b), and Micrographs (c and d) Through Origin of HIP MERL 76 Specimen S/N D9 Showing Typical Fracture Features and Microstructure

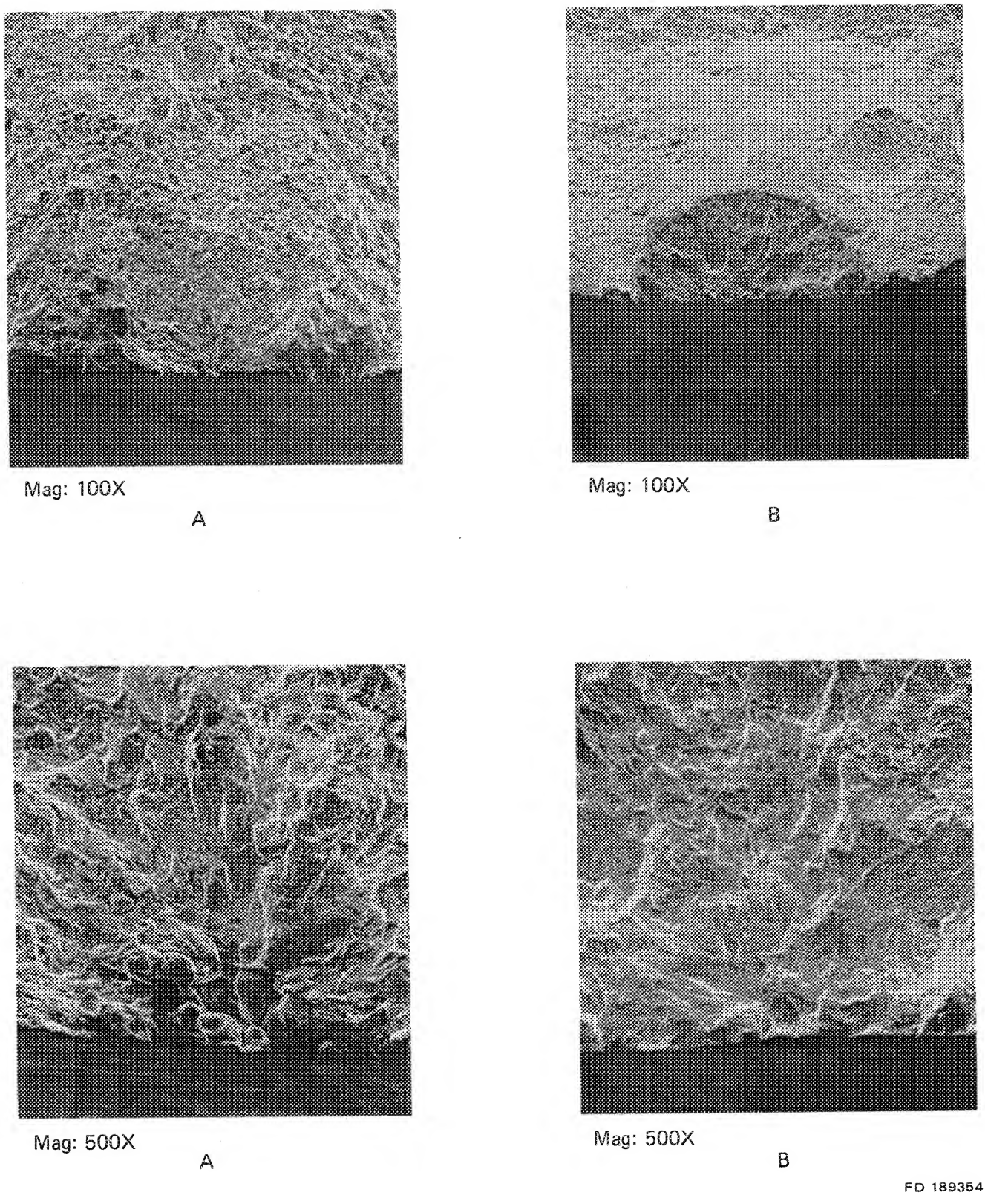

Figure 149. SEM Fractographs Showing Two Typical Origins on HIP MERL 76 Specimen S/N D2

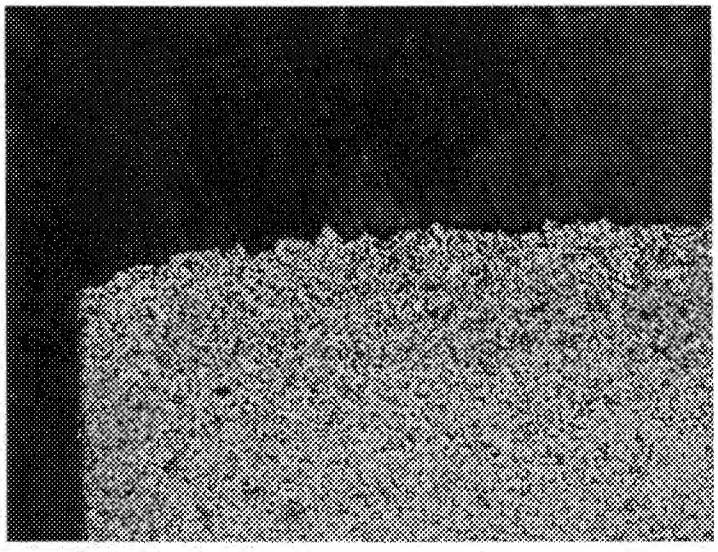

Mag: 100X

a

Mag: 6500X

b

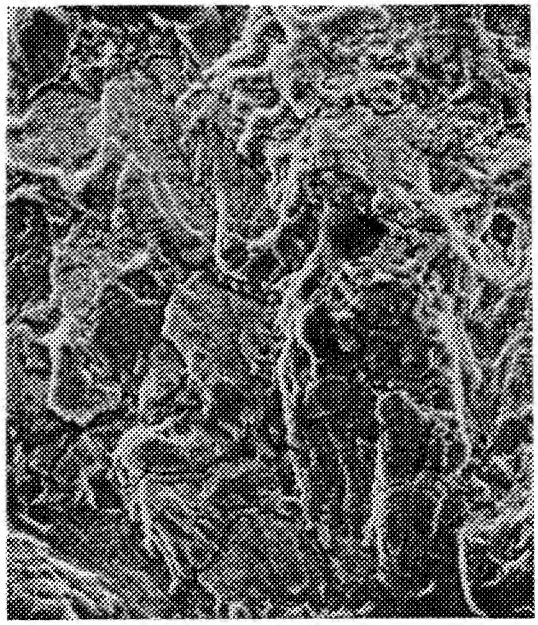

Mag: 1000X

c

FD 189355

Figure 150. Micrograph Through Typical Origin (a), and SEM (b) and TEM (c) Fractographs Showing Typical Transgranular Propagation on Fracture Face of HIP MERL 76 Specimen S/N D2

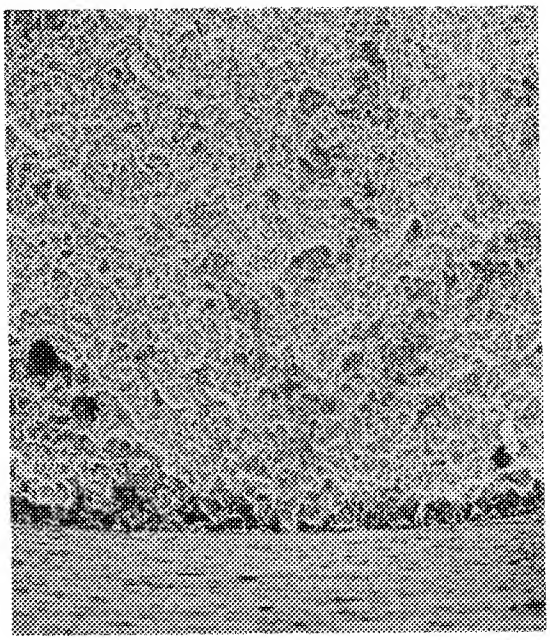

Mag: 100X

a

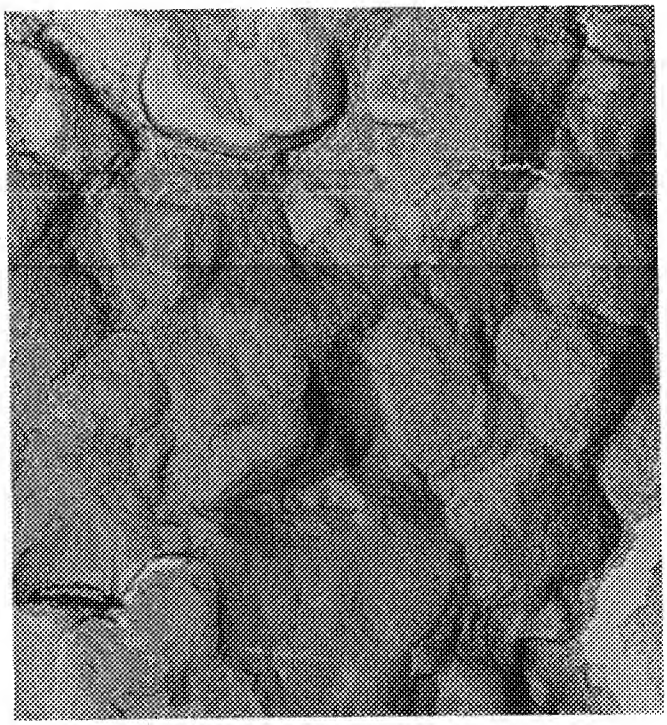

Mag: 3500X

b

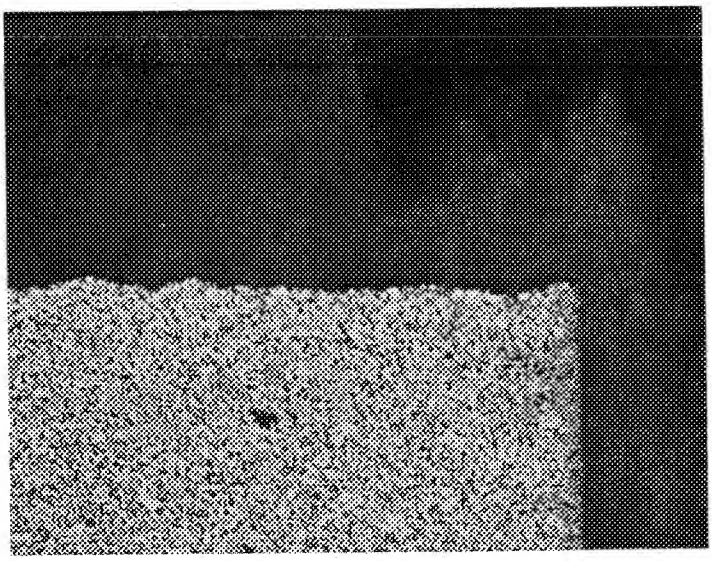

Mag: 100X

c

FD 189356

Figure 151. SEM Fractograph (a), TEM Fractograph (b), and Micrograph (c) Through Origin of HIP MERL 76 Specimen S/N F7 Showing Typical Features and Microstructure

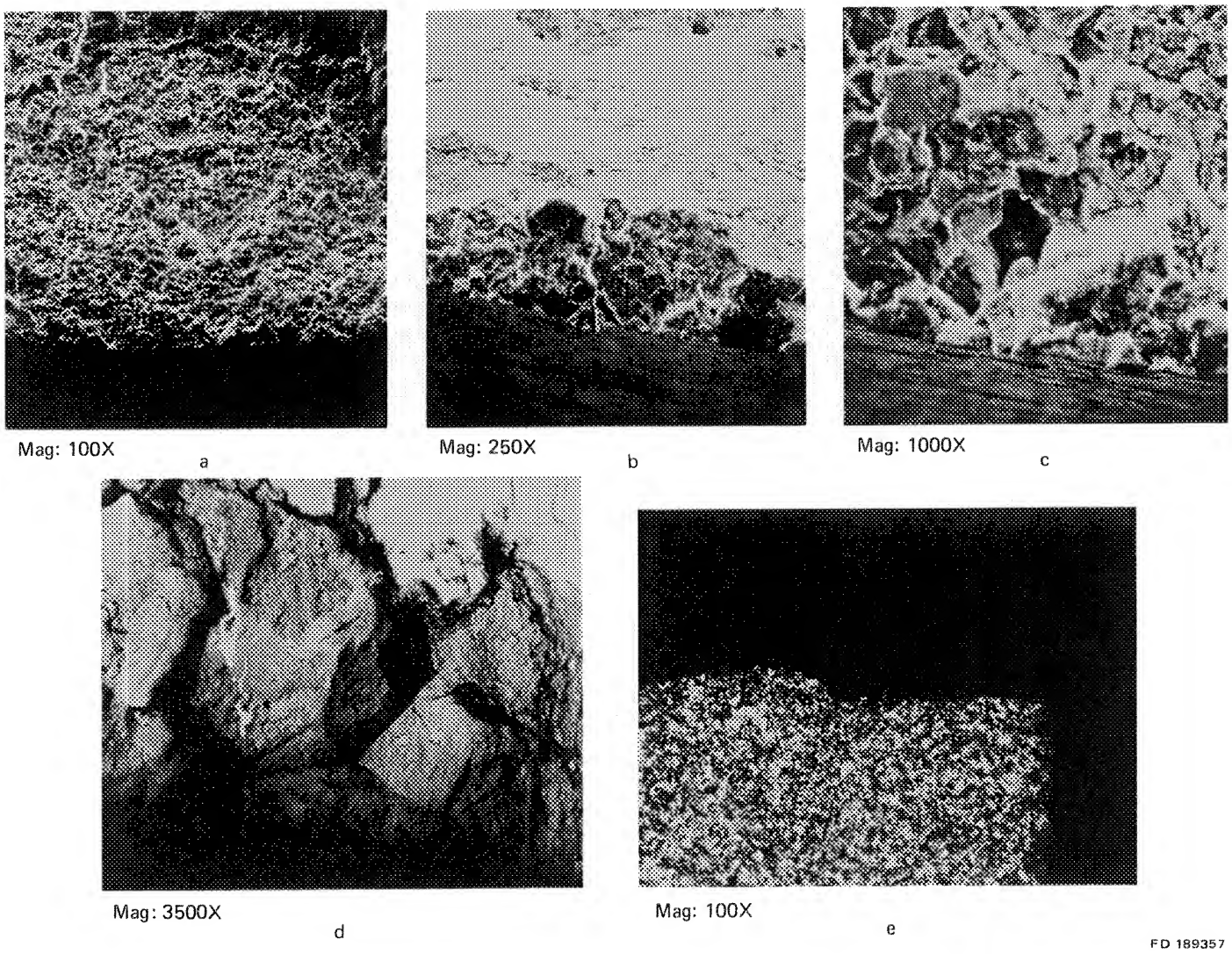

Figure 152. SEM Fractographs Showing Surface Origin (a) and Subsurface Void Origin (b and c); TEM Fractograph Showing Typical Intergranular Fracture Surface (d); Micrograph (e) Through Origin of HIP MERL 76 Specimen S/N F8

TABLE 22
SUMMARY OF FRACTOGRAPHIC AND METALLOGRAPHIC STUDIES

Material	*Spec S/N*	*Type* Test*	*Initiation*	*Propagation*	*ASTM Grain Size*
Waspaloy	A-2	C-11	Transgranular	Transgranular	3-5, Occasional 2
Waspaloy	A-7	C-L	Transgranular	Transgranular	3-5, Occasional 2
Waspaloy	A-11	C/D-H	Transgranular	Intergranular	Duplexed-3-6, Occasional 2, 1, Necklaced with 7 and finer
Waspaloy	A-14	C/D-L	Intergranular	Intergranular	Duplexed-4-5, and 7 and finer
Wrought Astroloy	1A	C-H	Transgranular	Transgranular	Duplexed-4-6 Necklaced With 7-8
Wrought Astroloy	4A	C-L	Transgranular	Transgranular	Duplexed-4-6 Necklaced With 7-8
Wrought Astroloy	8A	C/D-H	Intergranular	Intergranular	Duplexed-4-6 Necklaced With 7-8
Wrought Astroloy	10A	C/D-L	Intergranular	Intergranular	Duplexed-4-6 Necklaced With 7-8
HIP-Astroloy	DB-1	C-H	Transgranular	Transgranular	5-7, Occasional 4
HIP Astroloy	DB-5	C-L	Transgranular	Transgranular	5-7 Occasional 4
HIP-Astroloy	DB-10	C/D-H	Smeared	Intergranular	5-7, Occasional 4
HIP-Astroloy	CB-13	C/D-L	Smeared	Intergranular	5-7, Occasional 4
NASA IIB-7	1B	C-H	Smeared	Smeared	12.5-13.5
NASA IIB-7	4B	C-L	Smeared	Smeared	12.5-13.5
NASA IIB-7	9B	C/D-H	Heavily Oxidized	Intergranular	12.5-13.5
NASA IIB-7	10B	C/D-L	Heavily Oxidized	Intergranular	12.5-13.5
GATORIZED IN 100	7	C-H	Inclusion	Intergranular	12.5-14.5, Occasional 11.5
GATORIZED IN 100	3	C-L	Inclusion	Intergranular	12.5-14.5, Occasional 11.5
GATORIZED IN 100	9	C/D-H	Smeared	Intergranular	12.5-14.5, Occasional 11.5
GATORIZED IN 100	11	C/D-L	Smeared	Intergranular	12-5.-14.5, Occasional 11.5
HIP Plus Forged René 95	1	C-H	Transgranular	Transgranular	60% Unrecrystallized grains — 5-6, occasional 4. 40% Necklaced — Finer than 8
HIP Plus Forged René 95	3	C-L	Transgranular	Transgranular	60% Unrecrystallized grains — 5-6, Occasional 4. 40% Necklaced — Finer than 8
HIP Plus Forged René 95	4	C/D-H	Intergranular	Intergranular	60% Unrecrystallized grains — 5-6, Occasional 4. 40% Necklaced — Finer than 8
HIP Plus Forged René 95	13	C/D-L	Intergranular	Intergranular	60% Unrecrystallized grains — 5-6, Occasional 4. 40% Necklaced — Finer than 8
HIP MERL 76	D2	C-H	Voids	Transgranular	8.5-10.5
HIP MERL 76	D9	C-L	Voids	Transgranular	8.5-10.5, Occasional 7.5
HIP MERL 76	F7	C/D-L	Intergranular	Intergranular	8.5-10.5
HIP MERL 76	F8	C/D-H	a. Intergranular b. Subsurface Voids	Intergranular	8.5-10.5, Occasional 7.5

*C = Cyclic, C/D = Cyclic Dwell
H = High Strain Range
L = Low Strain Range

The tendency of the high-strength, fine-grained alloys to initiate fatigue cracks either intergranularly or at microstructural defects, such as voids or inclusions which are large relative to grain size, and the subsequent intergranular crack growth, even under relatively rapid (0.33 Hz) cycling, indicates higher susceptibility to grain boundary failure mechanisms (such as oxidation) compared to the coarse-grain alloys. The hold-time tests, where effects such as grain boundary oxidation would be expected to increase, resulted in intergranular propagation in all of the alloys and a change in initiation mode from transgranular to intergranular for all of the samples where failure mode at the origin could be distinguished. Only in the Waspaloy samples with a relatively coarse structure at the origin was the failure mode transgranular under cyclic/dwell conditions, further substantiating a strong relationship between grain size and failure mode. The apparent higher susceptibility of the fine grained alloys to intergranular failure modes and probably to grain boundary oxidation is assumed to be the reason for the substantially higher degradation shown by these alloys under cyclic/dwell conditions in both fatigue crack initiation and crack growth comparisons at 650°C.

FURTHER CREEP-FATIGUE EVALUATIONS

General

In addition to total strain range and mean stress, cyclic hold (dwell) times and cyclic creep strain magnitudes represent important variables which affect fatigue life. Actual engine components may experience dwell conditions which are not represented by the 900-sec strain-hold or stress-relaxation type of dwell cycle utilized previously in this program. For example, while a turbine disk bolthole may experience sufficient elastic constraint to locally relax under sustained externally applied loading, the highly stressed region of a disk-blade attachment may be kinematically free to creep. The stress-strain hysteresis loops which represent these types of cycles are significantly different. Improved LCF life prediction systems must be capable of accurately modeling the material behavior under both types of dwell cycles, including determination of the effect of hold times.

To determine the differences in LCF life due to different hold times and types of cyclic/dwell tests, axial strain control LCF tests of IN 100 were performed at 650°C (1200°F). Several tests with 30-sec and 120-sec dwell times at maximum tensile strain were conducted, all with a fully reversed strain cycle (R_ϵ = -1). In addition, several cyclic/dwell waveforms were evaluated to compare stress-hold with strain-hold types. All of the cycle types employed dwell only during peak tensile conditions of the stress-strain cycle. Table 23 describes the cycle types which were evaluated.

Test specimens and general test methods were the same utilized for other cyclic and cyclic/dwell tests contained in this report, except that for some of the desired waveforms the controlled parameter during the dwell was stress or load rather than strain, and the variable which determined switching into and out of the dwell period was not limited to time. Differences in test cycles are described in the following paragraphs.

Variable Hold-Time Testing

Strain hold times of 30 and 120 sec were used to determine the effect of dwell on LCF life in addition to the 900-sec dwell tests run previously. These tests utilized a fully reversed strain-time waveform with dwell at maximum tensile strain. All other test conditions and methods duplicated the 900-sec dwell tests.

Table 24 presents the results from this testing. Stress range and mean stress vs life curves appear in figures 153 through 156. Strain range vs life curves comparing the effect of strain dwell on LCF life are shown in figures 157 and 158. Also shown in these last two figures are the results from earlier Contractor testing, including cyclic (no dwell) and 900-sec cyclic/dwell data.

Increasing hold time per cycle could be expected to influence LCF life by increasing the time-dependent inelastic, or creep, strain component and also by increasing the exposure time of the material to the elevated temperature environment. Comparison of creep strain magnitudes for 30, 120, and 900-sec hold periods for the IN 100 alloy indicates that for all strain ranges of interest (1.2% $\Delta\epsilon_T$ or below), the cyclic creep strain components are very small (0.0001 m/m or less) and are the same within experimental measurement capability for all hold-time cycles. Consequently, under the conditions evaluated, changes in the creep strain component could not be directly related to reductions in life with increasing hold time per cycle. Figure 159 shows time per cycle vs LCF life results for the 0.33 Hz cyclic and all three cyclic/dwell conditions. The linear (log-log) relationship between cycle time and life for various strain ranges indicates that the systematically reduced LCF life is, in some way, due to increased exposure time of the alloy to the elevated temperature (650°C) environment.

TABLE 23
STRAIN-HOLD AND STRESS-HOLD CYCLE TYPES

	Dwell Control				
Cycle Type	*Begin Dwell at*	*Dwell Control*	*Reversed at*	*Initial R_ϵ*	*Remarks*
1a	Peak Strain	Peak Strain	900 sec[1]	-1	Stress relaxation dwell.
b	Peak Strain	Peak Strain	900 sec	0	Stress relaxation dwell; mean stress decreases during test.
2	Peak Stress	Peak Stress	Fixed max strain	-1	Creep dwell; requires high $\Delta\epsilon_c$ to obtain different stress ranges. $\Delta\epsilon_p$ and hold time per cycle decrease during test.
3	Peak Stress	Peak Stress	900 sec	-1	Creep dwell; moderate progressive increase in mean strain during test due to unreversed creep.
4	Peak Stress	Peak Stress	900 sec	0[2]	Creep dwell; significant progressive increase in mean strain during test due to unreversed creep.
5	Peak Stress	Peak Strain	900 sec	0	Modified stress relaxation dwell; mean stress constant during test, but significant unreversed creep contributions to failure.

[1]Tests of this type with hold times of 30 and 120 sec also conducted.
[2]Specimen S/N 48 run with this cycle type, except $R_\epsilon = 0.5$.

TABLE 24
STRAIN CONTROLLED LOW-CYCLE FATIGUE RESULTS FOR TASK II STRAIN DWELL TESTS OF IN 100 WITH VARIABLE DWELL TIME
Testing conducted in air at 650°C, Ramp Frequency = 0.33 Hz (20 cpm)

Spec S/N	*Type* Test*	*Strain R Ratio (min/max)*	*Dwell Time (sec)*	*Strain (m/m at $N_f/2$)*				*Mean Stress at $N_f/2$*		*Stress Range*		*Cyclic Stability*	*Cycles to Failure*	
				Range	*Elastic*	*Inelastic*	*Creep*	*MPa*	*ksi*	*Cycle 1*	*$N_f/2$*		*N_5%*	*N_f*
24	Cyclic/Dwell	-1	120	0.0126	0.0118	0.0008	0.0001	17	2.4	2088 MPa (302.8 ksi)	2054 MPa (297.9 ksi)	Stable	569	662
25	Cyclic/Dwell	-1	120	0.0100	0.0097	0.0003	<0.0001	6	0.8	1695 MPa (245.8 ksi)	1695 MPa (245.8 ksi)	Stable	4,554	4,995
26	Cyclic/Dwell	-1	120	0.0080	0.0079	0.0001	<0.0001	11	1.6	1340 MPa (194.3 ksi)	1346 MPa (195.1 ksi)	Stable	—	35,582**
32	Cyclic/Dwell	-1	120	0.0155	0.0132	0.0023	0.0005	-51	-7.3	2312 MPa (335.4 ksi)	2329 MPa (337.8 ksi)	Stable	230	249
34	Cyclic/Dwell	-1	30	0.0149	0.0127	0.0022	0.0003	-40	-5.8	2211 MPa (320.7 ksi)	2236 MPa (324.3 ksi)	Stable	284	328
35	Cyclic/Dwell	-1	30	0.0122	0.0117	0.0005	0.0001	-10	-1.4	2025 MPa (293.7 ksi)	1995 MPa (289.4 ksi)	Stable	531	600
27	Cyclic/Dwell	-1	30	0.0123	0.0117	0.0006	0.0001	-50	-7.2	2013 MPa (291.9 ksi)	1993 MPa (289.0 ksi)	Stable	713	806
36	Cyclic/Dwell	-1	30	0.0097	0.0095	0.0002	<0.0001	20	2.9	1674 MPa (242.8 ksi)	1669 MPa (242.1 ksi)	Stable	6,261	6,710
41	Cyclic/Dwell	-1	30	0.0084	0.0083	0.0001	<0.0001	-15	-2.1	1468 MPa (212.9 ksi)	1473 MPa (213.6 ksi)	Stable	28,513	29,886

*Cyclic tests conducted at 0.33 Hz (20 cpm)
Cyclic/Dwell tests have a hold time at the maximum tensile strain. Ramp frequency is the same as the cyclic tests.
**Test discontinued, no indication of failure

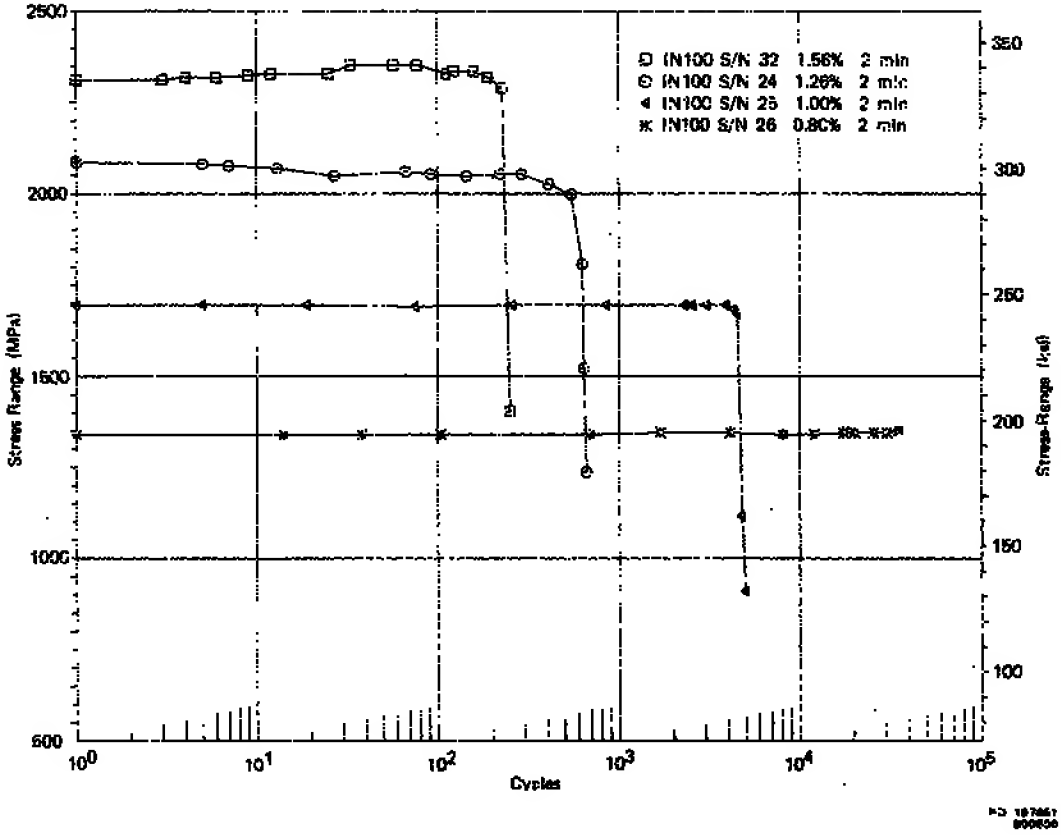

Figure 153. Stress Range vs Cycles for IN 100 (R_σ = -1, 120-sec Dwell)

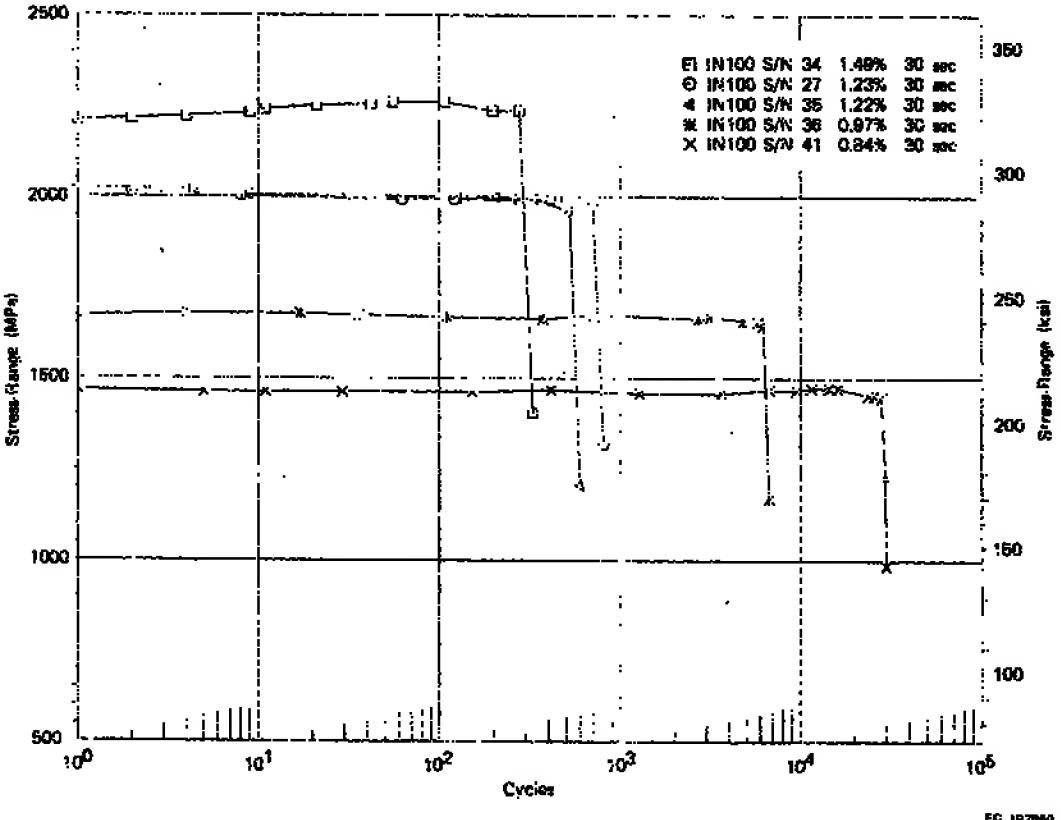

Figure 154. Stress Range vs Cycles for IN 100 (R_σ = -1, 30-sec Dwell)

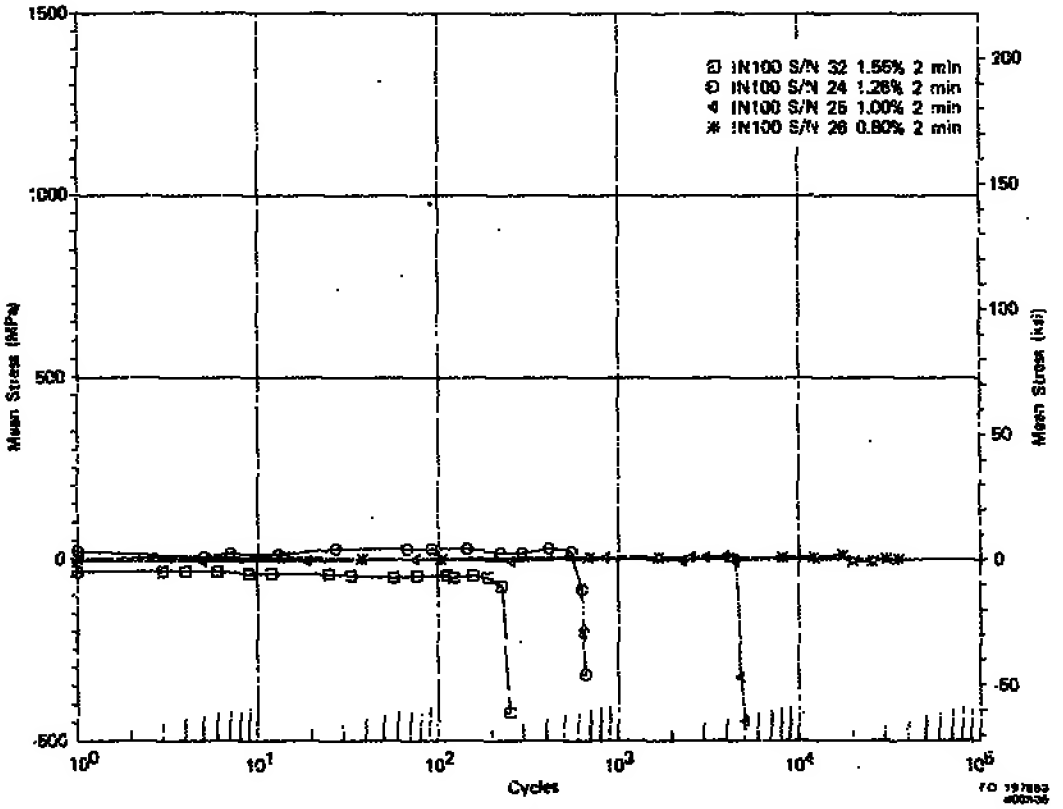

Figure 155. Mean Stress vs Cycles for IN 100 (R_σ = -1, 120-sec Dwell)

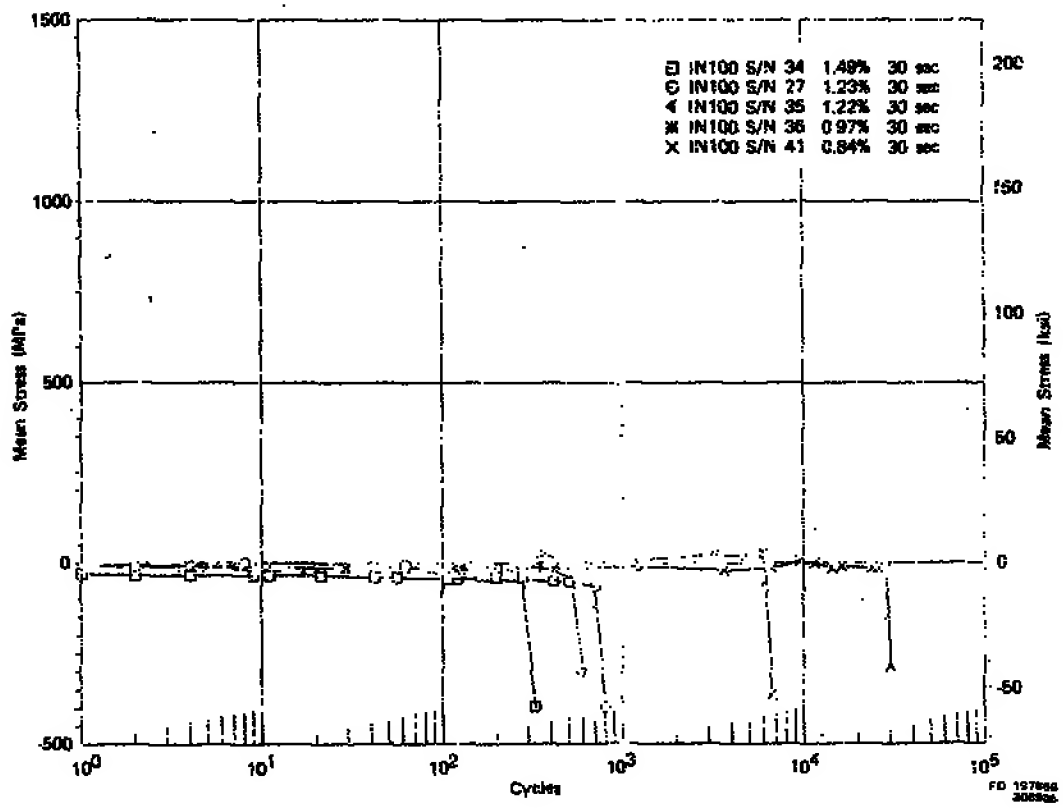

Figure 156. Mean Stress vs Cycles for IN 100 (R_σ = -1, 30-sec Dwell)

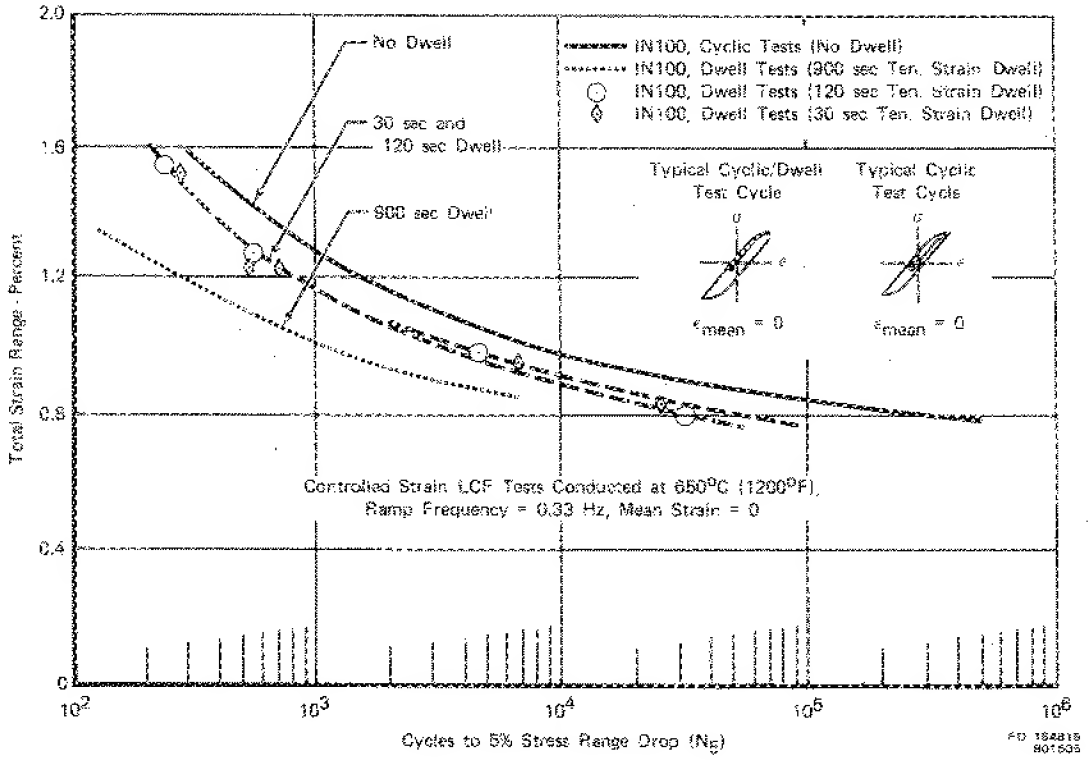

Figure 157. Effect of Strain Hold Time on Strain Control LCF Results of IN 100 (N_5 Life)

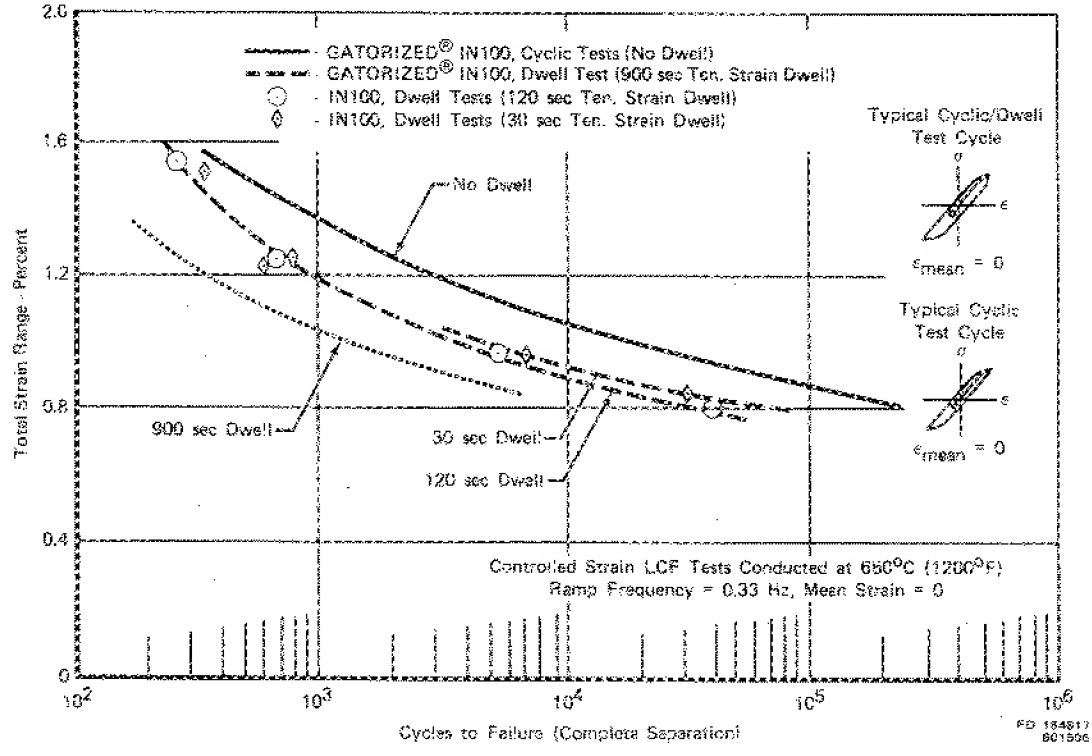

Figure 158. Effect of Strain Hold Time on Strain Control LCF Results of IN 100 (Failure)

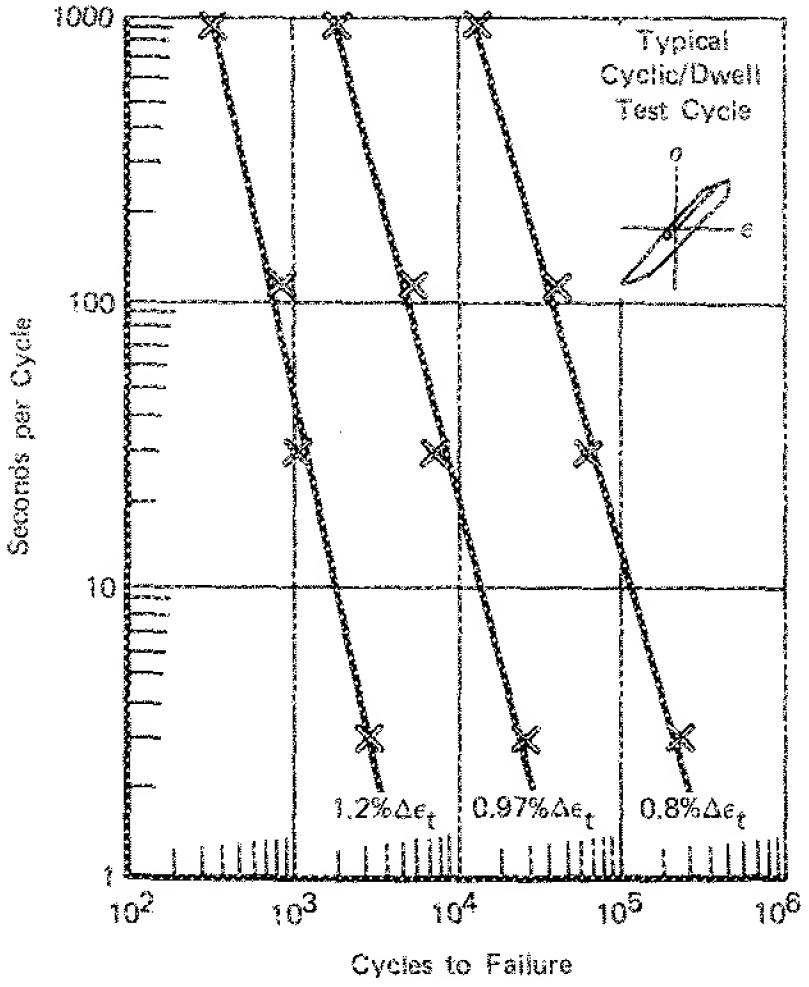

Figure 159. Effect of Cycle Time on LCF Life for IN 100

Creep-Fatigue Cycle Evaluations

Significant differences occur in the local stress-strain-time material response for different fracture critical locations of aircraft engine turbine disks. Boltholes in disk web areas, for example, may be sufficiently constrained by surrounding essentially elastic material so that their LCF-creep behavior may be approximated by a stress relaxation, or strain-dwell, cycle. Blade attachment areas at the disk rim, however, may experience some net section creep and, consequently, may be better represented by a creep dwell, or constant stress-hold, cycle.

Initial waveforms for this phase of testing were selected in an attempt to evaluate differences between a stress-hold cycle (creep dwell) and a strain-hold cycle (stress relaxation). Additional waveforms separated the contributions of mean stress and progressively increasing mean strains (due to cyclically unreversed creep) on the LCF life.

Table 23 describes the different dwell cycle types. Typical cycle schematics and resulting stress-strain-time responses appear in figures 13, 15, 16, and 160 through 163.

In order to investigate differences between a basic creep, or stress dwell cycle and the relaxation, or strain dwell cycle previously described, three tests were conducted using the waveform described in figure 160 and defined in table 23 as cycle type 2. Several tests were planned for the same peak stress condition with different strain ranges obtained by controlling the maximum strain limit. Use of this waveform produced several difficulties. In order to obtain sufficient creep to ensure significantly different strain ranges, the peak stress condition and the resulting total strain range were very high, causing low LCF lives. Also, dwell time per cycle continually decreased during the course of the test as the mean stress became increasingly compressive. Because of these difficulties, alternative stress-dwell waveforms were selected. Test results for this cycle are presented in table 25 and figure 164.

To eliminate differences in hold period duration, subsequent stress dwell cycles were selected to ensure a 900-sec dwell for best comparison with strain-dwell results. For dwell periods of the same duration, LCF life differences between a peak stress, or creep dwell, cycle and a peak strain, or relaxation dwell, cycle can be attributed to three factors: (1) differences in mean stress due to mean stress relaxation in the strain dwell cycle, (2) differences in mean strain due to cyclically unreversed creep in the stress dwell cycle, and (3) a slightly larger creep strain in the creep dwell cycle since all of the hold period is spent at peak stress.

The first creep dwell cycle was selected to produce a mean stress of zero with a 900-sec dwell, as shown in figure 161 and described in table 23 as cycle type 3. Results are presented in table 26. Figure 165 presents a plot of this data for comparison with strain-hold data. There appears to be no significant difference for the two cycle types at these conditions which involve nearly zero mean stresses for both cycle types and a minimum amount of accumulated creep strain (cyclically unreversed) for the stress-dwell cycle. Although the creep strain ranges are small for these cycles, it is apparent from the results that no significant differences in LCF life occur due to the basic cycle type (stress vs strain dwell).

The same creep-dwell cycle was further evaluated with an all-tensile strain cycle ($R_\varepsilon = 0$) to determine the effects of mean stress. The cycle is illustrated in figure 162 and described in table 23 as cycle type 4. This cycle produced significant cyclically unreversed creep in addition to the constant tensile mean stress and resulted in substantially reduced LCF life when compared to strain-dwell tests at similar starting conditions of strain range and mean stress. Results are presented in table 26 and plotted in figure 166.

TABLE 25

CONTROLLED STRAIN LOW-CYCLE FATIGUE RESULTS FOR TASK II CREEP DWELL TESTS OF IN 100

Testing conducted at 650°C, 0.33 Hz, Ramp Frequency

Spec S/N	Type[1] Test	Strain R Ratio (min/max)	Stress (Dwell)	Strain (m/m at N_f				Mean Stress at H_f		Stress Range		Cyclic Stability	Cycles to Failure		Dwell Period[3]	
				Range	Elastic	Inelastic	Creep	MPa	ksi	Cycle 1	N_f		N_d	N_f	Cycle 1	$N_f/2$
17	Creep/Dwell	-1	1165 MPa (169 ksi)	0.0180	0.0143	0.0037	0.0012	-98	-14.2	2446 MPa (354.7 ksi)	2524 MPa (366.1 ksi)	Harden	82	100	1 hr	30 min
18	Creep/Dwell	-1	1103 MPa (160 ksi)	0.0146	0.0131	0.0015	0.0004	-69	-9.9	2292 MPa (332.4 ksi)	2336 MPa (338.8 ksi)	Slight Hardening	309	368	1 hr	10 min
19	Creep/Dwell	-1	1103 MPa (160 ksi)	0.0160	0.0132	0.0028	0.0011	-124	-18.0	2370 MPa (343.7 ksi)	2469 MPa (358.1 ksi)	Harden	115	139	7 hr	20 min

[1]These tests are fully reversed strain tests with a hold period at a predetermined max stress (to allow creep to occur until the maximum strain limit is reached).

[2]N_d is defined as the life when the dwell time becomes zero, and the test continues as a 0.33 Hz cyclic test until failure.

[3]This is the time required for the specimen to creep to the maximum strain (time approximate).

Note -- this data does not indicate increasing creep rate because the creep strain component has decreased concurrently during the test.

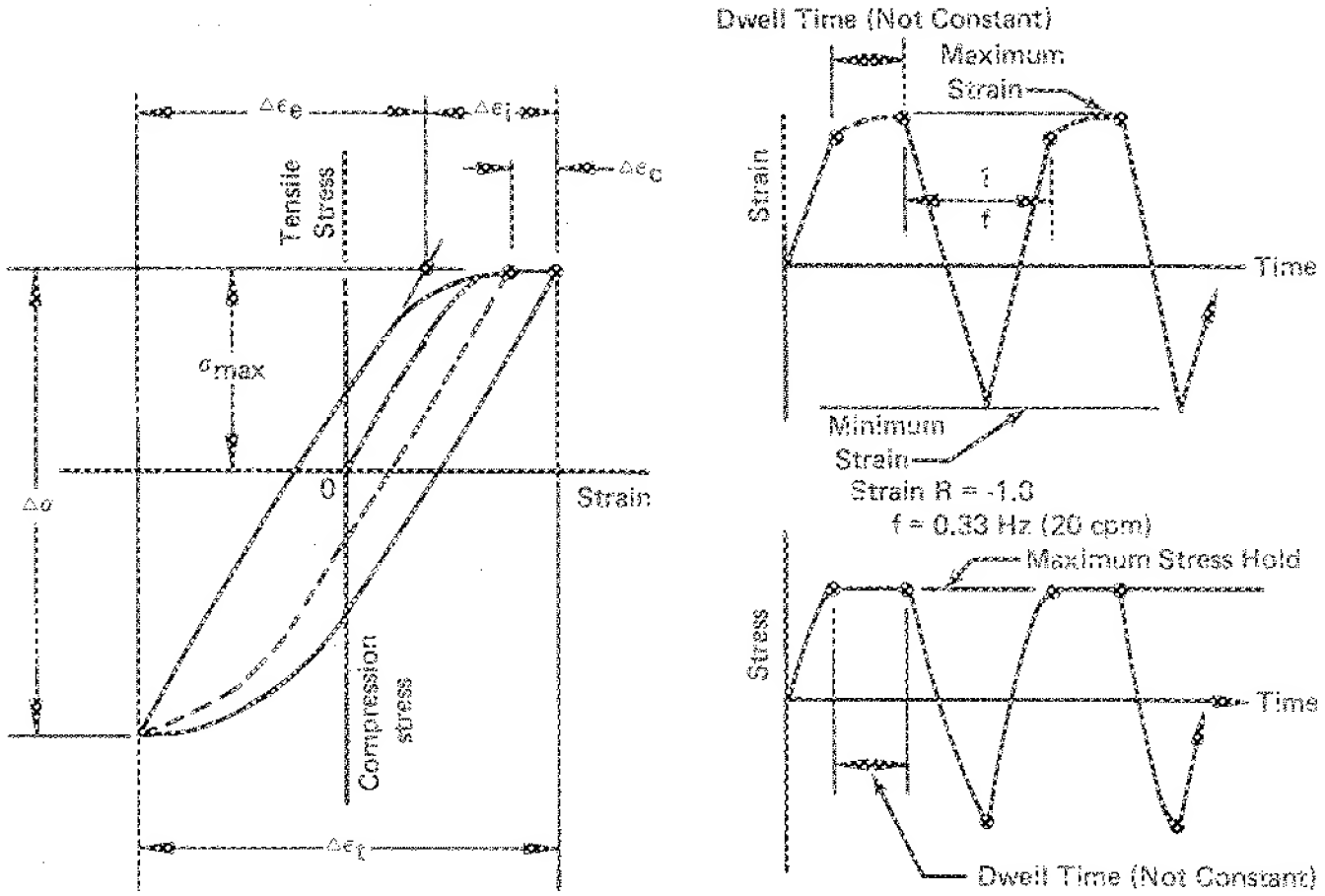

$\Delta\sigma$ = Total Stress Range
σ_{max} = Creep Stress (Held Constant to Allow Specimen to Creep)
$\Delta\epsilon_t$ = Total Strain Range
$\Delta\epsilon_i$ = Inelastic Strain Range
$\Delta\epsilon_c$ = Creep Strain Range
$\Delta\epsilon_e$ = Elastic Strain Range
Dwell Time = Hold Time at Max Stress, May Vary Due to Creep Rate
R = Strain Ratio, Minimum Strain/Maximum Strain
f = Ramp Frequency (Equivalent to 20 cpm Nondwell Tests)
E = $\Delta\sigma/\Delta\epsilon_e$

FD 135465

Figure 160. Typical Stress-Dwell LCF Test with Mean Strain Equal to Zero

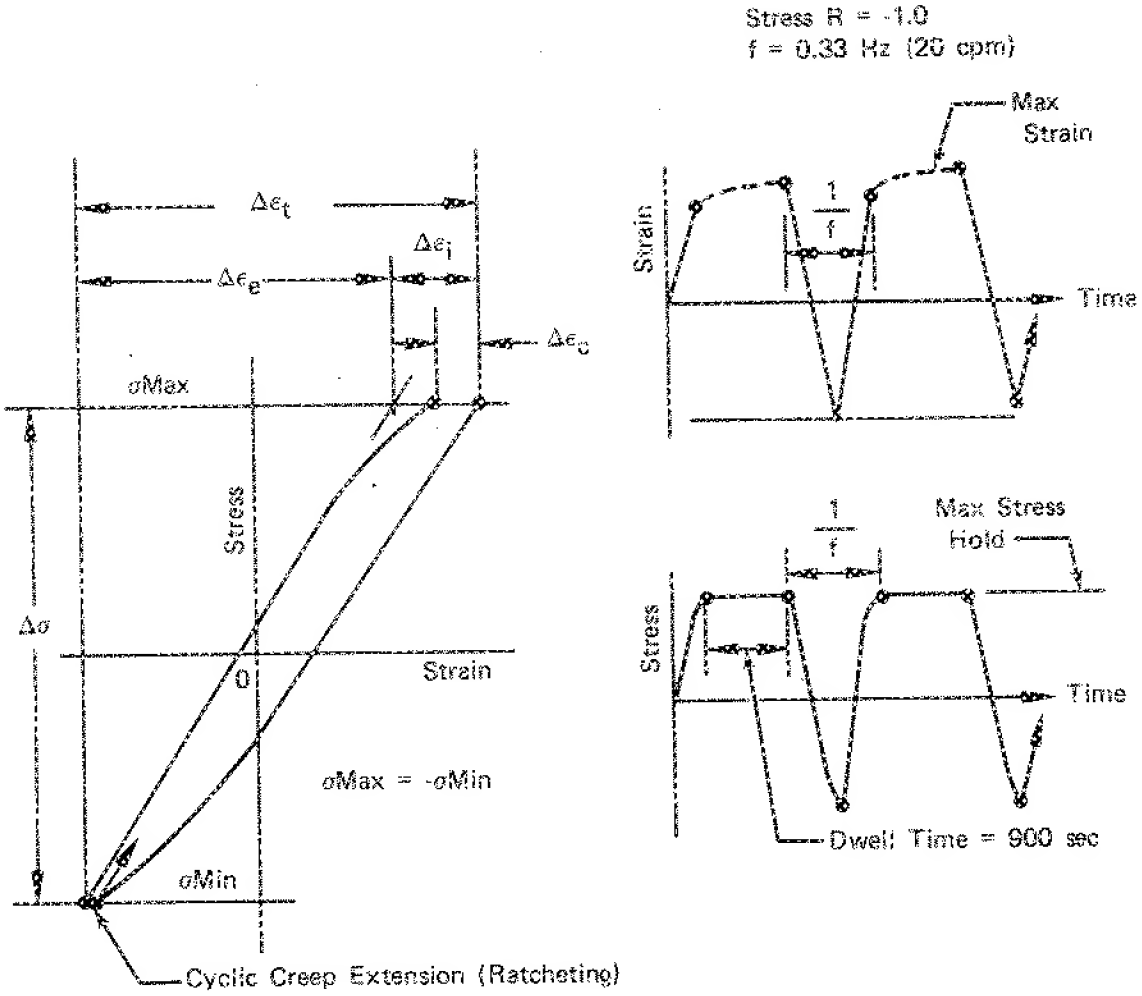

$\Delta\sigma$	= Total Stress Range
σMax	= Creep Stress (Held Constant to Allow Specimen to Creep) = -σMin
$\Delta\epsilon_t$	= Total Strain Range
$\Delta\epsilon_i$	= Inelastic Strain Range
$\Delta\epsilon_c$	= Creep Strain Range
$\Delta\epsilon_e$	= Elastic Strain Range
Dwell Time	= Hold Time at Max Stress, 900 sec
R	= Stress Ratio, Min/Max Stress
f	= Ramp Frequency (Equivalent to 20 cpm Nondwell Tests)
E	= $\Delta\sigma/\Delta\epsilon_e$

FD 162757
801680

Figure 161. Typical Stress-Dwell LCF Test with Mean Stress Equal to Zero (Stress-Limited Rather than Strain-Limited)

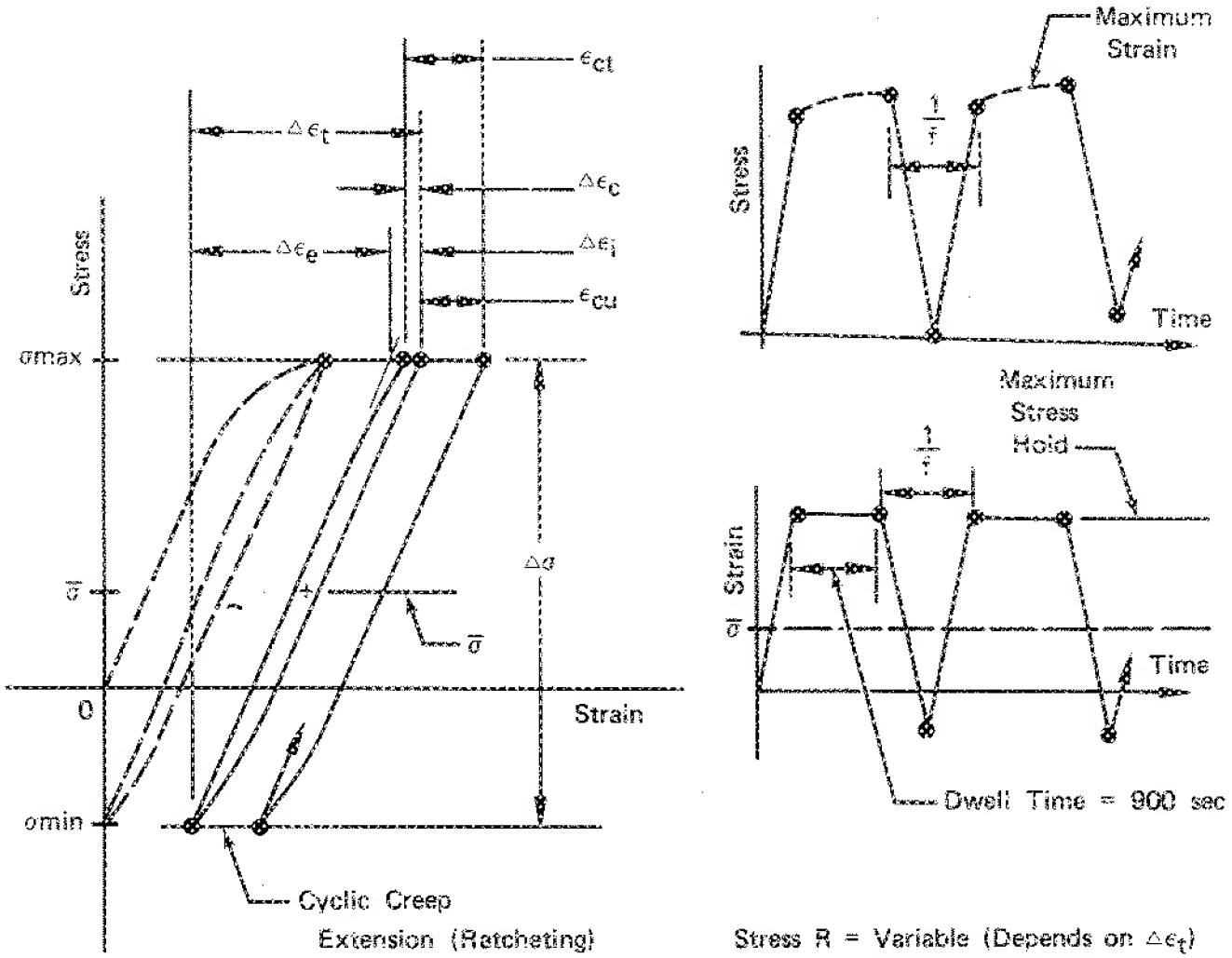

$\Delta\sigma$	= Total Stress Range
σmax	= Creep Stress (Held Constant to Allow Specimen to Creep)
σmin	= Minimum Stress (Stress Necessary to Set Minimum Strain = 0 at Start of Test)
$\bar{\sigma}$	= Tensile Mean Stress
$\Delta\epsilon_t$	= Total Strain Range
$\Delta\epsilon_i$	= Inelastic Strain Range
$\Delta\epsilon_{cr}$	= Cyclic Creep Strain Range (Reversed)
ϵ_{ct}	= Total Creep Strain per Cycle
ϵ_{cu}	= Unreversed Creep Strain per Cycle
$\Delta\epsilon_e$	= Elastic Strain Range
Dwell Time	= Hold Time at Maximum Stress, 900 sec
R	= Stress Ratio, Minimum Stress/ Maximum Stress
f	= Ramp Frequency (Equivalent to 20 cpm Nondwell Tests)
E	= $\Delta\sigma/\Delta\epsilon_e$

PD 164819

Figure 162. Typical Stress-Dwell, Stress Control LCF Test with Mean Stress Greater than Zero

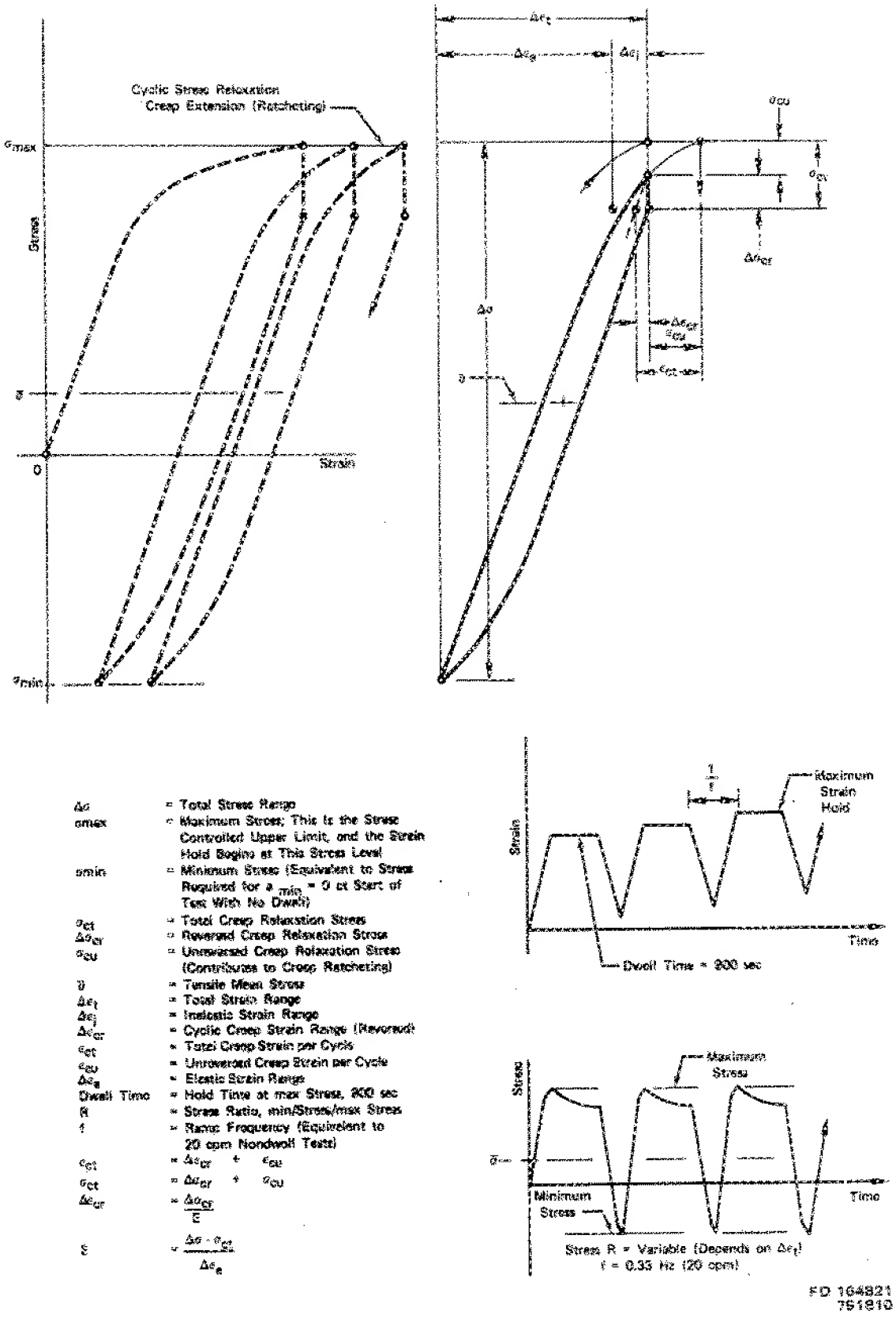

$\Delta\sigma$	= Total Stress Range
σ_{max}	= Maximum Stress; This is the Stress Controlled Upper Limit, and the Strain Hold Begins at This Stress Level
σ_{min}	= Minimum Stress (Equivalent to Stress Required for a R_{min} = 0 at Start of Test With No Dwell)
σ_{ct}	= Total Creep Relaxation Stress
$\Delta\sigma_{cr}$	= Reversed Creep Relaxation Stress
σ_{cu}	= Unreversed Creep Relaxation Stress (Contributes to Creep Ratcheting)
$\bar{\sigma}$	= Tensile Mean Stress
$\Delta\varepsilon_t$	= Total Strain Range
$\Delta\varepsilon_i$	= Inelastic Strain Range
$\Delta\varepsilon_{cr}$	= Cyclic Creep Strain Range (Reversed)
ε_{ct}	= Total Creep Strain per Cycle
ε_{cu}	= Unreversed Creep Strain per Cycle
$\Delta\varepsilon_e$	= Elastic Strain Range
Dwell Time	= Hold Time at max Stress, 900 sec
R	= Stress Ratio, min/Stress/max Stress
f	= Ramp Frequency (Equivalent to 20 cpm Nondwell Tests)
ε_{ct}	= $\Delta\varepsilon_{cr} + \varepsilon_{cu}$
σ_{ct}	= $\Delta\sigma_{cr} + \sigma_{cu}$
$\Delta\varepsilon_{cr}$	= $\frac{\Delta\sigma_{cr}}{E}$
E	= $\frac{\Delta\sigma - \sigma_{cu}}{\Delta\varepsilon_e}$

FD 164821
791810

Figure 163. Typical Strain-Dwell, Stress Control LCF Test with Mean Stress Greater than Zero

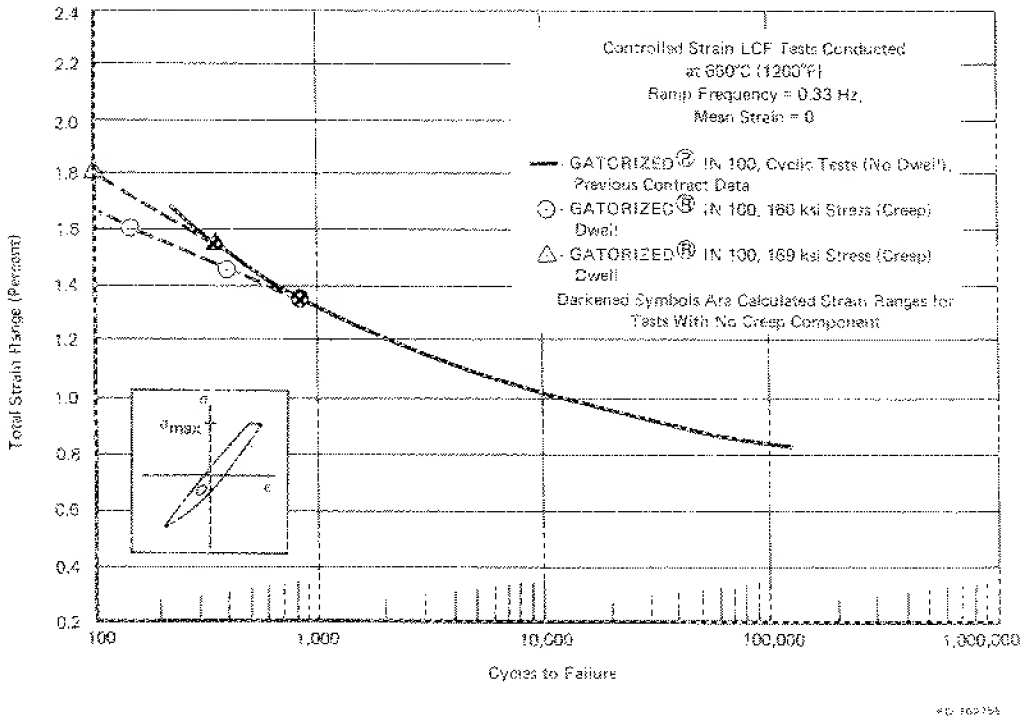

Figure 164. Strain Control LCF Results for IN 100 (with Stress Dwell and Strain Limits, Mean Strain Equal to Zero)

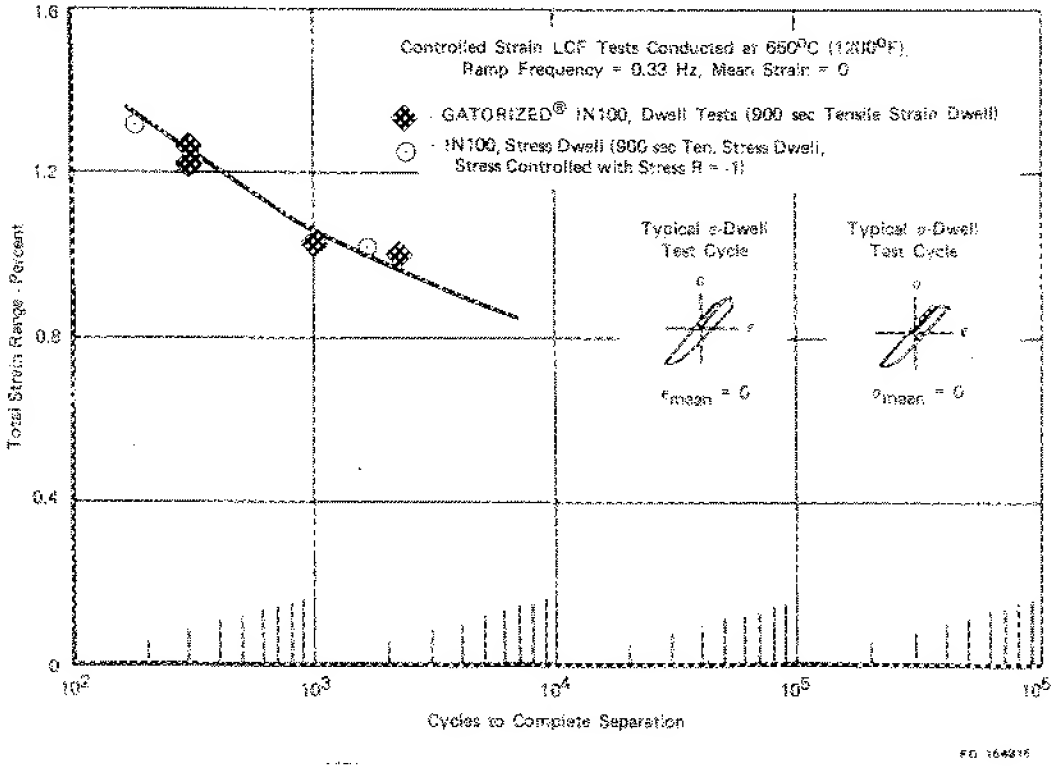

Figure 165. Comparison of the Effect of Stress-Hold Testing Modes on the LCF Properties of IN 100 (Mean Stress Equal to Zero)

TABLE 26

STRESS-HOLD VS STRAIN-HOLD TEST RESULTS FOR IN 100

AAll Tests Were Stress Limited, Testing Conducted at 650°C, 0.33 Hz Ramp Frequency

Spec S/N	Type[1] Test	Strain R (1st Cycle)	Strain R	Cyclic Strain (m/m at $N_f/2$) Range	Elastic	Inelastic	Creep	Average Unreversed Creep[2] (m/m)	Mean Stress (Hold Constant) MPa	ksi	Stress Range	Max Stress	Mean Strain[3] Cycle[1]	$N_f/2$	Failure[4]	True[5] Fracture Ductility (%)	Dwell Time (sec)	Cycles to Failure N_f
30	Creep/ Dwell	-1	-1.0	0.0102	0.0037	0.0005	0.0060	<<0.0001	0.0	0.0	1694 MPa (244.8 ksi)	842 MPa (122 ksi)	0.0009	0.0022	0.0016	5.8	900	1,771
31	Creep/ Dwell	-1	-1.0	0.0120	0.0114	0.0014	0.0006	<0.0001	0.0	0.0	2029 MPa (294.3 ksi)	1015 MPa (147 ksi)	0.0050	0.0043	0.0074	6.7	900	195
33	Creep/ Dwell	0	-0.64	0.0120	0.0116	0.0012	0.0007	0.0006	210	21.5	1926 MPa (280.8 ksi)	1178 MPa (171 ksi)	0.0064	0.0337	0.0528	14.2	900	93
37	Creep/ Dwell	0	-0.33	0.0094	0.0090	0.0004	0.0002	0.0002	373	54.1	1819 MPa (220.3 ksi)	1138 MPa (164 ksi)	0.0047	0.0294	0.0405	10.7	900	189
40	Creep/ Dwell	0	-0.17	0.0091	0.0078	0.0009	0.0003	0.0004	460	67.9	1313 MPa (190.4 ksi)	1124 MPa (163 ksi)	0.0041	0.0275	0.0440	12.2	900	105
46	Creep/ Dwell	0	-0.22	0.0092	0.0086	0.0002	0.0001	0.0003	432	62.7	1347 MPa (195.3 ksi)	1104 MPa (160 ksi)	0.0041	0.0246	0.0409	12.8	900	131
47	Creep/ Dwell	0	-0.034	0.0033	0.0003	<0.0001	<0.0001	<0.0001	501	72.6	1070 MPa (155.2 ksi)	1035 MPa (150 ksi)	0.0032	0.0136	0.0312	10.8	900	879
49[6]	Creep/ Dwell	0.5	+0.35	0.0043	0.0042	0.0001	<0.0001	0.0004	744	108.0	719 MPa (104.3 ksi)	1104 MPa (160 ksi)	0.0066	0.0357	0.0522	12.3	900	108
42	Strain/ Dwell	0	-0.70	0.0128	0.0117	0.0011	0.0005	0.0003	173	25.1	1997 MPa (289.7 ksi)	1172 MPa (170 ksi)	0.0064	0.0238	0.0404	7.7	900	132
43	Strain/ Dwell	0	-0.24	0.0092	0.0079	0.0008	0.0001	0.0002	421	61.1	1374 MPa (199.2 ksi)	1103 MPa (160 ksi)	0.0041	0.0197	0.0350	8.7	900	198
50	Strain/ Dwell	0	-0.033	0.0095	0.0064	<0.0001	<0.0001	<0.0001	485	70.5	1069 MPa (159.4 ksi)	1034 MPa (150 ksi)	0.0033	0.0132	0.0252	7.9	900	1,564

[1]Creep Dwell tests are stress controlled tests with a hold period at the max stress (to allow creep to occur during the hold time). Strain Dwell tests are stress controlled tests with a hold period at the max strain (to allow stress relaxation to occur during the hold period).

[2]Mean Strain does not stay constant but progressively increases during the test due to cyclic creep ratcheting.

[3]This creep component is the average unreversed creep per cycle which contributes only to mean strain extension (ratcheting). The total creep per cycle is equal to the sum of the cyclic creep component and the unreversed creep component.

[4]This value of mean strain is taken from the last complete cycle prior to failure, and is not equal to the true fracture strain.

[5]*True Fracture Ductility* is calculated based upon measured initial and final (after fracture) specimen gage section diameters: T.F.D. = 2 ln. $(d_o/d_f) \times 100\%$; d_o = original diameter, d_f = fracture diameter.

[6]This test was run at same peak stress as specimen S/N-46, but with half the total cyclic strain range to determine if peak stress or strain range was the critical parameter at these conditions.

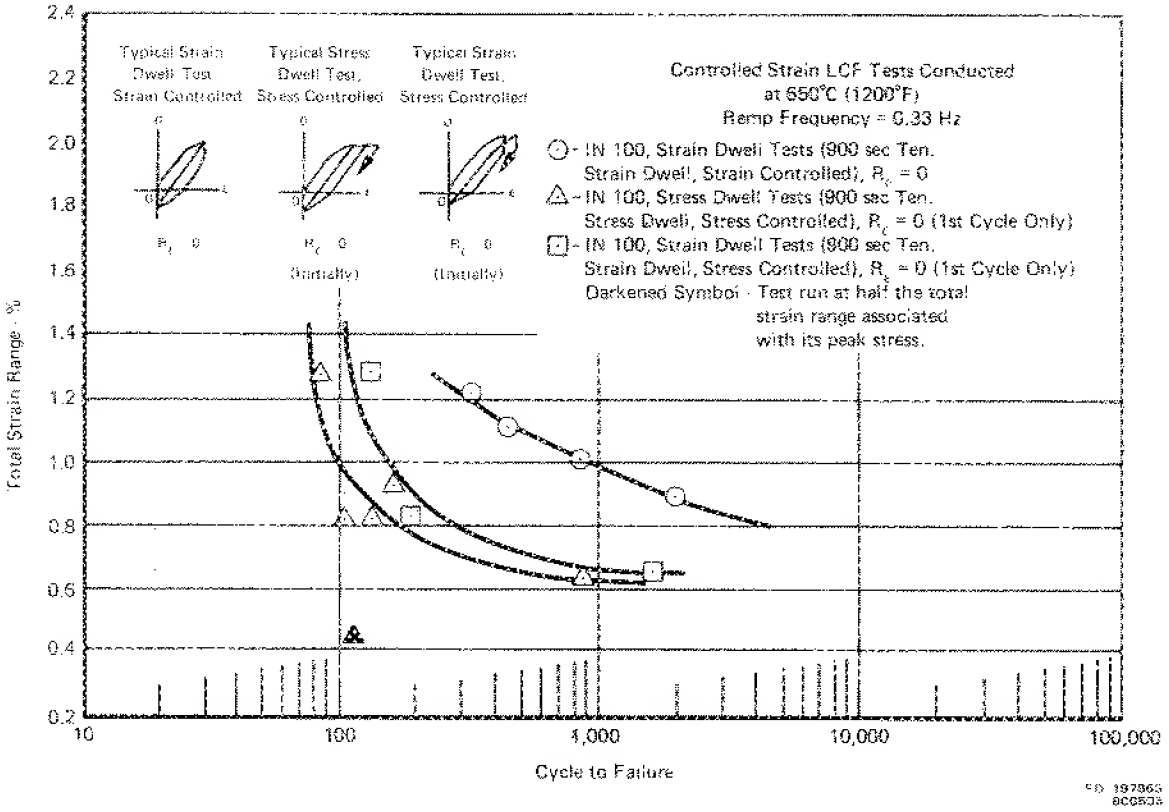

Figure 166. Comparison of Stress-Hold and Strain-Hold Testing Modes on the LCF Properties of IN 100 (Mean Stress Greater than Zero)

In an attempt to separate effects of the high net accumulated creep strain and the effects of mean stress, an additional dwell cycle was run with a constant peak (and mean) stress, but utilized a strain control dwell cycle to produce a cyclically unreversed creep component equal to zero. Figure 163 details the cycle described in table 23 as cycle type 5. Results are presented in table 26 and plotted in figure 166. Significant cyclically unreversed creep also occurred for these tests, but was substantially less (by approximately half) than the corresponding creep-dwell cycles. However, while LCF lives for both cycle types were not very different from each other, they were substantially lower than for the typical strain dwell test where mean stress relaxation occurs. Also differences in life for all three cycle types were *lowest* at high strain ranges where cyclically unreversed creep is maximum for the creep dwell test and mean stress differences between the three cycle types are minimum. Consequently, although complete separation of mean stress and cyclically unreversed creep strain effects was not attained, it appears that mean stress played a more important role than the unreversed creep strain in reducing LCF life for the stress-dwell cycles over strain-dwell cycles.

Results of standard creep tests, as well as comparisons of net creep, for both stress-dwell and strain-dwell conditions at several peak stress conditions are presented in figures 168 through 173.

One additional test was performed (S/N 48) utilizing a cycle type similar to that described as cycle type 4 in table 23, except that the total cyclic strain range was one-half that for other comparable stress-hold testing ($R_\epsilon = 0.5$). When plotted as a function of total strain range, as in figure 166, no correlation with the other data is found. However, when the data are replotted in figure 167 based on peak stress, it falls in reasonably well with the other results. Under these conditions, the rate of accumulation of unreversed creep was higher than for any of the other cycle types evaluated, as shown in figure 172. This testing indicates that the unreversed creep strain which accumulates in the creep dwell cycle significantly affects LCF life and must be considered along with mean stress in any approach to model LCF-creep interactions for unrestrained (creep-dwell) conditions, as has previously been suggested by Manson and Halford.[10]

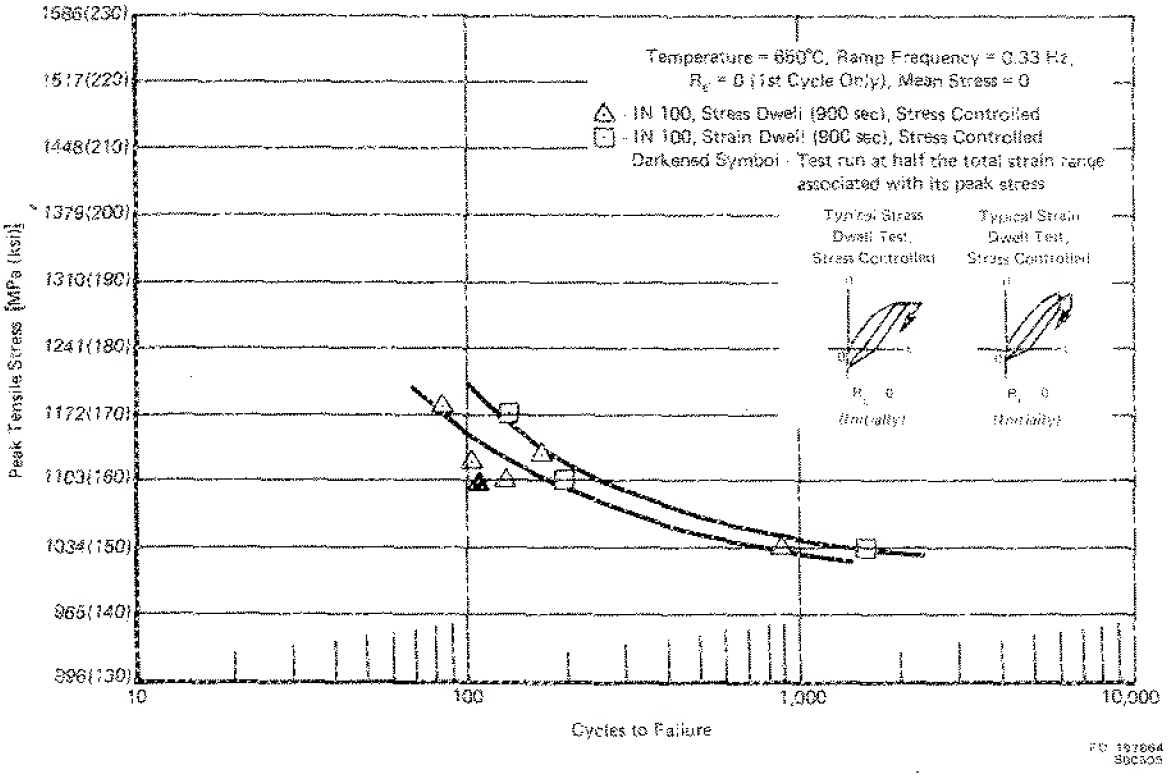

Figure 167. Comparison of Stress-Hold and Strain-Hold Testing Modes (Using Peak Tensile Stress as the Independent Variable) for IN 100

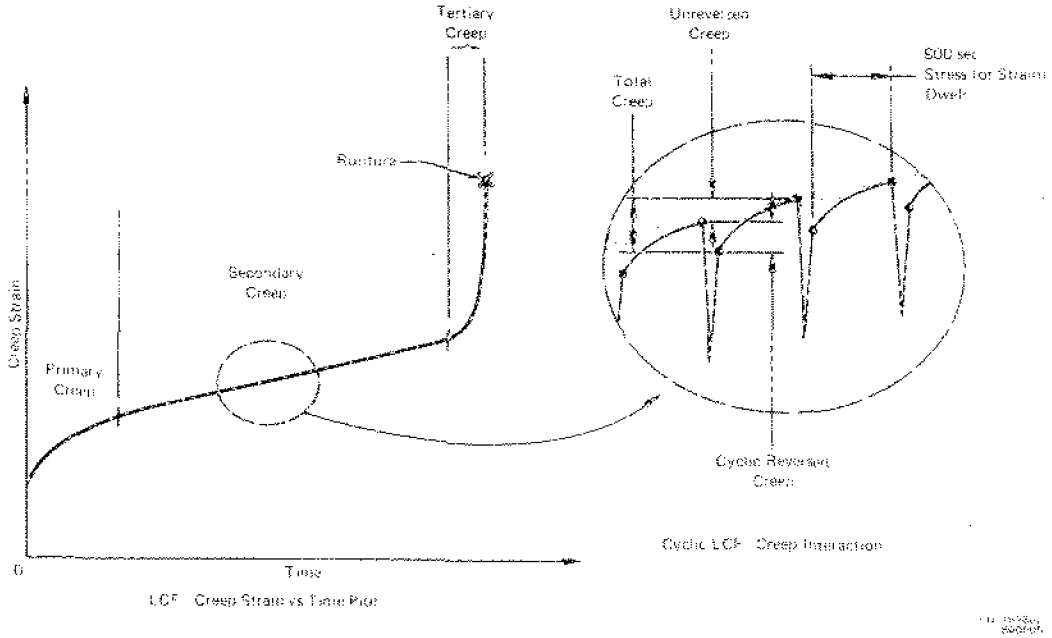

Figure 168. Typical Total Creep vs Time (or Cycles) Diagram for LCF — Creep Interaction Tests

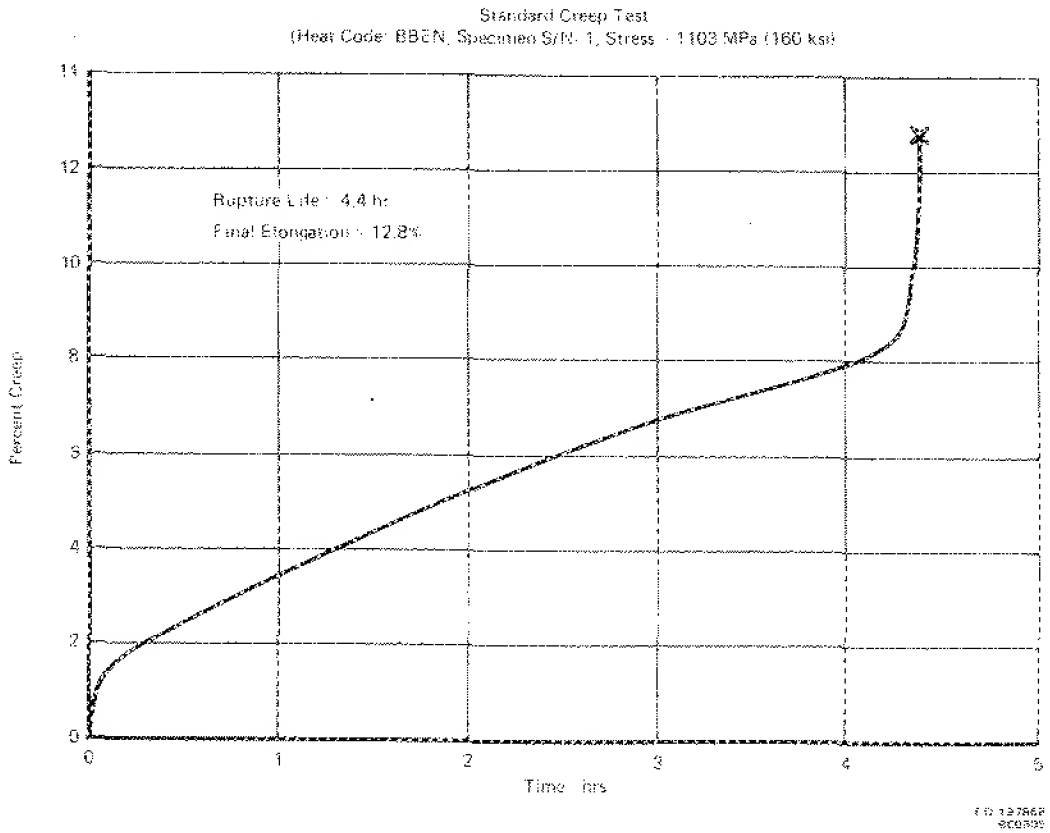

Figure 169. Creep vs Time Curve for IN 100 at 650°C, Maximum Stress = 1103 MPa

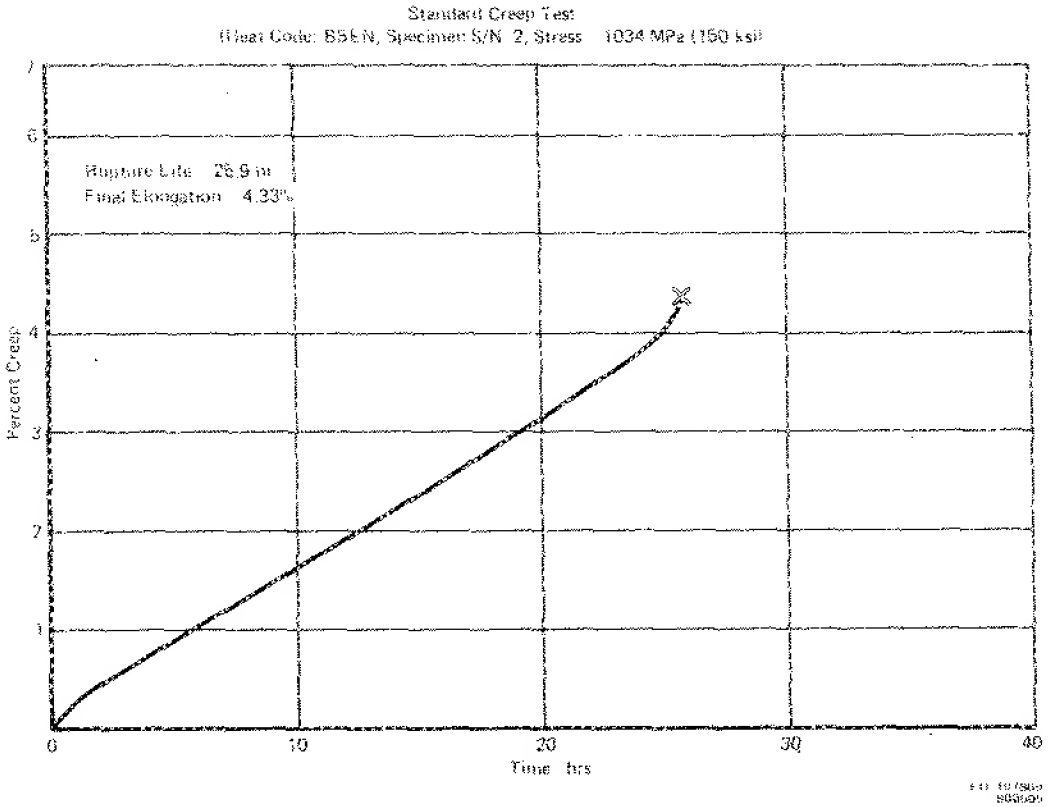

Figure 170. Creep vs Time Curve for IN 100 at 650°C, Maximum Stress = 1034 MPa

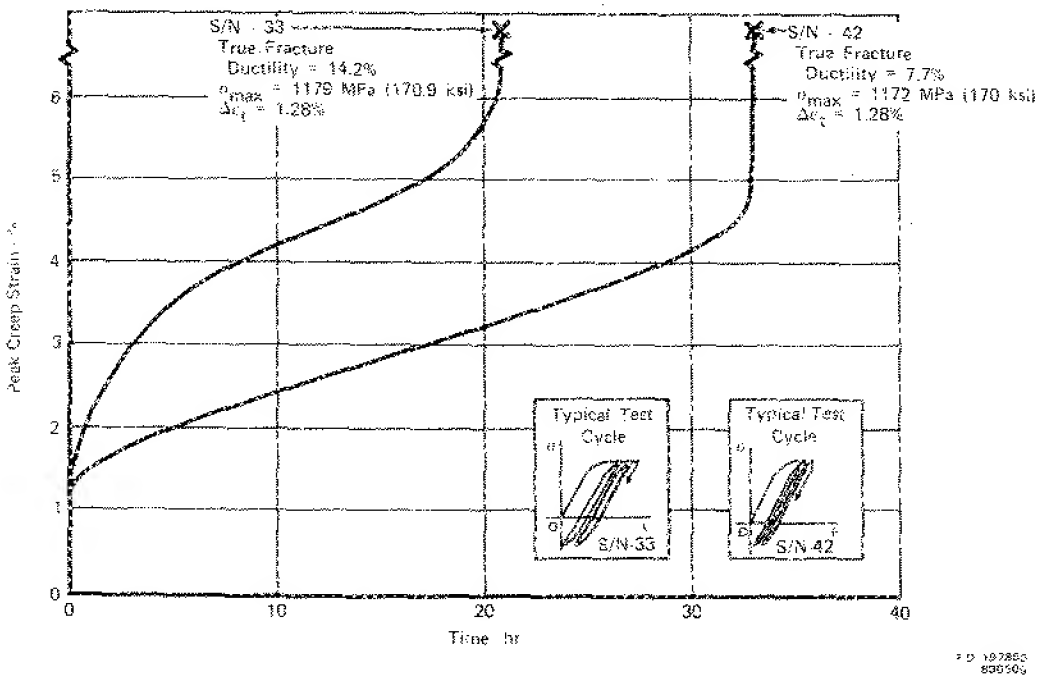

Figure 171. LCF - Creep Strain vs Time Curve for IN 100, Maximum Stress = 1175 MPa

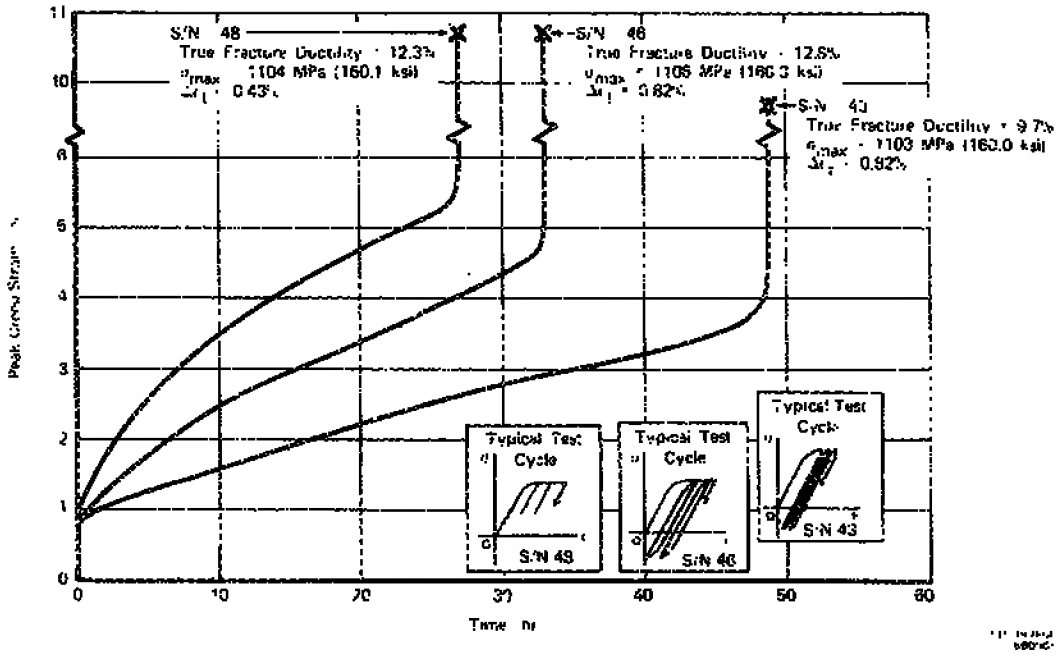

Figure 172. LCF - Creep Strain vs Time Curve for IN 100, Maximum Stress = 1100 MPa

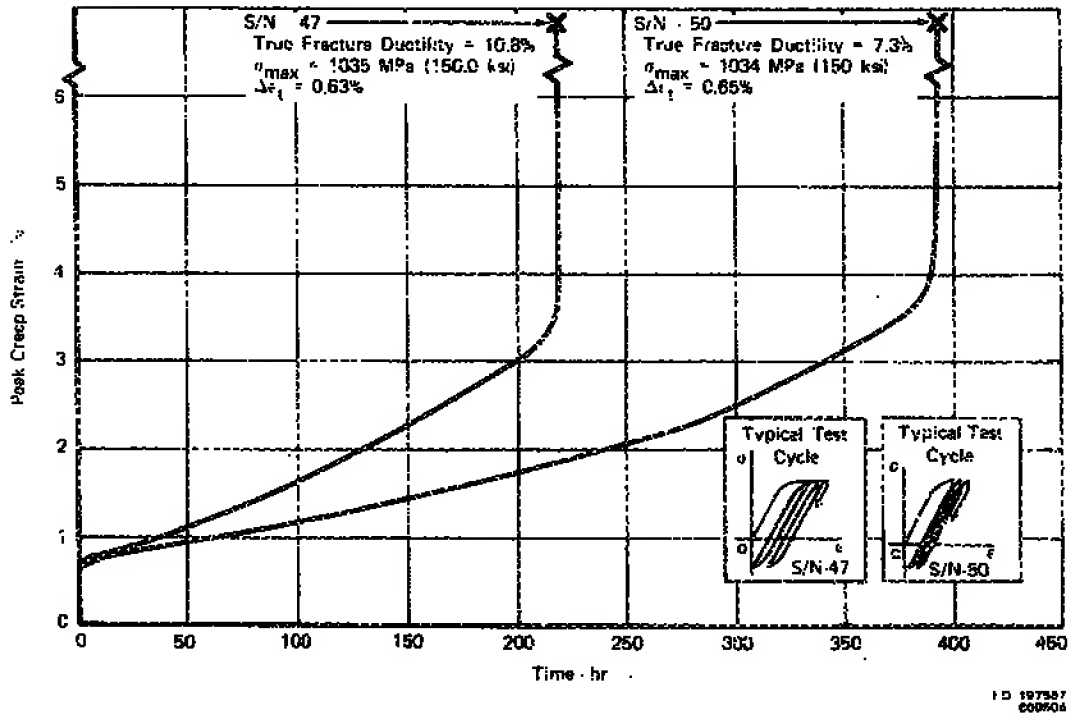

Figure 173. LCF Creep Strain vs Time Curve for IN 100, Maximum Stress = 1034 MPa

CONCLUSIONS AND SUMMARY OF RESULTS

Several turbine disk alloys representing various tensile strengths, processing histories, and microstructures were evaluated for resistance to fatigue crack initiation and propagation under both cyclic and cyclic/dwell conditions at 650°C. Effects of mean stress, inert environments, various cyclic/dwell conditions, and Contractor test methods were also evaluated for selected alloys and conditions. Results of this testing are summarized below:

Axial Strain Control LCF Tests

- *Fully Reversed Strain Cycle ($R_\varepsilon = -1$) Low Strain Ranges* — At total strain ranges of interest for aircraft turbine disk applications, LCF life is generally related to tensile strength. The rank order of the alloys tested from highest to lowest life for low strain ranges is shown in table 27.

- *Fully Reversed Strain Cycle ($R_\varepsilon = -1$), High Strain Ranges* — Rank order of the alloys by LCF initiation life changed substantially at higher strain ranges, approaching the rank order expected from monotonic tensile ductilities. For cyclic (0.33 Hz) tests, the rank order of the alloys from highest to lowest LCF initiation life is shown in table 28.

- *Fully Reversed Strain Cycle, Cyclic/Dwell* — Generally, the higher-strength, finer-grained alloys exhibited more significant reductions in fatigue life due to the dwell. At low strain ranges, the percent reductions in life for the alloys appears in table 29.

- *All-Tensile Strain Cycle ($R_\varepsilon = 0$)* — At total strain ranges of interest for turbine disk applications, LCF life again is generally related to tensile strength. The rank order, which approximates the $R_\varepsilon = -1$ results, from highest to lowest LCF life for low strain ranges is presented in table 30.

  LCF life at higher strain ranges is related to ductility, and the rank order is identical to the fully reversed test results.

- *Mean Stress, Mean Strain Effects* — In general, the effects of mean strain were found to be negligible for the conditions evaluated but the effects of mean stress were pronounced. At high strain ranges the mean stress was near zero and did not contribute to reduction in life. At low strain ranges, however, mean stresses were large and significantly reduced LCF life compared to tests run with comparable strain ranges but zero mean stress ($R_\varepsilon = 1$).

- *Contractor LCF Test Method Comparison* — Low-cycle fatigue data generated by P&WA and GE generally agreed. Cyclic (0.33 Hz) test data show the mean curve for P&WA testing to be greater in cyclic life than the mean curve for GE testing. However, the data were limited and variance was significant. Dwell (900-sec hold time) data agreed reasonably well. Differences in LCF life are probably attributable to specimen machining and surface preparation.

Fatigue Crack Growth Evaluations

- Crack growth rates generally increased with increasing tensile strength. Creek growth testing conducted with a 900-sec dwell at maximum tensile load in air showed the same trends as the 0.33 Hz testing with larger absolute differences in crack growth rates. See table 31 for rank ordering.

- Comparison of Contractor testing and data analysis procedures for HIP plus forged René 95 showed crack growth data obtained at 0.33 Hz for the K_t bar specimen to be approximately two times faster than that obtained from the compact type specimen. At 900-sec dwell times, K_t bar data was *much* faster than the CT specimens, with diminishing differences at low ΔK levels. Further investigation of these differences is needed.

- Waspaloy and IN 100 tested in an argon environment at 0.33 Hz demonstrated crack growth rates at low ΔK levels approximately a factor of 2 slower than the same alloys tested in air. Air and argon crack growth rates converged at higher ΔK levels. Oxidation appeared to degrade the cyclic crack growth rates of IN 100 slightly more than Waspaloy. Cyclic/dwell tests in argon were inconclusive.

Metallographic and Fractographic Evaluations

Metallographic and fractographic evaluations were performed on failed strain control LCF specimens of Waspaloy, wrought Astroloy, HIP Astroloy, HIP MERL 76, IN 100, HIP plus forged René 95 and NASA IIB-7. Results, where failure modes could be distinguished, can be summarized as follows:

- Crack initiation for cyclic tests was transgranular for all the alloys, except HIP MERL 76 and IN 100 where cracks initiated in voids and inclusions.

- Crack growth for cyclic tests of all the alloys was transgranular, except in the fine-grained IN 100.

- Crack initiation was generally intergranular for cyclic/dwell tests, except for the coarse-grained Waspaloy sample.

- Crack growth in all the cyclic/dwell test samples was intergranular.

Creep-Fatigue Cycle Evaluations

Results of additional creep-fatigue evaluations performed on the IN 100 samples at 650°C can be summarized as follows:

- Changing dwell time from zero to 30, 120, and 900 sec resulted in corresponding reductions in life with very minimal changes in cyclic creep strain range. Reductions in life are attributed primarily to exposure time at 650°C rather than cyclic creep deformation damage.

- Comparison of basic tensile stress-hold with tensile strain-hold cycles *showed no significant differences provided test variables, such as mean* stress, strain range, and hold time were comparable.

- Mean stress and accumulated creep strain (in stress-hold cycles) both significantly affected LCf life. Life differences between stress-hold and strain-hold cycles are attributed to mean stress and cumulative creep strains.

TABLE 27.
RANK ORDER FROM HIGHEST TO LOWEST LCF INITIATION LIFE FOR STRAIN RANGES BELOW APPROXIMATELY 1.0%, FULLY REVERSED STRAIN CYCLE

Tensile Strength	*LCF Life with 0.33 Hz Results*	*LCF Life with 900-sec Dwell Results*
NASA IIB-7	René 95 H+F	NASA IIB-7
René 95 H+F	HIP MERL 76	René 95 H+F
HIP MERL 76	NASA IIB-7	HIP MERL 76
IN 100	IN 100	IN 100
Wrought Astroloy	Wrought Astroloy	Wrought Astroloy
Waspaloy	HIP Astroloy	HIP Astroloy
HIP Astroloy	Waspaloy	Waspaloy

TABLE 28.
RANK ORDER FROM HIGHEST TO LOWEST LCF INITIATION LIFE FOR STRAIN RANGES ABOVE APPROXIMATELY 1.8%, 0.33 Hz, FULLY REVERSED STRAIN CYCLE

Tensile Ductility	*LCF Life with 0.33 Hz Results*
HIP Astroloy	Waspaloy
Wrought Astroloy	HIP Astroloy
Waspaloy	HIP MERL 76
HIP MERL 76	Wrought Astroloy
IN 100	René 95 H+F
René 95 H+F	IN 100
NASA IIB-7	NASA IIB-7

TABLE 29.
PERCENT REDUCTION OF LCF LIFE AS A RESULT OF 900-sec DWELL (Total Strain Range of 1.0%)

Alloy	*Reduction (%)*
René 95 H+F	89
IN 100	85
HIP MERL 76	84
NASA IIB-76	62
HIP Astroloy	45
Waspaloy	42
Wrought Astroloy	26

TABLE 30.
RANK ORDER FROM HIGHEST TO LOWEST LCF INITIATION LIFE FOR ALL-TENSILE STRAIN CYCLES, 0.33 Hz

LCF Life with Total Strain Range Below 1.0%	*LCF Life with Total Strain Range Above 1.8%*
René 95 H+F	Waspaloy
NASA IIB-7	HIP MERL 76
HIP MERL 76	René 95 H+F
IN 100	IN 100
Waspaloy	NASA IIB-7

TABLE 31
RANK ORDERING FROM BEST TO WORST CRACK GROWTH RATES, 0.33 Hz

Alloy	*0.2% Yield Strength at 650°C — MPa*
Waspaloy	967
HIP Astroloy	881
Wrought Astroloy	986
IN 100	1110
HIP MERL 76	1027
NASA IIB-7	1277
René 95 H+F	1122

REFERENCES

1. Cowles, B. A., D. L. Sims, and J. R. Warren, "Evaluation of the Cyclic Behavior of Aircraft Turbine Disk Alloys," NASA Report CR-159409, October 1978.

2. Shahani, V. and H. G. Popp, "Evaluation of Cyclic Behavior of Aircraft Turbine Disk Alloys," NASA Report CR-159433, June 1978.

3. deNeeve, P. F. and A. Wuerscher, "Evaluation of the Strain Behavior of an LCF Specimen," *Pratt & Whitney Aircraft of Canada* Internal Correspondence, 23 April 1970.

4. Jelic, F., P. Niessen, and D. J. Burns, "Temperature Dependence on Fatigue Crack Propagation in *Al-2.6 Mg Alloy*," *Fatigue at* Elevated Temperatures, ASTM STP 520, pp. 139-148, 1973.

5. Rudak, S. J., A. Saxena, R. J. Bucci, and R. C. Malcolm, "*Development of Standard* Methods of Testing and Analyzing Fatigue Crack Growth Rate Data," AFML-TR-78-40, May 1978.

6. Paris, P. C., *Fatigue — An Interdisciplinary Approach*, Proceedings 10th Sagamore Conference, Syracuse University Press, N. Y., 1964, p. 107.

7. Sims, D. L., C. G. Annis, and R. M. Wallace, "Cumulative Damage Fracture Mechanics at Elevated Temperatures," AFML-TR-76-176, Part III, April 1977.

8. Sha, G., "K-Solution of [General Electric] Surface Flaw Specimens," Pratt & Whitney Aircraft/Florida, April 1980.

9. Gell, M. and G. Leverant, "Mechanisms of High Temperature Fatigue," Fatigue at Elevated Temperatures, ASTM STP 520, pp. 37-67, 1973.

10. Manson, S. S., and G. R. Halford, "Treatment of Multiaxial Creep-Fatigue by Strainrange Partitioning," NASA TM X-73488, December 1976.

REPORT DOCUMENTATION PAGE

Form Approved
OMB No. 0704-0188

1. AGENCY USE ONLY (*Leave blank*)	2. REPORT DATE	3. REPORT TYPE AND DATES COVERED
	July 1980	Final Contractor Report

4. TITLE AND SUBTITLE

Evaluation of the Cyclic Behavior of Aircraft Turbine Disk Alloys, Part II

5. FUNDING NUMBERS

WU–None
NAS3–21379

6. AUTHOR(S)

B.A. Cowles, J.R. Warren, and F.K. Haake

7. PERFORMING ORGANIZATION NAME(S) AND ADDRESS(ES)

United Technologies Corporation
Pratt & Whitney Aircraft Group
Government Products Division
Box 2691
West Palm Beach, Florida 33402

8. PERFORMING ORGANIZATION REPORT NUMBER

E–14588

9. SPONSORING/MONITORING AGENCY NAME(S) AND ADDRESS(ES)

National Aeronautics and Space Administration
Washington, DC 20546–0001

10. SPONSORING/MONITORING AGENCY REPORT NUMBER

NASA CR–165123
FR–13153

11. SUPPLEMENTARY NOTES

Project Manager, Dr. R.V. Miner, Jr., NASA Lewis Research Center, Cleveland, Ohio.

12a. DISTRIBUTION/AVAILABILITY STATEMENT

Unclassified - Unlimited
Subject Category: 07

Available electronically at http://gltrs.grc.nasa.gov
This publication is available from the NASA Center for AeroSpace Information, 301–621–0390.

12b. DISTRIBUTION CODE

13. ABSTRACT ***(Maximum 200 words)***

This program followed two earlier NASA contracts which evaluated the cyclic behavior of several advanced aircraft turbine disk alloys. The alloys selected for this program included HIP MERL 76 which is an advanced alloy currently undergoing trial disk production development at Pratt & Whitney Aircraft under NASA MATE program sponsorship, HIP plus forged René 95 currently used by General Electric Corporation, GATORIZED® IN 100 which is an advanced alloy currently used by P&WA, and conventionally forged Waspaloy which is a current, widely used disk alloy produced from ingot. The objectives of this program included evaluation of an additional alloy from previous programs, providing a comparison of Contractor test methods, determination of crack initiation and early propagation mechanism for various alloys, and determination of the effects of mean stress or strain, various creep-fatigue cycle forms, and environment on crack initiation and crack growth behavior for selected alloys. As in earlier programs, the cyclic behavior of the alloys was evaluated from two aspects: crack initiation and crack propagation. The test methods utilized to establish this behavior were axially loaded strain control low-cycle fatigue tests for initiation and load-controlled cyclic crack growth rate fracture mechanics test for propagation. Tests were conducted with both cyclic and cyclic/dwell conditions at 650 °C (1200 °F).

14. SUBJECT TERMS	15. NUMBER OF PAGES
Strain control; Fatigue crack propagation; Low cycle fatigue (LCF); Life prediction; NASA IIB–7; IN 100; Waspaloy; Astroloy; HIP-Astroloy; Turbine disks; HIP MERL 76	196
	16. PRICE CODE

17. SECURITY CLASSIFICATION OF REPORT	18. SECURITY CLASSIFICATION OF THIS PAGE	19. SECURITY CLASSIFICATION OF ABSTRACT	20. LIMITATION OF ABSTRACT
Unclassified	Unclassified	Unclassified	